Kent Academic Repository

Shehata, Sara (2023) *Synthesis of ROMP polymers for biological applications.* **Doctor of Philosophy (PhD) thesis, University of Kent,.**

Downloaded from

The version of record is available from

This document version

DOI for this version

Licence for this version

Additional information

Versions of research works

Versions of Record

Author Accepted Manuscripts

Enquiries

University of Kent

Synthesis of ROMP polymers for biological applications

Sara Shehata

Thesis submitted to the University of Kent for the Degree of Doctor of Philosophy

School of Physical Sciences

September 2022

ABSTRACT

Ring opening metathesis polymerisation (ROMP) is a living polymerisation which allows for the synthesis of polymers with controlled length and composition, as well as narrow distribution of the molecular weights. Thanks to the availability of metal alkylidene catalysts at a cheap price, ROMP has become a versatile method for the preparation of materials for different applications, including optics and electronics, energy storage and nanomedicine among others.

This project explored the use of ROMP for the realisation of biologically relevant polymers. In particular, ROMP has been used in two applications. The first application involved the preparation of amphiphilic block copolymers consisting of ibuprofen and PEG, which were covalently linked to the polymer backbone via a cleavable bond. Ibuprofen and PEG respectively constituted the hydrophobic and hydrophilic portions of the block copolymer. Ibuprofen is a nonsteroidal anti-inflammatory drug (NSAID) which was selected in this study thanks to its potential role in chemoprevention and chemotherapy. The so synthesised amphiphilic block copolymer could self-assembled in aqueous environment to form nanoparticles with precise size and morphology, and that could entrap the drug within the hydrophobic core. This allowed for the studies of the drug release from the polymeric nanoparticles using both physiological and alkaline conditions. Our studies demonstrated a high stability of the synthesised nanoparticles under physiological environments, while slow drug release could be obtained under strong basic conditions. In the second application ROMP has been used for the preparation of amphiphilic cationic polymers for the development of antimicrobial materials. Homopolymers bearing pyridinium cations and SSA (self-associating amphiphilic salts) counterions were prepared. SSAs are a novel class of antimicrobial agents synthesised by the Hiscock group at the University of Kent. In this collaboration, the so synthesised homopolymers were studied for their antimicrobial activity against both Gram-negative and Gram-positive bacteria. The results demonstrated an antagonistic effect between the amphiphilic cationic ROMP polymer and the selected SSA.

DECLARATION

I declare that the work presented herein is my own and that the thesis was written in my own words. I certify that it has not been submitted for the purposes of a qualification at any other institution or for any other degree.

Sara Shehata

01 September 2022

ACKNOWLEDGMENTS

Firstly, I would like to express my gratitude to my supervisor Dr. Stefano Biagini for giving me the opportunity to join his group at the University of Kent. He not only has been a great supervisor, but also a very good friend who has always supported me in my good and bad moments. I thank him for all the wise advice he gave me during my three years of PhD and for always showing me the positive sides of a negative situation. I am grateful to have been his student. Secondly, I would like to thank my co-supervisor Dr. Christopher Serpell, who has adopted me and made me part of his research group. I thank him for all his creativity and wide knowledge of the medicinal world. I would also like to thank Dr. Aniello Palma for being such a great second supervisor and for leading so well all of my review meetings, and also Professor Jennifer Hiscock for the amazing collaboration we have created and for giving me the opportunity to learn new analytical techniques.

A special gratitude goes to my friends and colleagues Lee, Saeed, Prashant and Sena without whom I could not have survived the PhD experience. Thanks for all the laughs, lunches, dinners and drinks together, but especially thanks for having withstood me in every moment. Also, thanks for the chemistry and biology knowledge it has been shared with me.

Finally, I would like to thank my family for supporting my decision to move country and start this new experience far away from them, although I know it has been difficult for them. Thanks for always believe in me and for pushing me reaching the end goal.

DISSEMINATION

Peer-reviewed publication

Shehata, S., Serpell, C.J. and Biagini, S.C., 2020. Architecture-controlled release of ibuprofen from polymeric nanoparticles. *Materials Today Communications*, *25*, p.101562.

Collaborations

Birchall, L.T., Shehata, S., McCarthy, S., Shepherd, H.J., Clark, E.R., Serpell, C.J. and Biagini, S.C., 2020. Supramolecular behaviour and fluorescence of rhodamine-functionalised ROMP polymers. *Polymer Chemistry*, *11*(32), pp.5279-5285.

Birchall, L.T., Shehata, S., Serpell, C.J., Clark, E.R. and Biagini, S.C., 2021. Himic Anhydride: A retro Diels–Alder reaction for the organic laboratory and an accompanying NMR study. *Journal of Chemical Education*, *98*(12), pp.4013-4016.

TABLE OF CONTENTS

LIST OF ABBREVIATIONS

Abbreviation	Meaning
ACP	amphiphilic cationic polymers
AFM	atomic force microscopy
AMP	antimicrobial peptides
AMR	antimicrobial resistance
ATRP	atom transfer radical polymerisation
BASP	brush-arm star polymer
BHT	butylated hydroxytoluene
BRET	bioluminescence resonance energy transfer
BSI	incidence of bloodstream infections
CAC	critical aggregate concentration
$CDCl_3$	deuterated chloroform
COSY	correlated spectroscopy
COX	cyclooxygenase
CT	camptothecin
CUR	curcumin
DABCO	1,4-diazabicyclo[2.2.2]octane
DBASC	diblock brush-arm star copolymer
DCC	dicyclohexyl carbodiimide
DCM	dichloromethane
DDS	drug delivery systems
DFT	density functional theory
DLS	dynamic light scattering
DMAP	dimethylamino pyridine
DMF	dimethylformamide
DMSO	dimethyl sulfoxide
DNA	deoxyribonucleic acid
DOSY	diffusion ordered spectroscopy
DOX	doxorubicin
DOXY	doxorubicin salt
DP	degree of polymerisation
ECDC	European centre for disease prevention and control
EDC	1-ethyl-3-(3-dimethylaminopropyl)carbodiimide

EDU	1-[3-(dimethylamino)propyl]-3-ethylurea
EEA	European economic area
EPR	enhanced permeation and retention
ESI	electrospray ionisation
EU	European Union
FBS	foetal bovine serum
FDA	food and drug administration
FTIR	Fourier-transform infrared spectroscopy
GC	gas chromatography
GPC	gel permeation chromatography
GS	gentamicin sulphate
HBA	hydrogen bond acceptor
HBD	hydrogen bond donator
HDAC	histone deacetylase
HEC	hydroxyethylcellulose
HEG	hexaethylene glycol
HMBC	heteronuclear multiple bond correlation
HMQC	heteronuclear multiple quantum coherence
HPLC	high-performance liquid chromatography
HR-MS	high-resolution mass spectrometry
Ibu	ibuprofen
IUPAC	international union of pure and applied chemistry
LB	Luria broth
MALDI	matrix-assisted laser desorption/ionization
MCF	Michigan cancer foundation
MIC50	minimum inhibitory concentration
MRSA	methicillin-resistant Staphylococcus aureus
MS	molecular sieves
MSI-78	magainin derivative
MW	molecular weight
NB	norbornene
NBOC	nitrobenzyloxycarbonyl
NHC	*N*-heterocyclic carbene
NHS	*N*-hydroxysuccinimide esters

NIR	near infrared
NMR	nuclear magnetic resonance
NP	nanoparticle
NR	nile red
NSAID	nonsteroidal anti-inflammatory drugs
OD600	optical density 600 nm
ONB	oxanorbornene
PACT	photodynamic antimicrobial chemotherapy
PBS	phosphate buffered saline
PC	phosphatidylcholine
PDI	polydispersity index
PE	phosphatidylethanolamine
PEG	poly(ethylene glycol) methyl ether
PEI	poly ethyleneimine
PEN/PN/PNB	poly(norbornene)
PEO	poly(ethylene oxide)
PET	poly(ethylene terephthalate) or petroleum ether
PG	prostaglandins
PGA	poly(L-glutamic acid)
PLE	pig liver esterase
PSA	polysalicylate
PTXL	placlitaxel
PVP	Poly(vinyl alcohol)
RA	rheumatoid arthritis
RAFT	reversible addition fragmentation chain transfer polymerisation
RES	the reticulo-endothelial system
RET	retinal
RI	refractive index
RIF	rifampicin
RNA	ribonucleic acid
ROMP	ring opening metathesis polymerisation
ROP	ring-opening polymerisation
ROS	reactive oxygen species
RT	retention time

SAHA	suberoylanilide hydroxamic acid
SCID	severe combined immunodeficiency
SEC	size exclusion chromatography
SEM	scanning electron microscope
SLN	solid lipid nanoparticles
SMA	styrene-maleic anhydride copolymer
SP	spiropyran
SPR	surface plasmon resonance
SSA	supramolecular self-associating amphiphiles
ST	surface tension
TBA	tertrabutylammonium
TC	thiocresol
TEG	triethylene glycol
TEM	transmission electron microscopy
THF	tetrahydrofuran
TOF	time of flight
TS	transition state
UHPLC	ultra-high-performance liquid chromatography
UKHSA	UK Security Agency
UV	ultraviolet
VAN	vancomycin
VT	variable temperature
WHO	World Health Organisation
XRD	X-ray diffraction
ZP	zeta potential

CHAPTER 1. RING OPENING METATHESIS POLYMERISATION (ROMP)

1.1.   Introduction

The word **polymer** derives from the Greek words *polus* meaning "many" and *meres* meaning

"parts"[1]. Because of their size, polymers are also known as **macromolecules**, which simply means

"large (or long) molecules". The term "polymer" as we know it in modern times, was proposed by

Hermann Staudinger in 1920[2] who defined them as molecules of high molecular weight consisting

of small molecules covalently bonded to each other. Polymers play a very important role in

everyday life and in this respect are mainly divided into two categories, synthetic polymers such as

polyethylene or polystyrene (common plastic) and natural polymers such as proteins, consisting of

a precise selection of 20 different amino acids, but also cellulose, the main constituent of paper,

and natural rubber. Nature has always been the greatest exponent for the realisation of polymers

of advanced features as well as precise biological structure. Thus, polymer chemists have always

tried and still try to mimic these natural polymer characteristics in order to control properties such

as molecular weight, sequence distribution and dispersity. As such, living polymerisations have

been proven to be a convenient approach for the preparation of polymers with unique properties.

They are obtained by the sequential addition of different monomers, and this allows for the

manipulation of the polymer's physical properties. It is for this reason that living polymerisation

was chosen for this thesis project.

1.1.1.   Classification of polymers based on the polymerisation mechanism

Polymers can be classified according to their mechanism of polymerisation and are mainly divided

in *step-growth* polymerisation and *chain-growth* polymerisation[1,3].

Step-growth polymerisation, also known as *condensation* polymerisation, requires the

reaction of at least two molecules (either a monomer or an oligomer) containing different

functional groups such as carboxylic acids, amines or hydroxyl groups. The reaction of molecules

containing such functionalities can occur by elimination of a small molecule, such as water. As such, polycondensations involve classical reactions including esterification or amidation. In this type of mechanism, polymers of high molecular weight are typically obtained only at the end of the reaction. The most common examples of polymers prepared by this technique are nylon-6,6, obtained by the condensation of hexamethylenediamine and adipic acid, poly(ethylene terephthalate) (PET), obtained by the polyesterification of terephthalic acid and ethylene glycol, polycarbonates and polyurethanes (Figure 1.1).
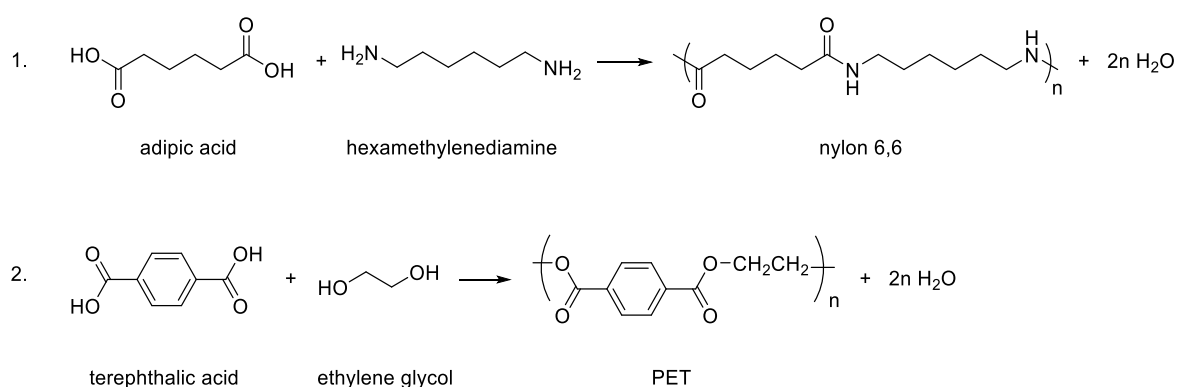
Fig. 1.1. Examples of step-growth polymerisation: 1) synthesis of nylon-6,6; 2) synthesis of PET.

Chain-growth polymerisation is also referred to as *addition* polymerisation and require the presence of initiation species, such as an anion, a cation or a radical (anionic, cationic and free-radical chain-growth polymerisations respectively) which reacts with a monomer, typically an alkene, in order to initiate the polymerisation. In this case, the polymerisation follows three main steps which are initiation, propagation and termination and in contrast to *step-growth* polymerisation, it affords polymers with high molecular weight early during the polymerisation. Furthermore, the polymerisation yield and the monomer conversion increase with time. An example of such polymerisation technique is the polymerisation of styrene shown in Figure 1.2. Living polymerisation is a type of *addition* polymerisation where, during the propagation step, the active site of the polymer is kept "alive" without any termination process interfering.

1. Initiation
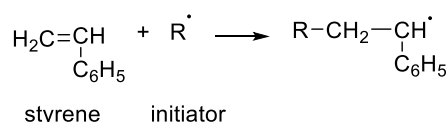
styrene   initiator

2. Propagation

3. Termination

polystirene
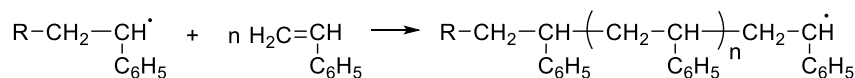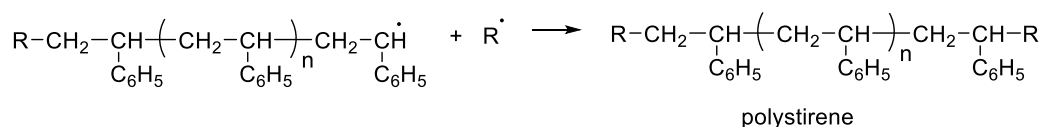
Fig. 1.2. Example of chain-growth polymerisation. The polymerisation of styrene is initiated by a radical formed by heating, followed by propagation of the polymer chain and termination to afford polystyrene.

1.2. Living Ring Opening Metathesis Polymerisation

1.2.1. Living Polymerisation

The concept of living polymerisation was first proposed by Ziegler in 1928[4] when his group started investigating the reaction of styrene and butadiene with organometallic compounds deriving from the main group. However, it was only in 1956 that the term "living polymerisation" was introduced by Szwarc following his work on living anionic polymerisation of styrene[5]. He defined a living polymerisation as a "reaction that is born through an initiation process, grows by a propagation process, and dies as a result of termination process (sic)"[6]. Because of the absence of a termination step, additional amount of monomer like styrene can be added into the reaction mixture where the monomers react with the chain ends, leading to polymer chain growth rather than forming a new chain. Therefore, living polymerisation is a type of chain-growth polymerisation. According to the IUPAC definition of living polymerisation[7], "the chain initiation is fast compared with the rate of chain propagation, so that the number of kinetic chain carriers is essentially constant throughout the polymerisation", meaning that the polymer obtained possess uniform length. In fact, living

polymers generally have very narrow molecular weight distributions which are characterised by the dispersity index (Đ) described by the equation 1.1.[8]:

$$Đ = \frac{M_w}{M_n}$$ **Eq. 1.1.**

where M_w is the weight average molecular weight and M_n is the number average molecular weight. Typically, these systems are statistically described in terms of a Poisson distribution[9] and possess dispersity values of Đ < 1.5.

Essential characteristics for a living polymerisation are therefore:

1. Rapid and complete initiation, where the rate of initiation (K_i) is greater than the rate of propagation (K_p).

2. Irreversible propagation steps.

3. Absence of chain transfer and chain termination.

4. Number-average molecular weight, M_n, proportional to the monomer conversion.

5. Narrow molecular weight distribution and control of molecular weight.

1.2.2. The Ring-Opening Metathesis Polymerisation

Ring opening metathesis polymerisation (ROMP) is a living polymerisation technique first discovered by Anderson and Merckling[10] in 1955 while working at the DuPont laboratories on the polymerisation of norbornene (highly strained bicyclic olefin) using the classical Ziegler-Natta catalyst (Ti(II) catalyst). In 1963, Eleuterio[11], another DuPont researcher, discovered that the polymerisation of bicyclic olefins catalysed by MoO_3/γ-$Al_2O_3/LiAlH_4$ afforded polymers containing single ring repeating units linked together via unsaturated bonds (*trans-* and *cis*-unsaturation). In 1970, Chauvin and Hérisson proposed the metallacyclobutane mechanism[12] for metathesis which was later supported by other scientists such as Grubbs[13] and Schrock[14]. Subsequently, Grubbs and Schrock synthesised a series of well-defined catalysts for ROMP, which made the synthesis of

polymers with controlled molecular weight distributions and block sequences a possibility. By the late 1990's, ROMP became one of the most versatile living polymerisation method for the realisation of diverse materials to be used in a wide range of applications. In 2005, Yves Chauvin, Robert H. Grubbs and Richard R. Schrock won the Nobel Prize in chemistry for the development of the metathesis method in organic synthesis[15].

ROMP is a chain-growth polymerisation technique where mono-, bi- or multi-cyclic olefins undergo ring opening (by breaking and reforming double bonds simultaneously) when initiated by metal alkylidene catalysts based on group VI or VIII metals (such as Mo and Ru). The polymerisation is controlled and living which makes the preparation of precise homo and block architectures possible, according to the type of initiator used. The initiator, in fact, must be tolerant to moisture or air and to most functional groups, in order to be widely utilised.

1.2.2.1.   The initiators

From the early 1960's to the early 1980's, many of the ROMP catalysts were based on transition metals such as Ti, V, Nb, Ta, Cr, Mo, W, Re, Co, Ir, Ru and Os and the majority of them were heterogeneous catalysts consisting of a two or three component mixture (e.g. MoO_3/γ-$Al_2O_3/LiAlH_4$, $MoCl_5/Et_3Al$, $WCl_6/EtAlCl_2/EtOH$)[11,16,17]. However, there were some limitations related to the use of these initiators which included lack of reaction control, chain-transfer steps (such as intramolecular "backbiting") and termination steps[18], leading to the formation of more propagating species which grow independently to each other at different polymerisation rates. For these reasons, efforts were shifted towards the preparation of homogeneous single component catalysts, specifically transition metal carbenes and metallacyclobutanes (also called transition metal alkylidenes)[19,18]. In 1982 Grubbs et al. synthesised the first titanacyclobutane initiator[20] capable of polymerising a series of norbornene compounds (upon heating to T > 60 °C) that possessed low dispersity of Đ < 1.2 and molecular weights nearly proportional to the amount of monomer used. The higher activity and the

improved initiation of these Ti catalysts (**1** and **2**, Figure 1.3) made it possible to prepare di- and tri-

block copolymers[21] with narrow molecular weight distribution.
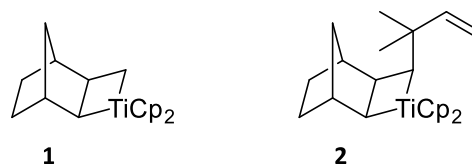
Fig. 1.3. The titanacyclobutane initiators prepared by Grubbs.

However, tungsten and molybdenum alkylidenes developed by Schrock and co-workers in

the late 1980's were the initiators that became the most used for almost 20 years. These catalysts

were imido-alkoxy based metal complexes with general formula M(=NAr)(=CHR)(OR')$_2$[22,23] where M

= Mo, W; Ar = aryl, R = aryl or alkyl; R' = CMe$_3$, CMe$_2$CF$_3$, CMe(CF$_3$)$_2$, C(CF$_3$)$_3$, aryl. By carefully

selecting the coordinating ligands around the metal centre, it was possible to modulate the activity

of the catalyst achieving both rapid initiation and propagation rates over a wide range of

monomers, thus enabling living polymerisations. The most used "Schrock initiators" were the

commercially available molybdenum-based catalysts **4** and **5** (Figure 1.4), which afforded

homopolymers and block copolymers with low dispersity[24]. However, the high oxophilicity of the

Mo and W metal centre made these catalysts unstable towards many polar functional groups (e.g.,

aldehydes and alcohols), as well as air and moisture. Therefore, extremely dry conditions were

required for storage and for conducting the polymerisation[6].
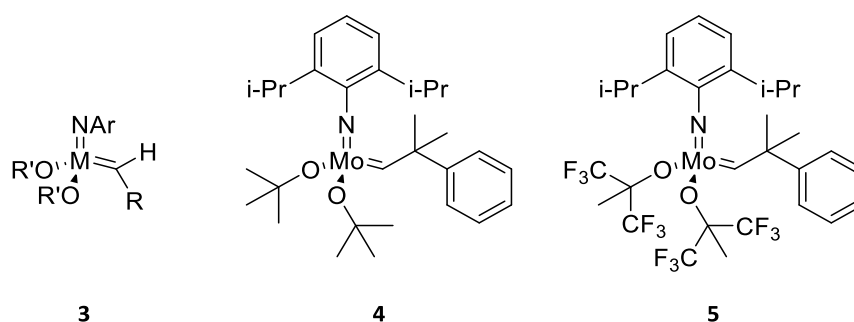
Fig. 1.4. The molybdenum and tungsten Schrock catalysts. Complex **3** shows the general formula.

In 1992, Grubbs *et al.*, synthesised the first well-defined ruthenium alkylidene catalyst which was easily obtained by the reaction of $RuCl_2(PPh_3)_3$ or $RuCl_2(PPh_3)_4$ with 2,2-diphenylcyclopropene affording the metal carbene complex $RuCl_2(PPh_3)_2(CH=CH=CPh_2)$[25] (**6**, Figure 1.5). Although this catalyst showed tolerance towards many functional groups, it was not active to a wide range of olefins. Since then, many ruthenium analogous with improved activity have been obtained by the subsequent modification of ligands. The so called "first generation Grubbs catalyst" ($RuCl_2(PCy_3)_2=CHPh$) (**7** (**G1**), Figure 1.5), first reported in 1996, was the most important ruthenium catalyst to be developed[26]. Catalyst **7** was more stable (reactions could be carried out in protic solvents and without exclusion of oxygen and moisture) but was considerably less active than the Schrock's molybdenum initiators[27]. By replacing the phosphine ligand in **7** with an *N*-heterocyclic carbene (NHC) ligand, it was possible to obtain a catalyst with a higher activity comparable to that of the Schrock-type initiators. This was the "second generation Grubbs catalyst" with formula (H_2IMes)-$(PCy_3(Cl_2)_2Ru=CHPh$ (**8** (**G2**), Figure 1.5), where H_2IMes = *N,N*-bis(mesityl)-4,5-dihydroimidazol-2-ylidene. Despite the higher activity and higher functional group tolerance of complex **8**, this initiator formed polymers with uncontrolled molecular weights and broad dispersities[28]. This is often the consequence of high propagation rates (K_p) relative to slow propagation rates (K_i), as well as competing chain transfer and "back-biting" reactions. Nevertheless, both first- and second-generation Grubbs initiators are still commercially available and are still being used for the preparation of polymers.
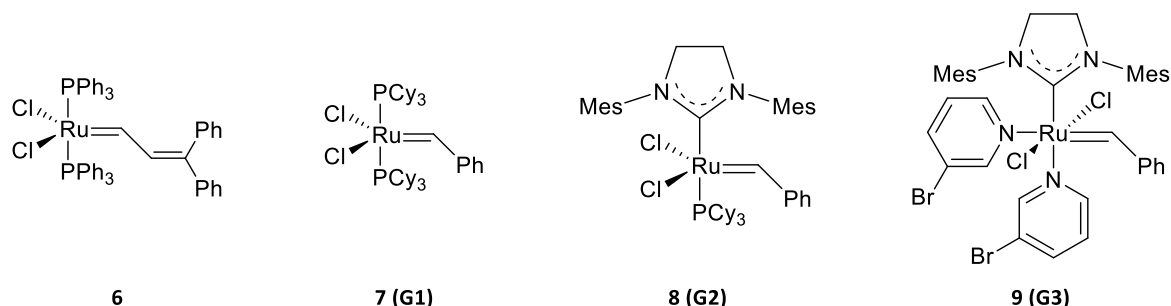
Fig. 1.5. Ruthenium-based catalysts (**7**, **8** and **9** are 1st, 2nd and 3rd generation Grubbs catalyst respectively).

In 2002, Grubbs and co-workers developed another ruthenium-based initiator, the so called "third generation Grubbs catalyst" **9** (**G3**) [(H$_2$IMes)(3-Br-py)$_2$-(Cl)$_2$Ru=CHPh] (Figure 1.5), which was obtained by the reaction of **8** with an excess of 3-bromopyridine (the reaction occurs via exchange of the phosphine ligand)[29]. This is a very simple reaction that can be completed within minutes and can form **9** with high yields (Scheme 1.1).
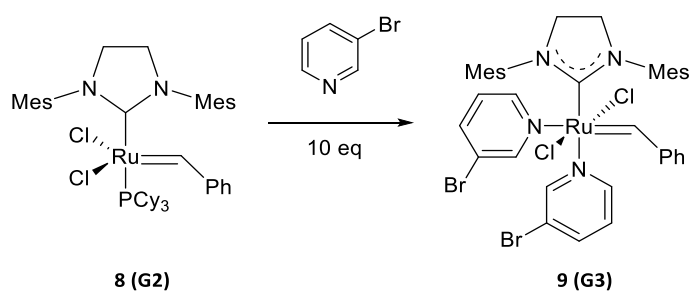
Scheme 1.1. Synthesis of the third generation Grubbs catalyst, **9**.

Grubbs third generation catalyst provides fast initiation (six order of magnitude higher than **8**) as a result of the labile nature of the pyridine ligand, high propagation rates and extreme functional group tolerance. It can afford homopolymers and copolymers with controlled architecture and very low dispersity. Furthermore, it is stable to air and moisture making it easier to handle.

Since then, many other ruthenium based catalyst have been developed, including water soluble catalysts bearing charged phosphines and NHC ligands, as well as poly(ethyleneglycol)-containing ligands [30,31,32] (respectively **10**, **11** and **12**, Figure 1.6).

Thanks to its commercial availability, relative cheapness and stability, Grubbs third generation catalyst is nowadays the most widely used initiator for ROMP.

10   **11**   **12**
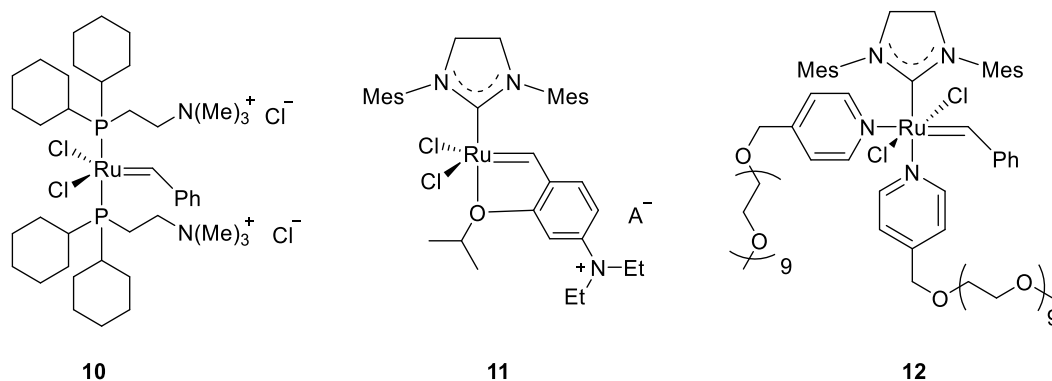
Fig. 1.6. Examples of water-soluble catalysts consisting of positively charged amines or PEG-containing ligands.

1.2.2.2.   The monomers

The most common monomers polymerised via ROMP are highly strained-bicyclic olefins particularly norbornene (NB) and its derivatives (e.g., norbornadienes and 7-oxonorbornenes). NB possess a ring strain energy of 27.2 kcal mol^{-1} and therefore can be polymerised with fast rates[33]. However, many other cyclic olefins, such as cyclobutenes[34], cyclooctenes[35] and cyclooctadienes[36] have been shown to polymerise under the ROMP conditions. Whereas, five-, six, and seven-membered ring olefins possess low ring strain and therefore do not readily polymerise[37,38,39] (Figure 1.7).

norbornene   norbornadiene   7-oxonorbronene   cyclobutene

cyclopentene   cyclohexene   cycloheptene   cyclooctene   cyclooctadiene
COE   COD
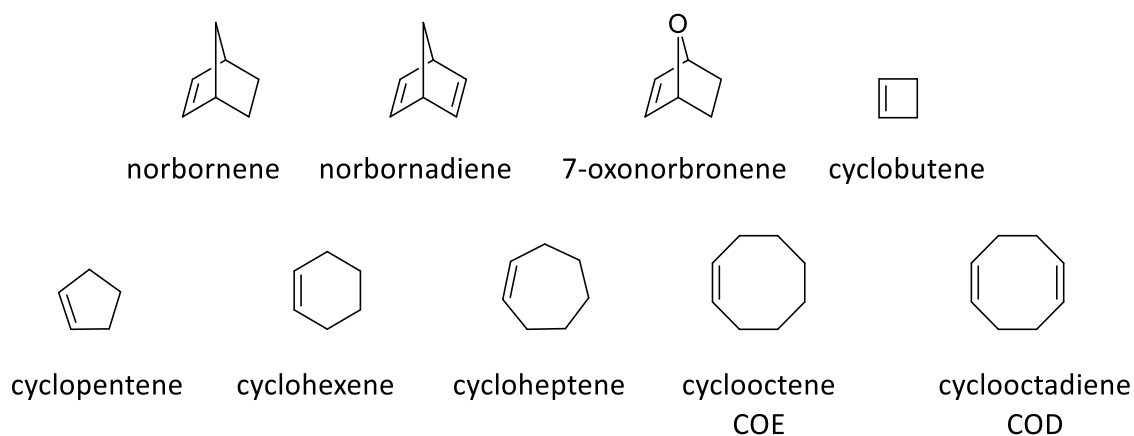
Fig. 1.7. Representative examples of high and low ring strain monomers tested for ROMP.

The high usage of NB monomers derives from their simplicity in preparation by a [4 + 2] Diels-Alder cycloaddition of cyclopentadiene (or furan) and an electron-deficient olefin.

Furthermore, a wide variety of NB compounds are commercially available. Typical NB monomers are constructed so they possess a polymerisable group and an anchor group which is a functional group that connects a functional unit to the cyclic olefin through a spacer or linker. In this way, many complex bioactive, electroactive[40] or liquid-crystalline[34] molecules have been incorporated within a polymeric material using esters, amides, acetals and many more functional groups. The presence of the anchor group alters the reactivity of the monomer and therefore the rates of the polymerisation, as well as affecting the formation of back-biting and chain transfer reactions. Furthermore, it is well known that *exo* isomers are more reactive then the *endo* ones where steric and electronic effects play a more important role[41,42]. It is important therefore, to carefully consider the nature of the functional group as well as the functional unit in order to obtain a successful polymerisation.

1.2.2.3.   Polymer architecture

ROMP is a type of living polymerisation which allows for the preparation of homo- and co- polymers with precise structure as well as controlled length and composition. Typical copolymer architectures include statistical (or random), block, alternating, graft and gradient copolymers, which are obtained by reacting a mixture of monomers together.

Statistical copolymers are obtained by the simultaneous combination of two or more monomers. The composition of the monomers in the polymer backbone is determined by the reactivity of each monomer and its active species. For instance, cyclobutene derivatives are more reactive then norbornene and its 5-substituted derivatives, which in turn react faster than cyclopentene and larger rings. Temperature and solvent can also be additional factors to consider while preparing statistical copolymers. *Alternating* copolymers consist of two species of monomeric units that are distributed in an alternating sequence with an −ABABAB- arrangement. They are typically formed via step polymerisation and occur due to each of the monomers adding preferentially to the other. In this way the homopolymerisation becomes absent from the reaction.

Block copolymers contain long sections of each co-monomer along the polymer backbone (-AB- or –ABA- arrangement). They are prepared by sequential addition of monomers and thanks to the living behaviour of ROMP, the polymerisation proceeds until all the monomer has been consumed, and therefore an additional different monomer can be added leading to continued polymerisation. Usually, the order in which the monomers are polymerised is not important for the realisation of diblock- or multiblock- copolymers with narrow molecular weight distribution. *Graft* copolymers are polymers with branched molecular structure consisting of a linear backbone and polymeric side chains (the grafts) attached to it which are of different chemical composition than the backbone (Figure 1.8).

Among the graft copolymers, there exists a widely used class of polymers nowadays, referred to as *molecular polymer brushes* (MPBs)[43]. They are densely grafted copolymers, where each repeating unit of the backbone possesses at least one side chain. There are three different grafting approaches that can be used for preparing MPBs with distinct properties, and they can be used alone or as a combination of approaches. These methods are called *grafting-from*, *grafting-to* and *grafting-through*.

a) Homopolymer

d) Block copolymer

b) Alternating copolymer

e) Graft copolymer

c) Statistical (random) copolymer
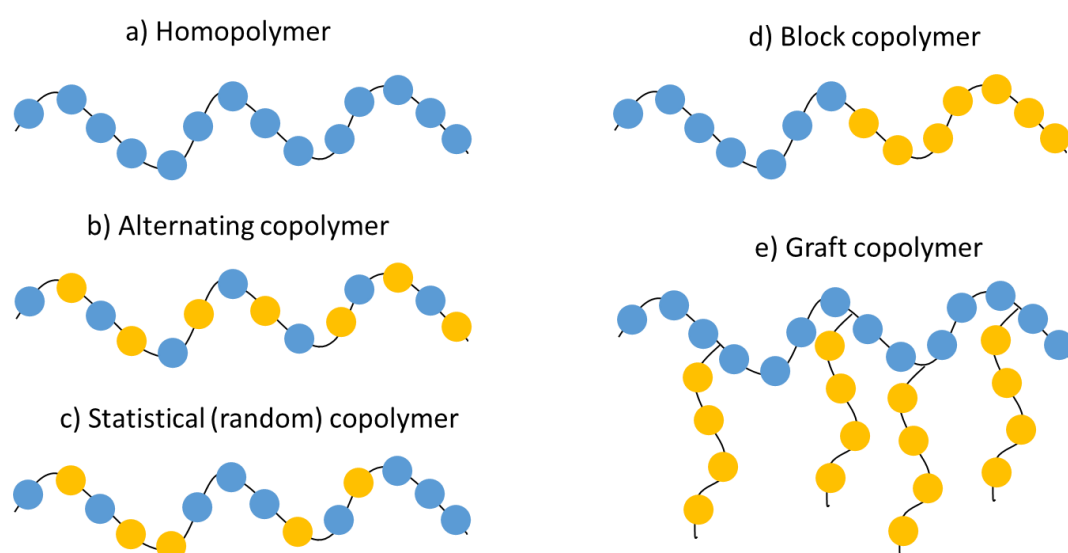
Fig. 1.8. Common polymer morphologies obtained by ROMP. The blue and the yellow circles refer to two different monomeric units.

In the *grafting-from* method the side chains grow from a backbone bearing a series of initiation sites (macroinitiator), while in the *grafting-to* method the side chains and the backbone contain functional groups allowing coupling reactions to happen between the two parts. In the *grafting-through* method a previously synthesised side chain, the macromonomer, is polymerised through its terminal group. It provides control over the grafting density and both length of the backbone and side chains. Therefore, it is the most frequently used in several fields including nanofabrication[44], nanomedicine[45] and functional materials[46]. It allows facile preparation of amphiphilic block-type polymer brushes as well as facile incorporation of more than one functional unit (or moiety).

1.2.2.4.   Mechanism of ROMP and thermodynamics

ROMP is a chain growth polymerisation process where a cyclic olefin is converted into an unsaturated polymer. The mechanism is similar to any olefin metathesis reaction, a carbon-carbon exchange process mediated by an alkylidene or carbene catalyst[47].

The general mechanism of ROMP[18,48] (Scheme 1.2) involves an initiation step where a cyclic olefin coordinates to the transition metal alkylidene complex. Subsequently, a metallacyclobutane intermediate is formed via the [2 + 2] cycloaddition between the two reagents. This is then followed by the [2 + 2] cycloreversion reaction which affords two new double bonds, including the new metal alkylidene. During the propagation step, the metal alkylidene formed allows for further reaction with cyclic olefins which combine to form the ROMP polymer chain. Thanks to the living behaviour, this step continues until all the monomer is consumed and the equilibrium is reached. The third step is the termination of the propagating species via addition of a specialised reagent which is used to remove and deactivate the transition metal complex from the end of the polymer chain, as well as to introduce a specific functional group in place of the metal.

metal   cyclic
alkylidene   olefin   metallacyclobutane
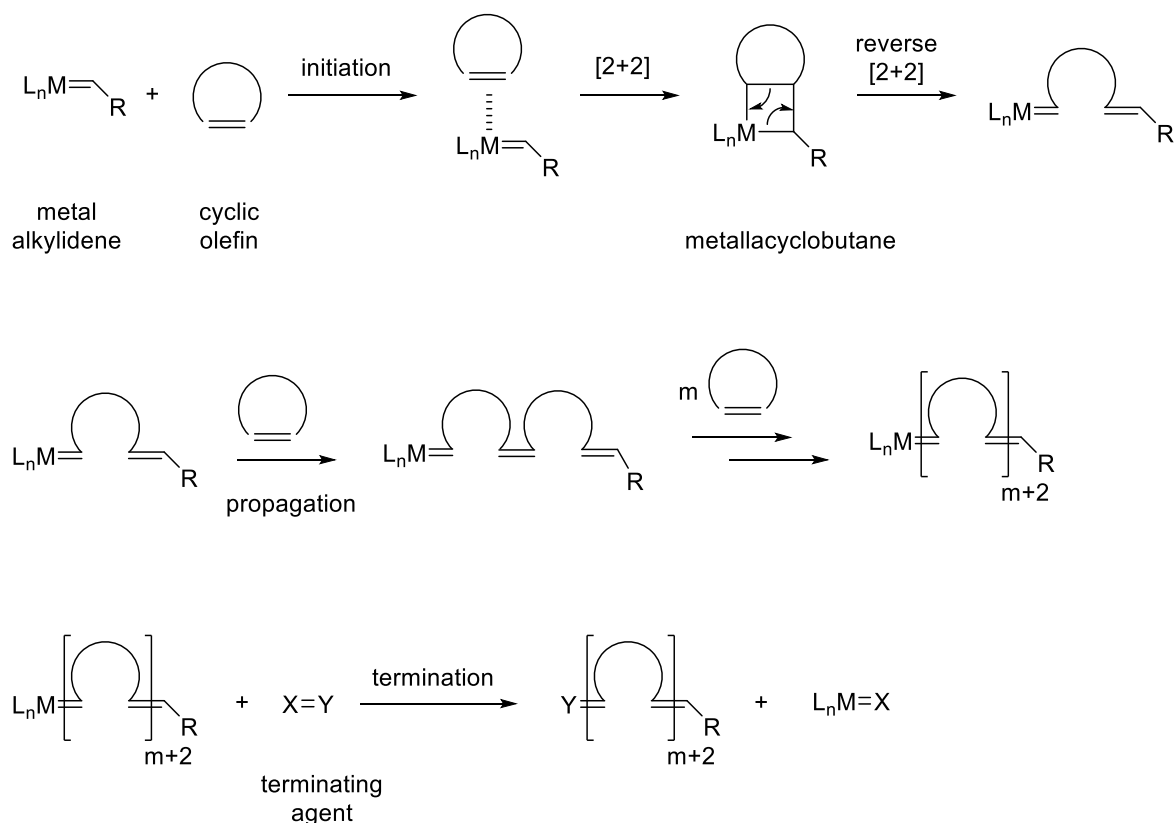
Scheme 1.2. General ROMP mechanism

Typically, the terminating agents are ethyl vinyl ether and benzaldehyde which respectively form a methylidene and a benzylidene end-capped polymer[6]. Ethyl vinyl ether presents an advantage over benzaldehyde; thanks to its volatility, it can easily be removed from the isolated polymer. However, the use of benzaldehyde can allow for end-group analysis via ^{1}H NMR, as it increases the intensity of the aromatic peak region for the phenyl group introduced during the initiation step at the other end of the polymer chain.

ROMP reactions are reversible, they exist in an equilibrium that can be controlled by the type of monomer used. The employment of strained cyclic olefins is crucial in order to shift the equilibrium from monomer to polymer, thus the release of the ring strain is the driving force of the reaction. In a study carried by Hyatt *et al.*[42], it was found that the rate determining step for the polymerisation of functionalised norbornenyl monomers initiated by the Grubbs third generation catalyst, was the formation of the metallacyclobutane ring, which was also found to be the highest energy transition state by DFT (density functional theory) calculations. However, the equilibrium of

13

the polymerisation can be affected by other conditions, such as temperature and monomer concentration. In fact, an increase in temperature causes an increase in the polymerisation rate due to high propagation and initiation constant rates (k_i and k_p). A prolonged reaction time can lead to inter- and intra-molecular chain-transfer reactions ("backbiting")[49]. These secondary reactions involve the metathesis of a double bond along the polymer backbone with an active metal alkylidene. This could be either a short growing chain consisting of an active terminus or an unreacted molecule of initiator itself. The result is the formation of different polymer chains, consisting of different polymerisation degree, that can grow independently from one another. In addition, as shown in Scheme 1.3, intermolecular reaction can lead to chain termination forming shorter polymer chains that cannot propagate even with further addition of monomers. Furthermore, backbiting reactions can lead to the formation of cyclic oligomeric species via intramolecular reaction of the active terminus of a polymer chain with another unsaturation along the polymer backbone.
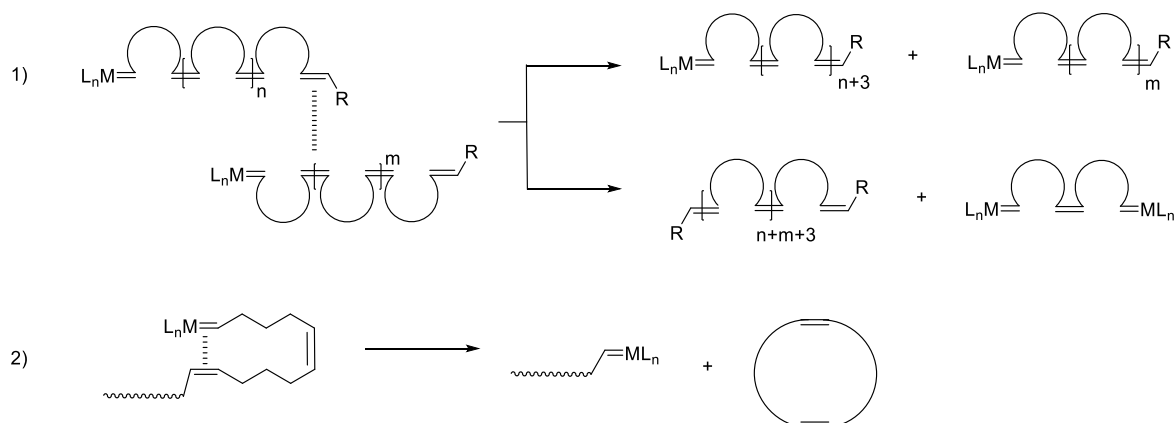
Scheme 1.3. Examples of intermolecular chain-transfer reaction (1) and intramolecular chain-transfer reaction or backbiting (2) with formation of multiple polymer chains in one case, and cyclic oligomeric species in the other case.

The overall effect is the broadening of the molecular weight distribution (Đ > 2.0) as well as the increase of the M_n. The M_n is not directly proportional to the monomer conversion and hence the polymerisation is not controlled. Therefore, these reactions prevent the polymerisation from

proceeding in a living fashion. Typically, the most favourable conditions for ROMP involve the use of high monomer concentrations, low temperature and short reaction times.

1.3.   Biologically related ROMP polymers

Ring opening metathesis polymerisation (ROMP) has gained interest as a versatile method for the preparation of biologically active polymers. Because of the control in tailoring their bulk physical properties, ROMP polymers have been widely used to prepare targeted delivery systems of drugs[50] or nucleic acids[51], antimicrobial polymers[52], carbohydrates[53] and peptide[54] containing polymers as well as synthetic mimics of DNA and RNA[55,56] in the form of delivery vehicles.

ROMP has gained interest due to its living behaviour which allows for the preparation of well-defined materials with precise block architectures, chain lengths, narrow molecular weight distributions and composition of pendant and end group functionalities. The ROMP process has the advantage of high functional group tolerance (e.g., hydroxyl groups, amides, and sulphate groups), and can therefore be applied with a wide range of functional monomers. They can form polymers with complex structures consisting of multiple recognition elements that can interact with multiple target receptors (i.e. oligomeric proteins or cell surfaces)[48]. Ruthenium catalysts **7**, **8** and **9** have been used in most applications of ROMP to bioactive polymer synthesis as they possess high tolerance towards air, moisture and functional groups. Fundamental to many bioactive polymer applications is their macromolecular architecture. Given that the biological environment is found to be in aqueous media, most of the polymers are constructed so that they are water soluble. The excellent compatibility of the ROMP polymers with water makes this polymerisation popular for many biological purposes, such as the targeted delivery of diagnostic and therapeutic agents.

The following sections will highlight advances in the synthesis of ROMP polymers for biomedical applications. In particular, we will discuss the synthetic approach, the importance of

architecture and linkages, and we will highlight the several experimental reports from literature with a major focus on ROMP for drug delivery and antimicrobial polymers.

1.3.1. Stimuli responsive drug curriers

The identification of new monomers is important in order to produce bioactive polymers with appropriate function. Most of methodologies use oxanorbornene (ONB) or norbornene (NB) monomers which generate polymers that cannot degrade (therefore cannot be metabolised) in physiological applications. Hence, appending the cargo to the polymer backbone via a cleavable linker partially solves the problem. Most of the biologically active ROMP polymers utilise linkers that respond to UV light or to different pH ranges allowing the drug molecule to be released and to interact with the desired biological target[48,57]. Shunmugam *et al.*, for instance, designed polymer carriers containing doxorubicin (DOX), a chemotherapeutic drug, via an hydrazone link[58] that can break and therefore release DOX at the mildly acidic pH of 5.5 − 6 (Figure 1.9, 1). Similarly, Sutthasupa and co-worker[59] synthesised molecular brushes bearing indomethacin conjugated to the poly(norbornene) backbone by an ester group. They demonstrated that the drug could be slowly released, for a period of up to 14 days, under acidic pH (5.7) when incubated at 37 °C. Johnson *et al.*[60] linked doxorubicin and camptothecin (CT) to a norbornene bivalent-brush polymer via click reaction. Drug release, in this case, was stimulated by exposure of the material to UV light. In each case, after the release of the drug, the polymer backbone remained intact. However, many research groups already demonstrated its non-cytotoxicity[58,59].
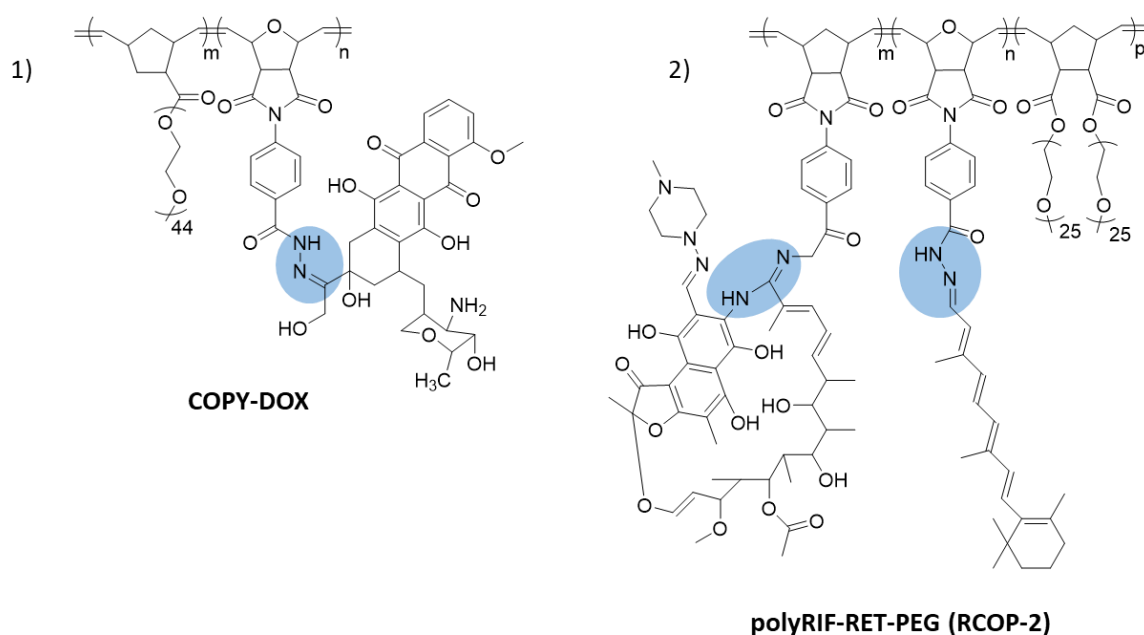
Fig. 1.9. Copolymers synthesised by Shunmugam *et al*. containing a pH-responsive linkage (hydrazone bond) highlighted in blue. 1) It's a block copolymer containing the chemotherapeutic doxorubicin (DOX); 2) It's a triblock copolymer containing a combination of the tuberculosis drug Rifampicin (RIF) and retinal (RET).

Although most of these applications introduced the drug into the polymer carrier via a covalent link, there are also few examples in which physical entrapment of the cargo was used. This will be discussed in the following section.

1.3.1.1. pH-responsive drug carriers

pH-Responsive drug carriers can be used to release the drug at specific targets including tumours. There are pH gradients that exist between the normal blood stream (pH 7.4) and the tumour extracellular environment (pH ~ 6.0 – 7.0)[61] which drops to a lower pH of 5.5 – 6.0 in endosomes and 4.5 – 5.0 in lysosomes[62]. Therefore, drug carriers that incorporate degradable linkage are used. The approach is to covalently link the drug into the polymer backbone by using hydrolytically labile bonds, such as ester[63], imine[64,65], acetal[66,67] oxime or hydrazone[68] bonds. Shunmugam *et al*.[58] developed a block copolymer (COPY-DOX) (1, Figure 1.9) consisting of hydrazone-tethered DOX and PEG chains in the norbornene backbone. COPY-DOX was prepared by adding a known amount of

DOX-containing norbornene and PEG-containing norbornene monomers polymerised by **G2** catalyst which afforded a block copolymer with a low dispersity index (Đ = 1.04). In a water solution, this copolymer formed micelles which were spherical in shape as confirmed by TEM and AFM. Shunmugam *et al*. demonstrated that such micelles were stable in physiological conditions while DOX release was fast if endo/lysosomes with a pH of 5.5 was used. In another study, Shunmugam *et al*.[69] prepared a polyRIF-RET-PEG copolymer (2, Figure 1.9) in which the tuberculosis drug Rifampicin (RIF) was conjugated along with retinal (RET) (which is known to reduce Rifampicin side effects) by an acylhydrazine linker. In a similar manner to the previous DOX polymer, polyRIF-RET-PEG was obtained by using the **G2** catalyst which afforded a polymer with Đ = 1.08. The amount of RET and RIF within the polymer was about 18 % and 13 % respectively. Thanks to the presence of PEG side chains, the polymer self-assembled in an aqueous environment forming spherical micelles and RIF was released under acidic conditions (pH 4.7 – 5.5). A different approach was used by Johnson's group[70], which developed a brush-arm star polymer (BASPs) bearing an acetal-based cross-linker and a doxorubicin (DOX)-branch-PEG macromonomer (each repeating unit simultaneously carries a PEG chain and DOX). Their strategy was to use a "brush-first" ROMP method in which the DOX-PEG macromonomer was first polymerised by the **G3** catalyst and then cross-linked with a bis-norbornene derivative which formed the core of DOX-BASP nanoparticles. The degradability under acidic conditions in this case was introduced by the addition of an acetal group within the cross-linker while DOX was linked to the branched polymer backbone via a click reaction (11 % of drug loading). Johnson *et al*. showed that while the BASP nanoparticles can be degraded under acidic conditions (pH 4.0), DOX can be released in 24 hours under a neutral pH of 7.4 after 24 hours. Placlitaxel (PTXL) is another anticancer drug (antineoplastic agent) commonly used in drug delivery. Cheng and co-workers[71], for instance, designed a diblock brush polymer containing a PEG-based norbornene macromonomer and a PTXL-based monomer. The two monomers were polymerised together in a 1:1 ratio by using the **G3** catalyst, which afforded a block copolymer with a narrow molecular weight distribution (Đ = 1.06). In this case, the conjugation of

PTXL was achieved using a cycloacetal-based linkage which exhibited limited acid-sensitivity (1, Figure 1.10). After the formation of unimolecular micelles in aqueous solution, release of PTXL was carried out at pH 5.5 showing that after 24 hours, only 28 % of the drug was released, while 90 % of free drug was reached after 10 days. Héroguez and co-workers[72] developed a new drug delivery system comprising of a histone deacetylase (HDAC) inhibitor, CI-994 (Tacedinaline), which revealed antitumor effects in cancer cells in culture (2, Figure 1.10). The latter was conjugated to a norbornene-based monomer through azide-alkyne click chemistry. In order to form nanoparticles with precise structure and size, a norbornene-polyethylene oxide (PEO) macromonomer was introduce. Co-polymerisation of the CI-994-norbornene monomer and the norbornene-PEO macromonomer was carried out using the **G1** catalyst. Differing from the previous cited examples, the release of CI-994 was tested directly by exposure of the NPs to acidic endosomes/lysosomes which were able to enter these vesicles by endocytosis. Through a bioluminescence resonance energy transfer (BRET) assay, they demonstrated that the NPs could release the drug over time, overcoming the limited activity that CI-994 presents if introduced on its own. In a follow-up study, Héroguez and co-workers[50] designed new NPs bearing another two types of HDAC inhibitors: Vorinosat (SAHA) and Trichostatin (NODH). With the same type of chemistry, they demonstrated the internalisation of their NPs into the endo/lysosomes where the acidic environment trigged the release of the inhibitors. A camptothecin (CT) brush poly(L-glutamic acid) (PGA) conjugate was prepared by Cheng and co-workers[73]. The brush polymer was obtained by attaching PGA to a poly-norbornene backbone leading to the formation of a water-soluble rod-like morphology. CT was subsequently introduced into the polymer structure by creating an ester group between the PGA chain and CT. The resulting polymer (CT-PGA) was found to have a very low dispersity index (Đ = 1.16) and a high drug loading of 27 wt%. Drug release was obtained in vitro at acidic pH (5.5) showing that the brush polymer possessed a half-life of 24 days.

Thus, ROMP polymers containing pH responsive linkages have shown to possess promising characteristic, making these systems highly suitable vehicles for drug delivery applications.

polyPTXL-PEG   **polyNB-PEG-CI994**
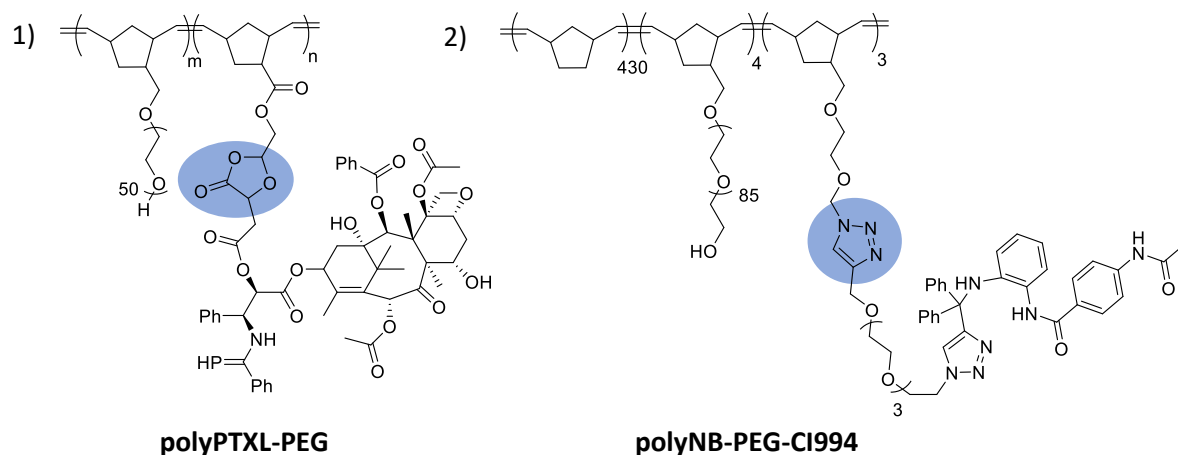
Fig. 1.10. pH responsive ROMP polymers. 1) Copolymer containing PTXL synthesised by Cheng *et al.*[71] where the drug is covalently linked to the polymer backbone via a cyclic acetal; 2) Triblock copolymer containing CI-994 synthesised by Héroguez *et al.*[72] where the drug is linked to the polymer backbone via click chemistry.

1.3.1.2.   UV light-responsive drug carriers

Irradiation of nanocarriers with UV light can be another effective strategy for the controlled release of chemotherapeutic drugs[74]. Many photoresponsive systems have been designed for their non-invasiveness and the possibility of spatiotemporal control. Absorption of light in these systems usually involves the functionalisation of drugs with photolytic functional groups such as the azobenzene group[75] and its derivatives, which undergo cis/trans isomerisation depending on the type of irradiation used. However, the spiropyran-merocyanine group[76] and o-nitrobenzyl derivatives have been the most commonly used[77,78,79,80].

Thanks to its 100 % grafting density, ROMP has been efficiently used to develop UV-responsive nanocarriers with high drug loading content. Using the graft-through ROMP method, Grubbs *et al.*[81] were able to develop a novel bivalent-brush polymer system in which each repeating unit comprised of a hydrophilic PEG and a drug molecule, namely DOX and CT (Figure 1.11). Both drugs were first functionalised with an o-nitrobenzyl derivative and then attached to the polymer backbone via a "click" coupling reaction. With this approach, Grubbs *et al.* synthesised homopolymers pDOX and pCT containing 12.6 % of DOX and 8.5 % of CT respectively. The **G3** catalyst was used to afford pDOX and pCT with low dispersity when the degree of polymerisation

(DPn) was kept below 50. Thanks to the use of a photocleavable linker, DOX and CT were released in response to 365 nm UV irradiation. After 10 minutes of irradiation, 50 % and 64 % of free DOX and CT were detected, respectively. Block copolymer pDOX50-pCT50 was also synthesised using an equimolar mixture of DOX and CT macromonomers which afforded a polymer that exhibited narrow and monomodal molecular weight distribution. Irradiation with UV light induced simultaneous release of both drugs after 10 minutes of exposure. In a follow-up study, Grubbs and co workers[82] prepared a bivalent-brush polymer containing DOX via a graft-to method. The macromonomer containing a PEG chain on one side, and an azide functionality on the other, was polymerised using **G3** first, and then reacted with a photocleavable DOX-alkyne derivative through a copper-catalysed azide-alkyne coupling. The photolytic nitrobenzyloxycarbonyl (NBOC) linker provided a polymer prodrug that released 70 % of free DOX when irradiated with UV light (365 nm) for a period of 10 minutes. Following Grubbs' work, Johnson and co-workers[83] designed BASP polymers through the use of the "brush-first" ROMP method. Two different bivalent macromonomers containing both PEG and the drug, namely DOX and CT, were polymerised together with a novel cross-linker containing a diester derivative of cisplatin (Pt-XL) using the **G3** catalyst, which resulted in a three-drug-loaded particle. Each of the three drugs were linked to the polymer backbone through different linkers which responded to distinct triggers. In fact, CT was released in response to cell culture media, cisplatin upon intracellular reduction (from Pt(IV) to Pt(II)), and DOX via irradiation with long-wavelength UV light, affording the first example of a multi-responsive drug carrier.
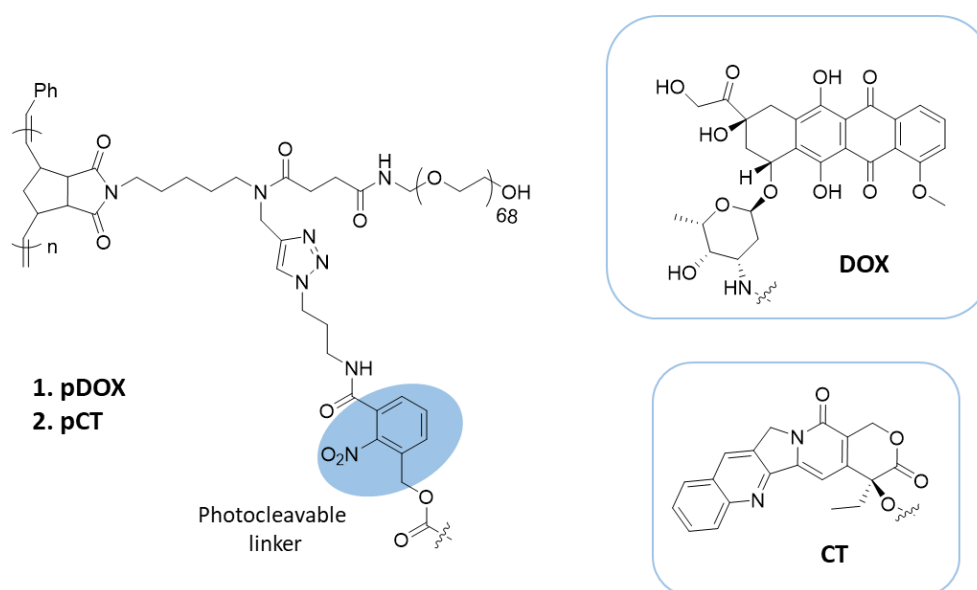
Fig. 1.11. Bivalent-brush polymer system prepared by Grubbs *et al*. comprising of a hydrophilic PEG and a drug molecule, namely DOX (1) and CT (2). O-nitrobenzyl, highlighted in blue, is used as the photocleavable linker. A similar polymer system was used by Johnson *et al*. in order to design brush-arm star polymers.

Although these UV-light responsive systems have shown effective drug release response, they suffer from several drawbacks such as low tissue penetration depth (~ 10 mm) of UV light and phototoxicity. This could be resolved by using drug nanoparticles that can undergo photolysis in response to NIR (near infrared) light which has shown better therapeutic performance and deeper tissue penetration[74,84].

1.3.1.3.   Physical entrapment

Although ROMP has been widely used for the preparation of drug delivery vehicles where the drugs have been covalently linked to the self-assembling material, there are few examples in literature where non-covalent interactions have been applied. The use of polymers as encapsulating carriers may be advantageous, as long as the micelles are sufficiently stable, due to a more efficient drug release process.

Wu and co-workers[85] developed water-soluble random polynorbornenes PNB-SPx-co-P3y-co-A1z bearing a hydrophobic moiety, a hydrophilic tail and a functional spiropyran (SP) (1, Figure 1.12). The latter was chosen in this study for its reversible photochromic behaviour. In fact,

irradiation of the hydrophobic SP with 365 nm UV-light leads to its isomerisation into the hydrophilic form, merocyanine (MC). Once spherical micelles were obtained, encapsulation of Nile red (NR) as a model for drug delivery was carried out by direct injection into the micelle solution reaching a 1.31 % of loading. Disruption of micelles and subsequent drug release occurred upon irradiation with UV-light (365 nm) and 40 % of NR could be reloaded into the micelles after irradiation with 530 nm visible-light. Encapsulation of drug molecules could be also achieved by the employment of nanoparticle systems derived from a norbornene based homopolymer. Shunmugam et al.[86], indeed, developed a norbornene-derived thiobarbiturate homopolymer (NTBH) in which the norbornene polymer backbone served as a hydrophobic moiety, while the thiobarbiturate was attached covalently to each repeating unit, serving as a hydrophilic head. Shunmugam et al. demonstrated that NTBH can change the molecular orientation according to the polarity of the solvent utilised. Self-assembly of this system in water solution formed bilayer vesicles that could encapsulate both hydrophobic and hydrophilic molecules such as NR and doxorubicin in its salt form (DOXY) respectively. NR release was studied both in lipophilic (octanol) and acidic environments (pH 3 – 6) while DOX release was obtained in octanol by the dialysis method.
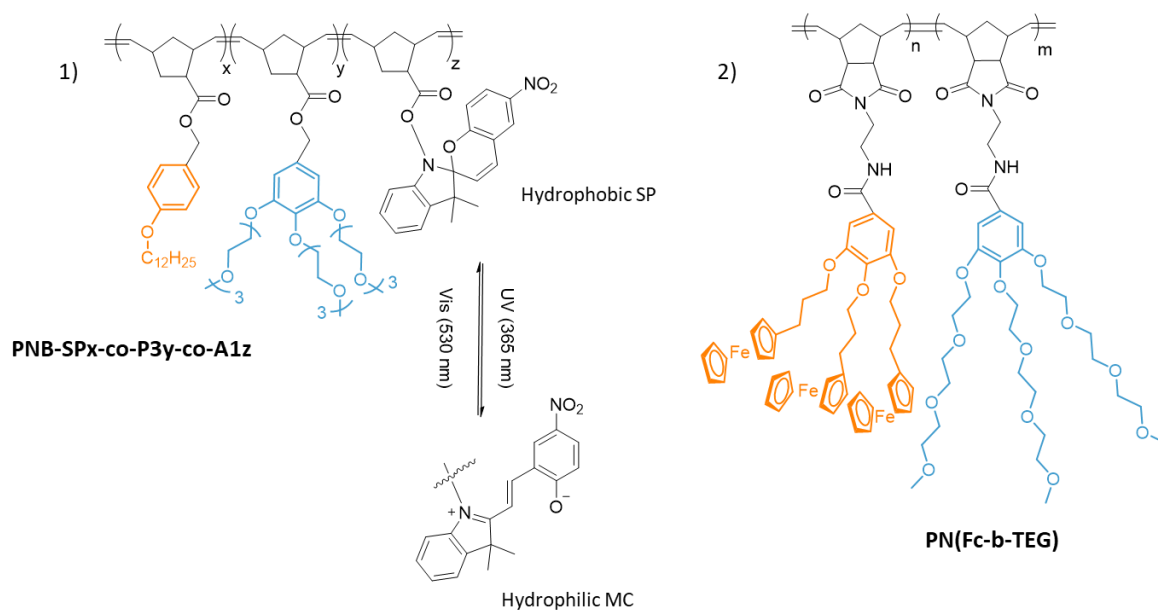
Fig. 1.12. ROMP polymers with amphiphilic properties used to encapsulate drug molecules. 1) Triblock copolymer synthesised by Wu et al. containing functional SP and used for the encapsulation of NR as drug model; 2) Block copolymer containing Fc and TEG prepared by Gu and co-workers. The polymer nanoparticles were used for the encapsulation of DOX.

Zhu and co-workers[87], prepared bottlebrush polyethylene glycol-polynorbornene-thiocresol block copolymers (PEG-PNB-TC) with amphiphilic properties. The polymeric micelles obtained by self-assembly of the polymer in water, were capable of loading 5 % of PTXL with an encapsulation efficacy of 80 % and furthermore, they were found to be stable for a period of up to 28 days if kept at 4 °C. PTXL release from PEG-PNB-TC micelles was studied *in vitro* using the dialysis method under the "sink condition" which showed that 70 % of the drug can be released in 12 hours. In addition, a synergistic effect between PTXL and curcumin (CUR) (a natural chemotherapy drug sensitizer added to improve the anticancer activity of PTXL) was obtained when the two drugs were co-loaded into the polymeric micelles at a PTXL/CUR ratio of 1:20, demonstrating the versatility of the encapsulation method for use in combination drug therapy. Gu and co-workers[88,89] designed amphiphilic copolymers containing the hydrophobic ferrocene (Fc) and the dendronized triethylene glycol (TEG) as the hydrophilic component (2, Figure 1.12). Grubbs third-generation catalyst **G3** was used to afford a block copolymer PN(Fc-b-TEG)[89] with high polymerisation rate (~ 15 min), high monomer conversion (> 99 %), high yield and narrow distribution of molecular weights. Self-assembly in water solution afforded globular nanoscale core-shell micelles which have been used to encapsulate DOX via dialysis with 7.4 % of drug-loading. Knowing that many biological processes (i.e., cellular respiration and apoptosis) involve redox reactions, Gu and co-workers designed nanoparticles that can release encapsulated DOX by addition of an oxidant, which oxidises Fc into hydrophilic ferrocenium (Fcium). In particular, oxidation with $FeCl_3$ afforded 45 % of free DOX within 12 h and 64 % after 96 h. A different approach was used by Barnes *et al*.[90], where a water soluble diblock brush-arm star copolymer (DBASC) was prepared by a core-first/graft-from strategy. Firstly, a γ-cyclodextrin (γ-CD) based norbornene compound (γ-CD-NB_8) was prepared (core-first); secondly, this was reacted with NB-functionalised hexaethylene glycol (NB-HEG) via the graft-from method using **G3**; finally, the resulting homo-arm star polymer was extended by adding NB-PEG which produced the corresponding DBASC (CD-(HEG_m-PEG_n)$_8$) with high molar mass (~ 300 kDa) and low dispersity (Đ = 1.2) (Figure1.13). The latter was found to be crystalline and porous with a

hydrodynamic diameter of ~10 nm. In this case, encapsulation of DOX·HCl occurred within the large

hydrophobic cavity of γ-CD in CD-(HEG$_m$-PEG$_n$)$_8$, which ended up being an efficient delivery vehicle

of DOX·HCl, that slowly released the drug and killed MCF-7 breast cancer cells.
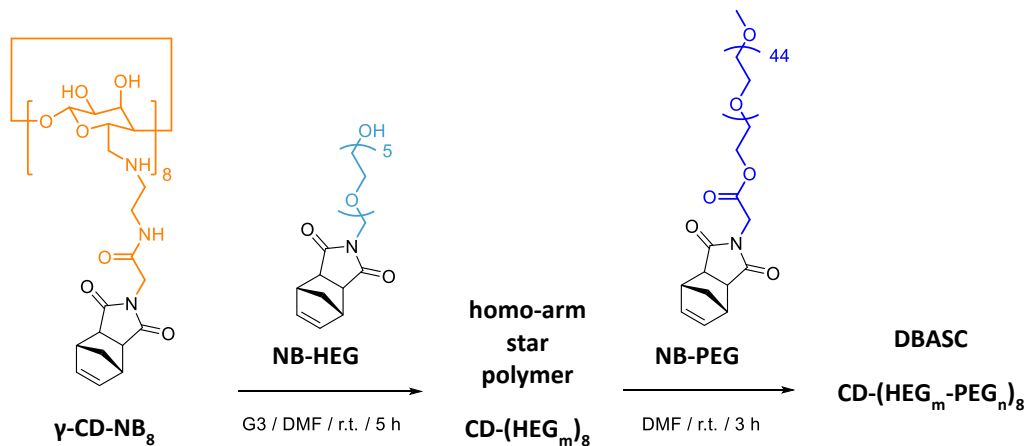
Fig. 1.13. Core-first/graft-from approach utilised by Barnes *et al*. for the preparation of CD-(HEG$_m$-PEG$_n$)$_8$.

1.3.2. Antimicrobial polymers

A series of antimicrobial ROMP polymers have been prepared as a promising class of therapeutics

capable of fighting microbial infections. In fact, compared to conventional antibiotics, they present

significantly less bacterial resistance, higher therapeutic stability and long term activity[91]. There are

two main classes of antimicrobial ROMP polymers: polymeric biocides and biocidal polymers[92].

Polymeric biocides are polymers containing a known antibiotic covalently attached to the

polymer backbone via side chains, whereas biocidal polymers are polymers with intrinsic

antimicrobial activity and are more common in the literature. The latter are usually constructed so

that they possess amphiphilic shape consisting of a hydrophobic domain and a cationic domain,

which are mainly quaternary ammonium[93], quaternary phosphonium[94], guanidinium[95] and tertiary

sulfonium[95] cations. The method of action of biocidal polymers is explained by the Shai-Matsuzaki-

Huang model[96], where the cationic domain of the antimicrobial polymer interacts with the bacterial

outer surface which is negatively charged. This leads to the intercalation of the hydrophobic portion

into the cell membrane and therefore alteration and disruption of its structure. Hereafter, some examples of ROMP polymers with antimicrobial activity are presented and discussed.

1.3.2.1.   Polymeric biocides

One of the first examples reported in the literature where a small molecule antibiotic was covalently attached to the ROMP polymer chain, leads to 1996. North *et al.*[97] synthesised penicillin functionalised poly(norbornene)s (PNB-PEN) (1, Figure 1.14) using the ruthenium initiator **G1**. In this case, the β-lactam antibiotic derivative was attached to the polymer backbone using an amide bond. Even though it was not possible to determine the dispersity of this polymer using GPC due to solubility issues, the author was able to provide evidence of the β-lactam ring being able to survive intact along the polymer backbone. In 1999, the Arimoto group[98] prepared multivalent ROMP polymers containing vancomycin (VAN) (2, Figure 1.14), a glycopeptide that binds via weak non-bonding interactions to the D-Ala-D-Ala residue of the bacterial peptidoglycan, thus interfering with its biosynthesis. Vancomycin was linked to the polymer backbone using a regioselective reductive amination, forming a secondary amine. Despite the high number of functionalities on the selected glycopeptide, polymers (PNB-VAN) were obtained (with 60 % yield) thanks to the high functional group tolerance of the Grubbs initiator, where in this case, **G1** was used. The multivalent ROMP polymer obtained was then tested against VREs (vancomycin resistant enterococci), showing a significant antimicrobial activity (8 to 60 fold) compared to vancomycin itself. Even though the authors claimed the polymer was obtained, no GPC data regarding molecular weight and molecular weight distribution were shown. Arimoto *et al.*[99] also tested the affinity of the vancomycin polymer to the bacteria cell wall by surface plasmon resonance (SPR). Two model peptides which mimic the peptidoglycan residue D-Ala-D-Ala (vancomycin susceptible) and D-Ala-D-Lac (vancomycin resistant) were used. The author claimed that the polymer possessed a higher binding affinity to the receptor compared to the monomer (norbornene containing drug) due to the "multi-valent or cluster effect", although these results did not entirely agree with the biological activity.

A different approach was used by Héroguez *et al.*[65], where pH-sensitive ROMP nanoparticles bearing gentamicin sulfate (GS) were prepared and tested against *Staphylococcus epidermidis* as the bacterial strain. Due to the presence of three amine groups, the antimicrobial GS was linked to a norbornenyl-poly(ethylene oxide) macromonomer (NB-PEO) via an imine bond (3, Figure 1.14). This was then polymerised in dispersion using the **G1** initiator, together with NB, which formed the hydrophobic core of the NPs, and NB-PEO macromonomer end-functionalised with a carboxylic group, which acted as an anchor group for the biomaterial surface. The polymerisation of these three monomers led to the precipitation of the polymer from the solvent and immediate formation of the NPs, where GS and the -COOH group were located on the external hydrophilic shell of the nanoparticles. DLS was used to determine the average diameter, which was found to be about 350 nm, and the dispersity which showed a narrow distribution (< 0.3). Drug release studies at acidic pH, followed by minimum inhibitory concentration (MIC_{50}) of the GS containing NPs, demonstrated that the MIC_{50} values decreased when lower pH was used (pH = 4 and 5). However, in the first 16 hours only 10 % of GS was released, and therefore MIC_{50} values were found to be higher compared to free GS (MIC_{50} > 3 µg/mL vs < 0.5 µg/mL). Using a similar technique, Héroguez *et al.*[100] developed vancomycin based ROMP nanoparticles, where this time the drug was linked to a NB-PEO macromonomer via an amide bond. Contrary to GS, vancomycin did not need to be released in order to provide antimicrobial activity. Once NPs of vancomycin were obtained, these were then grafted onto functionalised titanium surfaces (Ti90A16 V4 alloy), forming a new bactericidal biomaterial surface, where its activity was tested against gram positive *Staphylococcus aureus*. However, the MIC_{50} of the grafted NPs were found to be higher compared to the free vancomycin (MIC_{50} > 7 µg/mL vs < 0.8 µg/mL) and as the author claimed, this could be due to the high rigidity of the system which prevented it from reaching the active molecule and thus, decreased the kinetics of the antimicrobial activity.
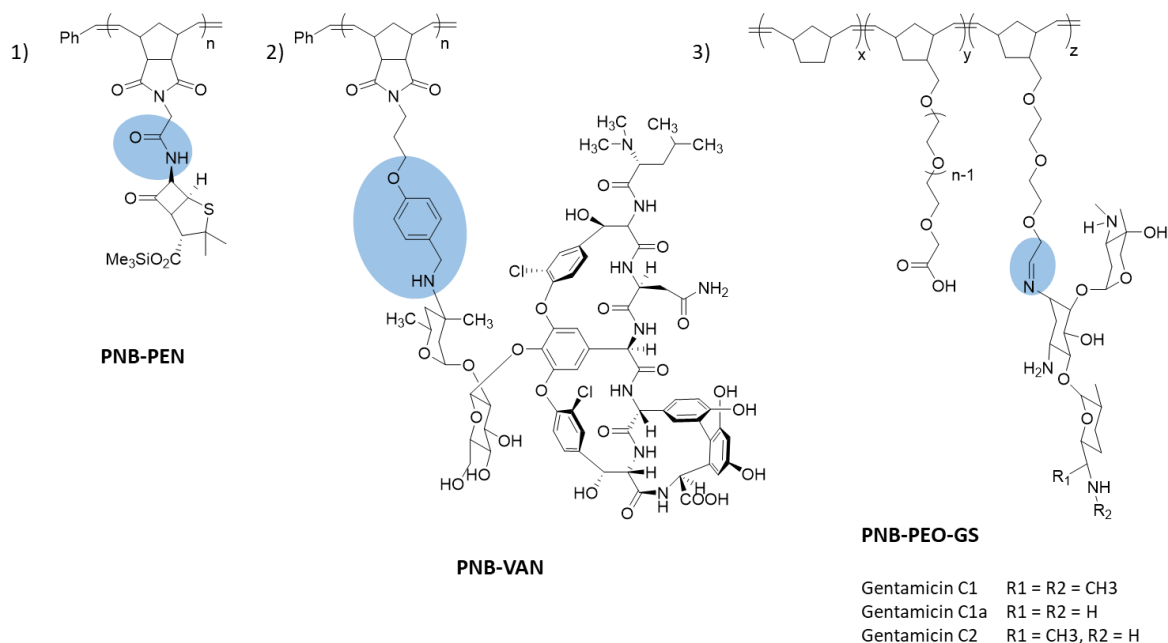
Fig. 1.14. Examples of antimicrobial molecules covalently attached to ROMP polymers. 1) ROMP polymer bearing penicillin derivative prepared by North *et al.*; 2) Vancomycin-based polynorbornene prepared by Arimoto *et al.*; 3) Triblock copolymer containing gentamicin sulphate as the antimicrobial drug: the polymer prepared by Héroguez *et al.* possess amphiphilic properties that allow for the realisation of NPs where GS is place on the hydrophilic shell.

1.3.2.2. Biocidal polymers

Amphiphilic cationic polymers (ACPs), also known as synthetic mimics of peptides, have been widely used in the development of antimicrobial materials as they have shown to mimic the structural properties of naturally occurring antimicrobial peptides (AMPs) with the advantage of being cheaper and at the same time more stable to physiological conditions.

One of the first sets of amphiphilic cationic ROMP polymers with antimicrobial properties was prepared by Coughlin *et al.*[101] in 2004. Four different monomers bearing Boc-protected amine and alkyl chains with different length in the norbornene bridge position were polymerised using a variant of **G2** and then deprotected in order to afford water soluble homo- and co-polymers with very low dispersity (Đ < 1.3) and different molecular weights ranging from oligomers to high polymers (M_n = 10 - 130 kDa) (1, Figure 1.15). The antimicrobial activity of the homopolymers against both Gram-positive (*B. subtilis*) and Gram-negative (*E. coli*) bacteria, as well as the hemolytic activity against human red blood cells, was found to increase with increasing hydrophobicity, with

poly3 being the most active against both *B. subtilis* and *E. coli* but the least selective towards the bacteria membrane (MIC_{50} = 25 µg/mL and HC_{50} < 1 µg/mL). Furthermore, it was reported that an increase in molecular weight did not significantly change the activity for any of the homopolymers prepared. In order to obtain better activity and selectivity, Coughlin *et al*. prepared random copolymers with different ratios of poly3 and poly2. The resulting copolymers were found to possess similar activity to that of poly3 (MIC_{50} = 40 µg/mL) while retaining the selectivity of poly2 (HC_{50} > 4000 µg/mL).

In another study, Coughlin and co-workers[93] developed amphiphilic polyONB bearing quaternary pyridinium, substituted with different alkyl chains (C_2 - C_{10} and phenylethyl) (2, Figure 1.15). The polymers were obtained using two different approaches: direct polymerisation of cationic monomers or post polymerisation modification of the pyridine functionalised polymer, using the **G3** initiator in both cases. However, due to the poor solubility of these polymers, molecular weight and dispersity could not be determined by GPC. Therefore, ^{1}H NMR end group analysis was used in the first instance, revealing a M_n of 3 kDa for each homopolymer, and MALDI-TOF was then used, revealing that a lower molecular weight was formed compared to the one determined theoretically (3 kDa vs 10 kDa respectively). This discrepancy was due to a slight deactivation of the **G3** catalyst by the pyridine ring. The resulting homopolymers were tested against *B. subtilis* and *E. coli* as representative bacteria. Even in this study, Coughlin *et al*. reported an increase in both antibacterial and hemolytic activity with an increase of the alkyl chain length (≥ C_6). Polymers with six or more carbons were found to be as potent as MSI-78 (a Magainin derivative), possessing an MIC_{50} < 12 µg/mL and a HC_{50} < 250 µg/mL. Arguably, in both mentioned studies, finding a balance between hydrophobicity and hydrophilicity is necessary in order to obtain the best activity and selectivity towards the bacterial cell. Furthermore, it has been demonstrated that an increase in hydrophobicity is important in order to enhance the binding of the polymer onto the lipid membrane and consequently lead to the cell death.
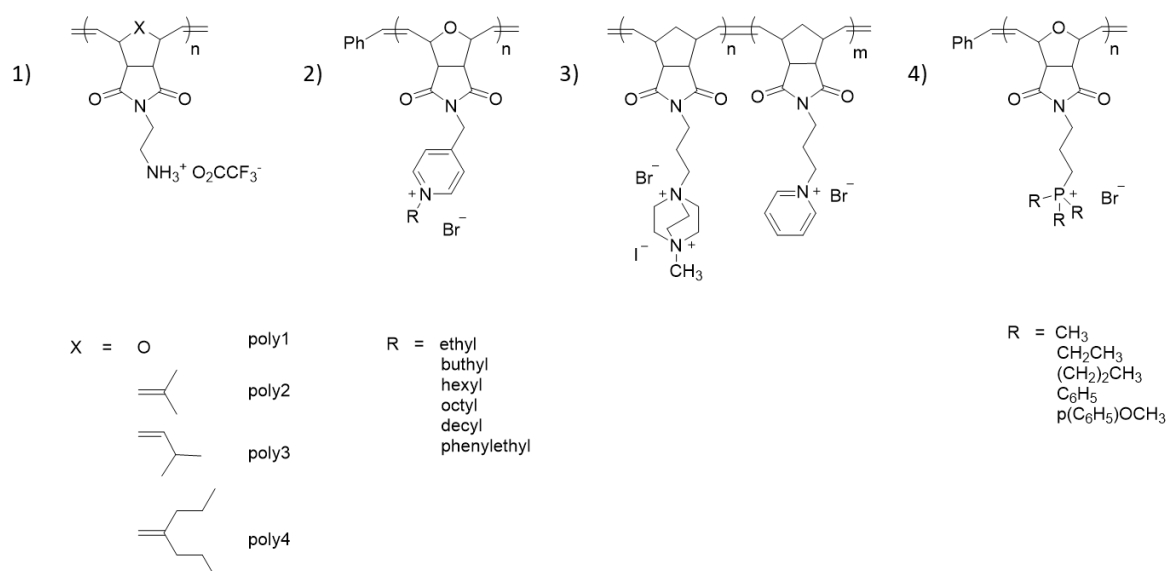
Fig. 1.15. Examples of amphiphilic cationic polymers (ACPs) with antimicrobial activity against Gram-positive and Gram-negative bacteria. 1) and 2) ACPs prepared by Coughlin *et al*. containing quaternary ammonium functionalities; 3) and 4) ACPs prepared by Eren *et al*. possessing DABCO and substituted phosphonium side chain respectively.

Similarly, Eren *et al*.[102] prepared polyONB bearing cationic species such as quaternary pyridinium and DABCO (1,4-diazabicyclo[2.2.2]octane) (3, Figure 1.15). Homopolymers and copolymers with theoretical molecular weights ranging from 3 kDa and 10 KDa were obtained using the **G3** initiator, although GPC results appeared to be higher in each case. According to the author, the presence of the double charge in DABCO containing polymers increased the antimicrobial activity against *S. aureus* by a factor of 16 compared to the mono-charged pyridinium containing homopolymers (MIC_{50}: 8 µg/mL vs 128 µg/mL for polymers with M_n = 10 kDa), whereas both DABCO and pyridinium based polymers stayed inactive towards *E. coli*. At the same time, DABCO containing polymers presented high hemolytic activity with HC_{50} > 2000 µg/mL for polymers with M_n of 10 kDa. Furthermore, copolymerisation of DABCO and pyridinium containing monomers, allowed for the formation of copolymers with increased cationic character and thus improvement in antimicrobial activity against Gram-positive bacteria (MIC_{50} = 16 µg/mL), while no activity was seen in the case of the Gram-negative bacteria. Additional studies carried out by the Eren group on the preparation of ACPs, involved the preparation of: (i) random and block copolymers functionalised with pyridinium group and ammonium group added via an amide bond to the polymer backbone[52]; (ii) polyONB

possessing aliphatic and aromatic phosphonium side chains[94,103] (4, Figure 1.15); (iii) ONB polymers containing aromatic phosphonium side chains conjugated with an acrylate containing vancomycin moiety[104]; (iv) copolymers bearing zinc(II) phthalocyanine (added as generators of reactive oxygen species, ROS, in photodynamic antimicrobial chemotherapy, PACT) and aromatic phosphonium functionalities[105]. In these studies, Eren *et al.* have demonstrated that the presence of phosphonium cations as well as increasing the hydrophobicity of the ACPs by addition of aromatic functionalities increased the biocidal activity against both Gram-positive and Gram-negative bacteria. However, the conjugation of vancomycin to these ACPs dropped the activity against *S. aureus*, while becoming completely inactive towards *E. coli*.

From the examples mentioned above, it has been demonstrated that activity and selectivity of ACPs is influenced by their multiblock structure (distribution of monomers within the polymer backbone). However, the polymer topology is another factor that needs to be considered. For instance, AMPs that possess a star shape[106] or a branched structure[107] have been shown to possess an increased biocidal activity and lower toxicity. Hartlieb *et al.*[108] developed multivalent bottlebrush ROMP copolymers with enhanced bioactivity and selectivity via the grafting-through method. Firstly, RAFT (reversible addition-fragmentation chain transfer) polymerisation was used in order to form NB-based macroinitiators (NB-P(BocAEAm), NB-P(NiPAAm) and NB-P(NiPAAm-stat-BocAEAm)) with intrinsic antimicrobial activity, which were then polymerised using ROMP. The final Boc-deprotection formed cationic bottlebrush copolymers with a very narrow molecular weight distribution ($Đ < 1.2$). In this study, the importance of the polymer structure for the design of ACPs was demonstrated. In fact, hetero-graft copolymers formed self-assembled morphologies where the hydrophobic units were trapped within the core shell, making them unavailable for cell membrane disruption, and thus decreasing the biocidal activity ($MIC_{50} > 1024$ µg/mL for *E. coli* and *S. aureus*). Homo-graft copolymers instead, behaved as linear antimicrobial polymers, and therefore, activity and selectivity towards both Gram-negative and Gram-positive bacteria were increased ($MIC_{50} = 64$ µg/mL for *E. coli* and *S. aureus*).

Table 1.1 summarises all the antimicrobial ROMP polymers discussed in this section, including both polymeric biocides and biocidal polymers. The microbes tested for each polymer system with the corresponding antimicrobial (MIC_{50}) and hemolytic activity (HC_{50}) are presented.

Table 1.1. Overview of MIC_{50} and HC_{50} values of antimicrobial ROMP polymers. n.a. = not available.

Polymer	Microbes tested	MIC_{50} (µg/mL)	HC_{50} (µg/mL)	Reference
Poly(NB-VAN)	*S. aureus*	2.3	n.a.	98
	Enterococcus	2		
Poly(NB-PEO-GS)	*S. epidermidis*	> 3	n.a.	65
Poly(NB-PEO-VAN)	*S. aureus*	> 7	n.a.	100
Poly(NB-NH$_3^+$) (poly3-*co*-poly2)	*B. subtilis*	40	> 4000	101
	E. coli	40		
Poly(ONB-Py-alkyl) (alkyl ≥ C$_6$)	*B. subtilis*	< 12	< 250	93
	E. coli	< 12		
Poly(ONB-DABCO)	*S. aureus*	8	> 2000	102
	E. coli	Inactive		
Poly(ONB-DABCO-Py)	*S. aureus*	16	2000	102
	E. coli	Inactive		
Poly(ONB-NR$_3^+$)-*co*-poly(ONB-PyR$^+$)	*S. aureus*	64	> 1000	52
	E. coli	256		
Poly(ONB-PPh$_3^+$)	*S. aureus*	8	99	94
	E. coli	16		
	C. albicans	128		
	M. tuberculosis	64		
Poly(ONB-DABCO)-VAN	*S. aureus*	64	> 2000	104
	E. coli	> 512		
	E. faecalis	256		
Poly(ONB-PPh$_3^+$)-VAN	*S. aureus*	32	> 2000	104
	E. coli	> 512		
	E. faecalis	16		
Poly(ONB-PPh$_3^+$)-*co*-poly(ONB-Zn)	*S. aureus*	16	512	105
	E. coli	256		
Homo-graft bottle brush copolymers	*S. aureus*	64	> 1024	108
	E. coli	64		
	P. aeruginosa	128		
	S. epidermidis	32		
Hetero-graft bottle brush copolymers	*S. aureus*	> 1024	> 1024	108
	E. coli	> 1024		
	P. aeruginosa	> 1024		
	S. epidermidis	64		

1.4.   Conclusion

The living behaviour of ROMP has allowed for the preparation of highly functionalised polymers with precise architectures and sequences. Initiators for ROMP have undergone extensive developments over many years, and the discovery of fast, active, functional group-tolerant ruthenium-based catalysts by the Grubbs group, have allowed for the synthesis of polymers that can be used in a wide range of fields, particularly the field of nanomedicine. Indeed, the ROMP technique has been used over the past 20 years for the realisation of novel biologically active materials, including carbohydrate-[109,53] and peptide-[110,111] containing polymers, but mostly, polymers containing drugs and polymers with antimicrobial activity which have been widely discussed in this chapter. Thanks to the control over the polymer sequence, many research groups have been able to synthesise block- and triblock- copolymers with amphiphilic properties that have led to the preparation of different self-assembled morphologies, which have allowed for the delivery of active molecules to specific targets. Thus, as demonstrated, ROMP has played an important role in the preparation of innovative materials that could not be obtained with other polymerisation techniques, and it will continue to be used in the future for the realisation of imaginative applications in biology.

1.5.   Project aims

The aim of this project was to use the ROMP polymerisation as a means for the preparation of biologically relevant polymers, for two different applications. The first one involved the preparation of a polymeric drug delivery system for the delivery of NSAIDs, namely ibuprofen, to tumours. An amphiphilic block copolymer containing PEG as the hydrophilic portion, and ibuprofen as the hydrophobic portion was synthesised. Its self-assembly properties as well as drug release process were then investigated. The second application involved the realisation of a novel class of antimicrobial polymers, in the form of amphiphilic cationic polymers, bearing SSAs (supramolecular self-associating amphiphiles). SSAs are a class of antimicrobial molecules synthesised within the

Hiscock group at the University of Kent. The aim of this collaboration was to study the physicochemical properties of monomers as well as polymers bearing SSAs as the anionic component. Finally, their antimicrobial activity towards both Gram-positive and Gram-negative bacteria was studied.

1.6.   References

1   J. R. Fried, *Polymer Science & Technology: Third Edition*, 2014.

2   U. Isopren, *Helv. Chim. Acta*, 1922, **5**, 785–806.

3   P. C. Hiemenz and T. P. Lodge, *Polymer chemistry, 2nd edn. CRC*, 2007, vol. 8.

4   K. Ziegler and K. Bähr, *Berichte der Dtsch. Chem. Gesellschaft*, 1928, **61**, 253–263.

5   M. Szwarc, M. Levy and R. Milkovich, *J. Am. Chem. Soc.*, 1956, **78**, 2656–2657.

6   R. H. Grubbs, *Handbook of Metathesis*, 2003, vol. 205.

7   A. D. Jenkins, R. F. T. Stepto, P. Kratochvíl and U. W. Suter, *Pure Appl. Chem.*, 1996, **68**, 2287–2311.

8   C. W. Bielawski and R. H. Grubbs, *Prog. Polym. Sci.*, 2007, **32**, 1–29.

9   P. J. Flory, *J. Am. Chem. Soc.*, 1940, **62**, 1561–1565.

10   M. L. Heilig, *N. G US Pat. 2721189*, 1955, **28**, 131–134.

11   H. S. Eleuterio, *H. S US Pat. 3074918*.

12   Y. He´risson, J. L. Chauvin, *Makromol. Chem.*, 1970, **141**, 161–176.

13   D. D. C. R. H. Grubbs, P. L. Burk, *J. Am. Chem. Soc.*, 1975, **97**, 3265–3267.

14   R. Schrock, S. Rocklage, J. Wengrovius, G. Rupprecht and J. Fellmann, *J. Mol. Catal.*, 1980, **8**, 73–83.

15   MLA style: The Nobel Prize in Chemistry 2005. NobelPrize.org. Nobel Media AB 2021. Wed. 9 Jun 2021., https://www.nobelprize.org/prizes/chemistry/2005/summary/, (accessed 10 June 2021).

16   G. Natta, G. Dall'Asta and G. Mazzanti, *Angew. Chemie Int. Ed. English*, 1964, **3**, 723–729.

17   N. Calderon, E. A. Ofstead, J. P. Ward, W. A. Judy, K. W. Scott, *J. Am. Chem. Soc.*, 1968, **90**, 4133.

18   K. J. Ivin, J. C. Mol, *Olefin Metathesis and Metathesis Polymerization*, 1997.

19   M. R. Buchmeiser, *Chem. Rev.*, 2000, **100**, 1565–1604.

20   D. A. Straus and R. H. Grubbs, *Organometallics*, 1982, **1**, 1658–1661.

21   L. F. Cannizzo and R. H. Grubbs, *Macromolecules*, 1988, **21**, 1961–1967.

22   R. R. Schrock, R. T. DePue, J. Feldman, C. J. Schaverien, J. C. Dewan and A. H. Liu, *J. Am. Chem. Soc.*, 1988, **110**, 1423–1435.

23   M. L. H. Green, *Endeavour*, 1986, **10**, 104.

24   D. J. Polym, B. L. Farmer, J. F. Rabolt and R. D. Miller, *J. Polym. Sci., Polym. Lett. Ed*, 1987, **20**, 1480.

25   S. T. Nguyen, L. k. Johnson and R. H. Grubbs, *J. Am. Chem. Soc*, 1992, **114**, 3975–3977.

26   P. Schwab, M. B. France, J. W. Ziller and R. H. Grubbs, *Angew. Chemie Int. Ed. English*, 1995, **34**, 2039–2041.

27   P. Schwab, R. H. Grubbs and J. W. Ziller, *J. Am. Chem. Soc.*, 1996, **118**, 100–108.

28   T. M. Trnka, J. P. Morgan, M. S. Sanford, T. E. Wilhelm, M. Scholl, T. L. Choi, S. Ding, M. W. Day and R. H. Grubbs, *J. Am. Chem. Soc.*, 2003, **125**, 2546–2558.

29   J. A. Love, J. P. Morgan, T. M. Trnka, and R. H. Grubbs, *Angew. Chemie Int. Ed.*, 2001, **41**, 4035–4037.

30   J. P. Gallivan, J. P. Jordan and R. H. Grubbs, *Tetrahedron Lett.*, 2005, **46**, 2577–2580.

31   D. D. Manning, L. E. Strong, X. Hu, P. Beck, L. L. Kiessling, T. Nishikawa, T. Ando, M. Kamigaito, M. Sawamoto, T. J. Macromolecules ; Deming, B. M. Novak, L. L. Macromolecules ; Kiessling, N. L. Pohl, M. C. Schuster, K. H. Mortell, A. D. Hegeman, R. V Weatherman, B. Mohr, D. M. Lynn and R. H. Grubbs, *J. Mol. Catal. A Chem*, 1996, **118**, 45.

32   J. C. Foster, S. Varlas, L. D. Blackman, L. A. Arkinstall and R. K. O'Reilly, *Angew. Chemie - Int. Ed.*, 2018, **57**, 10672–10676.

33   P. V. R. Schleyer, J. E. Williams and K. R. Blanchard, *J. Am. Chem. Soc*, 1970, **92**, 2377.

34   M. Weck, B. Mohr, B. R. Maughon and R. H. Grubbs, *Macromolecules*, 1997, **30**, 6430–6437.

35   K. Breitenkamp and T. Emrick, *J. Am. Chem. Soc.*, 2003, **125**, 12070–12071.

36   C. W. Bielawski, D. Benitez and R. H. Grubbs, *J. Am. Chem. Soc.*, 2003, **125**, 8424–8425.

37   P. A. Patton, C. P. Lillya and T. J. Mccarthy, *Mcromolecules*, 1986, **19**, 1266–1268.

38   P. Dounis, W. James Feast and A. M. Kenwright, *Polymer (Guildf).*, 1995, **36**, 2787–2796.

39   W. J. Neary and J. G. Kennemur, *Macromol. Rapid Commun.*, 2016, **37**, 975–979.

40   N. Zaami, C. Slugovc, A. Pogantsch and F. Stelzer, *Macromol. Chem. Phys.*, 2004, **205**, 523–529.

41   V. Lapinte, J. C. Brosse and L. Fontaine, *Macromol. Chem. Phys.*, 2004, **205**, 824–833.

42   M. G. Hyatt, D. J. Walsh, R. L. Lord, J. G. Andino Martinez and D. Guironnet, *J. Am. Chem. Soc.*, 2019, **141**, 17918–17925.

43   I. Choinopoulos, *Polymers (Basel).*, 2019, **11**, 298.

44   X. Sui, S. Zapotoczny, E. M. Benetti, P. Schön and G. J. Vancso, *J. Mater. Chem.*, 2010, **20**, 4981–4993.

45   M. Müllner, *Macromol. Chem. Phys.*, 2016, **217**, 2209–2222.

46   Q. Chen, *Int. J. Polym. Sci.*, 2021, **2021**, 1–15.

47   R. L. Kenyon, *Chem. Eng. News*, 1968, 46, 5.

48   R. H. Grubbs and E. Khosravi, *Handbook of Metathesis, Volume 3: Polymer Synthesis*, 2015, vol. 2.

49   C. Slugovc, *Macromol. Rapid Commun.*, 2004, **25**, 1283–1297.

50   P. Bertrand, C. Blanquart and V. Héroguez, *Biomolecules*, 2019, **9**, 60.

51   R. Gareth Davies, V. C. Gibson, M. B. Hursthouse, M. E. Light, E. L. Marshall, M. North, D. A. Robson, I. Thompson, A. J. P. White, D. J. Williams and P. J. Williams, *J. Chem. Soc. Perkin 1*, 2001, 3365–3381.

52   M. N. Islam, B. Aksu, M. Güncü, M. Gallei, M. Tulu and T. Eren, *J. Polym. Sci.*, 2020, **58**, 872–884.

53   T. Debsharma, B. Schmidt, A. Laschewsky and H. Schlaad, *Macromolecules*, 2021, **54**, 2720–2728.

54   P. Kelly, P. Anand, A. Uvaydov, S. Chakravartula, C. Sherpa, E. Pires, A. O'Neil, T. Douglas

and M. Holford, *Int. J. Environ. Res. Public Health*, 2015, **12**, 12543–12555.

55   M. Lis, F. Dorner, G. N. Tew and K. Lienkamp, *Langmuir*, 2016, **32**, 5946–5954.

56   A. Ö. Tezgel, P. Jacobs, C. M. Backlund, J. C. Telfer and G. N. Tew, *Biomacromolecules*, 2017, **18**, 819–825.

57   D. Dutta, W. Ke, L. Xi, W. Yin, M. Zhou and Z. Ge, *Wiley Interdiscip. Rev. Nanomedicine Nanobiotechnology*, 2020, **12**, 1–19.

58   V. Vijayakameswara Rao, S. R. Mane, A. Kishore, J. Das Sarma and R. Shunmugam, *Biomacromolecules*, 2011, **13**, 221–230.

59   S. Sutthasupa and F. Sanda, *Eur. Polym. J.*, 2018, **98**, 162–171.

60   J. A. Johnson, Y. Y. Lu, A. O. Burts, Y. Xia, A. C. Durrell, D. A. Tirrell and R. H. Grubbs, *Macromolecules*, 2010, **43**, 10326–10335.

61   F. Danhier, O. Feron and V. Préat, *J. Control. Release*, 2010, **148**, 135–146.

62   I. Mellman, *Annu. Rev. Biochem.*, 1986, **55**, 663–700.

63   Y. Gao, Y. Xiao, S. Liu and J. Yu, *J. Biomater. Sci. Polym. Ed.*, 2018, **29**, 160–180.

64   J. Mao, Y. Li, T. Wu, C. Yuan, B. Zeng, Y. Xu and L. Dai, *ACS Appl. Mater. Interfaces*, 2016, **8**, 17109–17117.

65   L. Pichavant, C. Bourget, M. C. Durrieu and V. Héroguez, *Macromolecules*, 2011, **44**, 7879–7887.

66   E. R. Gillies and J. M. J. Fréchet, *Bioconjug. Chem.*, 2005, **16**, 361–368.

67   Y. Gu, Y. Zhong, F. Meng, R. Cheng, C. Deng and Z. Zhong, *Biomacromolecules*, 2013, **14**, 2772–2780.

68   J. Z. Du, X. J. Du, C. Q. Mao and J. Wang, *J. Am. Chem. Soc.*, 2011, **133**, 17560–17563.

69   S. R. Mane, H. Dinda, A. Sathyan, J. Das Sarma and R. Shunmugam, *ACS Appl. Mater. Interfaces*, 2014, **6**, 16895–16902.

70   A. X. Gao, L. Liao and J. A. Johnson, *ACS Macro Lett.*, 2014, **3**, 854–857.

71   J. Zou, Y. Yu, Y. Li, W. Ji, C. K. Chen, W. C. Law, P. N. Prasad and C. Cheng, *Biomater. Sci.*,

2015, **3**, 1078–1084.

72   I. Denis, F. El Bahhaj, F. Collette, R. Delatouche, F. Gueugnon, D. Pouliquen, L. Pichavant, V.

Héroguez, M. Grégoire, P. Bertrand and C. Blanquart, *Eur. J. Med. Chem.*, 2015, **95**, 369–

376.

73   R. Baumgartner, D. Kuai and J. Cheng, *Biomater. Sci.*, 2017, **5**, 1836–1844.

74   H. Chen and Y. Zhao, *ACS Appl. Mater. Interfaces*, 2018, **10**, 21021–21034.

75   J. Lu, E. Choi, F. Tamanoi and J. I. Zink, *Small*, 2008, **4**, 421–426.

76   R. Tong, H. D. Hemmati, R. Langer and D. S. Kohane, *J. Am. Chem. Soc.*, 2012, **134**, 8848–

8855.

77   M. S. Kim and S. L. Diamond, *Bioorganic Med. Chem. Lett.*, 2006, **16**, 4007–4010.

78   H. Zhao, E. S. Sterner, E. B. Coughlin and P. Theato, *Macromolecules*, 2012, **45**, 1723–1736.

79   P. T. Wong, S. Tang, J. Cannon, D. Chen, R. Sun, J. Lee, J. Phan, K. Tao, K. Sun, B. Chen, J. R.

Baker and S. K. Choi, *Bioconjug. Chem.*, 2017, **28**, 3016–3028.

80   S. K. Choi, M. Verma, J. Silpe, R. E. Moody, K. Tang, J. J. Hanson and J. R. Baker, *Bioorganic

Med. Chem.*, 2012, **20**, 1281–1290.

81   J. A. Johnson, Y. Y. Lu, A. O. Burts, Y. Xia, A. C. Durrell, D. A. Tirrell and R. H. Grubbs,

Macromolecules, 2010, **43**, 10326–10335.

82   J. A. Johnson, Y. Y. Lu, A. O. Burts, Y. H. Lim, M. G. Finn, J. T. Koberstein, N. J. Turro, D. A.

Tirrell and R. H. Grubbs, *J. Am. Chem. Soc.*, 2011, **133**, 559–566.

83   L. Liao, J. Liu, E. C. Dreaden, S. W. Morton, K. E. Shopsowitz, P. T. Hammond and J. A.

Johnson, *J. Am. Chem. Soc.*, 2014, **136**, 5896–5899.

84   S. Mura, J. Nicolas and P. Couvreur, *Nat. Mater.*, 2013, **12**, 991–1003.

85   K. Feng, N. Xie, B. Chen, L. P. Zhang, C. H. Tung and L. Z. Wu, *Macromolecules*, 2012, **45**,

5596–5603.

86   S. R. Mane, V. N. Rao and R. Shunmugam, *ACS Macro Lett.*, 2012, **1**, 482–488.

87   Q. Yao, D. C. Gutierrez, N. H. Hoang, D. Kim, R. Wang, C. Hobbs and L. Zhu, *Mol. Pharm.*,

2017, **14**, 2378–2389.

88 X. Liu, G. Qiu, L. Zhang, F. Liu, S. Mu, Y. Long, Q. Zhao, Y. Liu and H. Gu, *Macromol. Chem. Phys.*, 2018, **219**, 1800273.

89 G. Qiu, X. Liu, B. Wang, H. Gu and W. Wang, *Polym. Chem.*, 2019, **10**, 2527–2539.

90 R. Li, X. Li, Y. Zhang, A. O. Delawder, N. D. Colley, E. A. Whiting and J. C. Barnes, *Polym. Chem.*, 2020, **11**, 541–550.

91 M. R. E. Santos, A. C. Fonseca, P. V. Mendonça, R. Branco, A. C. Serra, P. V. Morais and J. F. J. Coelho, *Materials (Basel).*, 2016, **9**, 1–33.

92 V. Bobbarala, *Concepts, compounds and the alternatives of antibacterials*, 2015.

93 T. Eren, A. Som, J. R. Rennie, C. F. Nelson, Y. Urgina, K. Nüsslein, E. B. Coughlin and G. N. Tew, *Macromol. Chem. Phys.*, 2008, **209**, 516–524.

94 N. C. Süer, C. Demir, N. A. Ünübol, Ö. Yalçin, T. Kocagöz and T. Eren, *RSC Adv.*, 2016, **6**, 86151–86157.

95 J. M. Sarapas, C. M. Backlund, B. M. deRonde, L. M. Minter and G. N. Tew, *Chem. - A Eur. J.*, 2017, **23**, 6858–6863.

96 K. Matsuzaki, *Biochim. Biophys. Acta - Biomembr.*, 1999, **1462**, 1–10.

97 S. C. G. Biagini, V. C. Gibson, M. R. Giles, E. L. Marshall and M. North, *Chem. Commun.*, 1997, 1097–1098.

98 H. Arimoto, K. Nishimura, T. Kinumi, I. Hayakawa and D. Uemura, *Chem. Commun.*, 1999, **2**, 1361–1362.

99 H. Arimoto, T. Oishi, M. Nishijima and T. Kinumi, *Tetrahedron Lett.*, 2001, **42**, 3347–3350.

100 L. Pichavant, H. Carrié, M. N. Nguyen, L. Plawinski, M. C. Durrieu and V. Héroguez, *Biomacromolecules*, 2016, **17**, 1339–1346.

101 M. F. Ilker, K. Nüsslein, G. N. Tew and E. B. Coughlin, *J. Am. Chem. Soc.*, 2004, **126**, 15870–15875.

102 A. P. Kaymaz, İ. Acaroğlu-Degitz, M. A. Yapaöz, A. D. Sezer, S. Malta, B. Aksu and T. Eren,

Materialia, 2019, **5**, 100246.

103 N. C. Süer, T. Arasoglu, H. Cankurtaran, M. Okutan, M. Gallei and T. Eren, *Turkish J. Chem.*, 2021, **45**, 986–1003.

104 İ. Acaroğlu Degitz, B. Hakkı Gazioğlu, M. Burak Aksu, S. Malta, A. Demir Sezer and T. Eren, *Eur. Polym. J.*, 2020, **141**, 110084.

105 E. Ahmetali, P. Sen, N. C. Süer, B. Aksu, T. Nyokong, T. Eren and M. K. Şener, *Macromol. Chem. Phys.*, 2020, **221**, 1–14.

106 S. J. Lam, E. H. H. Wong, N. M. O'Brien-Simpson, N. Pantarat, A. Blencowe, E. C. Reynolds and G. G. Qiao, *ACS Appl. Mater. Interfaces*, 2016, **8**, 33446–33456.

107 R. Namivandi-Zangeneh, R. J. Kwan, T. K. Nguyen, J. Yeow, F. L. Byrne, S. H. Oehlers, E. H. H. Wong and C. Boyer, *Polym. Chem.*, 2018, **9**, 1735–1744.

108 S. Laroque, M. Reifarth, M. Sperling, S. Kersting, S. Klöpzig, P. Budach, J. Storsberg and M. Hartlieb, *ACS Appl. Mater. Interfaces*, 2020, **12**, 30052–30065.

109 C. Fraser and R. H. Grubbs, *Macromolecules*, 1995, **28**, 7248–7255.

110 S. C. G. Biagini and A. L. Parry, *J. Polym. Sci. Part A Polym. Chem.*, 2007, **45**, 3178–3190.

111 J. Zhu, H. Sun, C. E. Callmann, M. P. Thompson, C. Battistella, M. T. Proetto, A. S. Carlini and N. C. Gianneschi, *Chem. Commun.*, 2020, **56**, 6778–6781.

CHAPTER 2. NSAIDs BASED ROMP NANOPARTICLES: SYNTHESIS, SELF-ASSEMBLY AND DRUG RELEASE.

2.1. Introduction

According to the World Health Organisation (WHO), cancer is the primary cause of death worldwide, with breast, lung, colon, rectum and prostate cancers being the most common ones[1]. The global cancer statistic have estimated 19.3 million of new cases of cancer and nearly 10 million deaths in 2020[2]. The main causes of cancer are due to high body mass index, lack of physical activity, use of tobacco and alcohol consumption[1]. There are several therapeutic strategies, including surgery, radiotherapy, chemotherapy and targeted drug therapy. Surgery is the main treatment used; radiotherapy and chemotherapy can inhibit the rapid growth of tumours, although these therapeutic strategies have a major drawback of killing normal, healthy cells[3]. A novel and more promising method for the cure and survival rate of cancer patients, involve the development and application of targeted drug delivery systems (DDSs).

2.1.1. Targeted drug delivery systems

Drug delivery systems (DDSs) are methods and formulations used to transport a specific biologically active substance in the body with the purpose of achieving a desired therapeutic effect. Five generations of DDSs have been developed over the last decades and targeted DDSs belong to the fourth generation[4]. The aim of targeted DDSs is improving the treatment effectiveness while reducing the side effects typical of conventional drug molecules. This is obtained by delivering the drug to a specific target within the body and therefore by maximising the concentration of the drug at the specific site of action, while minimizing its concentration to the nontargeted region[5]. Furthermore, this type of drug delivery is independent from the method and route of administration[6]. The target (or site of action) is the specific organ, tissue, a cell or a group of cells that are in chronic or acute conditions and that therefore require to be treated with specific drugs. The ideal targeted DDS has to be non-toxic, biodegradable or biocompatible and stable but also it

has to stay inert before reaching the target of interest[7]. Furthermore, such targeted DDSs need to be constructed so that they release a specific amount of the drug at specific times[8]. In this way a reduction in administration frequency can be achieved. They can be used to treat different diseases but their main application in the nanomedicine field is for cancer therapy[7].

There are two main types of targeting strategies: "passive" and "active" targeting[9]. The "passive" targeting is commonly referred to as the enhanced permeation and retention (EPR) effect, which is based on the accumulation of the DDS at the target of interest due to systematic blood circulation and extravasation. Thanks to their physicochemical properties (e.g., size and surface), nanoparticles (NPs) are mostly used in the "passive" targeting strategy. They can enter the blood vessels and reach the targeted site by avoiding the uptake by the reticulo-endothelial system (RES). The EPR effect is more efficacious for intravenous administered NPs[10].

The "active" targeting refers to specific interactions between the DDS and the targeted site, mainly ligand-receptor interactions. The drug carrier is formulated so that it possesses specific ligands, such as antibodies or peptides, that can bind overexpressed receptors present at the targeted site[11]. However, this interaction is possible only when the ligand and the receptor are in close proximity to one another (< 0.5 nm)[9]. Furthermore, the target can be reached only by blood circulation and extravasation, followed by intracellular retention and distribution, meaning that even the "active" targeting relies on the EPR effect.

There are several drug carriers that have been developed to be used as advanced delivery systems. These include: (i) liposomes[12], vesicles consisting of phospholipid bilayers that can be loaded with either hydrophilic or hydrophobic drugs; (ii) non-metallic NPs[13], such as silicon and carbon based NPs. They possess several advantages, such as low cost, biocompatibility, biodegradability and low toxicity; (iii) polymeric NPs, which are subcategorised into natural polymer NPs[14], polymeric micelles[15] obtained by the self-assembly of amphiphilic polymers, and colloidal polymeric NPs[16] where the drug is either dispersed within the polymeric matrix or confined within a cavity.

In the next section the focus is on the use of polymeric NPs in the form of polymer-drug conjugates (or polyprodrugs) which can form polymeric micelles.

2.1.2. Polymer-drug conjugates

The development of polymer-drug conjugates as targeted DDSs has become prevalent in recent years, following their first introduction to the market 30 years ago[17]. The first polymer-drug conjugate approved by the FDA (Food and Drug Administration) is a protein-based DDS where the protein is covalently linked to a mPEG (monomethoxy poly(ethylene glycol)) chain. Such system, Adagen (pegademase bovine), entered the market in 1990[17] as an enzyme replacement therapy for the adenosine deaminase deficiency[18] used in patients with severe combined immunodeficiency (SCID). Several others have been later approved by the FDA, such as Oncaspar[19] in 1994 used to treat acute lymphoblastic leukaemia, and Pegasys[20] in 2002 used to treat chronic hepatitis C. Whereas numerous polymer-drug conjugates are in clinical phases I, II or III. For instance, Onzeald[21], is a polymer-small molecule drug conjugate where the chemotherapeutic drug, irinotecan, is covalently linked to a PEG chain via an ester bond and it has progressed to phase III trials. Onzeald can be potentially used in brain cancer therapy, and it is designed so that it can attenuate or potentially eliminate the irinotecan side effects.

The last few decades have seen increased efforts in the development of polymer-drug conjugates. These include polymer systems in which the incorporated drug can be a small molecule drug[22], a peptide[23], a protein[24] as well as an antibody[25].

2.1.2.1. Designing polymer-drug conjugates

Polymer-drug conjugates, also called polymeric prodrugs, are systems where the drug (a biologically active component) is covalently linked to a polymer chain. In this system, the drug stays inactive during its delivery to the site of action, such as an organ, a tissue or a cell, and can be activated only by specific metabolic processes that lead to the cleavage of a specific bond (ester, imine, disulphide

etc.) between the drug and the polymer. There are several advantages associated with the use of polyprodrugs, such as an increase in the drug water solubility, an enhancement of drug bioavailability, protection of the drug during its circulation to the site of action and an improvement in pharmacokinetics[26]. In contrast to non-covalent encapsulation strategies (dispersion of the drug within the polymeric matrix or confinement within a cavity), polyprodrugs have the advantage of precise structure and high drug-loading rate[22]. Furthermore, such DDSs are constructed not only to target a specific organ, tissue or cell, but also to release a specific amount of the drug at specific times[8].
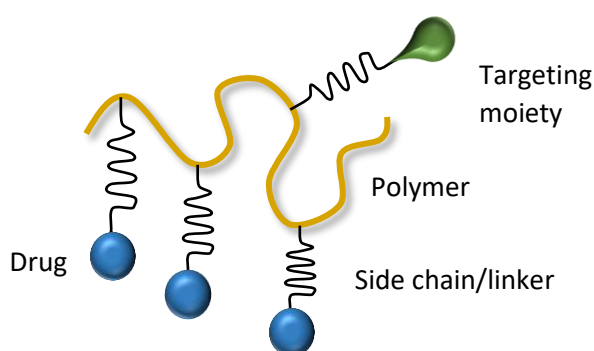
Fig. 2.16. Representation of a polymer-drug conjugate.

In general, a polymeric prodrug consists of a combination of components: a polymeric backbone, one or more drugs, a linker (or spacer) consisting of a functional group that can be cleaved under specific metabolic conditions and sometimes a targeting moiety can be added in order to obtain the "active" targeting (Figure 2.1)[26]. There are several factors to consider in order to efficiently construct a polyprodrug system, including chemical structure (typically well established and approved polymers are used[27]), molecular weight (oligomers, macromers, polymers), steric hindrance and the reactivity between the polymer and the drug. In general, both entities possess functional groups such as -COOH, -OH, - SH and -NH$_2$ so that coupling agents such as DCC (dicyclohexyl carbodiimide), EDC (1-ethyl-3-(3-dimethylaminopropyl)carbodiimide) and NHS (N-hydroxysuccinimide esters) are being employed. The bonds that result from the coupling of these functional groups need to be stable enough in order to avoid the release of the drug during the circulation to the target, but also labile enough so that they can be cleaved at the site of action

45

via specific processes, which include enzymatic degradation[28], hydrolysis under mild acidic pH[29], reduction[30] (mainly of disulphide bonds) or oxidation with ROS species[31].

The ideal drug carriers should be either biocompatible or inert biodegradable polymers as they can break down inside the body to produce nontoxic natural byproducts such as water and carbon dioxide, and therefore can be easily eliminated by the body[27]. However, non-degradable polymers have also been employed and tested for their cytotoxicity[32,33].

2.1.2.2. Nanoparticles of polymer-drug conjugates

By tuning the physicochemical properties of polymer-drug conjugates it is possible to construct polymeric NPs, which behave as drug carriers in the nanometre scale. Polymeric NPs are obtained by either precipitation or emulsification in the presence of a surfactant, or most commonly by the self-assembly in aqueous environment of block copolymers possessing amphiphilic properties. This allows for the preparation of polymeric micelles, core-shell structures where the hydrophobic polymer core is sequestered within a hydrophilic corona[15]. Polymeric micelles possess several advantages such as incorporation of non-water soluble drugs within the hydrophobic core and consequently enhancement of their bioavailability, as well as high-drug loading and controlled drug release achieved by slow degradation of the polymer matrix[34].

2.1.2.2.1. Properties of nanoparticles

There are several factors to take into consideration when constructing a polymeric NP, such as particle size, shape, surface charge and PEGylation. Each of these factors can contribute towards the circulation time, clearance, selective tissue distribution and intracellular fate[35].

- *Particle size*: polymeric NPs of size ranging from 20 nm to 100 nm are good candidates for *in vivo* applications, as they can circulate in the blood for a long period of time. On contrary, it has been demonstrated that large particles of diameter > 1 μm tend to be opsonized and

accumulate in the liver with potential capillary occlusion. Whereas smaller particles with diameter < 5 nm are rapidly cleared from the bloodstream through the kidneys[36].

- *Particle shape*: spherical NPs are the most common used in clinical and pre-clinical setting as they can be rapidly internalised into cells[37]. However, other morphologies such as rod-shaped (cylindrical[38]) NPs have shown a higher cellular uptake compared to spherical NPs[39]. For instance, Wooley *et al.*[39] prepared folate-functionalised NPs possessing both cylindrical and spherical shape. In this study, cylindrical NPs have been internalised to a greater extent than the sphere ones as it was hypothesised that cylinders could bind multiple receptors thanks to their longer dimension. In this study, the formed multivalent interaction allowed for a more efficient cellular uptake.

- *Surface charge*: typically, positively charged NPs have a higher non-specific internalisation rate in the majority of cells and shorter blood circulation half-life compared to neutral and negatively charged NPs. The latter have also been demonstrated to less accumulate in the liver and spleen[35,40].

- *PEGylation*: it has been proven that an increase of NPs circulation half-life is achieved by making the NP surface more hydrophilic. This is usually obtained by creating copolymers possessing PEG. PEG is a hydrophilic and relatively inert polymer that, when introduced in a NP formulation, helps preventing the NPs opsonisation as they remain undetected by the RES system[9]. However, although PEGylated NPs possess an increased systematic circulation time, there are still some limitations regarding the NPs cell internalisation. In some cases, the i.v. administered NPs are still directed to the liver and the spleen[41]. Other hydrophilic polymers have also been employed, such as PVP (poly vinyl alcohol) and PEI (poly ethyleneimine)[42].

It is evident, from these observations, the complexity of the NP-cell interaction and therefore being able to generate the best drug carrier can be sometimes challenging. It is critical to take into

considerations all these factors in order to obtain the best blood circulation time and cellular uptake.

2.1.3. Nonsteroidal anti-inflammatory drugs (NSAIDs) in cancer therapy

Nonsteroidal anti-inflammatory drugs (NSAIDs) are the most common prescribed drugs worldwide. They possess antipyretic, analgesic and anti-inflammatory properties and are hence used mainly to reduce fever, pain and inflammation. However, in the last few decades they have found application in the treatment and prevention of cancer. The relationship between chronic inflammation and cancer has been first discovered in 1863 by Virchow[43]. His hypothesis was based on the fact that cell proliferation was enhanced by chronic inflammation at the injured tissue. In a sense, tumours act as wounds that fail to heal[44].

Several epidemiological studies have been carried out to study the effect of NSAIDs in reducing the cancer risk of different types of cancer including breast[45,46], prostate[47], colorectal[48] and ovarian[49] cancers. Some of these studies revealed a reduction in cancer risk associated with the NSAIDs administration, but some others did not find any association between the two[50]. Furthermore, the long-term use of NSAIDs often causes several side effects such as cardiovascular, gastrointestinal and renal side effects[51], associated with oral administration.

The mechanism of NSAIDs in the cancer treatment is still not very clear, but it is thought that they act by inhibiting the cyclooxygenase (COX) which is the enzyme responsible for the conversion of the arachidonic acid (AA) to prostaglandins (PGs). PGs are a group of lipids consisting of 20 atoms of carbon, also known as eicosanoids and are responsible of inflammatory responses at the site of tissue damaged or infected[52]. However, an overexpression of PGs, mediated by the COX-2 isoform, is also thought to be responsible for promoting cancer growth and metastasis[53]. In particular, the pro-inflammatory prostaglandin E_2 (PGE_2) has been found to be overexpressed in many tumours including colon[54], breast[55], lung[56] and head and neck[57] cancers. Therefore,

suppressing the formation of PGE_2 by inhibiting COX using NSAIDs could have a chemotherapeutic value.

2.1.3.1. NSAIDs based nanoparticles

The majority of NSAIDs based nanoparticles present in literature are lipid based NPs such as liposomes and solid lipid nanoparticles (SLNs). In these cases, the NSAID drug gets encapsulated within the NP matrix for the management of pain and inflammation. The main purpose is to overcome some of the side effects associated with their oral administration, rather than for cancer treatment[58]. Although some other examples in the literature demonstrate the use of NPs of NSAIDs for use in tumour therapy[59].

Harding *et al.*[60], for instance, prepared solid lipid nanoparticles (SLNs) by microwave assisted one-pot microemulsion using indomethacin, ketoprofen and nimesulide as NSAIDs drugs. The SLNs were prepared to be used as anti-inflammatory formulation with the intention of reducing the gastrointestinal and renal side effects typical of NSAIDs. In this instance, the microwave approach allowed for the encapsulation of the drug at the same time the SLN was forming, giving rise to a high drug loading. Other formulations include polymeric NPs where NSAIDs are physically entrapped within the polymer matrix. Carvalho and co-workers[61], used indomethacin as anti-inflammatory drug and studied its encapsulation properties as well as drug release from a mixture of EUDRAGIT® L100 (anionic copolymer based on methacrylic acid and methyl methacrylate (1:1)), PEG and polysorbate 80. Even in this case, the NP was formulated for inflammatory management.
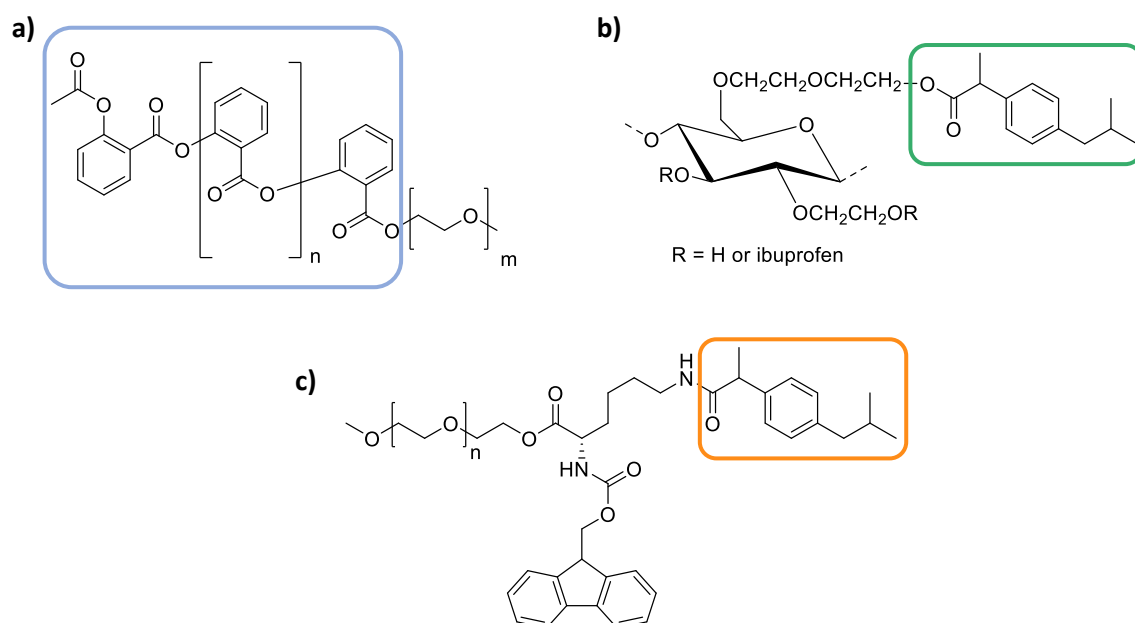
Fig. 2.17. examples of polymer-drug conjugates containing NSAIDs. a) PSA-PEG synthesised by Serpell *et al.*[62]; b) HEC-ibuprofen conjugate synthesised by Edgar *et al.*[63]; c) PEG-Fmoc-ibuprofen conjugate for the delivery of PTX prepared by Guo *et al.*[59]

Polymer-drug conjugates of NSAIDs are also present in literature. Guo *et al.*[59] prepared a polymer carrier for the anticancer drug paclitaxel (PTX) based on a PEG chain consisting of ibuprofen and Fmoc covalently linked via amide bond. In this case the NSAID drug was introduced as the COX inhibitor, while PTX was playing the role of the anticancer agent. Polysaccharides have also been used as drug carriers[64]. An example is the polymer-drug conjugate prepared by Edgar *et al.*[63] via the esterification of ibuprofen with hydroxyethylcellulose (HEC) which possesses hydrophilic properties. The prodrug system showed slow release of ibuprofen by hydrolysis of the ester bond, meaning that the release was long enough to minimise the stomach exposure. Moscatelli and co-workers[65], instead, prepared NPs derived by the conjugation of ibuprofen to different types of methacrylates via ester bond in order to obtain pH-responsive drug carriers. The NPs were prepared by emulsion polymerisation in water. The emulsion was capable of loading enough drug so that a small quantity of the drinkable formulation would be required in order to reach the minimum therapeutic dose of ibuprofen (200 mg). Serpell *et al.*[62] developed a novel prodrug system where the polymer backbone consisted only of salicylic acid. The so formed polysalicylate (PSA) conjugated

to PEG could form NPs that under specific physiological conditions could slowly release salicylic acid. In this way the need of a polymer backbone for the conjugation of the drug was eliminated. Figure 2.2 shows some of the aforementioned polymer-NSAIDs conjugates.

2.1.4. Aim of the study

Taking into consideration the potential role of NSAIDs as therapeutic agents for the treatment of different type of cancers, novel polymeric NPs were synthesised in this project. The aim was to prepare polymer-drug conjugates of NSAIDs, namely ibuprofen. To achieve this, the ring opening metathesis polymerisation (ROMP) was used in order to obtain polymers with controlled length and composition. Amphiphilic block copolymers containing ibuprofen and PEG, as the hydrophobic core and the hydrophilic corona components, were synthesised and then self-assembled in aqueous environment in order to obtain NPs of different morphologies. The drug release of ibuprofen from polymeric NPs was studied *in vitro* using both physiological and alkaline conditions. Figure 2.3 shows a schematic representation of the work done in this project.

PEG(OMe)
Ibuprofen (Ibu)

Self-assembly
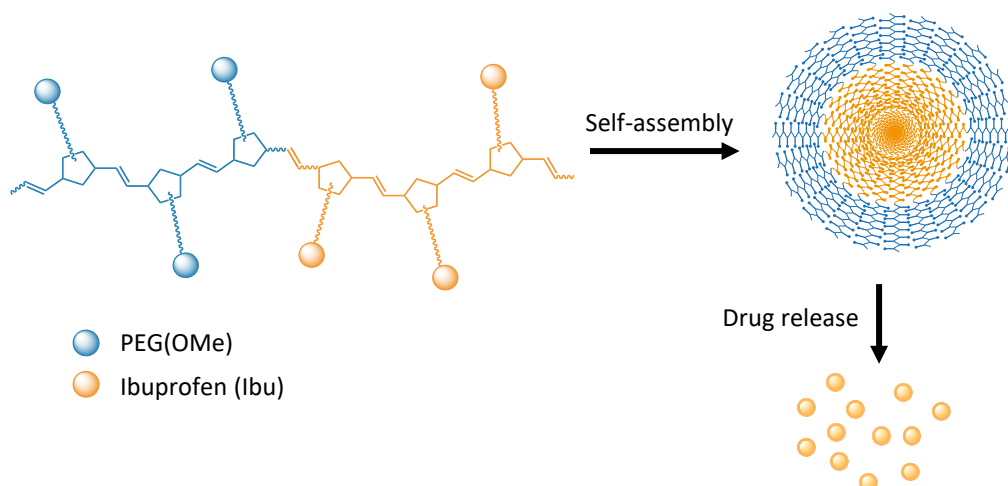
Drug release

Fig. 2.18. Schematic representation of an amphiphilic block copolymer which undergo self-assembly forming spherical aggregates. Under precise condition these polymeric NPs can release the chemotherapeutic drug.

The work carried out in this chapter was peer-reviewed and published in Materials Today Communications[66].

2.2. Results and discussion

2.2.1. Monomer synthesis

The monomers required to obtain the desired ROMP homopolymers and copolymers were not commercially available and therefore they were synthesised as shown in the following sections. The selected monomers contained a norbornene system connected to a specific moiety, such as an NSAIDs drug or a poly(ethylene glycol) chain, through a linker. It is known from literature that the linker/side chain can affect the rate of the ROMP polymerisation and that the *exo* isomers react faster than the *endo* isomers[67,68]. For this reason, *exo* monomers were synthesised and used for the preparation of ROMP polymers. However, the corresponding *endo* isomers were also prepared as these were more readily available and useful to optimise reaction conditions for the synthesis of drug conjugates but were not polymerised.

2.2.1.1. Synthesis of Ibuprofen based norbornene monomer (NB-Ibu)

Scheme 2.1 shows the synthetic pathway used to prepare both *endo-* and *exo-* ibuprofen based norbornene monomers (NB-Ibu) **5a** and **5b** respectively. The first step (I) was the thermal isomerisation of *endo*-carbic anhydride **1a** to *exo*-carbic anhydride **1b**[69]. The *endo* adduct **1a** was heated neat, with no solvent, at 180 °C using a heating mantle for 2 hours followed by purification of the crude product by recrystallisation with toluene. This afforded the *exo* adduct **1b** with a yield of 14 %. The low yield was mainly due to the incomplete conversion of the *endo* adduct to the *exo* one; typically, only > 55 % of *exo* is formed at the end of the reaction (determined by GC)[69]. Therefore, repeated recrystallisation were required in order to obtained *exo*-carbic anhydride **1b** with a purity > 95 %. Within our group, it was experimentally determined that *endo*-carbic anhydride was 2.4 times more soluble in toluene then its *exo* isomer (0.1 mg/mL and 0.04 mg/mL respectively; experiments were conducted by Lee Birchall at the University of Kent). The mechanism of the reaction involved the retro Diels Alder of the *endo* adduct at high temperatures, forming cyclopentadiene and maleic anhydride. The so formed diene and dienophile reacted together in a

[4 + 2] cycloaddition affording the thermodynamically stable *exo* adduct. However, because the *endo* isomer is the kinetically favoured product and due to the reversible nature of the isomerisation, a large amount of *endo* was still present at the end of the reaction. Many research groups[70,71,72] carried out the recrystallisation of the crude product using benzene, however, due to its toxicity, in our research group it was decided to use toluene. It is worth noting that under standard Diels Alder conditions, the *endo* adduct is preferentially formed due to the frontier molecular orbital interaction and the stabilisation between p-orbitals in the C=O of maleic anhydride and those in the C=C bonds of cyclopentadiene[73]. Furthermore, as demonstrated by Sakata and Fujimoto[73], the transition state (TS) of the *endo* adduct is 1.9 kcal/mol lower than the TS of the *exo* adduct, making the *endo* isomer to be the major product (kinetically favoured product). However, the *exo* isomer is 0.5 kcal/mol more stable than the *endo* isomer (thermodynamically favoured product). Therefore, when thermal conditions are used, enough energy can be given to the reaction to go through the higher activation energy barrier and thus the *exo* adduct is formed as the major product.

Scheme 2.4. Synthetic pathway for the preparation of *endo* and *exo* ibuprofen containing norbornene monomers **5a** and **5b**.

In the second step (II), as shown in Scheme 2.1, compounds **1a** and **1b** were reacted with 1 eq of 5-amino pentanol **2** in a condensation reaction where triethyl amine was used in catalytic amounts[74]. The reaction afforded the alcohol derivatives **3a** and **3b** with a yield of 98 % and 71 % respectively. The lower yield for compound **3b** was caused by a loss during the work up conditions. No purification through column chromatography was performed in this step. In the third step (III), the Steglich esterification of compounds **3a** and **3b** respectively with ibuprofen **4** was carried out using EDC (N-ethyl-N'-(3-dimethylaminopropyl)carbodiimide) as the coupling agent and DMAP (dimethylamino pyridine) as catalyst[75]. Compounds **5a** and **5b** were obtained both as a colourless oil after purification by column chromatography (EtOAc/PET 2:3) with a yield of 43 % and 73 % respectively.
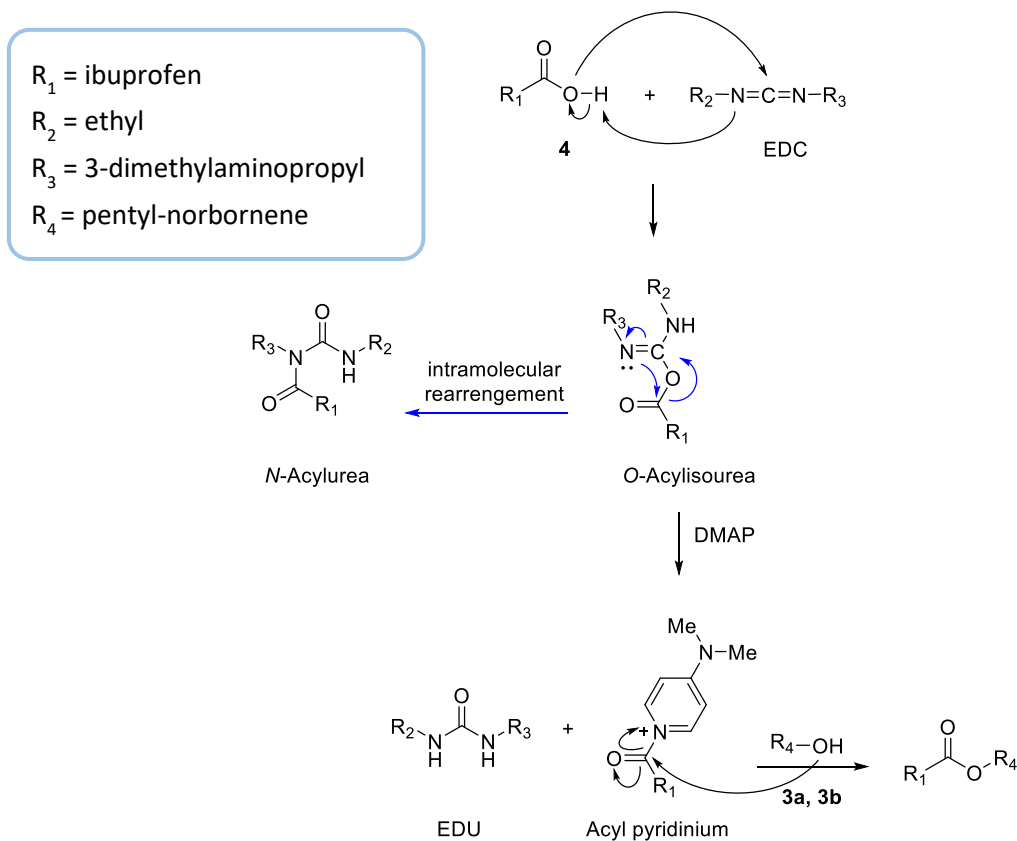
Fig. 2.19. Mechanism of the Steglich esterification between compounds **3a/3b** and compound **4**.

The mechanism of the Steglich reaction[75] (Figure 2.4) involved the initial reaction between the carboxylic acid **4** and EDC to form the O-acylisourea intermediate which then reacted with

DMAP to form an acyl pyridinium species. The latter then reacted with the alcohol derivatives **3a** and **3b** to form the desired esters **5a** and **5b**. Amines are better nucleophiles compared to alcohols so in this reaction DMAP is usually introduced to avoid the formation of the *N*-acylurea byproduct via intramolecular rearrangement of the *O*-acylisourea intermediate (Figure 2.4). At the end of the reaction EDU (1-[3-(dimethylamino)propyl]-3-ethylurea) was formed. Thanks to its high solubility to water, it was very simple to remove it from the reaction mixture using a H_2O/EtOAc extraction.

2.2.1.1.1. Gas chromatography and ^1H NMR of *endo-* and *exo*-carbic anhydride

Gas chromatography (GC) was used to determine the formation of *exo*-carbic anhydride **1b** and its purity after each recrystallisation. Each sample was prepared at a concentration of 1 mg/mL in DCM. 1 µL of sample was injected (speed of 50 µL/s and pre injection delay of 500 ms) into a Split inlet heated to 250 °C (split flow was set to 10 mL/min). Helium was used as the inert mobile phase with a flow rate of 1 mL/min. The oven was initially heated to 60 °C and then brought to 325 °C, while a capillary column (Phenomenex ZB-5MSPlus, 20 m length and 180 µm diameter) was used and the maximum temperature set to 325 °C.

GC was first run on the *endo*-carbic anhydride **1a** which was purchased from Acros Organics with 99 % purity. Under the conditions mentioned above, it was determined that compound **1a** eluted from the column at 3.11 minutes. Consequently, by peak comparison, it was simple to determine the formation of the *exo* adduct **1b** during the reaction. Furthermore, by integration of the area underneath each peak it was possible to determine the *endo*:*exo* ratio, and hence the purity of the *exo* adduct. Table 2.1 summarises the results obtained by GC for the pure *endo*, the crude product and first, second and third recrystallisation. As shown in this table, while *endo* possessed a retention time (RT) of ~ 3.11 minutes, the *exo* isomer eluted from the column at a slightly lower RT of ~ 2.95 minutes. After thermal isomerisation of compound **1a**, the crude product contained an *exo*:*endo* ratio of 83:17, hence *exo* was formed as the major product. After each

recrystallisation it was possible to remove the *endo* adduct and to obtain compound **1b** with a purity of 98 %. Chromatograms are shown in Figures S61 – S65, Appendix 1.

Table 2.2. Overview of the GC data obtained for pure endo, crude product and recrystallisation steps.

	Peak[a]	RT (min)	Area (%)	*Exo* purity (%)[b]
Pure endo	1	-	-	-
	2	3.106	100.0	
Crude product	1	2.952	100.0	83
	2	3.059	20.9	
1st recrystallisation	1	2.964	100.0	93
	2	3.092	7.24	
2nd recrystallisation	1	2.958	100.0	96
	2	3.077	4.24	
3rd recrystallisation	1	2.970	100.0	98
	2	3.092	2.49	

[a] peak 1 refers to the *exo* adduct, while peak 2 refers to the *endo* adduct. [b] The % of *exo* in the sample was calculated as the area % of *exo* divided by the total area % (area % of *exo* + area % of *endo*).

^{1}H NMR spectroscopy was also used to monitor the progress of the *endo/exo* isomerisation and to determine the purity of **1b**. This is shown in Figure S38, Appendix 1. The ^{1}H NMR spectra of *endo-* and *exo*-carbic anhydride are discussed and compared to each other (Figure 2.5). Carbic anhydride is a symmetrical molecule, therefore five main protons can be identified. In order to assign each proton to each peak in the ^{1}H NMR spectrum, COSY NMR was run and obtained. The alkene proton 1, is the easiest to assign as it is well known that alkene protons are deshielded as a result of the π-bond. Proton 1 is, thus, found to be a triplet in both **1a** (red spectrum) and **1b** (blue spectrum) at 6.33 ppm and 6.34 ppm respectively. In the *endo* adduct, protons 3 and 4 are two multiplets at 3.52 ppm and 3.59 ppm respectively. However, the same protons 3 and 4 in the *exo* isomer are a triplet at 3.46 ppm and a doublet at 3.01 ppm. Therefore, the proton's coupling and the chemical shift are affected by the configuration of the two isomers. Due to the rigidity of bicycle ring, the bridgehead protons 2' and 2" are in chemically different environments and thus two distinguished peaks are obtained[76]. The bridgehead protons are indeed geminal protons and give rise to an AB system where the two protons couple with each other and hence two doublets are obtained (AB-type quartet). Because the difference of frequencies Δν between the nuclei is not high

enough compared to the coupling constant J ($\Delta v < 10\,J$), *second order* spectra are obtained. This leads to the observation of the "roofing effect" where the intensity of the internal peaks is greatly enhanced, while the intensity of the outer peaks becomes smaller (see Figure 2.5). The coupling constant for the AB system ($J_{2'-2''}$) is calculated and found to be 9.3 Hz for **1a** and 8.7 Hz for **1b**. In the *endo* isomer, the bridgehead protons are slightly deshielded compared to the *exo* ones. In both cases a doublet of triplets and a broad doublet are obtained at 1.81/1.58 ppm and 1.67/1.45 ppm respectively for compound **1a** and **1b**. From COSY NMR it is found that proton 2' couples with 2" and 3, resulting in a doublet of triplets. Proton 2" is found to couple with 2', 3 and 1 (long range coupling), however because the coupling constants $J_{2''-3}$ and $J_{2''-1}$ are relatively small, only a broaden doublet can be observed. The integration for each peak is also obtained and as expected each peak integrates for 2H due to the symmetry of the molecule, excluding protons 2' and 2" which integrate for 1H each.
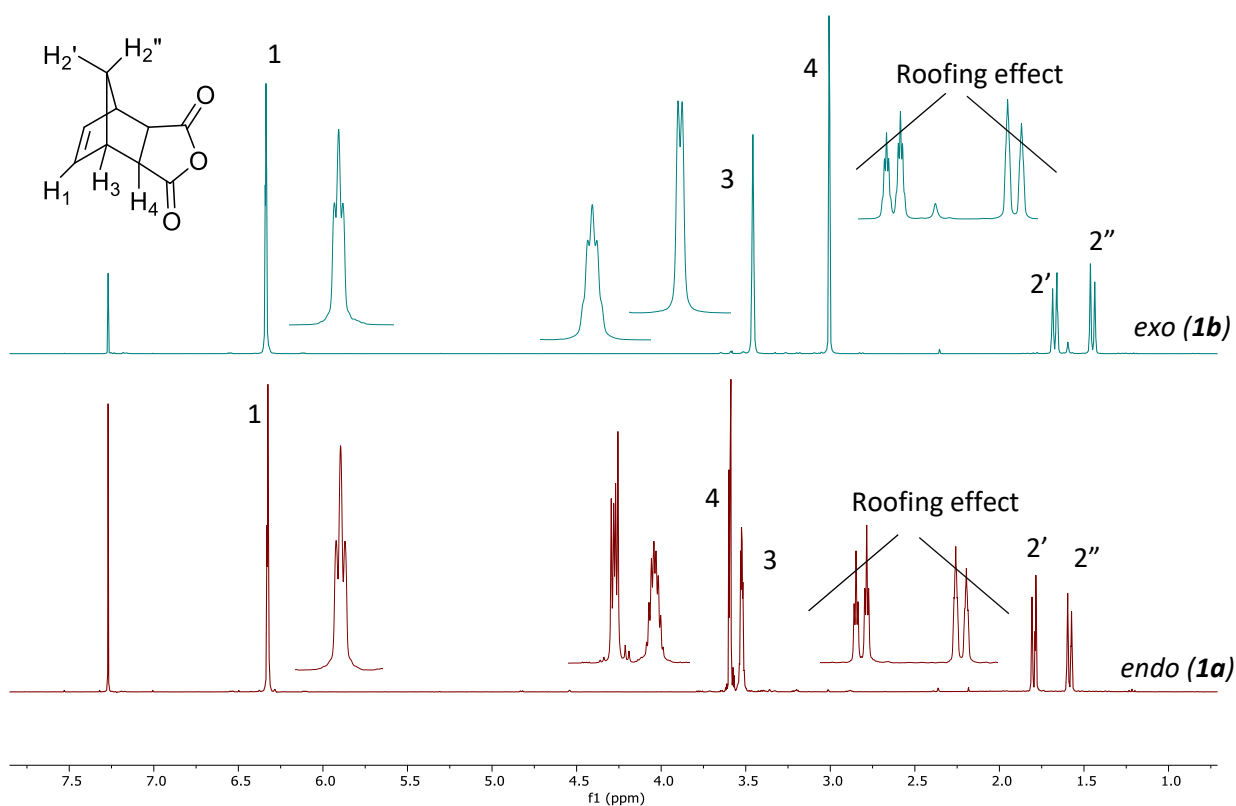
Fig. 2.20. ^{1}H NMR in CDCl$_3$ of *endo*-carbic anhydride **1a** (red spectrum) and *exo*-carbic anhydride **1b** (blue spectrum).

Formation of *endo* and *exo* compounds **3** and **5** was confirmed by ^{1}H NMR. Figure 2.6 shows the comparison of ^{1}H NMR spectra between compounds **3a** and **3b**. As noted, the stereoisomerism affects the chemical shift and multiplicity of each proton within the two compounds. The alkene proton 1 in the *endo* isomer **3a** is a triplet at 6.09 ppm, while in the exo isomer **3b** the same proton is found to be shifted downfield at 6.29 ppm. Interestingly, the resonance of protons 3 and 4 in **3a** are switched in comparison to its starting material **1a** (red spectrum, Figure 2.5): proton 3 is shifted downfield at 3.39 – 3.36 ppm, while proton 4 is shifted upfield at 3.24 – 3.23 ppm. This behaviour is not seen in the *exo* isomer **3b**, where protons 3 and 4 retain the same sequence of their starting material **1b**, while being shifted downfield due to the proximity of the N atom (3.27 ppm and 2.68 ppm for protons 3 and 4 respectively). Protons 6 and 10 in the alkyl chain are easy to identify as each of them only couple with two protons (protons 7 and 9 respectively) forming two triplets. Proton 10 is shifted upfield due to the proximity to the -OH group (3.60 ppm and 3.64 ppm in compound **3a** and **3b** respectively). Proton 6 is shifted downfield as it is close to the less electronegative N atom (3.33 ppm and 3.48 ppm in compound **3a** and **3b** respectively). The remaining alkyl protons 7, 8 and 9 should form three distinguished doublets of triplets (or quintets) as each of them couples with two chemically different CH_2, however, in both **3a** and **3b**, they form multiplets in the range between 2 ppm and 1 ppm, and in some cases tend to coalesce to each other as well as with the bridgehead protons 2' and 2". The latter are more easily individualised in **3b** than **3a** (see Figure 2.6).
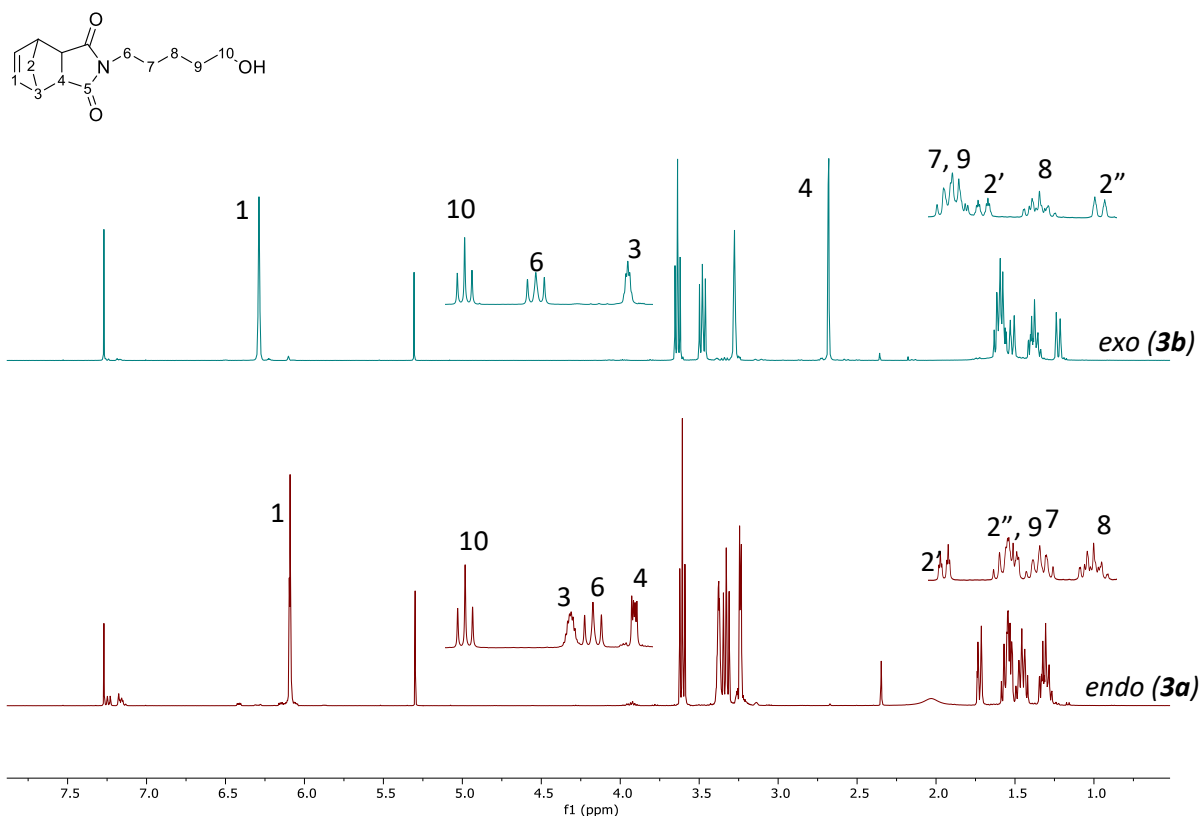
Fig. 2.21. ^{1}H NMR spectra in CDCl$_3$ of compounds **3a** and **3b** with compound structure and carbon numbering.

Compounds **5a** and **5b**, NB-Ibu monomers, were obtained by coupling compounds **3a** and **3b** with ibuprofen **4**. Consequently, the ^{1}H NMR spectra for these compounds is very similar to the spectra obtained for their alcohol derivatives **3a/3b** with the addition of the ibuprofen peaks. Figure 2.7 shows the ^{1}H NMR spectra of *endo* and *exo* NB-Ibu monomers. As expected, the addition of ibuprofen to **3a/3b** slightly changes the chemical shift of protons 1 – 10 but does not affect the multiplicity, except from proton 10 for which, in both **5a** and **5b**, a triplet of doublets is obtained. This might be due to a long range coupling with proton 12 caused by the mobility of the alkyl chain. In the aromatic region, two peaks are found: protons 15 and 16 form two doublets at 7.18 ppm and 7.08 ppm in compound **5a** and at 7.19 ppm and 7.10 ppm in compound **5b**. Proton 12 couples with the CH$_3$ 13 forming a quartet at 3.67 ppm, while the coupling of 13 with 12 gives rise to a doublet at 1.48 ppm. Proton 18 couples with CH 19 forming a doublet at 2.43 ppm, proton 19 couples with (CH$_3$)$_2$ 20 forming a septet at 1.84 ppm whilst the coupling with 18 is not seen, and finally protons 20 couple with 19 giving rise to a doublet at 0.88 ppm. It is noted that the resonance of the

59

ibuprofen protons is the same for both *endo* and *exo* compounds. This is most likely due to the distance of the ibuprofen moiety in respect to norbornene ring.
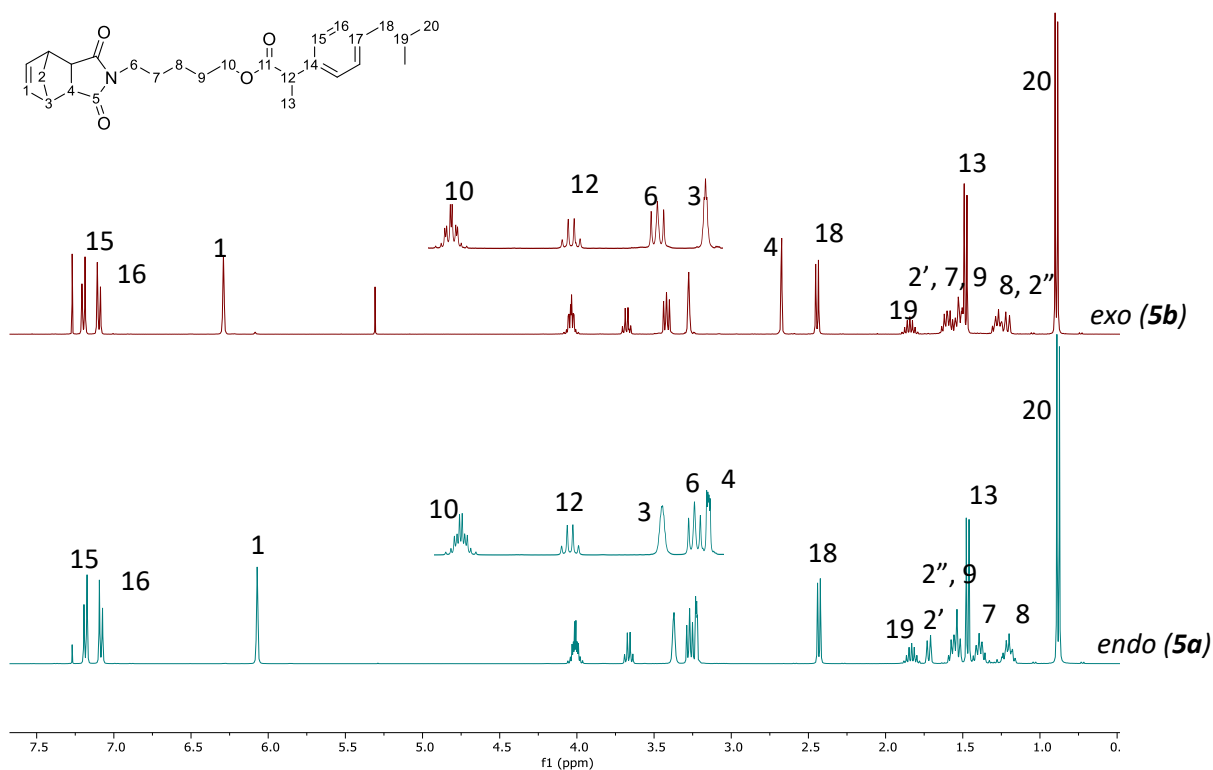
Fig. 2.22. ^{1}H NMR spectra in CDCl$_3$ of compounds **5a** (blue) and **5b** (red) with compound structure and carbon numbering.

2.2.1.2. Synthesis of PEG based norbornene monomer (NB-PEG)

As shown in Scheme 2.2, four steps were required to obtain the PEG based monomers **10a** (*endo*) and **10b** (*exo*). The first step (I) was the thermal isomerisation from *endo*-carbic anhydride **1a** to its *exo* form **1b** (description in Section 2.2.1.1). The second step (II) was the condensation of compound **1a** and **1b** respectively with glycine **6**, that afforded the pure *endo*- and *exo*-glycine derivatives **7a** and **7b** after recrystallisation from ethyl acetate[77] with a yield of 35 % and 49 % respectively. To obtain a better living group, compounds **7a** and **7b** were reacted (step III) with an excess of thionyl chloride, which was used both as a chlorinating agent and solvent[78]. This afforded the *endo*- and *exo*-glycinoyl chloride derivatives **8a** and **8b** with a yield of 91 % and 94 % respectively. These latter compounds were reacted in the last step (IV) with poly(ethylene glycol) methyl ether (PEG) (Mn =

550) **9,** in the presence of stochiometric Et$_3$N[77], in order to form the *endo* and *exo* monomers **10a**

and **10b** (NB-PEG) with a yield of 87 % and 86 % respectively. The so formed monomers would

confer water solubility to the polymer in due course.
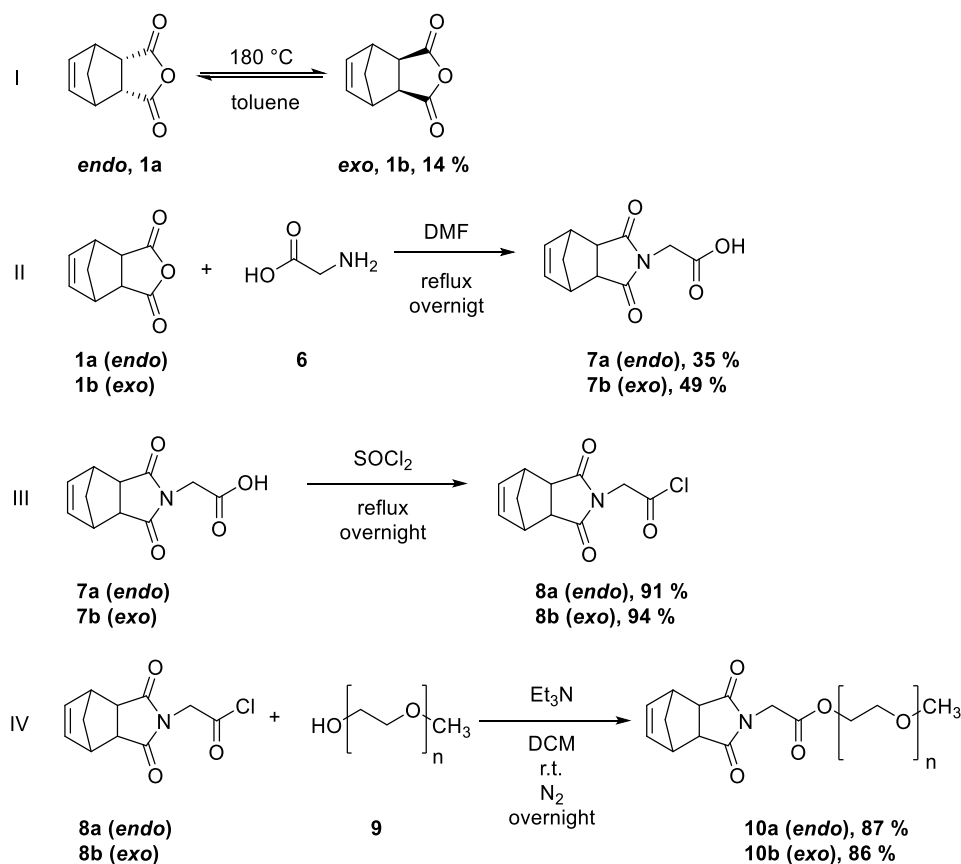
Scheme 2.5. Synthetic pathway for the preparation of PEG containing norbornenyl monomers, **10a** (*endo*) and **19b** (*exo*).

2.2.1.2.1. ^{1}H NMR of compounds 7, 8 and 10

As mentioned above, compounds **7a** and **7b** were obtained by the simple condensation of carbic

anhydride (**1a** and **1b**) with glycine **6**. Glycine is an amino acid of simple structure, consisting of only

one NMR relevant proton. This allow for an easy interpretation of the NMR spectra of compounds

7a and **7b**, as well as compounds **8a** and **8b**, which are the chlorinated version of the glycine based

norbornene. In Figure 2.8, blue spectrum, is shown the ^{1}H NMR spectrum of *exo*-glycine derivative

7b. This does not substantially differ from the *exo*-carbic anhydride (**1b**) spectrum (red spectrum,

Figure 2.5) in terms of multiplicity, while the chemical shift of each proton changes due to the

introduction of the glycine moiety. Proton 1 is a triplet at 6.31 ppm, protons 3 and 4 are shifted downfield at 3.32 ppm (triplet) and 2.78 ppm (doublet) respectively. Proton 6 is the CH$_2$ on the glycine which does not couple to any other protons in the molecule and therefore forms a singlet at 4.28 ppm. Interesting is instead the behaviour of the bridgehead protons 2' and 2". In the *exo*-carbic anhydride **1b** proton 2' is the most upfield between the two bridgehead protons and due to the coupling with 2" and the alkene proton 1, forms a doublet of triplets. However, in **7b**, proton 2' is found to be the most downfield, while proton 2" is the most upfield. This same behaviour does not occur on the *endo* isomer **7a** as shown in Figure S11, Appendix 1. It is not entirely clear what caused the environments of the two protons to "flip", but this is not of importance for confirming the formation of compound **7b**.
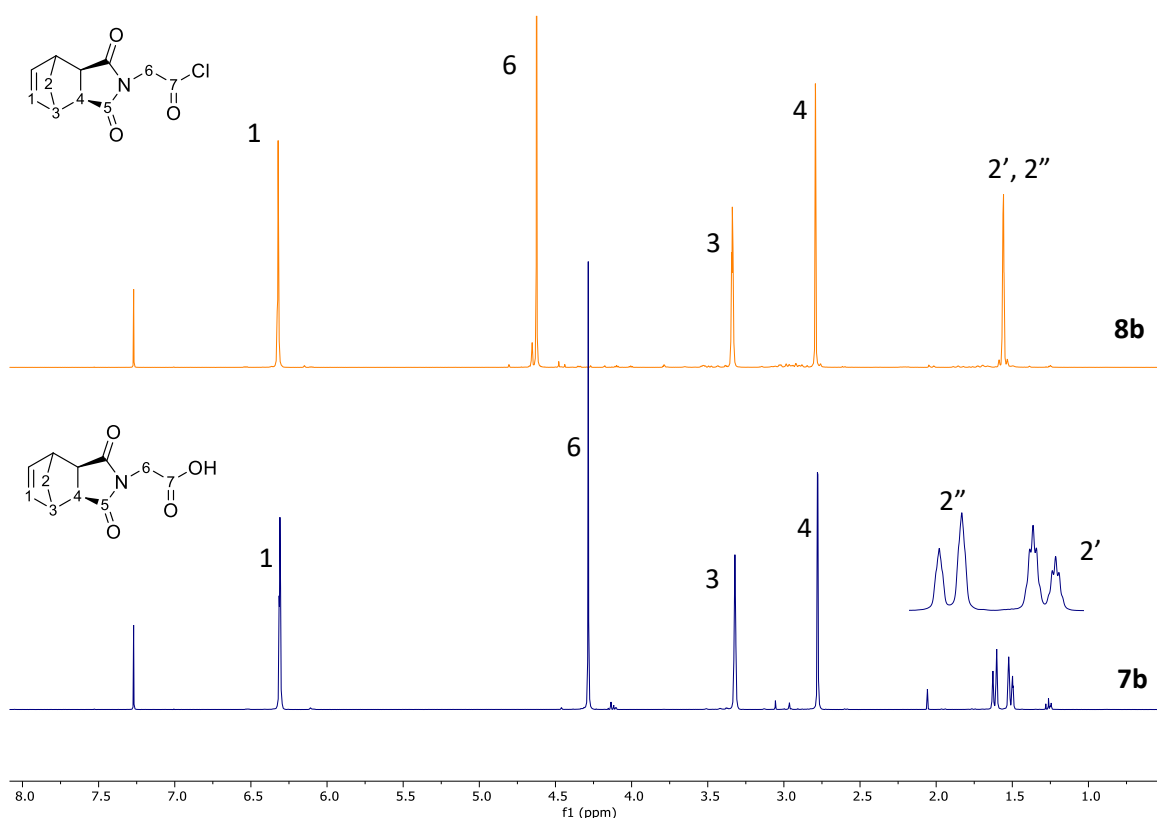
Fig. 2.23. ^{1}H NMR spectra in CDCl$_3$ of *exo* **7b** (blue) and *exo* **8b** (orange). Compound structures are shown as well as carbon numbering.

As regards to the *exo*-glycinoyl chloride derivative **8b**, it is expected to obtain a very similar spectrum of **7b**, with a downfield shift of each proton caused by the introduction of a more

electronegative Cl atom. As shown in the orange spectrum in Figure 2.8, this effect is most seen on proton 6 which is the closest to the Cl. The chemical shift of proton 6 goes from 4.28 ppm in **7b** to 4.62 ppm in **8b**. This can be enough for confirming that compound **8b** has been successfully obtained. Interestingly, the addition of Cl has an effect on the bridgehead protons, which coalesce together forming a broad singlet at 1.56 ppm. This effect is however not seen on the *endo*-glycinoyl chloride derivative **8a**, as shown in Figure S15, Appendix 1.
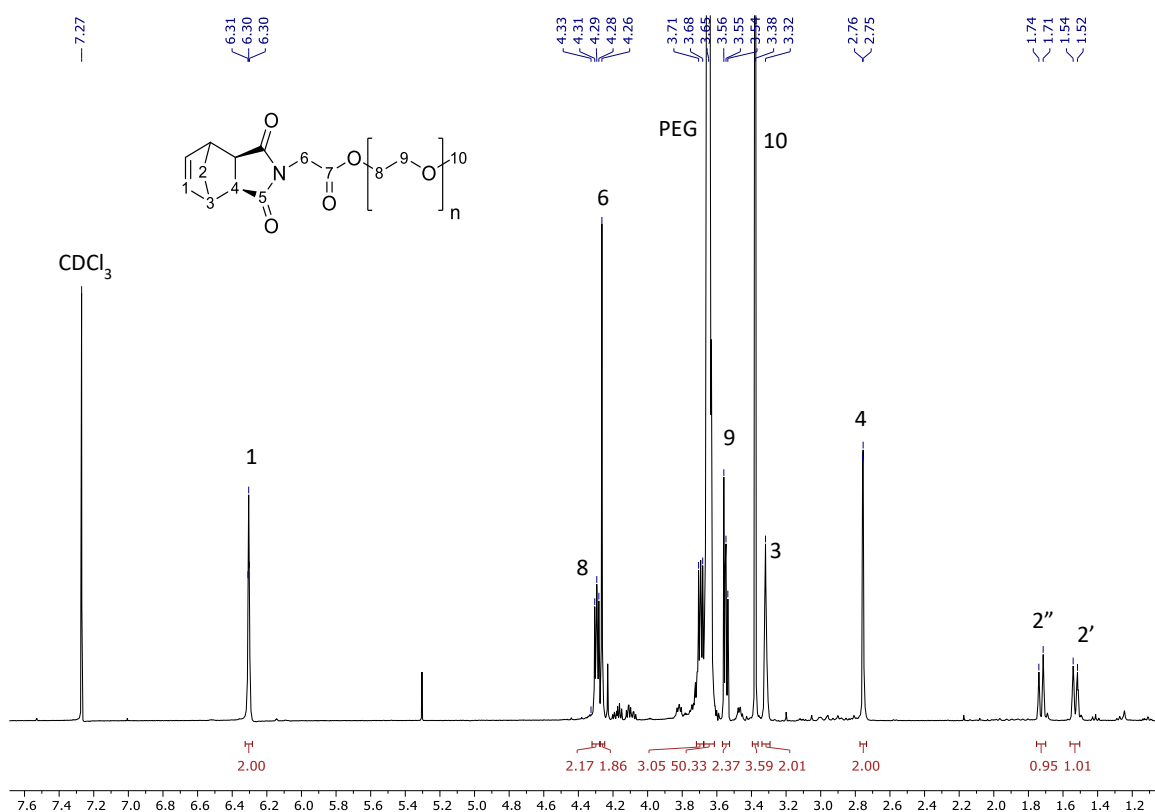
Fig. 2.24. ^{1}H NMR in CDCl$_3$ of monomer **10b**. Structure and numbering is also shown.

The reaction of **8a** and **8b** with PEG-methyl ester **9** afforded monomers **10a** and **10b**, where the *exo* isomer **10b** (NB-PEG) was the one used for the following polymerisations. Figure 2.9 shows the ^{1}H NMR spectrum of compound **10b**: in this case, the chemical shift of protons 1 – 6 appears to be the same of compound **7b**, although the bridgehead protons are slightly shifted downfield in **10b**. The selected PEG for this reaction possesses a molecular weight of 550 g/mol, meaning that it is consisting of about 12 ethoxy repeating units. As a result, the NMR spectrum present a broad and

very intense peak at 3.65 ppm which integrates for 48H: two CH_2 (protons 8 and 9) multiplied by 12 repeating units. However, it is still possible to identify two multiplets that integrates for 2H each at both sides of the PEG peak. These are protons 8 and 9 at both extremities of the PEG polymer chain (4.29 ppm and 3.55 ppm respectively). At 3.38 ppm there is a singlet that integrates for 3H and it is identified as proton 10, the CH_3 group at the end of the PEG chain. The ^1H NMR of its *endo* isomer **10a** is shown in Figure S19, Appendix 1.

2.2.1.3. ESI-MS analysis of NB-Ibu and NB-PEG monomers and their intermediates

The formation of NB-Ibu (**5b**) and NB-PEG (**10b**) monomers and their intermediates was also confirmed by liquid chromatography mass spectroscopy (LC-MS). In this case the electrospray ionisation (ESI) source was used. ESI is a soft source of ionisation, which means that no fragmentation occurs, therefore determination of the molecular ion is possible[79]. For each compound the ESI in the positive mode was used, therefore the compounds were ionised so that they acquire a positive charge (either H^+ or Na^+).

Table 2.3. Low resolution ESI-MS results obtained for compounds **3b**, **5b**, **7b** and **10b**.

	m/z [M+H]$^+$	
	Theoretical	Actual
3b	250.1	250.2
5b	438.3	438.2
7b	244.1	244.1
10b	742.58	742.4

Table 2.2 summarises the mass/charge (m/z) ratio results obtained for compounds **3**, **5**, **7** and **10**. These values are not affected by the stereoisomerism of *endo* and *exo*, therefore only the results for the *exo* isomers were recorded. Compound **8** could not be analysed by ESI-MS as it is readily hydrolysed to its glycine form **7**. Whilst for compounds **3b**, **5b** and **7b** it was possible to obtain a simple m/z spectrum mainly consisting of one peak (Figures S41 – S43, Appendix 1), this could not be obtained in the case of the NB-PEG monomer (**10b**). As shown in Figure 2.10 (b), the

m/z spectrum for **10b** consists of a series of peaks with different *m/z* ratio and different intensity, which are placed so that they form a Poisson distribution of the *m/z*. This is the typical spectrum found in polymers, due to the fact that polymers never exist as only one polymer chain, but they rather exist as a distribution of polymer chains with different lengths. When PEG was reacted with compound **8** to form **10**, a new polymer was formed and hence the *m/z* spectrum of **10b** followed the *m/z* spectrum pattern of a polymer. For clarity, this has been compared with the spectrum of PEG$_{550}$ (Figure 2.10, a).
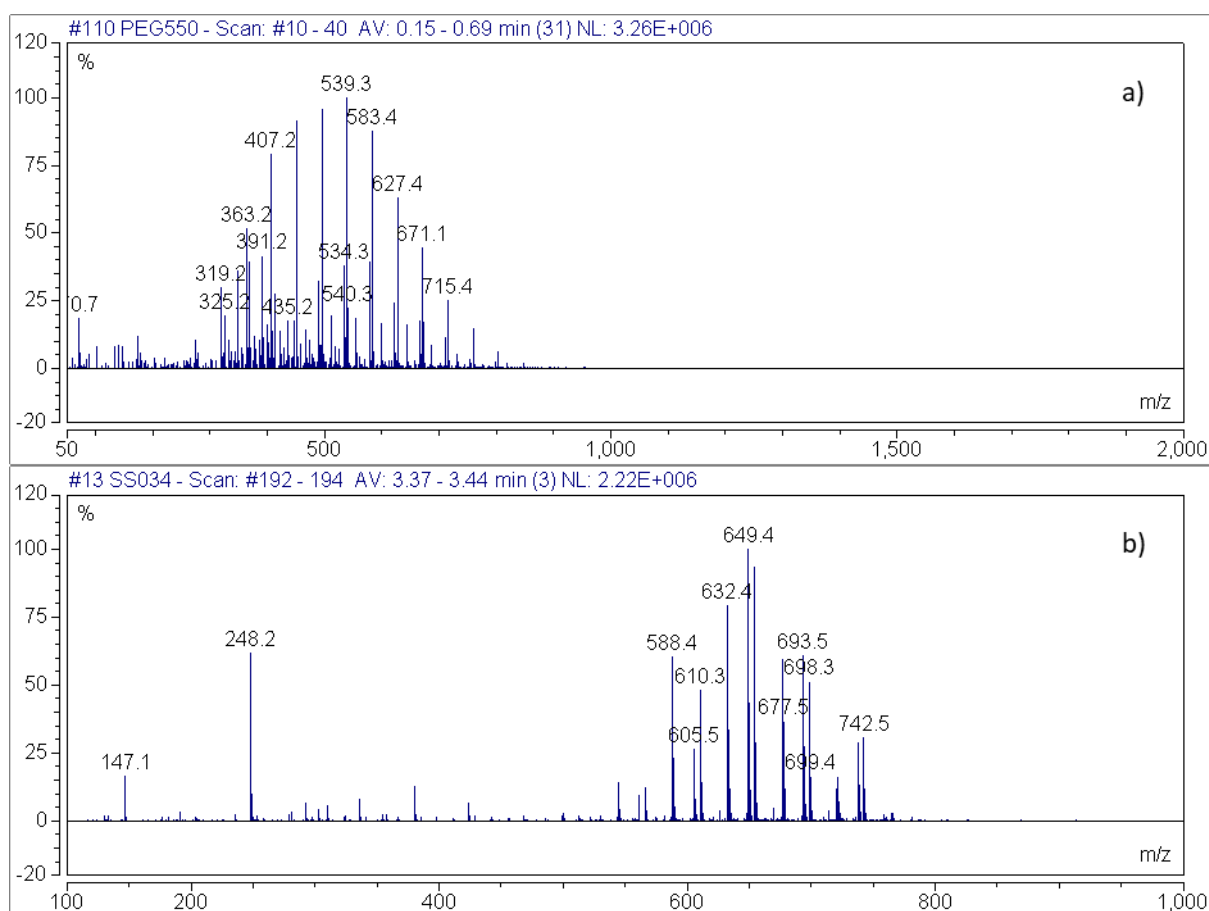
Fig. 2.25. Low resolution ESI-MS spectra of: a) PEG (M$_n$ = 550) and b) NB-PEG monomer (**10b**) in comparison.

2.2.2. Polymers synthesis

As shown in Scheme 2.3, monomers **5b** (NB-Ibu) and **10b** (NB-PEG) were polymerised using the commercially available 3rd generation Grubbs catalyst (H$_2$IMes)(3-bromopyridine)$_2$-(Cl)$_2$Ru=CHPh (**G3**), in anhydrous DCM using ethyl vinyl ether as terminating agent. The resulting homopolymers,

poly5b and **poly10b**, were then purified by precipitation with diethyl ether affording sticky brown solids in high yield, 98 % and 92 % respectively[77]. In both cases, the polymerisations were carried out using a ratio monomer to catalyst [M]/[C] of 20:1 and at a monomer concentration of 0.045 M. From kinetic studies, it was determined that both monomers polymerised to completion in less than 10 minutes.
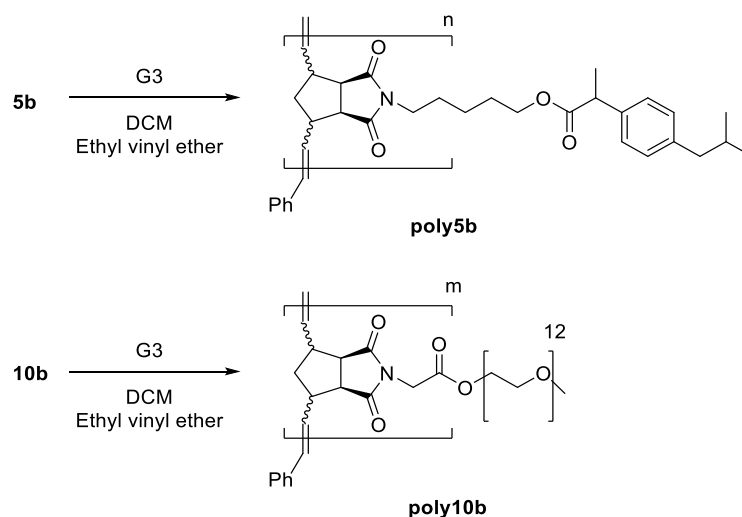
Scheme 2.6. Homopolymerisation of monomers **5b** and **10b** to afford homopolymers **poly5b** and **poly10b** respectively.

To obtain the block copolymer **poly5b-b-poly10b**, the NB-Ibu monomer **5b** was firstly polymerised using a ratio [M]/[C] of 20:1 and dry DCM as solvent. After 10 minutes an equimolar quantity of NB-PEG monomer **10b** was added to the reaction mixture giving an overall ratio [M]/[C] of 40:1. Statistical copolymer **poly5b-co-poly10b** was prepared by adding both monomers (1:1 molar ratio) at the same time, to a solution of **G3** in anhydrous DCM. In each case the polymerisation was terminated by adding few drops of ethyl vinyl ether to the reaction mixture and block and statistical copolymers were purified by precipitation with diethyl ether (Scheme 2.4).
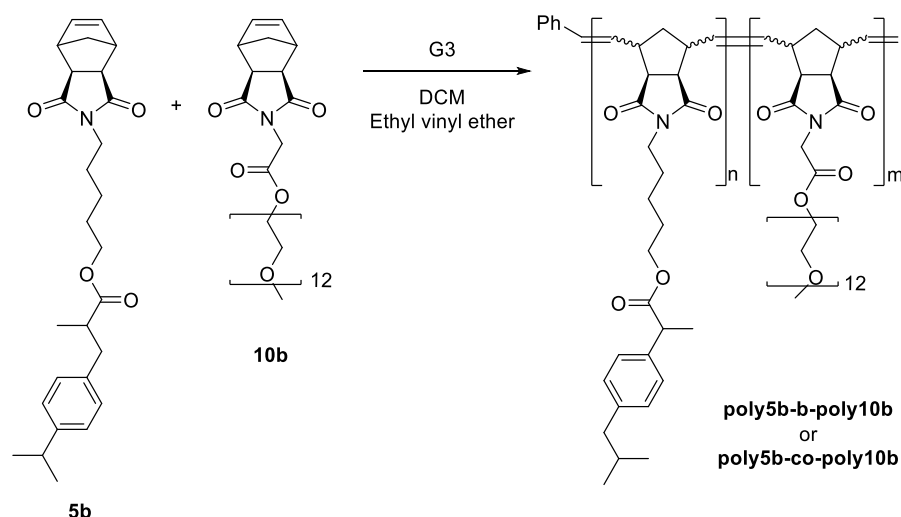
Scheme 2.7. Block and statistical copolymerisation of monomers **5b** and **10b** to afford **poly5b-b-poly10b** and **poly5b-co-poly10b** respectively.

2.2.2.1. ^{1}H NMR of homo- and co-polymers

NMR spectroscopy was one of the analytical methods used to determine the success of the polymerisation. The most important characteristic of a polymer ^{1}H NMR spectrum is the broadening of the peaks. This is mainly due to poor molecular rotation as well as repeating units being situated in marginally different chemical environments. This means that, the same proton placed in different repeating units possess a slightly different chemical shift leading to an apparent broadening of the peak.

Figure 2.11 shows the ^{1}HNMR spectra of the ibuprofen and PEG containing homopolymers, **poly5b** and **poly10b**. The polymerisation of **5b** and **10b** was successful as demonstrated by the broadening of the peaks. As noted, the ^{1}H NMR spectra of both homopolymers do not differ too much from their monomer spectra. Especially, the chemical shift of the protons in the ibuprofen and PEG moieties is not altered by the formation of a polymer chain as expected. Therefore, these protons can be easily assigned by comparison with their monomer spectrum. However, few changes in the norbornene proton resonances can be detected. As mentioned in Chapter 1 (Section 1.2.2.4), during ROMP, a metallacyclobutane intermediate forms between the alkene bond in the norbornene ring and the metal alkylidene complex (**G3**). This eventually opens via a [2 + 2]

67

cycloreversion forming two new double bonds that connect each repeating unit along the polymer backbone. This effect is seen in the ^{1}H NMR spectra of polymers by the disappearance of the typical triplet at 6.3 ppm (alkene peak in the monomer) and the appearance of two broad peaks between 6.0 ppm and 5.0 ppm in the polymer spectrum. The formation of two broad peaks is attributed to the presence of both *cis* and *trans* double bonds (proton 1) along the polymer backbone. The polymerisation is not stereospecific in the reaction conditions used, therefore, the formation of either *cis* or *trans* double bonds is not controlled. In fact, the selectivity towards *cis* or *trans* varies significantly with catalyst[80], monomer, solvent[81] and temperature[82] used. In addition to the changes in proton 1, the bridgehead protons 2 are also affected by the formation of the polymer chain. While in the monomers the bridgehead protons are found to be in chemically different environments, in the polymer this should not be the case and protons 2 should be seen as one peak that integrates for 2H. However, the NMR spectrum of **poly10b** still shows two distinct peaks at 2.16 ppm and 1.58 ppm each of them integrating for 1H. These are found to be slightly deshielded in comparison to protons 2 in monomer **10b**. Different is the case of **poly5b**, where the bridgehead protons are now found to be as one peak at 3.0 ppm with integration of 2H. Therefore, the change in the chemical environment of the bridgehead protons is dependent on the type of monomer used.

The ^{1}H NMR spectra of block and statistical copolymers (**poly5b-b-poly10b** and **poly5b-co-poly10b**) shown in Figure S27 and S29, Appendix 1, also demonstrated that the co-polymerisations were successful. Since monomers were added into the reaction mixture in a 1:1 molar ratio, the ^{1}H NMR spectra offered a straightforward interpretation. The formation of the polymer backbone was confirmed by the broadening of the peaks and by the presence of the *cis/trans* peaks between 6.0 ppm and 5.0 ppm. Furthermore, both ibuprofen and PEG peaks were present, and their integration was in a 1:1 ratio as expected. However, by NMR spectroscopy it was not possible to distinguish between block and statistical copolymers and therefore the ^{1}H NMR spectra as well as the ^{14}C NMR spectra appeared to be indistinguishable between one another.
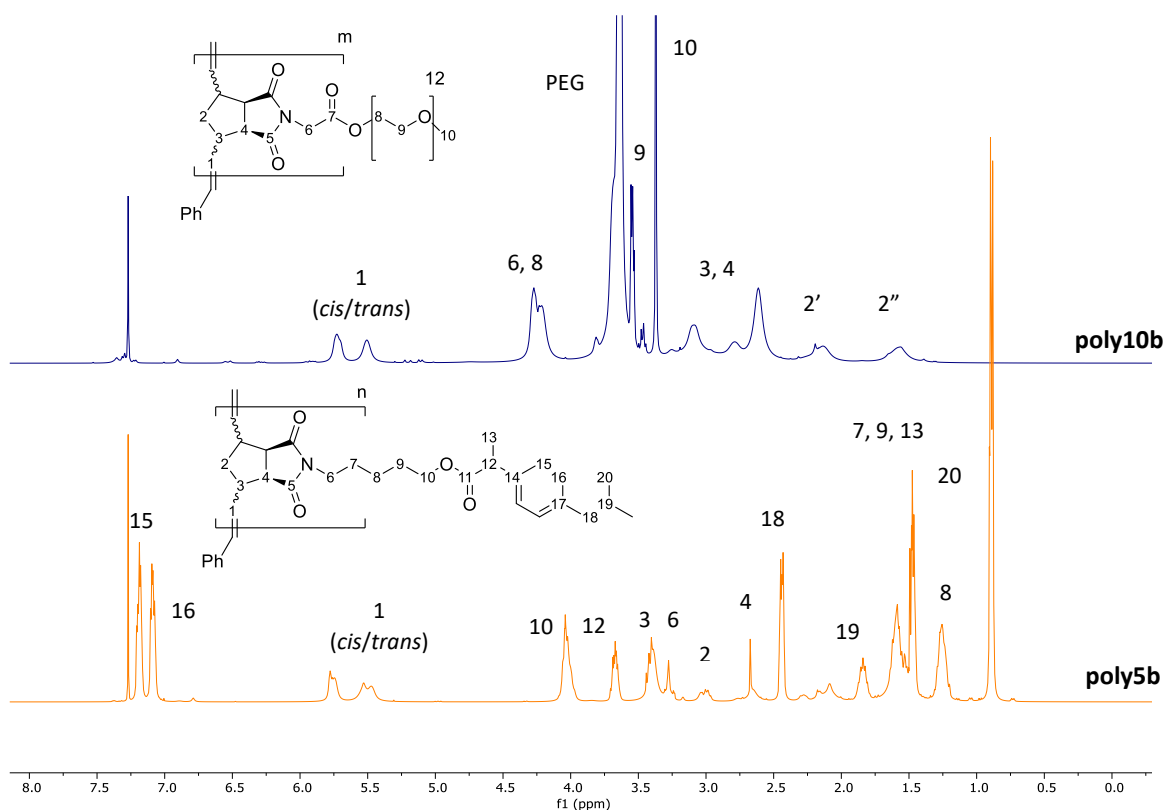
Fig. 2.26. ^{1}H NMR spectra of **poly5b** (orange) and **poly10b** (blue). Polymer structures and carbons numbering are also shown.

2.2.2.2. Quantitative ^{1}H NMR of copolymers

Although the co-polymerisations of **5b** and **10b** were carried out using an equivalent molar ratio of the two monomers, four different copolymers with different ratio of NB-Ibu and NB-PEG were obtained. Two of which were block copolymers and two were statistical copolymers. Since ROMP is a living polymerisation, copolymers with controlled length and composition are typically formed. Therefore, obtaining copolymers with non-consistent NB-Ibu/NB-PEG ratio is mainly caused by experimental errors during the weighing process.

The quantitative ^{1}H NMR spectroscopy (qNMR) has been widely used in both academia and industry for the absolute and relative quantification of multi-components in a mixture[83]. While in the absolute quantification an internal standard is used to determine the concentration and purity of an analyte of interest, in the relative quantification the internal standard is not introduced. In this case, integrals of interest are compared with one another allowing to measure accurate ratios

of different species in the same sample. Here, the qNMR was used to accurately determine the ratio of NB-Ibu and NB-PEG within the polymer backbone and eventually use it to determine the structure-activity relationship. In this experiment it was important that all of the signals had fully relaxed between pulses, therefore a relaxation delay d1 of 90 seconds was set up. As shown in Figure 2.12 (a), the peaks chosen are highlighted in orange and blue. The orange box is related to the aromatic protons 20 and 21 in the ibuprofen moiety, while the blue box corresponds to protons 6 and 8 in the PEG moiety (Figure 2.12, b). These were chosen as both integrated for 4H, but mostly because they did not overlap any other peak, allowing for accurate integration.
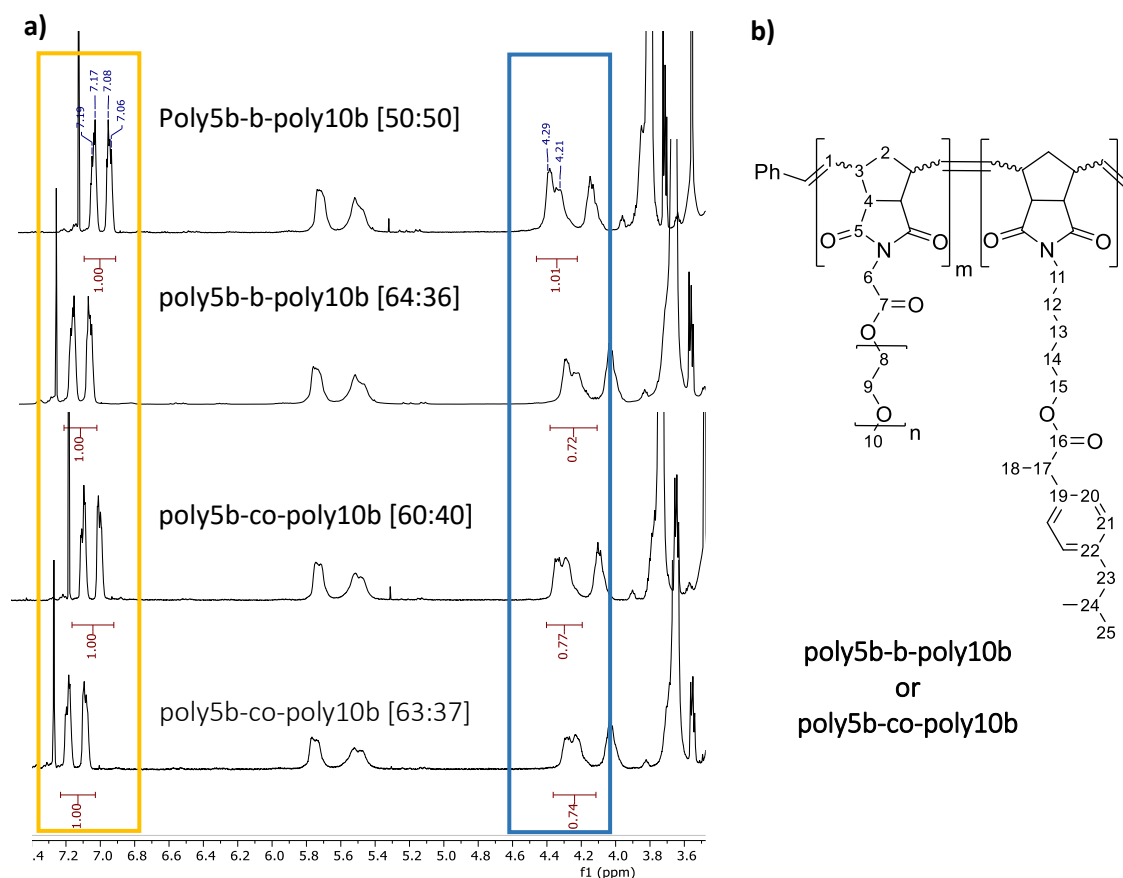
Fig. 2.27. a) qNMR of block and statistical copolymers. Protons 6/8 and 20/21 are integrated and compared to one another. b) Copolymer structure with carbons numbering.

As shown in Figure 2.12, two block copolymers **poly5b-b-poly10b** with 50:50 and 64:36 NB-Ibu/NB-PEG ratio were obtained, as well as two different statistical copolymers **poly5b-co-poly10b**

with 60:40 and 63:37 NB-Ibu/NB-PEG ratio were obtained (results are summarised in Table 2.4, Section 2.2.2.4).

2.2.2.3. Kinetic studies on homopolymerisation

The kinetic of ROMP polymerisation catalysed by ruthenium-based initiators **G1**, **G2** and **G3** has been widely studied over the years[84,85]. It is known from literature that the rate of living polymerisations follow a first order dependency on the monomer and the initiator[86]. This is also known as pseudo-first order kinetics, meaning that the polymerisation is second order overall, but it is first order in respect to monomer and catalyst. Because the concentration of the catalyst remains constant throughout the reaction, its consumption is so small that the change in concentration becomes negligible. The rate law for living polymerisations is therefore described as followed:

$$rate = k[M][C] = k'[M] \qquad \textbf{Eq. 2.1.}$$

where *k* is the rate constant, [M] is the concentration of the monomer, [C] is the concentration of the catalyst and *k'* is the new rate constant which includes the concentration of the catalyst.

Therefore, the rate of disappearance of the monomer, M, is:

$$\frac{d[M]}{dt} = -k'[M] \qquad \textbf{Eq. 2.2.}$$

To which it is possible to determine the pseudo first order equation:

$$ln\left(\frac{M}{M_0}\right) = -k't \qquad \textbf{Eq. 2.3.}$$

where *t* is the time, M_0 is the initial concentration of monomer and M is the concentration of monomer at time *t*.

In this project, ^{1}H NMR spectroscopy was used to study the kinetic of homopolymerisation of monomers **5b** (NB-Ibu) and **10b** (NB-PEG) and thus determine the rate of monomer conversion.

To a solution of monomer **5b** or **10b** in DCM with an initial concentration of 0.046 M, Grubbs 3rd generation catalyst was added. Aliquots of 50 µL were taken from the reaction mixture at predefined time points and then quenched with a solution of ethyl vinyl ether in DCM. The solvent was evaporated and $CDCl_3$ added in order to monitor the monomer to polymer conversion by ^1H NMR. Due to the low concentration of the NMR samples prepared, 1024 scans were used for each analysis. The so obtained spectra were baseline- and phase- corrected before integration of the peaks was carried out. The comparative integration of the alkene peak at ~ 6.3 ppm on the monomers and the *cis/trans* peak at 5.0 – 6.0 ppm on polymers, allowed for the determination of monomer conversion over time. These values were then converted into $\ln([M]/[M]_0)$ and plotted against time.
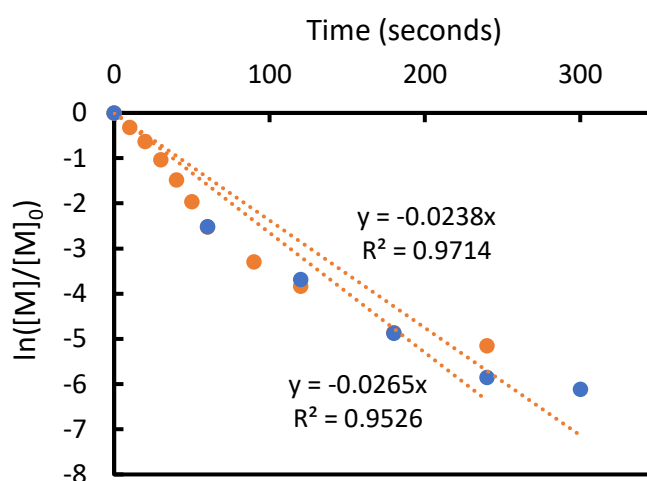
Fig. 2.28. Plot of $\ln([M]/[M]_0)$ vs time for the ROMP of monomers **5b** (orange) and **10b** (blue). Reaction was carried out at room temperature in DCM at an initial monomer concentration of 0.046 M. Aliquots were taken from the reaction mixtures at 10, 20, 30, 40, 50, 60, 90, 120, 180 and 240 seconds in the case of **5b**, and at 60, 120, 180, 240 and 300 seconds in the case of **10b**. These were quenched with ethyl vinyl ether and then analysed with ^1H NMR spectroscopy.

The living character of the polymerisation was confirmed by the plot of $\ln([M]/[M]_0)$ versus time shown in Figure 2.13. As expected, the plot showed linearity meaning that the polymerisation of both monomers followed a first order kinetics. In both cases the reaction was fast, and the monomers were consumed within 5 minutes, with a monomer conversion of 99.4 % for **5b** and 99.8 % for **10b**. From the angular coefficient of the straight line, it was possible to determine the rate

constant *k'* which proved to be equal to 2.65×10^{-2} L · mol^{-1} · s^{-1} for the polymerisation of monomer

5b (orange line, Figure 2.13) and equal to 2.38×10^{-2} L · mol^{-1} · s^{-1} for the polymerisation of monomer

10b (blue line, Figure 2.13). By knowing the value of the constant rate, it was then possible to

determine the half-life $t_{1/2}$ of the polymerisation, which was the time required for the monomer

concentration to decrease one-half its initial value. The half-life for a first order kinetics was

calculated using the following equation:

$$t_{1/2} = \frac{ln2}{k'}$$
Eq. 2.4.

By using equation 2.4, the half-life for the polymerisation of monomer **5b** was calculated

to be 26 seconds, while 29 seconds were required to decrease the concentration of monomer **10b**

of one-half of its initial concentration.

Table 2.4. Kinetic data for the ROMP of monomers **5b** and **10b** using G3 initiator.

	Reaction time (s)	Monomer conversion (%)	k' (L · mol^{-1} · s^{-1})	$t_{1/2}$ (s)
5b	240	99.4	2.65×10^{-2}	26
10b	300	99.8	2.38×10^{-2}	29

Table 2.3 summarises the kinetic data obtained for the homopolymerisation of the

ibuprofen containing monomer **5b** and the PEG containing monomer **10b**. Kinetic studies for the

copolymerisation of **5b** with **10b** to obtain block and statistical copolymers **poly5b-b-poly10b** and

poly5b-co-poly10b were not carried out. However, as the plots ln([M]/[M]$_0$) vs time for both

homopolymerisations possessed very similar trend, it could be assumed that the copolymerisation

would behave in the same manner. In these reactions, the copolymerisations were carried out for

a total of 20 minutes in order to obtain complete conversion of the two monomers.

Stacked ^{1}H NMR spectra for the homopolymerisation studies of **5b** and **10b** are shown in

Figures S39 and S40, Appendix 1.

2.2.2.4. Gel Permeation Chromatography (GPC) of polymers

Gel Permeation Chromatography (GPC) also referred to as Size Exclusion Chromatography (SEC) is the most common technique used to determine molecular weight and distribution of polymers[87]. it is relatively low cost, simple and provides accurate and reliable information about the molecular weight distribution of polymers. The principle is similar to Liquid Chromatography (LC) as it is consisting of a liquid mobile phase and a solid stationary phase. However, the separation of the components within the sample relies on the size, or rather the hydrodynamic volume, of the polymers rather than chemical properties. The stationary phase (column) is consisting of extremely small porous beads, therefore bigger polymers elute faster than smaller ones, which instead require more time to exit the column as they can enter the pores in the beads.

In this study, each polymer was dissolved in THF which was also used as mobile phase. The samples were injected with a flow rate of 1 mL/min into a 2xPLgel 5µm MIXED-C (300 x 7.5 mm) column with temperature set to 40 °C. The polymers were then detected using a refractive index (RI) detector and compared to a polystyrene calibration curve.

As mentioned in Section 2.2.2.2, four different copolymers were prepared and subsequently tested for their self-assembly properties and drug release. Two of them the block copolymers, **poly5b-b-poly10b** and two of them the statistical copolymers **poly5b-co-poly10b**. Here in Figure 2.14, the molecular weight distribution of homopolymers **poly5b** and **poly10** and their copolymer counterparts is shown. As expected, both homopolymers and copolymers possessed a very narrow molecular weight distribution as also indicated by their dispersity values shown in Table 2.4 (Đ < 1.6). This is typical of living polymerisations, where the fast initiation step and the irreversible propagation step allow for the preparation of polymers with low dispersity and controlled molecular weights. The M_n values obtained by GPC analysis were in fact comparable to those calculated theoretically (Table 2.4). Although the dispersity values were lower than 1.6 for each polymer, the introduction of the PEG chain into the ROMP backbone, slightly increased the polymer dispersity due to PEG being a polymer chain itself that possessed its own average

distribution. This could be better seen when comparing the Đ values between the ibuprofen containing homopolymer **poly5b** and the PEG containing homopolymer **poly10b**: the first was obtained with Đ = 1.27, while the second possessed a dispersity value of Đ = 1.36. As a consequence, both block and statistical copolymers were obtained with a higher molecular weight distribution.
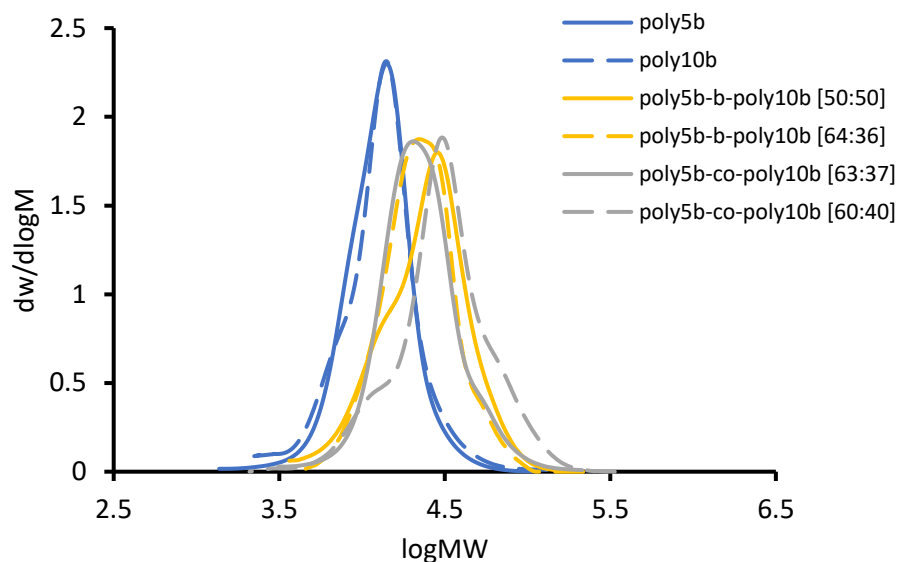
Fig. 2.29. Molecular weight distribution of homopolymers and copolymers. Homopolymers are indicated by the blue lines, whereas block and statistical copolymers are indicated by the yellow and grey lines respectively.

Table 2.5. Polymerisation characteristics of block and statistical copolymer derived from **5b** and **10b**.

Polymer	Yield (%)	n:m:G3 (th)[a]	n:m[b]	% NB-Ibu[c]	% NB-PEG[c]	M_n (th)	M_n GPC	M_w GPC	Đ[d] (M_w/M_n)
Poly5b*	98	20:1	/	100	/	8 800	11 100	13 600	1.27
Poly10b*	92	20:1	/	/	100	15 000	11 000	14 200	1.36
Poly5b-b-poly10b	78	20:20:1	26:14	64	36	21 900	19 300	24 900	1.29
Poly5b-co-poly10b	76	20:20:1	25:15	63	37	22 000	19 300	26 200	1.36
Poly5b-b-poly10b	65	20:20:1	20:20	50	50	23 600	19 600	28 300	1.44
Poly5b-co-poly10b	76	20:20:1	24:16	60	40	22 700	23 900	30 700	1.56

***poly5b** and **poly4** were both obtained with > 99 % of monomer conversion in 5 min. [a] Theoretical feed ratio. [b] Observed feed ratio calculated by quantitative ^{1}H NMR analysis. [c] Determined by quantitative ^{1}H NMR analysis. [d] Polydispersity determined by GPC in THF and reported relative to polystyrene standards.

Table 2.4 summarises the polymer properties obtained for the synthesised homo- and co-polymers. The GPC results, including the number average (M_n) and weight average (M_w) molecular weights as well as the dispersity values are here shown.

2.2.2.5. The importance of an active catalyst

Grubbs 3rd generation catalyst is a very active initiator, tolerant to air and moisture. However, if not handled carefully it can oxidise and therefore it can lose its activity. As determined by Jones *et al*.[88], in the presence of traces of air there is an increase in the rate of decay of **G3** caused by competing oxidation that yields benzaldehyde. For someone that uses **G3** for the first time this cannot be noticed immediately, however it is very simple to know when **G3** is being oxidised. In fact, a simple visual analysis can be carried out, due to **G3** changing colour from green in its active form to brown in its oxidised form (Figure 2.15, c).

The first polymerisation experiments carried out during this project used a deactivated **G3** initiator due to an old batch being dispatched from Sigma-Aldrich. The results did not meet the criteria of living polymerisation: very broad molecular weight distributions and high dispersity values were obtained for the homopolymerisations of **5b** and **10b**. Kinetic studies were also carried out resulting in very long polymerisation time compared to those obtained with the employment of active **G3**. For instance, when using the oxidised **G3,** the conversion of **5b** was only > 85 % after 4 hours while 40 minutes were required for **10b** to reach > 90 % of conversion (Figure 2.15, b). On contrary, active **G3** afforded **poly5b** and **poly10b** with > 99 % monomer conversion in less than 5 minutes (Figure 2.15, a).

Table 2.6. Polymerisation results obtained for oxidised/not active initiator versus active initiator.

	Polymer	Reaction time[a)]	Monomer conversion (%)	M_n (Th)	M_n GPC	M_w GPC	Đ (M_w/M_n)
Oxidised G3	Poly5b	4 h	> 85	8 800	95 800	210 600	2.20
	Poly10b	40 min	> 99	15 000	47 700	103 100	2.16
Active G3	Poly5b	4 min	> 99	8 800	11 100	13 600	1.27
	Poly10b	5 min	> 99	15 000	11 000	14 200	1.36

[a)] Reaction conditions: [Monomer]/[Catalyst] = 20:1; CH_2Cl_2; 25 °C.

As shown Table 2.5, there is a significant difference between the polymers synthesised with active **G3** and oxidised **G3**. It is evident that homopolymers obtained with the active initiator presented lower molecular weights and narrower distributions of the polymer chains when

compared to those obtained with the employment of deactivated **G3**. As shown in Table 2.5, dispersity values greater than 2.0 were obtained when the polymerisation was carried out with the deactivated catalyst. Furthermore, for these polymers, the number average molecular weight, M_n, was much greater than the theoretical M_n (almost one order of magnitude bigger). This could be due to the slow initiation step which led to secondary metathesis or "back-biting" reactions. This caused the formation of chain transfer processes which could give longer polymer chains but also broaden the molecular weight distribution. The initiation step was, on contrary, faster when active **G3** was used and thus provided polymers with M_n values that were comparable to those obtained theoretically.
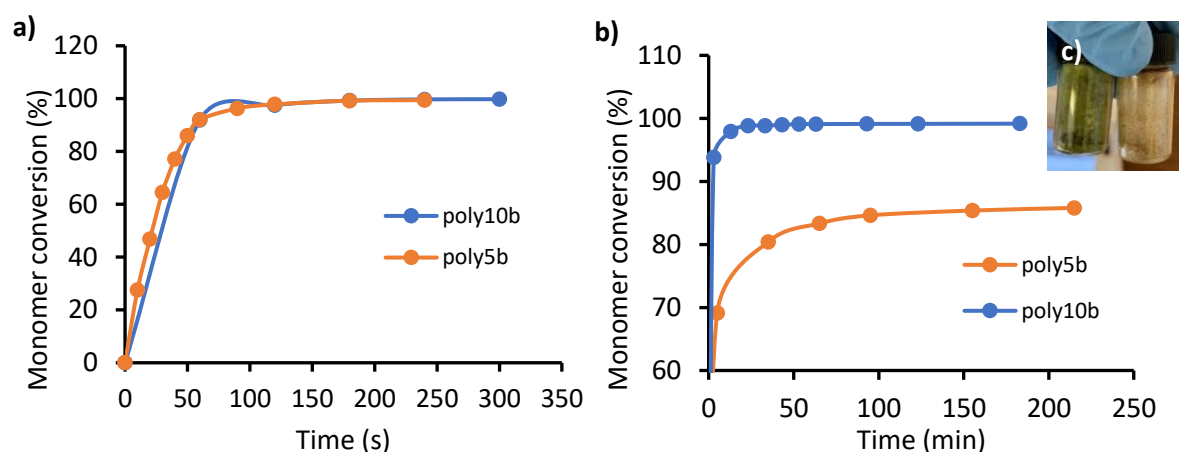
Fig. 2.30. Kinetic results for the homopolymerisation of **5b** (orange) and **10b** (blue). a) Conversion of **5b** and **10b** using active **G3**. 50 μL of aliquots were taken at predefined time points and quenched with a solution of ethyl vinyl ether in DCM. The samples were dried and analysed by ^{1}H NMR). b) Conversion of **5b** and **10b** using the deactivated **G3**. The polymerisation was carried out inside of an NMR tube using CDCl3 as solvent. The reaction was monitored by ^{1}H NMR every 10 minutes. c) Image of active G3 to the left (green) and deactivated G3 to the right (brown).

It is therefore important, when using **G3**, to maintain the catalyst under inert atmosphere in order to slow down the oxidation process, and if possible, to keep it away from light. The initiator can be either transferred into a Schlenk tube to facilitate the vacuum/nitrogen cycles or it can be kept in its bottle and flushed with nitrogen after each use.

2.2.3. Self-assembly of block and statistical copolymers

The synthesised block copolymer **poly5b-b-poly10b** possessed amphiphilic properties. It consisted of a hydrophilic portion, the PEG-containing block, and a hydrophobic portion, the ibuprofen-containing block. It is known from literature that, in aqueous solutions, amphiphilic copolymers can self-assemble into a variety of structures including micelles, vesicles, nanotubes, nanofibers and lamellae[89]. The self-assembly process is governed by a combination of weak, non-covalent forces including hydrogen bonding, hydrophobic effects, electrostatic interactions and Van der Waals forces which together can ensure the stability of the system in solution[89]. The first main force involved in the self-assembly process is the *hydrogen bond* formation between the water molecules and the hydrophilic portion of the amphiphile which gives rise to an enthalpic gain in solvation. The second one is the *hydrophobic effect*[90] which causes the self-aggregation of the non-polar portion of the amphiphile. The introduction of the hydrophobic chains in water leads to the disruption of the hydrogen bonding network that surrounds the hydrophilic chains and in returns leads to a rearrangement of the molecules of water around the non-polar chains. The latter are attracted to each other due to the hydrophobic interaction and form aggregated structures which are entropically favoured and are generated so that the water disruption is minimised. In this way micellar structures consisting of a hydrophobic core and a hydrophilic corona are obtained.

There are several factors that can affect the shape and size of the polymeric aggregates in solution, including the polymerisation degree, polymer concentration, nanoprecipitation solvent, temperature and pH. Knowing that polymer self-assembly by nanoprecipitation is solvent-dependent[92], self-assembly of the copolymers was obtained by dissolving the polymer (20 mg) in 1 mL of three different solvents (acetone, THF, acetonitrile), to which deionised water (10 mL) was added dropwise, over a 20 min period to the stirred solution to give a polymer with a final concentration of 2 mg/mL. In this stage, the copolymers formed NPs suspension through solvent exchange between the organic solvent and deionised water. The aggregate solution was subsequently transferred into a dialysis membrane, sealed and dialysed against distilled water for

24 h (water was changed three times over this period) to remove residual organic solvent. The self-assembly was then analysed by dynamic light scattering (DLS) and transmission electron microscopy (TEM). DLS data were recorded using a polyphospholipid refractive index of 1.45. TEM samples were analysed on Formvar coated copper grids, to which a negative stain of uranyl acetate was added, allowing for better contrast for nanostructures comprised of low molecular weight atoms (C, H, N) under the electron beam.

2.2.3.1. Dynamic light scattering studies

DLS is a very powerful tool for the study of the diffusion behaviour of macromolecules and the determination of aggregates in solution[93]. This technique can determine the size, intended as hydrodynamic diameter d_H, of particles by measuring the Brownian motion of macromolecules in solution, which is caused by the constant collision with solvent molecules. The motion of macromolecules depends on their size, temperature and solvent viscosity. When a monochromatic beam of light hits the particles in solution, the light scatters in all directions depending on the shape and size of the particles. Due to the Brownian motion, the distance between the particles constantly changes and thus the scattering intensity fluctuates over time. By analysing the intensity fluctuations of the scattered light, it is then possible to determine the diffusion coefficient (D) and therefore the hydrodynamic diameter of particles by using the Stokes-Einstein equation (Eq 2.5):

$$D = \frac{k_B T}{3\pi\eta d_H}$$

Eq. 2.5.

Where k_B is the Boltzmann constant (1.38×10^{-23} kg m^2 s^{-2} K^{-1}), T is absolute temperature (K) and η is the viscosity of the solvent. Generally, large particles diffuse slowly and thus adopt similar

positions at different time points, whereas small particles diffuse faster and therefore do not adopt

a specific position.
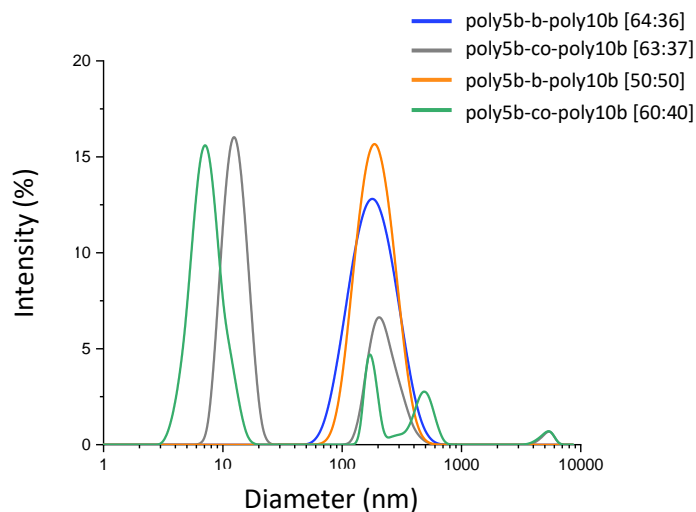
Fig. 2.31. DLS particle size distributions of poly5b-b-poly10b [64:36] and poly5b-co-poly10b [63:37] from acetone and poly5b-b-poly10b [50:50] and poly5b-co-poly10b [60:40] from acetonitrile.

Figure 2.16 shows the DLS particle distribution for the block copolymer **poly5b-b-poly10b**

[64:36] (PDI = 0.2) and the statistical copolymer **poly5b-co-poly10b [63:37]** (PDI = 0.4) which were

self-assembled in acetone, whereas of the block copolymer **poly5b-b-poly10b [50:50]** (PDI = 0.5)

and statistical copolymer **poly5b-co-poly10b [60:40]** (PDI = 0.7) which were self-assembled in

acetonitrile (DLS distribution for all of the investigated systems is shown in Figure S66, Appendix 1).

As shown in the intensity (%) vs diameter (nm) graph, for all of the four self-assembled polymers, a

broad distribution of the particle size was obtained. This was also confirmed by the polydispersity

index (PDI) values calculated by the instrument, which were determined to be between 0.2 and 0.7.

As known from literature, in fact, highly monodisperse particle solutions are characterised by PDI ≤

0.1, while PDI of 0.1 – 0.4 and PDI > 0.4 give rise to moderately and highly disperse particle solutions

respectively[94]. By this means, it could be assumed that self-assembly of both statistical and block

copolymers in acetone afforded NPs with narrower size distribution compared to those obtained

by nanoprecipitation from acetonitrile. Although, in both cases NPs of non-uniform size were

obtained. Nevertheless, the statistical copolymers presented, as expected, a different distribution of the particle size compared to the block copolymers which were much larger. For example, the largest peak (67 % by intensity) seen for **poly5b-co-poly10b [63:37]** was for particles at 13 nm. Because of the random distribution of the PEG and ibuprofen side chains tethered to the norbornene backbone, this was interpreted as the polymer collapsing in on itself, forming single chain nanoparticles[95]. A small amount of these NPs (32 %) formed random aggregates of a bigger size (230 nm) that precipitated in solution. TEM analysis of **poly5b-co-poly10b [63:37]** confirmed an absence of ordered self-assembly (Figure 2.19, Section 2.2.3.2). Block copolymers **poly5b-b-poly10b [64:36]** and **poly5b-b-poly10b [50:50]** instead behaved as non-ionic amphiphilic polymers and in water formed NPs in the size range of 50–600 nm as shown in Figure 2.16 with an average diameter of 196 nm.

2.2.3.2. Transmission electron microscopy (TEM) studies

Transmission electron microscopy (TEM) is a technique commonly used in combination with DLS for the study of self-assembly processes. By irradiation of the specimen (sample deposed onto a grid) with a high energy beam of electrons, the TEM microscope allows for the development of images of individual nanoscale objects. TEM is, therefore, used to visualise sample morphology but also to quantify structural features, such as particle size of the self-assembly systems. Although TEM possesses several advantages, there are still some challenges associated with the sample preparation. During the drying process, some self-assemblies can rearrange giving rise to a collection of images that are not representative of the sample in its native environment. However, for self-assemblies that are stable under drying conditions, useful information can be obtained[96].

Figure 2.17 (a) shows the TEM image obtained for the block copolymer **poly5b-b-poly10b [64:36]** self-assembled from acetone. The image revealed that the self-assembly of the block copolymer produced NPs with different sizes, which was in accordance with the results obtained

by DLS where high PDI values were determined. More specifically, two different particle size distributions could be seen. As shown in figure 2.17 (b) and 2.17 (c), the copolymer **poly5b-b-poly10b [64:36]** possessed a distribution of smaller NPs with size ranging from 10 nm to 50 nm and a distribution of bigger NPs with size ranging from 60 nm to 240 nm. Furthermore, examining the histogram in Figure 2.17 (b) in more detail, it was possible to identify two additional different particle distributions which were centred at 70 nm and 120 nm respectively. However, this could be due to the low number of images taken for this sample which led to a low counting, n < 200, and therefore results could not be taken as representative for the whole self-assembly solution.
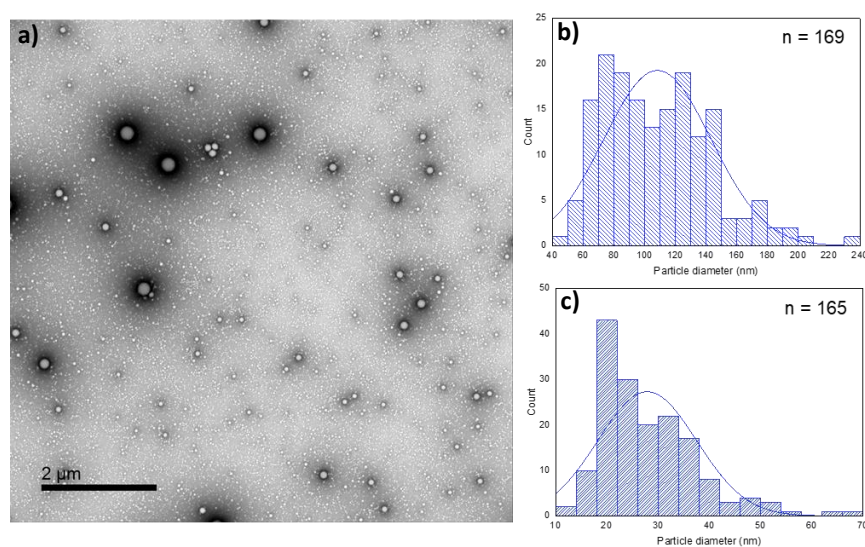
Fig. 2.32. a) TEM image of block copolymer **poly5b-b-poly10b [64:36]** self-assembled from acetone; b) distribution of the larger particles of image (a) with average size (108 ± 35)nm; d) distribution of the smaller particles of image (a) with average size (28 ± 9)nm.

The TEM results did not entirely correspond to the DLS measurements, which provided a greater average diameter, as is common due to the solvation sphere measured by DLS, and the compacting effect of the vacuum in TEM. Furthermore, Figure 2.17 (c) indicated that the formation of smaller NPs was dominant, and that they possessed an average diameter of 30 nm.

As a results of the DLS and TEM analysis, it was not possible to assume with certainty that micellar structures (core-shell structures) were obtained. The micellization is in fact a dynamic

phenomenon where *n* monomeric amphiphilic molecules *S* associate to form micelles S_n ($nS \rightleftharpoons S_n$). This is an equilibrium process whereby the monomeric amphiphiles constantly migrate from one micelle to another until the equilibrium is reached and micelles with similar size are formed (monodisperse distributions are obtained)[97]. For this reason, it could be assumed that **poly5b-b-poly10b [64:36]** did not form micellar structures but rather aggregates that adopted a spherical shape. The same behaviour was found for **poly5b-b-poly10b [50:50]** self-assembled in acetone, THF and acetonitrile.

Of all the samples analysed, here **poly5b-b-poly10b [50:50]** self-assembled from acetonitrile is shown in Figure 2.18 and described. Figure 2.18 (c) and (d) show the nanoparticle distribution for bigger and smaller spherical NPs respectively. In this case more counts were taken, n ~ 500, and therefore the sample showed a more regular distribution of bigger and smaller NPs in the TEM compared to **poly5b-b-poly10b [64:36]** self-assembled from acetone. The **poly5b-b-poly10b [50:50]** formed bigger NPs with an average size centred around 80 nm while the smaller NPs possessed a diameter of ~ 20 nm. These results were in agreement with the DLS analysis as also in this case a broad distribution of the particle size was obtained. However, due to the effect of the TEM preparation process contrasting with DLS, overall smaller NPs size values were obtained. TEM analysis of the **poly5b-co-poly10b** samples in all cases showed irregular supramolecular morphologies (Figure 2.19 and Figs. S36–38, ESI) and only big random agglomerates were visible.
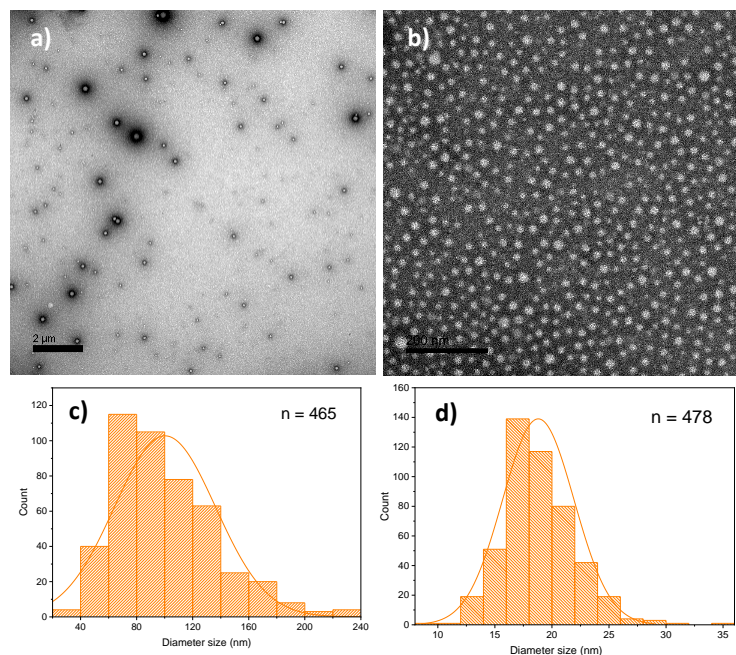
Fig. 2.33. a) TEM of larger NPs of **poly5b-b-poly10b [50:50]** scale 2000 nm; b) TEM of smaller NPs of **poly5b-b-poly10b [50:50]** scale 200 nm; c) and d) size distribution for **poly5b-b-poly10b [50:50]** in acetonitrile TEMs for a) (100 ± 36)nm and b) (19 ± 3)nm respectively.

Table 2.6 shows the diameters obtained by TEM for the self-assembly systems investigated. As demonstrated, for the acetone systems, a higher ratio of hydrophobic portion in the block copolymer (**poly5b-b-poly10b [64:36]**) seemed to give rise to smaller NPs with a higher diameter (d = 28 nm) compared to the one obtained for the block copolymer consisting of an equal hydrophobic/hydrophilic ratio (d = 20 nm). On contrary, bigger NPs possessed a lower diameter when compared to the **[50:50]** polymer (108 nm vs 118 nm). However, the difference was minimal (< 10 %) meaning that the values could be affected by many factors including the rate of drop addition of deionised water to the polymer solution as well temperature at the time of the experiment. Furthermore, as mentioned before, the results obtained for **poly5b-b-poly10b [64:36]** might not be taken as representative as only 169 counts were considered for the determination of the average NP diameter.

As regards to **poly5b-b-poly10b [50:50]**, this polymer was synthesised in a bigger scale and therefore more sample was available for the study of the organic solvent effect. While the dissolution of the polymer in acetone and THF did not considerably affect the size of both small and

big NPs, this seemed to change when acetonitrile was used. Small NPs obtained from acetonitrile system possessed a diameter of 19 nm, while a diameter of 100 nm was obtained for the bigger ones (versus 118 nm in acetone and 110 nm in THF). Therefore, the higher the polarity of the solvent used for nanoprecipitation (dielectric constant of acetonitrile ε = 37.5), the lower the size of the NPs obtained in solutions. However, even in this case the difference was minimal and therefore changing the solvent for nanoprecipitation did not seem to drastically change the size of the NPs nor their shape.

Further experiments need to be done in order to confirm the validity of the results. For instance, increasing the length of the polymer chain as well as increasing the hydrophilic portion within the block copolymer.

Table 2.7. table comparing the diameter of all the self-assemblies obtained. Different organic solvents were used to dissolved block copolymers **poly4-b-poly2 [64:36]** and **[50:50]** affording NPs with comparable size.

Polymer	Solvent	d (nm)$_{small\ NPs}$[a,b]	d (nm)$_{big\ NPs}$[a,c]
Poly5b-b-poly10b [64:36]	$CO(CH_3)_2$	28 ± 9	108 ± 35
Poly5b-b-poly10b [50:50]	$CO(CH_3)_2$	20 ± 3	118 ± 38
Poly5b-b-poly10b [50:50]	THF	20 ± 2	110 ± 29
Poly5b-b-poly10b [50:50]	CH_3CN	19 ± 3	100 ± 36

[a] Determined by TEM. [b] Average size of smaller NPs. [c] Average size of larger NPs. (See Figures S67-S70, Appendix 1).

In any case, **poly5b-b-poly10b [50:50]** and **poly5b-co-poly10b [60:40]** (PDI = 0.7 by DLS) systems prepared from acetonitrile afforded two comparable polymer sequences that allowed for the investigation of any differences in the release of ibuprofen against differences in polymer sequence architecture.
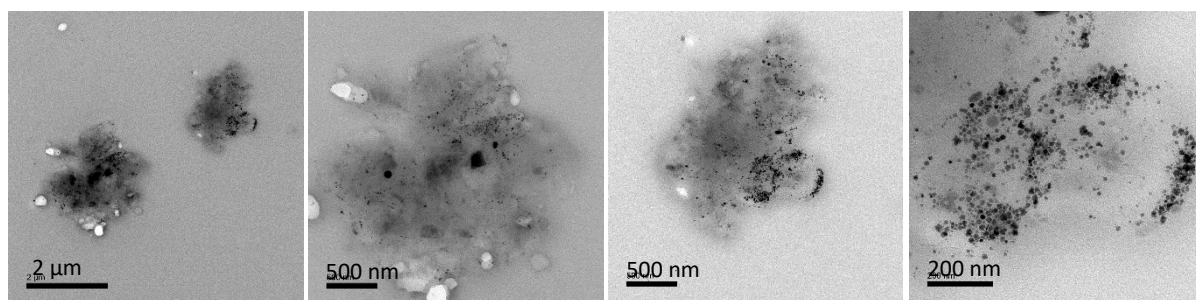
Fig. 2.34. TEM images of **poly4-co-poly2 [60:40]** self-assembled from acetone.

85

The TEM images obtained for all the polymers (block and statistical copolymers) self-assembled by nanoprecipitation from acetone, THF and acetonitrile are shown in Figures S67 – S74, Appendix 1.

2.2.3.3. Critical Aggregate Concentration (CAC) of block copolymers

The critical aggregate concentration (CAC) is the concentration above which single polymeric chains with amphiphilic properties start to form aggregates in an aqueous solution. Typically, at low concentrations, amphiphiles stay at the surface of the liquid, with the hydrophilic portion interacting with the water, while the hydrophobic portion migrate from the interface (e.g. interact with the air). When more molecules of amphiphiles are added to the water, a decrease in surface tension is seen and when the surface of the water is saturated with molecules, these are then collected as aggregates in water. This is the critical aggregate concentration. There are several methods used to determine the CAC of polymeric NPs, including spectrofluorometry[98,99], conductometry[100], DLS[99] and tensiometry[101]. In this study the latter method was used to measure the CAC of **poly5b-b-poly10b [50:50]** self-assembled from acetone, THF and acetonitrile as a function of the surface tension (ST).

As mentioned in Section 2.2.3, self-assemblies of **poly5b-b-poly10b [50:50]** were prepared so that the final concentration in water solution was 2 mg/mL after dialysis. The latter was then serially diluted in order to obtain at least 10 samples with decreasing concentrations. The polymer concentration and surface tension values were plotted on a graph and the CAC values, together with the ST values, were determined on the intercept of two straight lines, at the point where the surface tension no longer decreased with increasing of the polymer concentration.
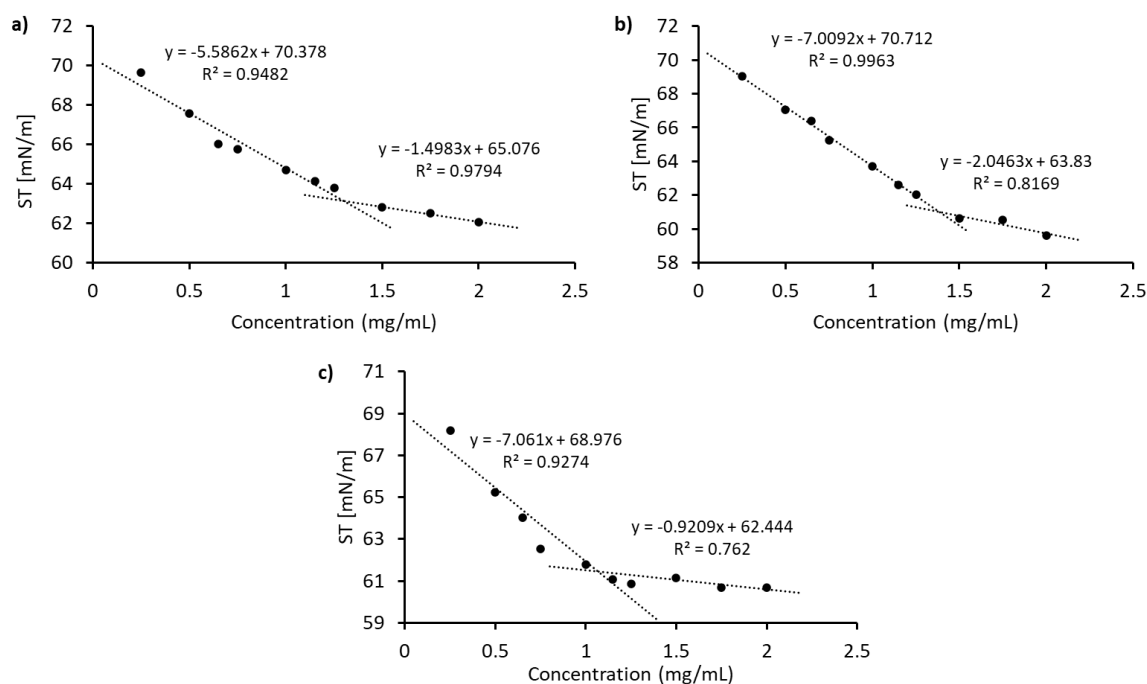
Fig. 2.35. Concentration vs surface tension (ST) of **poly5b-b-poly10b [50:50]** self-assembled from a) acetone, b) THF, c) acetonitrile.

Figure 2.20 shows the change in surface tension of the **poly5b-b-poly10b [50:50]** self-assemblies as a function of the polymer concentration in solution. As shown in all three cases, the surface tension decreased with increasing in concentration and when the CAC was reached, the ST change was minimal. As shown in Table 2.7, **poly5b-b-poly10b [50:50]** self-assembled from acetone and THF started to aggregate at a concentration of 1.30 mg/mL and 1.39 mg/mL respectively. However, the CAC value obtained for **poly5b-b-poly10b [50:50]** self-assembled from acetonitrile was lower and it was found to be 1.06 mg/mL. The lower CAC value for this system could be the reason for the smaller NP size of 100 nm obtained by TEM when compared to those obtained by nanoprecipitation from acetone and THF (118 nm and 110 nm respectively).

Table 2.8. CAC and ST values obtained for **poly5b-b-poly10b [50:50]** self-assembled from acetone, THF and acetonitrile.

poly5b-b-poly10b [50:50]	CAC (mg/mL)	ST (mN/m)
$(CH_3)_2CO$	1.30	63.1
THF	1.39	61.0
CH_3CN	1.06	61.5

The CAC for the synthesised statistical copolymers **poly5b-co-poly10b** was not determined as both DLS and TEM showed that random aggregates that precipitated in aqueous solution were obtained. Instead, CAC of **poly5b-b-poly10b [64:36]** could not be run due to sample unavailability at the time of the experiment.

2.2.4. Release of ibuprofen from polymeric nanoparticles

Poly5b-b-poly10b [50:50] self-assembled from acetone, THF and acetonitrile, as well as **poly5b-co-poly10b [60:40]** self-assembled from acetonitrile, were placed in different sets of tubes to which 2 M aqueous NaOH (pH 14.3), phosphate buffered saline (PBS, pH 7.4), foetal bovine serum (FBS, pH 7.3), pig liver esterase 30 units/mL in water (PLE, pH 7), and unbuffered water (pH 7) were added to give a final concentration of 1 mg/mL. The samples were incubated at 40 °C in a thermocycler. Each sample was removed at predefined time points (2 hr, 4 hr, 8 hr, 24 hr, 48 hr, 96 hr), frozen to quench the reaction and analysed afterwards by HPLC (Fig. S41). A gradient processing method was used, starting from 28 % methanol in water with 0.1 % of formic acid. Samples (10 μL) were run at 35 °C at a flow rate of 4 mL/min. Absorbance was monitored at λ = 225 nm. The instrument was calibrated using standard solutions of ibuprofen in methanol (50, 100, 150, 200, 250 ppm, Figure S77, Appendix 1).

Figure 2.21 illustrates the release of ibuprofen using 2 M NaOH in water. In the case of NPs obtained from the block copolymer, the majority of ibuprofen was released within the first 10 hours with a release percentage of 97 % in the acetonitrile and the acetone systems, and 90 % for the system prepared in THF. In the following hours, for a period of up to four days, only a small amount of ibuprofen was released with the NP reaching complete degradation in 24 hours. This was in accordance with the results obtained from TEM, for which each solvent system used afforded NPs that were very similar in size (diameter of 100 – 120 nm). Therefore, changing the solvent used for

precipitation of the micelles did not alter the degradation kinetics significantly. On contrary release of ibuprofen for the statistical copolymer self-assembled from acetonitrile, the hydrolysis was faster, and the majority of the drug was released within the first 2 hours (89 %). By a prior calibration of the instrument, it was also possible to quantify the concentration of the released drug which after 96 hours was in agreement with the theoretically expected value for quantitative hydrolysis which was 170 ppm for **poly5b-b-poly10b [50:50]** and 210 ppm for **poly5b-co-poly10b [60:40]**. The faster release of the statistical copolymer was consistent with higher accessibility of hydroxide ions to the ester linkages in a single chain polymer compared to bigger spherical structure adopted by the block copolymer.
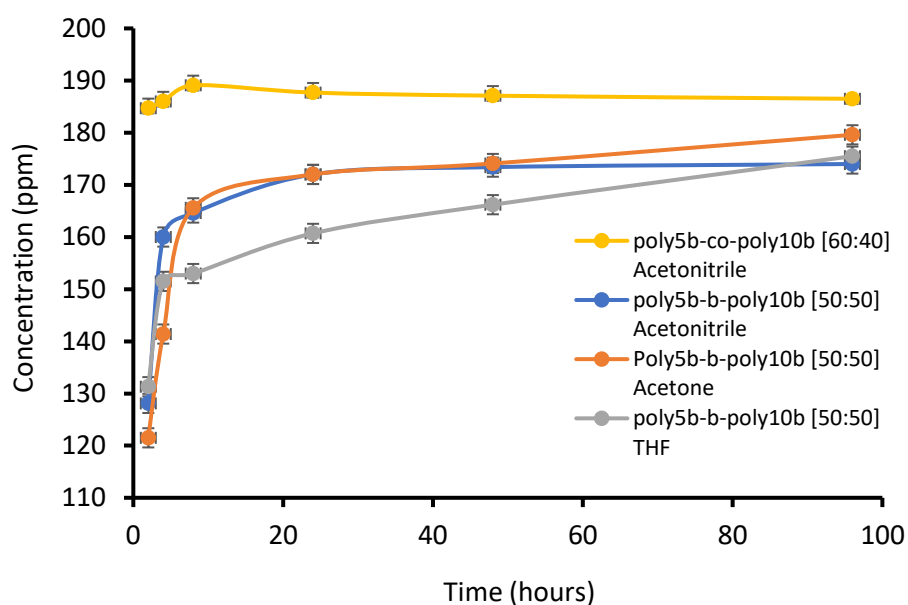
Fig. 2.36. Concentration of ibuprofen released (ppm) vs reaction time (hours) in 2 M NaOH solution in water. The concentrations are determined by calibration using standards of ibuprofen in methanol at 50, 100, 150, 200 and 250 ppm.

In the media which mimic physiological conditions more closely (PBS, FBS and PLE), the hydrolysis of ibuprofen from both of the copolymers **poly5b-b-poly10b [50:50]** and **poly5b-co-poly10b [60:40]** was much slower, with none of these media causing release of ibuprofen (measurable by HPLC) at a temperature of 40 °C over a period of 96 hours. This suggested that the shielding of the polymer-drug ester linkage within the hydrophobic core of the micelle retarded

chemical hydrolysis as well as impeding access of enzymes[102]. The resistance to enzymatic degradation from the **poly5b-co-poly10b [60:40]** contrasted with the basic chemical hydrolysis result, consistent with formation of single-chain nanoparticles by chain collapse, which provided a steric barrier to enzymes but not ions.

Figure 2.22 shows the typical chromatogram profile obtained for the release of ibuprofen from polymeric NPs. In the HPLC conditions used, ibuprofen eluted at a retention time (RT) of ca. 3.2 min with a purity of > 99 %.
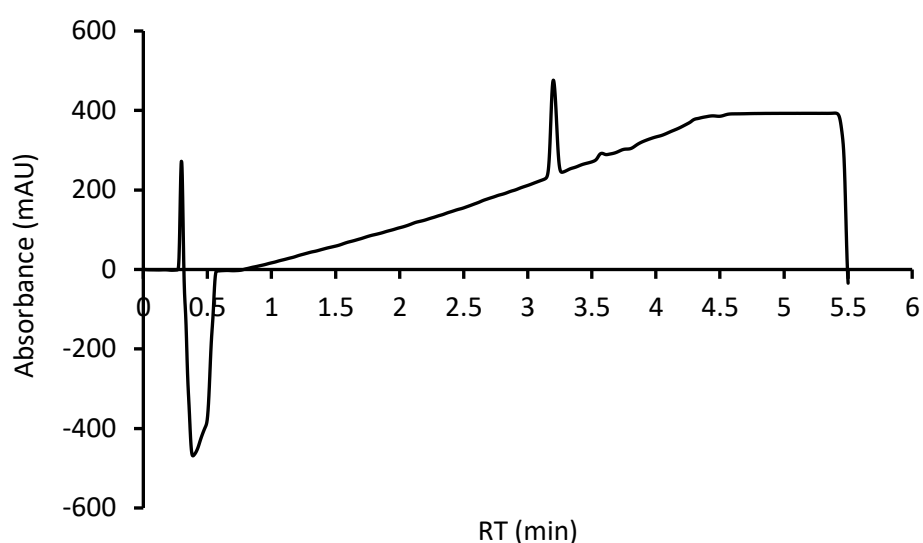
Fig. 2.37. Chromatogram retention time (min) vs absorbance (mAU) of ibuprofen.

Unfortunately, these experiments were carried out before the lock down caused by Covid-19. Consequently, analysis on the statistical copolymer self-assembled from acetone and THF could not be run. With the premises that changing the solvent system for NP formation did not significantly change the drug release process, the decision on focusing on the follow-up work was taken.

2.2.5. Synthesis of NSAIDs based NB monomers containing an imine linkage

Following the unsuccessful results for the release of ibuprofen from polymeric NPs using physiological conditions, another approach was taken. As mentioned in Chapter 1, Section 1.3.1.1, the pH in the tumour extracellular environment slightly decreases in comparison to the normal blood stream: from 7.4 to ~ 6.0 − 7.0[103], which eventually drops to lower pH of 5.5 − 6.0 in endosomes and 4.5 − 5.0 in lysosomes[104]. Many research groups developed polymer-drug conjugates where the drug was covalently linked to the polymer backbone through linkages that could degrade under mild acidic conditions, including imine[32,105], acetal[106,107] and hydrazone[108] bonds. For instance, Dai *et al.*[32] synthesised polymeric NPs containing doxorubicin (DOX), where the drug was attached to the block copolymer poly(2-(diisopropylamino)ethyl methacrylate-b-poly-(4-formylphenyl methacrylate-co-polyethylene glycol mono-methyl ether methacrylate) (abbreviated to PDPA-b-P(FPMA-co-OEGMA)) via an imine bond (Schiff base). The so formed polymer gave rise to spherical micelles that could undergo charge-conversion (from negative to positive charge) at pH ~ 6.5, followed by cellular internalisation into the tumour cells where DOX was released at pH ~ 5.5.

Reaction conditions
pTsOH, Toluene Dean-Stark
Pyrrolidine, DCM 4 Å MS, N₂
Ti(EtO)₄, THF, reflux, N₂
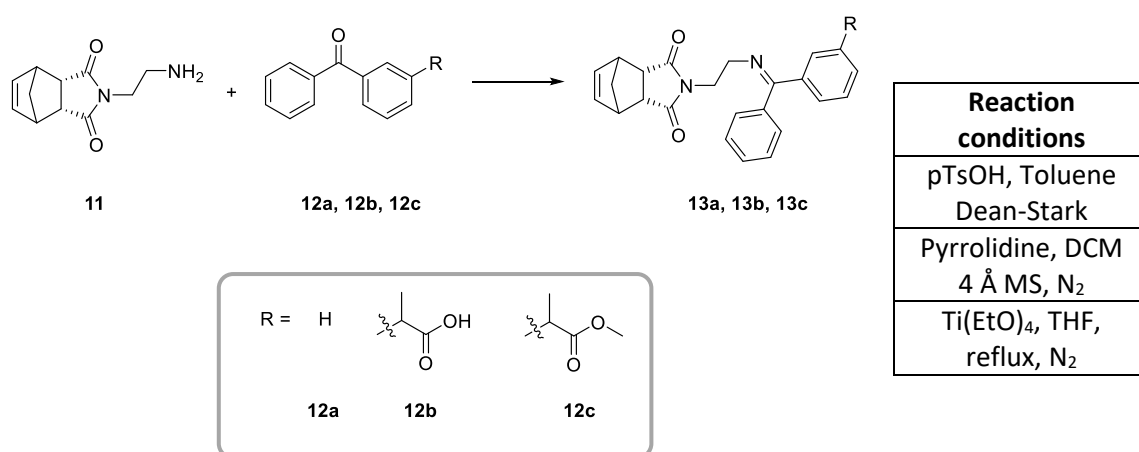
Scheme 2.8. Synthetic scheme for the preparation of compound **13a**, **13b** and **13c** respectively the benzophenone, the ketoprofen and the ketoprofen methyl ester containing NB monomers. Different reaction conditions have been attempted.

Following the results obtained by Dai and co-workers, in this study the synthesis of a NB monomer consisting of an imine bond between the NB ring and the drug was attempted. In order to obtain such a system, ketoprofen was employed. Ketoprofen is a propionic acid derivative of ibuprofen and possesses a ketone group. For this reason, it was selected as the drug of the study. Initially the formation of the imine bond was tested between the primary amine **11** (NB-NH$_2$)[109] and benzophenone **12a**, which was cheaper then ketoprofen and hence selected for the reaction conditions optimisation (Scheme 2.5). Compounds **11** and **12a** were reacted together in the presence of catalytic p-toluenesulfonic acid (pTsOH) in toluene using a Dean-Stark trap[110]. The reaction was carried out for 24 hours and the final product isolated by flash chromatography (EtOAC:PET 6:4) with a yield of 37 %. The formation of compound **13a** was confirmed both by ^{1}H NMR and by X-ray diffraction as shown in Figure 2.23 and Figure 2.24. Due to the nature of the substituents to the double bond, only one product could be formed.
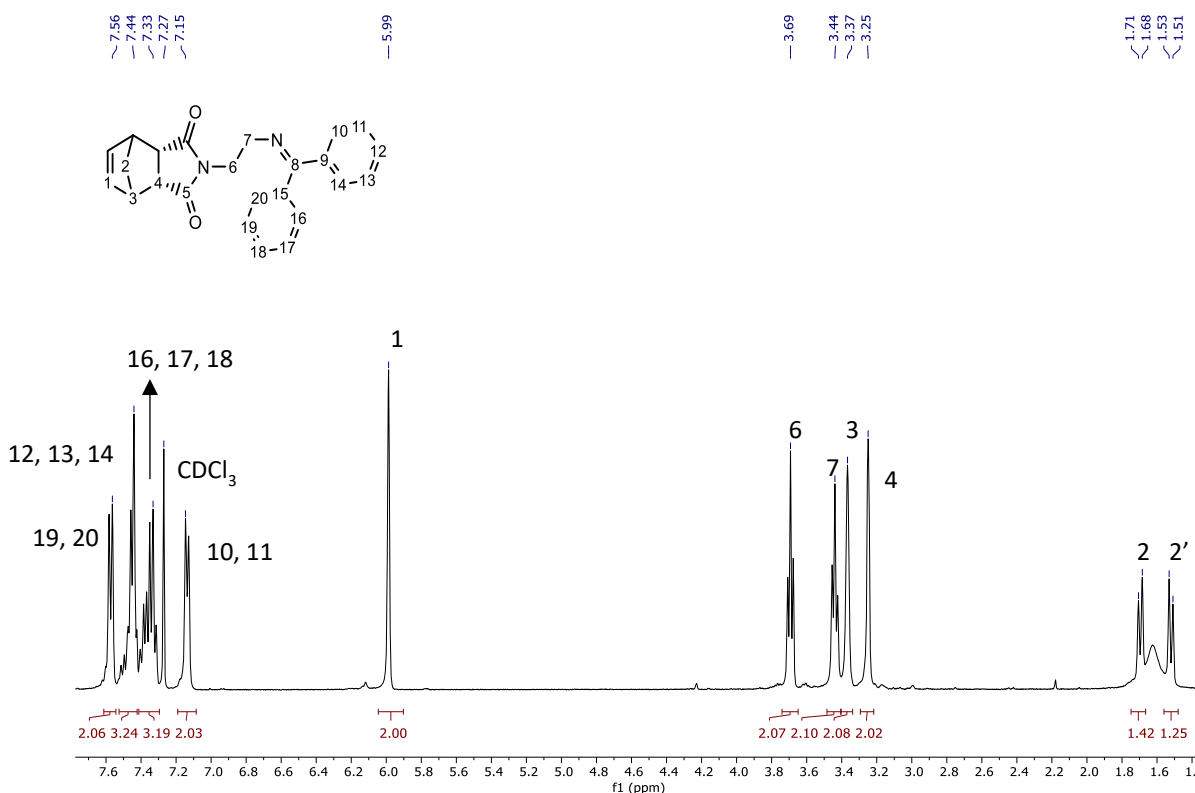
Fig. 2.38. ^{1}H NMR in CDCl$_3$ of compound **13a**, including compound structure and carbon numbering. Each peak has been assigned for each proton. b) Ball and stick representation of the single crystal X-ray structure of *endo*-**13a**.

Single crystals of **13a** were obtained by slow evaporation from acetone. A suitable crystal was mounted at 250 K and collected at the same temperature on a SuperNova, Dual, Cu at home/near, AtlasS2 diffractometer. The experiment was run by Lee Birchall. The ketoimine bond C=N distance was measured and found to be 1.2760 Å, which was significantly shorter than the single bond C-N (1.4557 Å) and the ethylene C-C bond (1.5244 Å) as a demonstration of the effective formation of **13a**.
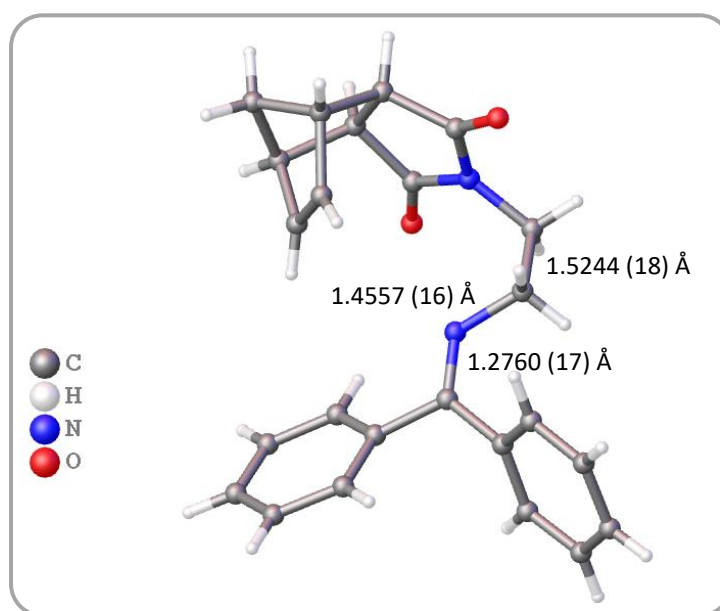
Fig. 2.39. Crystal Data for $C_{24}H_{22}N_2O_2$ (M =370.43 g/mol): triclinic, space group P-1 (no. 2), a = 6.0805(3) Å, b = 10.1042(5) Å, c = 15.8303(7) Å, α = 94.167(4)°, β = 94.199(4)°, γ = 99.270(4)°, V = 953.78(8) Å^3, Z = 2, T = 249.99(11) K, μ(CuKα) = 0.655 mm^{-1}, Dcalc = 1.290 g/cm^3, 7115 reflections measured (8.9° ≤ 2Θ ≤ 144.09°), 3641 unique (R_{int} = 0.0237, R_{sigma} = 0.0313) which were used in all calculations. The final R_1 was 0.0416 (I > 2σ(I)) and wR_2 was 0.1144 (all data).

The same conditions were applied for the reaction of the primary amine **11** with ketoprofen **12b** and ketoprofen methyl ester **12c** (obtained by the reaction of **12b** in MeOH with catalytic H_2SO_4). However, in both cases no reaction occurred due to the poor solubility of NB-NH$_2$ in toluene. The same issue was encountered when the synthesis of compound **13a** was subsequently repeated. In a second attempt, compounds **12a**, **12b** and **12c** were each reacted with compound **11** using anhydrous DCM as solvent, molecular sieves (4 Å) and catalytic pyrrolidine at 40 °C[111] (Scheme 2.5). Even in this case, no reaction occurred probably due to the equilibrium being shifted more towards the reagents rather than the product caused by inefficient deprotonation of the hemiaminal. Cogan

and Ellman[112] successfully prepared a series of *N*-sulfinyl ketimines by the condensation of sulfinamides and ketones using Ti(IV) salts to promote the imine formation but were also previously used for the reaction of ketones with amines[113]. In particular Ti(OEt)$_4$ afforded the desired products with high yield even when ketones with more substantial steric demand where employed. Here, compounds **12a**, **12b** and **12c** were each reacted with compound **11** in the presence of 2 equivalents of Ti(OEt)$_4$ using THF as solvent and heating to reflux under anhydrous conditions (Scheme 2.5). Unfortunately, Ti(OEt)$_4$ hydrolysed to form TiO$_2$ which was difficult to remove even by Celite® filtration and subsequent flash chromatography. Furthermore, characterisation by IR spectroscopy did not show formation of the desired product. However, drying THF more carefully (e.g. benzophenone-sodium still) could have avoided the formation of TiO$_2$ in the reaction mixture and therefore maintaining active the catalyst throughout the reaction.

Due to time constrain and due to the unsuccessful results, no further experiments were carried out. However, future work could be looking into optimising the Ti(OEt)$_4$ catalysed reaction conditions.

2.3. Conclusion

The synthesis and development of polymeric NPs containing NSAIDs drugs, namely ibuprofen, to be used in nanomedicine was investigated in this study[66]. The ring opening metathesis polymerisation, ROMP, was used as a versatile tool for the preparation of block and statistical copolymers of controlled length and composition. The highly ring strained cyclic olefine norbornene (NB), was selected as the monomeric unit as it allowed for the easy linkage of ibuprofen in one case and PEG in the other case, both via an ester bond. PEG was introduced in the monomeric unit for its hydrophilic properties which allowed for the formation of amphiphilic polymers that could self-assembled in aqueous environment forming NPs of specific size and shape.

As demonstrated by the GPC results, the highly active **G3** initiator afforded homopolymers as well as block and statistical copolymers, containing ibuprofen and PEG, with very narrow distribution of the molecular weights (Đ < 1.5) and M_n values that were very close to those obtained theoretically. The slightly higher dispersity values obtained for the homo- and co-polymers bearing PEG was a reflection of the PEG chain (M_n = 550) which possessed an average distribution itself.

The so synthesised block copolymer possessed amphiphilic properties and therefore could form self-assembly morphologies when added to water. In particular, as determined by TEM microscopy, small aggregates with average diameter of 19 - 28 nm and big aggregates with diameter of 100 – 120 nm were formed at the same time. Although the self-assembly process by nanoprecipitation was carried out using three different organic solvents, namely acetone, THF and acetonitrile, no specific effect was found in terms of size and shape during the formation of the NPs, thus demonstrating the versatility of the synthesised ROMP polymers. It also highlighted the importance of using a specific sequence within the polymer backbone. In fact, a random distribution of the hydrophilic/hydrophobic portions, in the statistical copolymer, did not afford specific self-assembly morphologies, but rather single chain nanoparticles which in solution aggregated with each other and eventually precipitated as big agglomerates.

The drug releasing process was also investigated against both block and statistical copolymer systems in order to further evidencing the differences between a controlled system, such that of the block copolymer, with the statistical one. Although no ibuprofen was released for a period of up to four days at 40 °C under physiological conditions (PBS, FBS and PLE), NPs could undergo degradation under basic conditions (2 M NaOH). It was determined that ibuprofen could be slowly released from polymeric NPs (> 90 % in 10 hours), while the hydrolysis was faster in the case of the single chain NPs. In this case, the majority of the drug (90 %) was released within the first two hours as a consequence of the easy access of the hydroxy ions to the ester bond.

Despite the fact that hydrolysis was not successful when systems that mimic physiological conditions were employed, it could be argued that the so formed polymeric NPs are very stable under those conditions. Therefore, they could still find an application as nanotherapeutics since no drug will be released before reaching the site of action, for instance the tumour cells. Potentially, they could also be used in chemoprevention for people with a high risk of developing cancers, as well as in diagnostic as the polymeric NPs would not release their payload prematurely under physiological conditions. Another application would include the treatment of rheumatoid arthritis (RA) since NSAIDs are known to help managing the chronic pain, inflammation and swelling that are typical of RA[114]. The use of NSAIDs based NPs would help reduce the long term administration of the drug, as well as reducing the side effects typical of NSAIDs oral administration (gastrointestinal ulceration, bleeding and renal distruption[115]).

Given the mild acidic pH values that are present in the tumour extracellular environment, some efforts have been made in the development of drug delivery candidates that possessed a bond, between the polymer and the drug, that could cleave under these conditions. Therefore, attempts to synthesise monomers consisting of an imine bond have been made. To this purpose, another NSAIDs drug, ketoprofen, has been used, however, after several attempts using different reaction conditions, a ketoprofen based NB monomer could not be obtained.

2.4. References

1   World Health Organisation, Cancer, https://www.who.int/news-room/fact-sheets/detail/cancer, (accessed 5 June 2022).

2   H. Sung, J. Ferlay, R. L. Siegel, M. Laversanne, I. Soerjomataram, A. Jemal and F. Bray, *CA. Cancer J. Clin.*, 2021, **71**, 209–249.

3   E. J. Mun, H. M. Babiker, U. Weinberg, E. D. Kirson and D. D. Von Hoff, *Clin. Cancer Res.*, 2018, **24**, 266–275.

4   A. Tewabe, A. Abate, M. Tamrie, A. Seyfu and E. A. Siraj, *J. Multidiscip. Healthc.*, 2021, **14**, 1711–1724.

5   K. Rani and S. Paliwal, *Sch. J. Appl. Med. Sci.*, 2014, **2**, 328–331.

6   V. P. Torchilin, *Eur. J. Pharm. Sci.*, 2000, **11**, S81–S91.

7   G. Liu, L. Yang, G. Chen, F. Xu, F. Yang, H. Yu, L. Li, X. Dong, J. Han, C. Cao, J. Qi, J. Su, X. Xu, X. Li and B. Li, *Front. Pharmacol.*, 2021, **12**, 1–22.

8   Y. Zhou, B. Zhang, Y. Yu, H. Shen, Q. Meng, H. Hu, L. Zhou, Y. Zhang, B. Yu and Y. Shen, *Polym. Chem*, 2018, **00**, 1–3.

9   Y. H. Bae and K. Park, *J Control Release*, 2011, **153**, 198–205.

10   F. Danhier, *J. Control. Release*, 2016, **244**, 108–121.

11   T. Lammers, F. Kiessling, W. E. Hennink and G. Storm, *J. Control. Release*, 2012, **161**, 175–187.

12   M. L. Matteucci and D. E. Thrall, *Vet. Radiol. & ultrasound Off. J. Am. Coll. Vet. Radiol. Int. Vet. Radiol. Assoc.*, 2000, **41**, 100–107.

13   Y. C. Chen, X. C. Huang, Y. L. Luo, Y. C. Chang, Y. Z. Hsieh and H. Y. Hsu, *Sci. Technol. Adv. Mater.*, 2013, **14**, 44407–44430.

14   N. C. Ngwuluka, N. A. Ochekpe and O. I. Aruoma, *Polymers (Basel).*, 2014, **6**, 1312–1332.

15   Z. L. Tyrrell, Y. Shen and M. Radosz, *Prog. Polym. Sci.*, 2010, **35**, 1128–1143.

16   S. K. Sahoo and V. Labhasetwar, *Drug Discov. Today*, 2003, **8**, 1112–1120.

17   S. N. S. Alconcel, A. S. Baas and H. D. Maynard, *Polym. Chem.*, 2011, **2**, 1442–1448.

18   A. M. Flinn and A. R. Gennery, *Orphanet J. Rare Dis.*, 2018, **13**, 1–7.

19   A. R. Ettinger, *J. Pediatr. Oncol. Nurs.*, 1995, **12**, 46–48.

20   D. L. Barnard, *Curr. Opin. Investig. Drugs*, 2001, **2**, 1530–1538.

21   A. Mehrabian, M. Mashreghi, S. Dadpour, A. Badiee, L. Arabi, S. Hoda Alavizadeh, S. Alia Moosavian and M. Reza Jaafari, *Technol. Cancer Res. Treat.*, 2022, **21**, 1–21.

22   T. Musumeci, C. A. Ventura, I. Giannone, B. Ruozi, L. Montenegro, R. Pignatello and G. Puglisi, *Int. J. Pharm.*, 2006, **325**, 172–179.

23   B. M. Cooper, J. Iegre, D. H. O' Donovan, M. O. ¨ Lwegård Halvarsson and D. R. Spring, *Chem. Soc. Rev*, 2021, **50**, 1480.

24   T. A. Wright, R. C. Page and D. Konkolewicz, *Polym. Chem.*, 2019, **10**, 434–454.

25   R. S. Zolot, S. Basu and R. P. Million, *Nat. Rev. Drug Discov.*, 2013, **12**, 259–260.

26   J. Khandare and T. Minko, *Prog. Polym. Sci.*, 2006, **31**, 359–397.

27   N. Kamaly, B. Yameen, J. Wu and O. C. Farokhzad, *Chem. Rev.*, 2016, **116**, 2602–2663.

28   C. O'Sullivan and C. Birkinshaw, *Polym. Degrad. Stab.*, 2002, **78**, 7–15.

29   S. R. Mane, A. Sathyan and R. Shunmugam, *ACS Appl. Nano Mater.*, 2020, **3**, 2104–2117.

30   X. Hu, J. Hu, J. Tian, Z. Ge, G. Zhang, K. Luo and S. Liu, *J. Am. Chem. Soc.*, 2013, **135**, 17617–17629.

31   S. Lee, A. Stubelius, N. Hamelmann, V. Tran and A. Almutairi, *ACS Appl. Mater. Interfaces*, 2018, **10**, 40378–40387.

32   J. Mao, Y. Li, T. Wu, C. Yuan, B. Zeng, Y. Xu and L. Dai, *ACS Appl. Mater. Interfaces*, 2016, **8**, 17109–17117.

33   P. A. Bertin, D. D. Smith and S. B. T. Nguyen, *Chem. Commun.*, 2005, 3793–3795.

34   H. M. Aliabadi and A. Lavasanifar, *Expert Opin. Drug Deliv.*, 2006, **3**, 139–162.

35   E. Blanco, H. Shen and M. Ferrari, *Nat. Biotechnol.*, 2015, **33**, 941–951.

36   M. Elsabahy and K. L. Wooley, *Chem. Soc. Rev.*, 2012, **41**, 2545–2561.

37   N. S. Lee, L. Y. Lin, W. L. Neumann, J. N. Freskos, A. Karwa, J. J. Shieh, R. B. Dorshow and K. L. Wooley, *Small*, 2011, **7**, 1998–2003.

38   J. C. Brendel, S. Catrouillet, J. Sanchis, K. A. Jolliffe and S. Perrier, *Polym. Chem.*, 2019, **10**, 2616–2625.

39   K. E. Zhang, R. Rossin, A. Hagooly, Z. Chen, M. J. Welch and K. L. Wooley, *J. Polym. Sci. Part A Polym. Chem.*, 2008, **46**, 7578–7583.

40   F. Alexis, E. Pridgen, L. K. Molnar and O. C. Farokhzad, *Mol. Pharm.*, 2008, **5**, 505–515.

41   K. Park, *J. Control. Release*, 2010, **142**, 147–148.

42   A. S. Deshmukh, P. N. Chauhan, M. N. Noolvi, K. Chaturvedi, K. Ganguly, S. S. Shukla, M. N. Nadagouda and T. M. Aminabhavi, *Int. J. Pharm.*, 2017, **532**, 249–268.

43   F. Balkwill and A. Mantovani, *Lancet*, 2001, **357**, 539–545.

44   Z. Werb and L. M. Coussens, *Nat. Publ. Gr.*, 2002, **420**, 860–867.

45   S. Kim, D. L. Shore, L. E. Wilson, E. I. Sanniez, J. H. Kim, J. A. Taylor and D. P. Sandler, *BMC Cancer*, 2015, **15**, 960.

46   T. Dierssen-Sotos, I. Gómez-Acebo, M. de Pedro, B. Pérez-Gómez, S. Servitja, V. Moreno, P. Amiano, T. Fernandez-Villa, A. Barricarte, A. Tardon, M. Diaz-Santos, R. Peiro-Perez, R. Marcos-Gragera, V. Lope, E. Gracia-Lavedan, M. H. Alonso, M. J. Michelena-Echeveste, A. Garcia-Palomo, M. Guevara, G. Castaño-Vinyals, N. Aragonés, M. Kogevinas, M. Pollán and J. Llorca, *BMC Cancer*, 2016, **16**, 660.

47   A. C. Vidal, L. E. Howard, D. M. Moreira, R. Castro-Santamaria, G. L. Andriole and S. J. Freedland, *Clin. Cancer Res.*, 2015, **21**, 756–762.

48   E. H. Ruder, A. O. Laiyemo, B. I. Graubard, A. R. Hollenbeck, A. Schatzkin and A. J. Cross, *Am. J. Gastroenterol.*, 2011, **106**, 1340–1350.

49   B. Trabert, R. B. Ness, W. H. Lo-Ciganic, M. A. Murphy, E. L. Goode, E. M. Poole, L. A. Brinton, P. M. Webb, C. M. Nagle, S. J. Jordan, H. A. Risch, M. A. Rossing, J. A. Doherty, M. T. Goodman, G. Lurie, S. K. Kjær, E. Hogdall, A. Jensen, D. W. Cramer, K. L. Terry, A. Vitonis, E. V Bandera, S. Olson, M. G. King, U. Chandran, H. Anton-Culver, A. Ziogas, U. Menon, S. A. Gayther, S. J. Ramus, A. Gentry-Maharaj, A. H. Wu, C. L. Pearce, M. C. Pike, A. Berchuck, J. M. Schildkraut and N. Wentzensen, *J. Natl. Cancer Inst.*, 2014, **106**, 1–11.

50   A. E. Prizment, A. R. Folsom and K. E. Anderson, *Cancer Epidemiol. Prev. Biomarkers*, 2010, **19**, 435–442.

51   R. S. Y. Wong, *Adv. Pharmacol. Sci.*, 2019, **2019**, 1–10.

52   E. Ricciotti and G. A. Fitzgerald, *Arterioscler. Thromb. Vasc. Biol.*, 2011, **31**, 986–1000.

53   Z. Zhang, F. Chen and L. Shang, *Cancer Manag. Res.*, 2018, **10**, 4631–4640.

54   B. Rigas, I. S. Goldman and L. Levine, *J. Lab. Clin. Med.*, 1993, **122**, 518–523.

55   D. Wang and R. N. DuBois, *Semin. Oncol.*, 2004, **31**, 64–73.

56   T. L. McLemore, W. C. Hubbard, C. L. Litterst, M. C. Liu, S. Miller, N. A. McMahon, J. C.

Eggleston and M. R. Boyd, *Cancer Res.*, 1988, **48**, 3140–3147.

57   M. Hambek, M. Baghi, J. Wagenblast, J. Schmitt, H. Baumann and R. Knecht, *Head Neck*, 2007, **29**, 244–248.

58   W. Badri, K. Miladi, Q. A. Nazari, H. Greige-Gerges, H. Fessi and A. Elaissari, *Int. J. Pharm.*, 2016, **515**, 757–773.

59   M. Zhao, Y. Huang, Y. Chen, J. Xu, S. Li and X. Guo, *Bioconjug. Chem.*, 2016, **27**, 2198–2205.

60   R. M. Shah, D. S. Eldridge, E. A. Palombo and I. H. Harding, *Int. J. Pharm.*, 2016, **515**, 543–554.

61   D. Dupeyrón, M. Kawakami, A. M. Ferreira, P. R. Cáceres-Vélez, J. Rieumont, R. B. Azevedo and J. C. T. Carvalho, *Int. J. Nanomedicine*, 2013, **8**, 3467–3477.

62   S. Akkad and C. J. Serpell, *Macromol. Rapid Commun.*, 2018, **39**, 1–5.

63   K. Abbas, M. Amin, M. A. Hussain, M. Sher, S. N. Abbas Bukhari and K. J. Edgar, *RSC Adv.*, 2017, **7**, 50672–50679.

64   P. Prasher, M. Sharma, M. Mehta, S. Satija, A. A. Aljabali, M. M. Tambuwala, K. Anand, N. Sharma, H. Dureja, N. K. Jha, G. Gupta, M. Gulati, S. K. Singh, D. K. Chellappan, K. R. Paudel, P. M. Hansbro and K. Dua, *Colloids Interface Sci. Commun.*, 2021, **42**, 100418.

65   A. Agostini, U. Capasso Palmiero, S. D. A. Barbieri, M. Lupi and D. Moscatelli, *Nanotechnology*, 2018, **29**, 225604.

66   S. Shehata, C. J. Serpell and S. C. G. Biagini, *Mater. Today Commun.*, 2020, **25**, 101562.

67   S. C. G. Biagini, M. P. Coles, V. C. Gibson, M. R. Giles, E. L. Marshall and M. North, *Polymer (Guildf).*, 1998, **39**, 1007–1014.

68   C. Slugovc, *Macromol. Rapid Commun.*, 2004, **25**, 1283–1297.

69   L. T. Birchall, S. Shehata, C. J. Serpell, E. R. Clark and S. C. G. Biagini, *J. Chem. Educ.*, 2021,

98, 4013–4016.

70   D. Craig, *J. Am. Chem. Soc*, 1951, **73**, 4889–4892.

71   J. B. Matson and R. H. Grubbs, *J. Am. Chem. Soc.*, 2008, **130**, 6731–6733.

72   J. P. Cole, J. J. Lessard, C. K. Lyon, B. T. Tuten and E. B. Berda, *Polym. Chem.*, 2015, **6**, 5555–5559.

73   K. Sakata and H. Fujimoto, *European J. Org. Chem.*, 2016, **2016**, 4275–4278.

74   Y. C. Teo and Y. Xia, *Macromolecules*, 2015, **48**, 5656–5662.

75   M. Tsakos, E. S. Schaffert, L. L. Clement, N. L. Villadsen and T. B. Poulsen, *Nat. Prod. Rep.*, 2015, **32**, 605–632.

76   K. Tori, Y. Hata, R. Muneyuki, Y. Takano, T. Tsuji and H. Tanida, *Can. J. Chem.*, 1964, **42**, 926–933.

77   S. C. G. Biagini and A. L. Parry, *J. Polym. Sci. Part A Polym. Chem.*, 2007, **45**, 3178–3190.

78   F. Xu, B. Simmons, R. A. Reamer, E. Corley, J. Murry and D. Tschaen, *J. Org. Chem.*, 2008, **73**, 312–315.

79   M. and T. H. Ho, CS; Lam, CWS; Chan, MHM; Cheung, RCK; Law, LK; Lit, LCW; Ng, KF; Suen, *Clin Biochem Rev*, 2003, **24**, 3–12.

80   B. K. Keitz, A. Fedorov and R. H. Grubbs, *J. Am. Chem. Soc.*, 2012, **134**, 2040–2043.

81   B. Al Samak, V. Amir-Ebrahimi, D. G. Corry, J. G. Hamilton, S. Rigby, J. J. Rooney and J. M. Thompson, *J. Mol. Catal. A Chem.*, 2000, **160**, 13–21.

82   X. Yang, S. R. Gitter, A. G. Roessler, P. M. Zimmerman and A. J. Boydston, *Angew. Chemie - Int. Ed.*, 2021, **60**, 13952–13958.

83   S. K. Bharti and R. Roy, *TrAC - Trends Anal. Chem.*, 2012, **35**, 5–26.

84   M. G. Hyatt, D. J. Walsh, R. L. Lord, J. G. Andino Martinez and D. Guironnet, *J. Am. Chem. Soc.*, 2019, **141**, 17918–17925.

85   D. J. Walsh, S. H. Lau, M. G. Hyatt and D. Guironnet, *J. Am. Chem. Soc.*, 2017, **139**, 13644–13647.

86   A. H. E. Müller and K. Matyjaszewski, *Controlled and Living Polymerizations*, 2010.

87   W. W. Schulz, *Modern size-exclusion liquid chromatography: Practice of gel permeation and gel filtration chromatography*, 1980, vol. 195.

88   V. Forcina, A. García-Domínguez and G. C. Lloyd-Jones, *Faraday Discuss.*, 2019, **220**, 179–195.

89   D. Lombardo, M. A. Kiselev, S. Magazù and P. Calandra, *Adv. Condens. Matter Phys.*, 2015, **2015**, 1–22.

90   N. T. Southall, K. A. Dill and A. D. J. Haymet, *J. Phys. Chem. B*, 2002, **106**, 521–533.

91   A. Blanazs, S. P. Armes and A. J. Ryan, *Macromol. Rapid Commun.*, 2009, 30, 267–277.

92   H. Phan, R. I. Minut, P. McCrorie, C. Vasey, R. R. Larder, E. Krumins, M. Marlow, R. Rahman, C. Alexander, V. Taresco and A. K. Pearce, *J. Polym. Sci. Part A Polym. Chem.*, 2019, **57**, 1801–1810.

93   J. Stetefeld, S. A. McKenna and T. R. Patel, *Biophys. Rev.*, 2016, **8**, 409–427.

94   S. Bhattacharjee, *J. Control. Release*, 2016, **235**, 337–351.

95   C. K. Lyon, A. Prasher, A. M. Hanlon, B. T. Tuten, C. A. Tooley, P. G. Frank and E. B. Berda, *Polym. Chem.*, 2015, **6**, 181–197.

96   A. Rizvi, J. T. Mulvey, B. P. Carpenter, R. Talosig and J. P. Patterson, *Chem. Rev.*, 2021, **121**, 14232–14280.

97   T. F. Tadros, ed. R. A. B. T.-E. of P. S. and T. (Third E. Meyers, Academic Press, New York,

2003, pp. 423–438.

98   Y. Nakahara, T. Kida, Y. Nakatsuji and M. Akashi, *Langmuir*, 2005, **21**, 6688–6695.

99   Ö. Topel, B. A. Çakir, L. Budama and N. Hoda, *J. Mol. Liq.*, 2013, **177**, 40–43.

100   A. Chatterjee, S. P. Moulik, S. K. Sanyal, B. K. Mishra and P. M. Puri, *J. Phys. Chem. B*, 2001, **105**, 12823–12831.

101   L. J. White, N. J. Wells, L. R. Blackholly, H. J. Shepherd, B. Wilson, G. P. Bustone, T. J. Runacres and J. R. Hiscock, *Chem. Sci.*, 2017, **8**, 7620–7630.

102   L. N. Woodard and M. A. Grunlan, *ACS Macro Lett.*, 2018, **7**, 976–982.

103   F. Danhier, O. Feron and V. Préat, *J. Control. Release*, 2010, **148**, 135–146.

104   I. Mellman, *Annu. Rev. Biochem.*, 1986, **55**, 663–700.

105   L. Pichavant, C. Bourget, M. C. Durrieu and V. Héroguez, *Macromolecules*, 2011, **44**, 7879–7887.

106   E. R. Gillies and J. M. J. Fréchet, *Bioconjug. Chem.*, 2005, **16**, 361–368.

107   Y. Gu, Y. Zhong, F. Meng, R. Cheng, C. Deng and Z. Zhong, *Biomacromolecules*, 2013, **14**, 2772–2780.

108   J. Z. Du, X. J. Du, C. Q. Mao and J. Wang, *J. Am. Chem. Soc.*, 2011, **133**, 17560–17563.

109   L. T. Birchall, S. Shehata, S. McCarthy, H. J. Shepherd, E. R. Clark, C. J. Serpell and S. C. G. Biagini, *Polym. Chem.*, 2020, **11**, 5279–5285.

110   R. Wang, M. Ma, X. Gong, G. B. Panetti, X. Fan and P. J. Walsh, *Org. Lett.*, 2018, **20**, 2433–2436.

111   S. Morales, F. G. Guijarro, J. L. García Ruano and M. B. Cid, *J. Am. Chem. Soc.*, 2014, **136**, 1082–1089.

112   D. A. Cogan and J. A. Ellman, *J. Am. Chem. Soc.*, 1999, **121**, 268–269.

113   M. Selva, P. Tundo and C. A. Marques, *Synth. Commun.*, 1995, **25**, 369–378.

114   M. Del Grossi Paglia, M. T. Silva, L. C. Lopes, S. Barberato-Filho, L. G. Mazzei, F. C. Abe and C. de Cassia Bergamaschi, *PLoS One*, 2021, **16**, 1–23.

115   M. J. Thun, S. Jane Henley and C. Patrono, *Nonsteroidal anti-inflammatory drugs as anticancer agents: Mechanistic, pharmacologic, and clinical issues*, 2002, vol. 94.

CHAPTER 3. CATIONIC ROMP POLYMERS CONTAINING SUPRAMOLECULAR SELF-ASSOCIATING AMPHIPHILIC (SSA) MOLECULES AND THEIR ANTIMICROBIAL ACTIVITY.

3.1. Introduction

For decades infections in humans have been kept in check by the development of antimicrobial drugs use. However, the treatment options have become more and more limited due to the rapid evolution of antimicrobial resistance (AMR). The World Health Organisation (WHO) has declared that AMR is one of the top 10 global public health threats that humanity is facing[1] and is primarily caused by the misuse and overuse of antimicrobials. Microorganisms such as bacteria, viruses, fungi, and parasites mutate and change their composition over time making the drugs used to treat them not effective anymore. Therefore, AMR refers to the ability of the cells to survive at higher concentrations of drugs than the typical lethal dose. For example, a study carried out by the European Centre for Disease Prevention and Control (ECDC) has estimated that since 2007 about 3,300 people die in the EU/EEA (European Union/European Economic Area) each year as a direct consequence of an infection due to AMR[2]. The latest data published by the UK Health Security Agency (UKHSA) in November 2021, showed a decrease in antibiotic resistant bloodstream infections from 65,583 in 2019 to 55,384 in 2020 which was the lowest since 2016[3]. In the same way, the number of deaths caused by AMR decreased in 2020 where 2,228 deaths were estimated compared to 2,596 in 2019[3]. However, it is important to highlight that this decline is mainly due to the restrictions that took place during the pandemic caused by Covid-19, where less social mixing and enhanced hand hygiene have played an important role, rather than the discovery of new antibiotics. For instance, the total consumption of antibiotics, intended as daily doses per 1,000 inhabitants, has decreased by 10.9 % between 2019 and 2020.

Figure 3.1 shows the incidence of bloodstream infections (BSIs) caused by 8 main pathogens (also known as superbugs) per 100,000 people between 2016 and 2020. It is evident that for each pathogen there is an increase in BSI between 2016 and 2019, while the infection decreased in 2020

as a result of the reduced contact between individuals due to Covid-19 pandemic. *Escherichia coli*, for instance, caused a BSI rate of 73.0 per 100,000 population in 2016 with an increase to 77.7 in 2019, and a decrease to 66.9 in 2020.
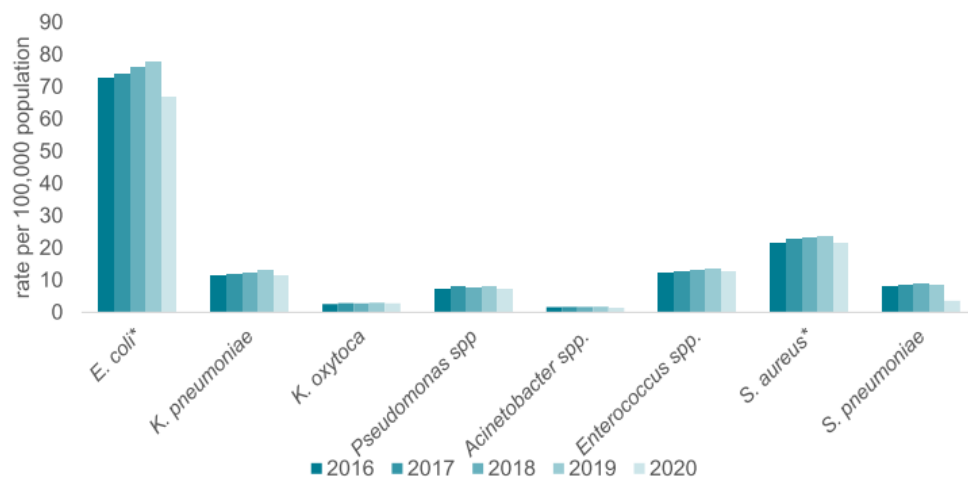
Fig. 3.1. Incidence per 100,000 population of 8 main pathogen bloodstream infection in England between 2016 and 2020. Figure was taken from the 2020 – 2021 report of the WHO[3]. This image contains public sector information licensed under the Open Government Licence v3.0.

3.1.1. Polymer therapeutics with antimicrobial activity

In order to overcome the issue caused by antimicrobial resistance, in recent years scientists have focused their attention into the development of antimicrobial polymers which mimic the biophysical and physicochemical properties of naturally occurring antimicrobial peptides (AMPs)[4]. They present, in fact, higher therapeutic stability and slower evolution of resistant strain bacteria compared to traditional small molecule antibiotics[4,5]. Typically, conventional antibiotics inhibit bacterial metabolic processes such as cell growth and cell division by acting on DNA and RNA synthesis as well as wall or protein synthesis. In response to the antimicrobial action, some bacteria enter a dormant cell state caused by the slowing of cellular metabolism. In this way bacterial cells do not actively divide and become intrinsically more resistant to antibiotics[6,7]. On the other hand, AMPs act by targeting the lipid bilayer bacterial cell membrane which is not involved in any of the typical resistance mechanisms[8,9]. This way, the bacterial cells can be killed without harming human cells and especially without inducing resistance (Figure 3.2). Naturally occurring AMPs, such as

Meganin-2[10], Protegrin 1[11], Indolicidin[12] and β-defensin 3[13], are amphiphilic peptides mainly composed of nonpolar side chain amino acids such as tryptophan and polar/cationic amino acid units such as lysine and arginine. As shown in Figure 3.2, the cationic residues (red in Figure 3.2) are attracted electrostatically to the bacterial cell membrane, which is mainly composed of anionic groups, while the hydrophobic residues (blue) are inserted into the non-polar membrane core, thus initiating membrane disruption. This mechanism is less specific and therefore more difficult for the bacteria to avoid. Furthermore, because the bacterial cell membrane is highly negatively charged compared to those of human cells, AMPs are more selective to bacteria over human cells[14,15].
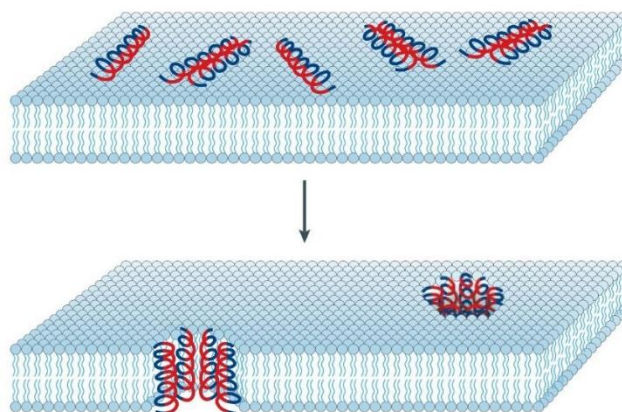
Fig. 3.2. Representation of antimicrobial peptides (AMPs) inducing bacterial cells death. Here, the AMPs interact first with the cell membrane fallowed by insertion into the bilayer. The hydrophobic portion of AMPs (blue) align with the lipid region, while the hydrophilic portion (red) of the AMPs form the internal core. Reproduced by permission from Springer Nature Customer Service Centre GmbH (reference 8).

Due to the poor bioavailability and the high production costs of AMPs, in the past decade several research groups have started developing synthetic polymers that possessed similar physicochemical features to natural AMPs, which is the key for improved antimicrobial activity. In order to selectively target and disrupt bacterial cell membranes, polymers with cationic and hydrophobic groups have been developed (amphiphilic cationic polymers, ACPs)[16]. Such polymers can be prepared either by the polymerisation of monomers bearing antimicrobial functionalities, or by modification of the polymer structure via post-polymerisation reactions[17]. Different polymerisation techniques have been employed in order to prepare synthetic antimicrobial

polymers. These include living free radical polymerisations such as atom transfer radical polymerisation (ATRP)[18,19] and reversible addition fragmentation chain transfer polymerisation (RAFT)[20,21], but also ring-opening polymerisation (ROP)[22] and ring-opening metathesis polymerisation (ROMP) for which examples have been widely discussed in Chapter 1, Section 1.3.2.2. Examples are shown in Figure 3.3.
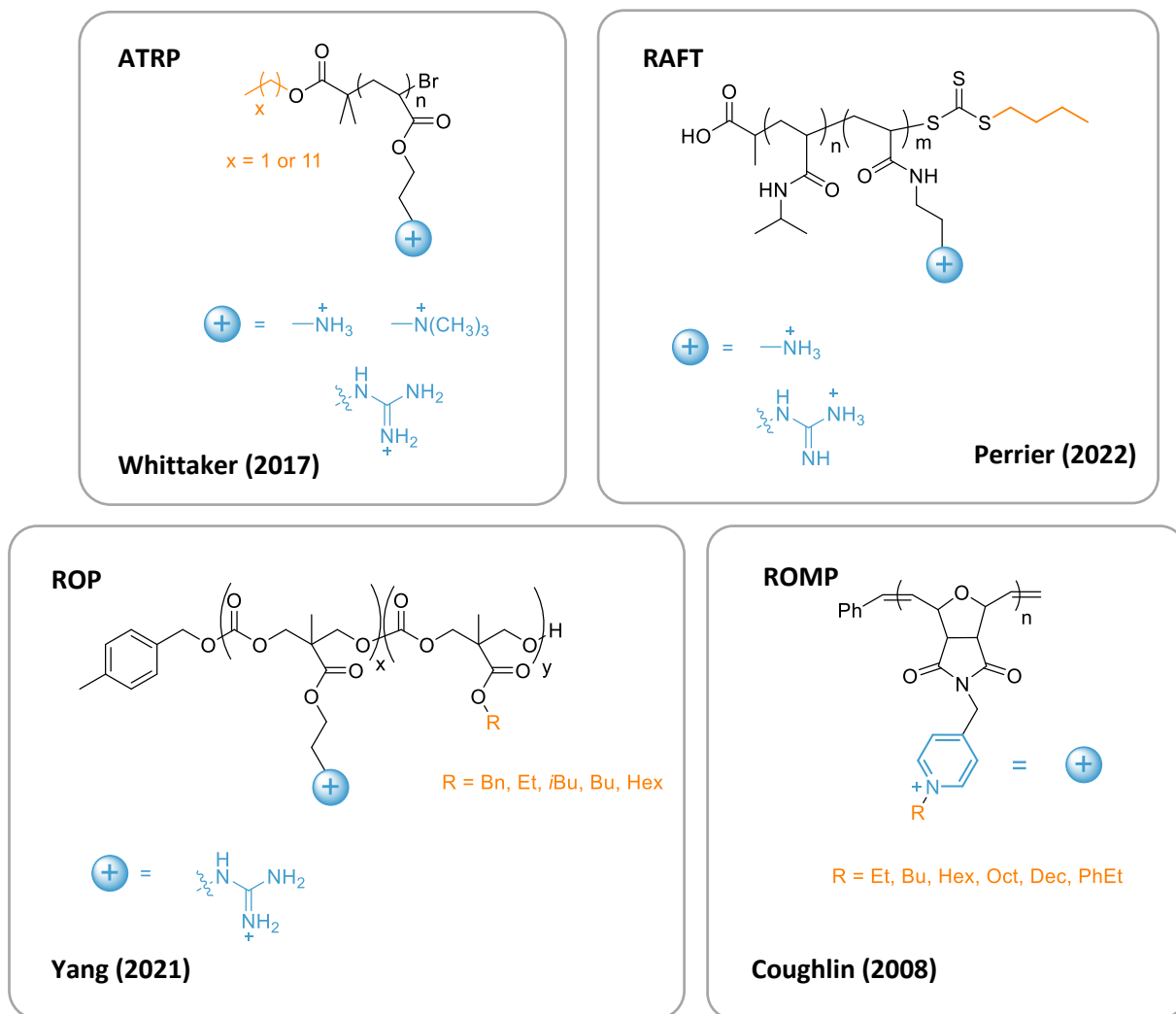
Fig. 3.3. Examples of polymers possessing antimicrobial activity synthesised using ATRP, RAFT, ROP and ROMP in the preparation of polyacrylates, polymethacrylates, polycarbonates and polynorbornenes respectively.

When designing antimicrobial polymers, several parameters need to be considered:

(i)   The amphiphilic balance: excessive hydrophobicity can generate polymers with poor water solubility and high toxcity, while very low hydrophobicity leads to poor antimicrobial activity[23].

(ii)   The cationic group structure: for instance, doubly-charged amine species such as DABCO show higher activity compared to monocharged amines such as the pyridinium cation[24], whilst improvement in antimicrobial activity can be achieved by the use of phosphonium cations[25,26].

(iii)   The molecular weight (MW): high MW affects properties such as solubility, diffusion and aggregation, and at the same time increases the toxicity towards human cells[23].

(iv)   The polymer topology: this includes homopololymers, random and block copolymers[24] but also branched and star shape polymers[27,28]. Generally random copolymers show higher antimicrobial activity compared to block copolymers as the latter tend to form nanoparticles in solution upon self-assembly, thus encapsulating the cationic units into the core shell. Examples are discussed in Chapter 1, Section 1.3.2.2.

Taking all of these parameters into account, in this project we were interested in developing a novel antimicrobial polymer prepared via ROMP in the form of a drug delivery system, where the drugs used are urea/thiourea sulfonate anions synthesised within the Hiscock group at the Univeristy of Kent. These molecules are identified as supramolecular self-associated amphiphilic salts and are known as SSAs.

3.1.2. Supramolecular self-associating amphiphiles (SSAs)

The Hiscock group have studied and developed a new class of molecules, named SSAs (supramolecular self-associating amphiphiles) which have been demonstrated to possess antimicrobial activity against both Gram-positive (methicillin-resistant *Staphylococcus aureus*,

MRSA)[29] and Gram-negative bacteria (*Escherichia coli*)[30,31]. SSA molecules are urea/thiourea sulfonate-based salts and are constructed so that they possess an anionic hydrogen bond accepting (HBA) group, a urea/thiourea moiety that acts as both a HBA and HBD (hydrogen bond donating) group and a hydrophobic region (Figure 3.4).
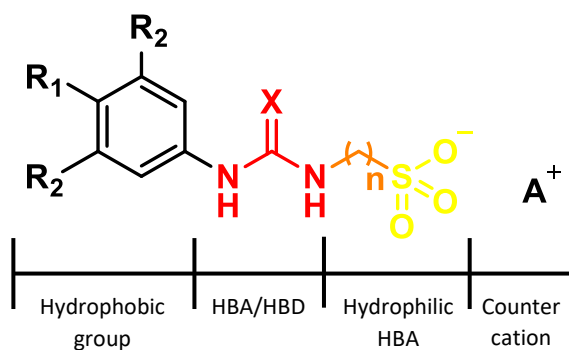
Fig. 3.4. General structure of SSAs. They possess a hydrophobic group (black), an HBA/HBD moiety (red) where X is usually an O or an S atom, a spacer (orange), a hydrophilic HBA (yellow) and a counter cation (A$^+$).

A library of about 50 SSAs has been prepared by Hiscock *et al*. via alteration of the substituents R_1 and R_2 in the hydrophobic group (small substituents such as CF_3, OMe, NO_2, NH_2, H, but also aromatic rings such as benzothiazole, naphthalene, anthracene have shown to alter the acidity of the NHs[32]) and/or the spacer between the urea/thiourea and the sulfonate groups (n = 1, 2 or 3). Different counter cations, mainly TBA (tertrabutylammonium), pyridinium, potassium and sodium have also been employed[32].

Owing to the presence of two HBA groups (the O/S on urea/thiourea moiety and the SO_3^-) and one HBD group (the NHs on the urea/thiourea), a so-called "frustrated" system is obtained. In this system an intramolecular hydrogen bond cannot be formed between the HBA and HBD groups of the same molecule and therefore an interaction between different molecules occurs. This means that the anionic component of SSAs can adopt multiple self-associative hydrogen bonding modes simultaneously[33] as shown in Figure 3.5 (b). Hiscock *et al*. have shown that in the solid state (via X-ray diffraction), SSAs can form: (i) a urea/thiourea dimer, (ii) a urea/thiourea-anion stacking and (iii) a urea/thiourea-urea/thiourea stacking (*syn* or *anti*) modes that can be manipulated by changing

the chemical composition, the solvent, but also by modifying the counter cation[34]. For instance, it was found that the presence of a weakly coordinating cation, such as TBA, tend to form urea-anion dimers, while the presence of strongly coordinating cations, such as K^+ and Na^+, preferentially form urea-urea stackings[34]. However, it's important to note that the binding modes determined through solid state studies may differ to the modes that SSAs form in the solution state, as self-association can be altered by the presence of a solvent. The Hiscock group have widely demonstrated[35] that, in the solution state, SSAs can form aggregates in both DMSO and water. In the first case, dimeric species with hydrodynamic diameters < 10 nm are formed, while in the second case SSAs tend to form larger aggregates with diameters > 100 nm. These larger structures have been determined by a combination of ^1H NMR, DLS and tensiometer which is used for the determination of the critical aggregate concentration (CAC). Furthermore, they could be visualised by transmission and fluorescence (when possible) microscopy. The presence of dimeric species in DMSO were also confirmed to exist in the gas-phase, determined by high resolution mass spectrometry (HR-MS), and in the solid phase, using X-ray diffraction (XRD).

Whilst in many cases the cationic component of amphiphilic salts is the one that carries the antimicrobial activity, Hiscock *et al*. have demonstrated that it is the anionic component of SSAs that form interactions with the bacterial membrane, thus causing bacterial cell disruption. The interaction of SSAs with the bacterial phospholipid bilayer was studied by solution state ^1H NMR using a SMA (styrene-maleic anhydride copolymer) phospholipid nanodisc[36]. It was hypothesised that SSAs preferentially interact with phosphatidylethanolamine (PE) and phosphatidylglycerol (PG) over phosphatidylcholine (PC) phospholipid head groups. Since PC is found to be prevalent at the outer surface of eukariotic cells, SSAs would be more selective towards the bacterial cell membrane and thus are not toxic to human cells. As shown in Figure 3.5 (c), SSAs are hypothesied to complex both PE and PG through a combination of hydrogen bond formation and electrostatic interactions. In the case of PC, only weak electrostatic interactions are possible between the sulfonate group of SSAs and the tertiary ammonium group of PC, therefore the general complexation is weak. The

quantification of small molecules:phospholipid interactions[36] was studied by Hisckock *et al.* on three SSA models using a novel solution-state 1D ^{1}H NMR assay.
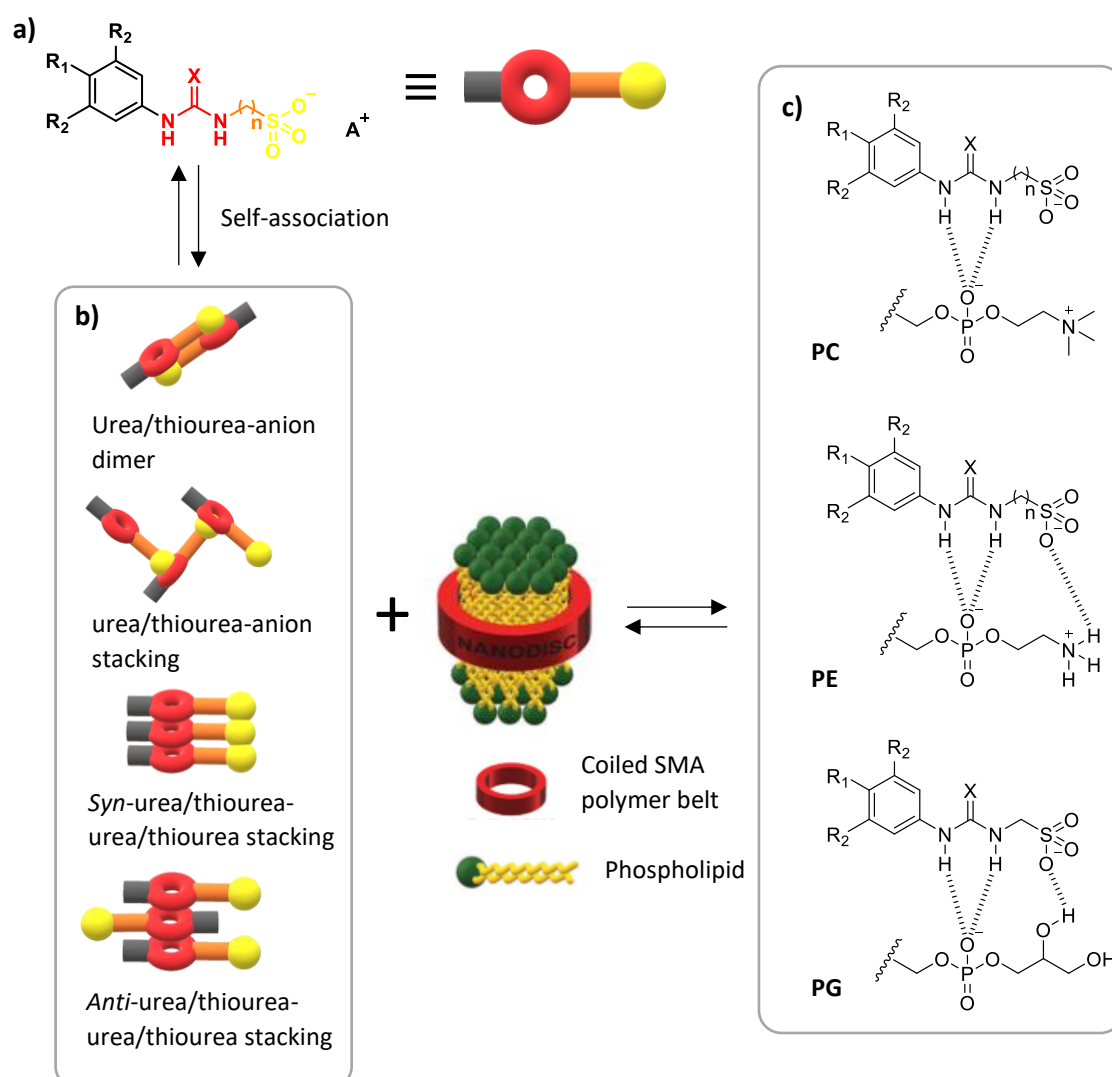
Fig. 3.5. Scheme showing: (a) a representative structure of the SSA; (b) a representation of the hydrogen bonding modes adopted by the anionic component of SSAs; (c) hypothesised interaction of SSA with the phospholipid bilayer of bacteria cell membrane. Figure adapted from reference 36.

3.1.3. Aim of the study

In collaboration with the Hiscock group, it was decided to develop a novel polynorbornene system bearing the antimicrobial SSA molecules synthesised within their group. In particular, it was decided to synthesise pyridine derived norbornene (NB) and oxanorbornene (ONB) molecules (**4b** and **9**, Scheme 3.1, a) taking inspiration from the paper published by Tew *et al.*[17] in 2008, where amphiphilic polyoxanorbornene (polyONB) bearing quaternary alkyl pyridinium side chains showed

113

bacterial growth inhibition against *B. subtilis* and *E. coli*. These pyridine-based NB and ONB

molecules were then reacted with two different SSAs (**SSA-1** and **SSA-2**) in order to form four

different monomers (**mon1 – mon4**) in the form of salts, which were then polymerised via ROMP

in order to obtain four novel amphiphilic homopolymers (**poly1 – poly4**) (Scheme 3.1, b). Both

monomers and polymers were then tested against Gram-positive (MRSA) and Gram-negative (*E.*

coli) bacteria.
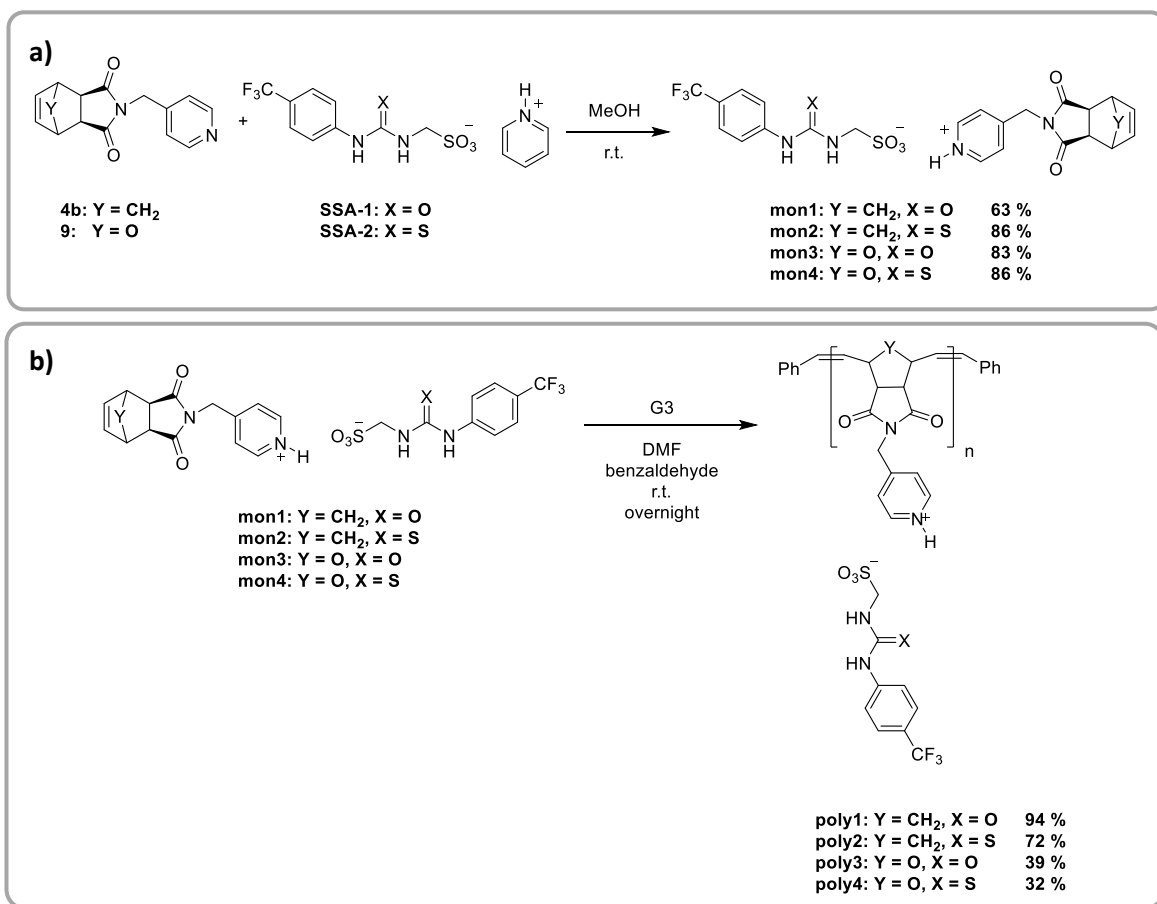
Scheme 3.1. a) synthesis of **mon1 – mon4** and b) synthesis of homopolymers **poly1 – poly4** carried out in this project.

3.2. Results and discussion

3.2.1. Monomer synthesis

The monomers required to synthesise the desired ROMP polymers were not commercially available and therefore they were synthesised as shown in the following sections. The monomers were pyridinium-based NB or ONB molecules, where the counter anion was the urea- or thiourea-sulfonate SSA (**SSA-1** and **SSA-2** respectively).

It is known from the literature that *exo* isomers react faster than the *endo* isomers[37], and therefore *exo* monomers were synthesised and used for the preparation of ROMP polymers. However, each reaction was first tested on the *endo* isomer as it is commercially available at a cheaper price (Chapter 2, Section 2.2.1).

3.2.1.1. Synthesis of pyridine-based NB intermediate, 4a and 4b

Scheme 3.2 shows the synthetic pathway used to obtain the *endo*/*exo*-NB derived pyridine **4a** and **4b**. These were obtained with a modification from the literature procedure[17]. In the first step, *endo*- and *exo*-carbic anhydride (**1a** and **1b**) were each reacted with 1 molar equivalent of 4-(aminomethyl)pyridine **2** at room temperature using DCM as a solvent. The reactions occurred rapidly, in each case a white solid precipitated after only two minutes from the complete addition of reactant **2**. However, the reactions were left to stir for 1 hour in order to make sure that all carbic anhydride was consumed. The white solid was filtered and washed with DCM, affording the open amides, **3a** (*endo*) and **3b** (*exo*), with yields of 90 % and 92 % respectively. In the second step, **3a** and **3b** were each dissolved in a solution of 0.5 M of methanolic HCl. The reactions were heated for 50 minutes at 50 °C[38] and the pure products, as the closed amides, were obtained by neutralisation with saturated NaHCO$_3$ solution and then extraction with DCM. Compounds **4a** (*endo*) and **4b** (*exo*) were obtained as white solids with yields of 81 % and 83 % respectively.
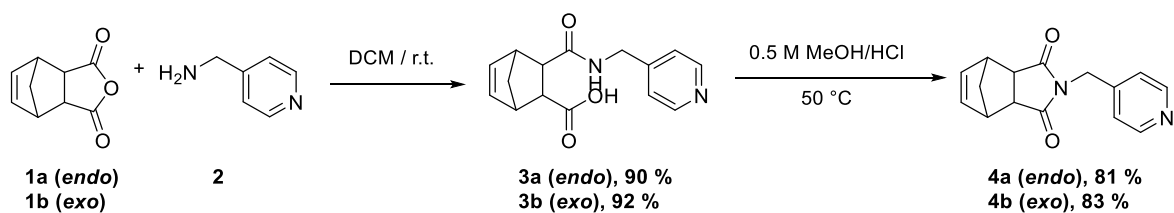
Scheme 3.2. Synthetic scheme for the preparation of pyridine containing NB intermediate.

The formation of both *endo* and *exo* compounds **3** and **4** was confirmed by ^{1}H NMR. It is important noting that in each case, *endo* and *exo* compounds possess slightly different NMR spectra. Due to the difference in stereochemistry between *endo* and *exo* compounds, the chemical environment of each proton differs, and this has therefore an effect on their chemical shift and on their multiplicity. For instance, ^{1}H NMR spectra in DMSO-d_6 of compounds **3a** and **3b** show some differences (Appendix 2, Figures S1 and S5); since compound **3** is asymmetric, the characteristic alkene peaks of norbornene are found at different frequencies. This is particularly noticeable on *endo* isomer **3a**, where two doublets of doublets that integrate for 1H each are present in the typical alkene region, at 6.19 ppm and 5.94 ppm. On the contrary, in the *exo* isomer **3b**, the alkene peaks are present as a multiplet that integrates for 2H at 6.24-6.21 ppm, therefore they are slightly more deshielded in comparison to the *endo* alkene protons (peaks are shifted downfield). Formation of compound **3** is also confirmed by the presence of the NH peak, which in both cases results in a triplet due to the coupling with the CH$_2$ in para position to the pyridine ring. The peak integrates for 1H and it resonates at 8.34 ppm and 8.52 ppm for compound **3a** and **3b** respectively.

The behaviour of the bridgehead protons on the norbornene ring is also interesting. For the *endo* isomer **3a** we can observe the typical "roofing effect" of an AB system, where second order spectra are obtained, and in fact we can determine a doublet of doublets centred at 1.28 ppm that integrates for 2H. However, the *exo* isomer **3b** shows a different behaviour where two distinct doublets with integrations of 1H at 2.25 ppm and 1.25 ppm are observed, as if the spectrum is first order. The difference between the Larmor frequencies of the coupled nuclei (Δv) in **3a** and **3b** is calculated using MestReNova[39] (Δv*endo* = 24 Hz; Δv*exo* = 400 Hz). In the *exo* isomer it is found that Δv

is larger compared to the coupling constant (J_{AB} = 8.23 Hz) and the ratio $\Delta v/J_{AB}$ = 50 is typical of first order NMR spectra. Whereas, in the *endo* isomer Δv is closer to the coupling constant (J_{AB} = 7.4 Hz) and thus a second order effect is obtained.

No major difference is noted between **3a** and **3b** when comparing the aromatic protons on the pyridine ring. This is due to the large distance between the pyridine and the norbornene ring and therefore the chemical shift for the aromatic protons is not affected as strongly by the isomerisation.

Compounds **4a** and **4b** were obtained by ring closing of **3a** and **3b** in methanolic HCl. The latter are symmetric molecules and thus the NMR spectra for *endo-* and *exo*-NB pyridine-based intermediates (**4a** and **4b**) are comprised of a lower number of protons compared to their open counterparts (**3a** and **3b**). For instance, as shown in Figure S7 (Appendix 2), the alkene proton of the *exo* isomer **4b** in DMSO-d_6 is now a triplet at 6.32 ppm that integrates for 2H. The CH_2 in para position to the pyridine ring does not couple to any other close proton and is therefore a singlet at 4.57 ppm. The same CH_2 protons in **3b** are found to form a quartet of doublets at 4.27 ppm, due to the protons not being magnetically equivalent. By COSY NMR it is determined that the CH_2 protons are coupling to each other as well as to the closest aromatic proton. Furthermore, the formation of **4a** and **4b** is confirmed by the absence of the NH proton. In **4b**, it can also be seen that the peaks related to the bridgehead protons are close to one another, meaning that the "roofing effect", usually obtained for rigid systems like carbic anhydride and its derivatives, is more pronounced (Δv = 100 Hz, J_{AB} = 9.80 Hz).

3.2.1.2. Synthesis of pyridine-based ONB intermediate, 9

ONB (**7**) was selected due to the ease of synthesis, in fact, the Diels-Alder [4+2] cycloaddition of furan (**5**) and maleic anhydride (**6**) was carried out under very mild conditions, at room temperature in THF for 1 hour[40] (Scheme 3.3). The product **7** was obtained by recrystallisation in the reaction

solvent with a yield of 71 %. In general, during this reaction, only the *exo* isomer is formed, which constitutes the only known exception to the rule where the *endo* isomer is predominantly formed.
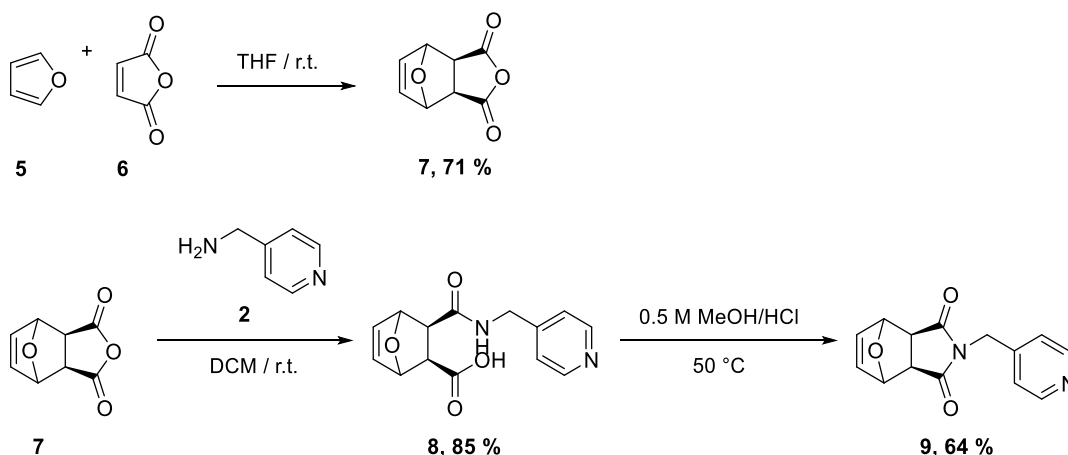
Scheme 3.3. Synthetic scheme for the preparation of pyridine containing ONB intermediate, **9**.

The stereochemistry of this reaction has been widely studied both experimentally[41,42,43], using NMR spectroscopy, and theoretically[44], using computational methodologies. Lee and Herndon[45] studied the reaction between furan and maleic anhydride using NMR spectroscopy. They demonstrated that the reaction in acetonitrile at 40 °C with a reactant concentration of 1.50 M, formed initially only the *endo* adduct. However, at 24 minutes the concentration of *endo* and *exo* was the same, while after 48 hours only *exo* was evident in the reaction mixture. They also demonstrated that at lower concentrations (0.5 M), the reaction became faster and the *exo* adduct was obtained after 50 minutes. Lee and Herndon were able to calculate the rate constant (k_{endo} and k_{exo}) for the formation of *endo* and *exo* isomers and found that $k_{endo} > 500 \, k_{exo}$, which corresponded to an activation energy difference (ΔEa) of 15.9 kJ/mol in favour of the *endo* adduct (kinetically favoured). However, the *exo* adduct was 7.9 kJ/mol more stable than *endo* (thermodynamically favoured), and due to the reversibility of the process, only the *exo* isomer was eventually formed in the reaction. Later, using quantum chemical calculations, Svatos *et al.*[46] were able to show that in acetonitrile the energy of the transition state (TS) for the *endo* isomer was only 0.3 kJ/mol higher than the *exo* isomer. This means that the preference for a given stereoisomer was only determined

by the stability of the product, which was calculated to be 11.5 kJ/mol higher for the *exo* adduct (Figure 3.6).
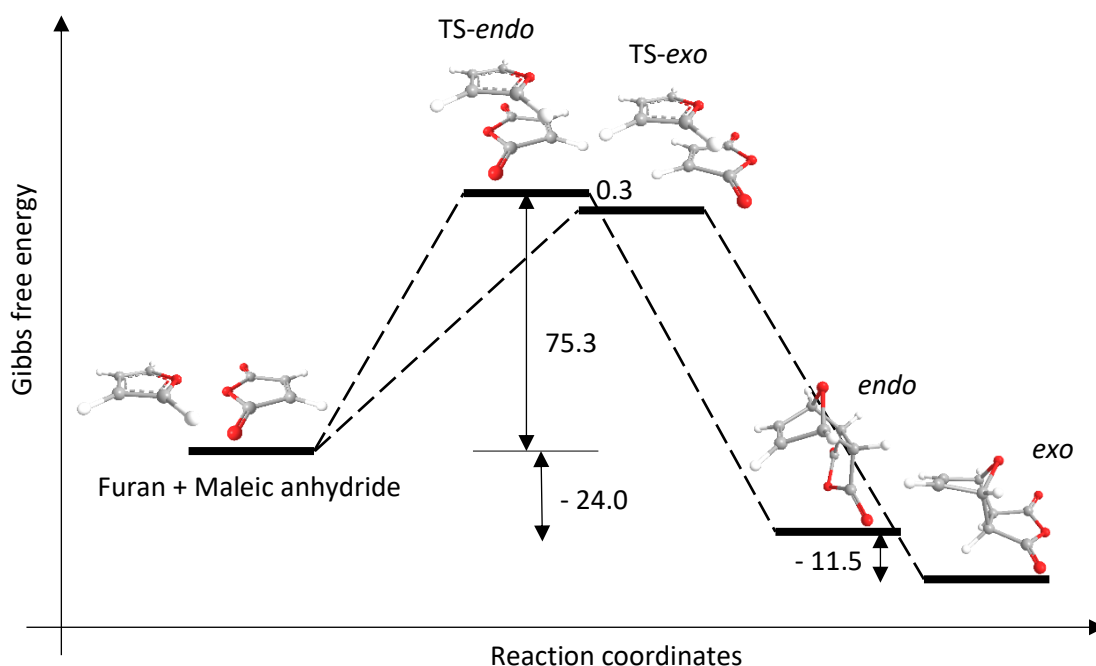
Fig. 3.6. Gibbs free energy profile for the [4+2] cycloaddition of furan and maleic anhydride with preferential formation of the exo adduct. The figure is an adaptation from reference 46.

In the second step (Scheme 3.3), oxanorbornene **7** was reacted with 1 eq of 4-(aminomethyl)pyridine **2** at room temperature using DCM as the solvent. The reaction gave a white precipitate that was filtered after 1 hour, affording the open form **8** with a yield of 85 %. Subsequently, ring closing of compound **8** in 0.5 M methanolic HCl afforded the pyridine containing ONB intermediate **9**, which was isolated by neutralisation with saturated $NaHCO_3$, followed by extraction in DCM. Compound **9** was obtained pure as a pale pink solid with a yield of 64 %.

^{1}H NMR and ^{13}C NMR in $CDCl_3$ (Figures S9 and S10, Appendix 2) confirmed the attainment of compound **7**, where chemical shift and multiplicity were comparable with those found in literature[40]. The ^{1}H NMR is composed of three peaks: the alkene peak is a triplet at 6.59 ppm, while the other two protons are a triplet and a singlet at 5.47 and 3.19 ppm respectively, each of them integrating for 2H. The ^{13}C NMR consists of four peaks: at 169.94 ppm the C=O is found, at 137.02

ppm, it is the alkene carbon, while at 82.24 and 48.73 ppm the two tertiary carbons on the ONB ring are found.

^{1}H NMR in DMSO-d$_6$ of compound **8** (Figure S11, Appendix 2) is very similar to the one obtained for **3b** (*exo* isomer), however, while maintaining the same multiplicity, the protons on the ONB ring are shifted downfield due to the presence of the oxygen atom on the norbornene bridge. Thus, the two alkene peaks are present as a multiplet at 6.48-6.46 ppm (compared to 6.24-6.21 ppm of **3b**) that integrate for 2H; the protons vicinal to the alkene ones are two singlets that integrate for 1H each at 5.11 and 4.97 ppm, while the two protons vicinal to the C=O group couple with each other and the protons next to the alkene giving rise to a quartet at 2.65 ppm that integrates for 2H. The aromatic protons and the CH$_2$ in the para position to the pyridine are instead not affected by the O atom on the norbornene ring and so the chemical shift values are the same as those obtained for compound **3b**.

In the same way as compound **4b**, the pyridine-based ONB **9** is a symmetric molecule, thus the ^{1}H NMR in CDCl$_3$ (Figure S13, Appendix 2) gives rise to a simpler spectrum composed of six peaks. The aromatic protons couple with each other forming two doublets at 8.55 and 7.19 ppm; the alkene peak is a triplet at 6.56 ppm that integrates for 2H; the proton closest to the alkene couples with the alkene proton and with the proton vicinal to the C=O giving rise to a triplet at 5.32; the two remaining protons are present both as singlets at 4.65 ppm (CH$_2$) and 2.93 ppm (CH-C=O); the NH is not present here.

3.2.1.3. Synthesis of urea- and thiourea-sulfonate salts, SSA-1 and SSA-2

Preparation of urea/thiourea-sulfonate pyridinium salts, **SSA-1** and **SSA-2**, was carried out following the procedure developed by Hiscock *et al*[34,32]. Isocyanate **10** and isothiocyanate **11** were reacted with 1 eq of aminomethane sulfonic acid **12**, in pyridine and heated to 60 °C overnight. Pyridine was used here both as a reactant and a solvent. In both reactions, products **SSA-1** and **SSA-2**

precipitated in solution forming a white suspension that was filtered and then washed with EtOAc to remove any trace of pyridine. As shown in Scheme 3.4, **SSA-1** and **SSA-2** were obtained cleanly with a yield of 74 % and 85 % respectively.

10: X = O
11: X = S

12

SSA-1: X = O, 74 %
SSA-2: X = S, 85 %

Scheme 3.4. Synthetic scheme for the preparation of **SSA-1** (urea-sulfonate pyridinium salt) and **SSA-2** (thiourea-sulfonate pyridinium salt).

SSA-1 and **SSA-2** were selected for this study for different reasons: (i) for the simplicity of their synthesis; (ii) because they contained a pyridinium cation that allowed easy proton transfer reactions with **4b** and **9**; (iii) because they were structurally similar to each other, allowing to carry out structure-activity relationship studies; (iv) because their physicochemical as well as antimicrobial properties were widely studied by Hiscock and co-workers. The successful synthesis of both SSAs was confirmed by ^{1}H NMR and ^{13}C NMR in DMSO-d_6 as they were found to match the values previously published by Hiscock *et al*. (Appendix 2, Figures S15 – S18). Since these compounds have been widely discussed in their publications, their characterisation and properties will not be discussed in this thesis.

3.2.1.4. Synthesis of NB and ONB monomers bearing SSA-1 and SSA-2

Scheme 3.5 shows the synthetic approach used for the preparation of the four monomers containing SSAs. **SSA-1** and **SSA-2** were reacted with an excess (1.2 eq) of norbornene **4b** and oxanorbornene **9** in MeOH, at room temperature for a period of up to 2 hours. The reaction of these four compounds in different combinations led to the formation of four new monomers (**mon1 – mon4**). These were obtained by precipitation from DCM, which was used to remove the excess

121

of **4b/9** and the pyridine formed during the reaction. Monomers **mon1** – **mon4** were obtained as white/light pink powders with a yield of 63 %, 86 %, 83 % and 86 % respectively. In the case of **mon3**, however, a different purification method was used. The ^{1}H NMR of **mon3** after precipitation with DCM, showed the presence of the methanol peak that could not be removed even under extreme conditions, such as heating to 100 °C under *vacuum*. This was due to formation of a hydrogen bond between MeOH and the product which contained a number of HBA atoms. Therefore, MeOH was removed by dissolution of **mon3** in water using a sonicator bath heated to 40 °C, followed by evaporation of the solvent using a rotary evaporator.

4b: Y = CH₂
9:   Y = O

SSA-1: X = O
SSA-2: X = S

mon1: Y = CH₂, X = O   63 %
mon2: Y = CH₂, X = S   86 %
mon3: Y = O, X = O   83 %
mon4: Y = O, X = S   86 %
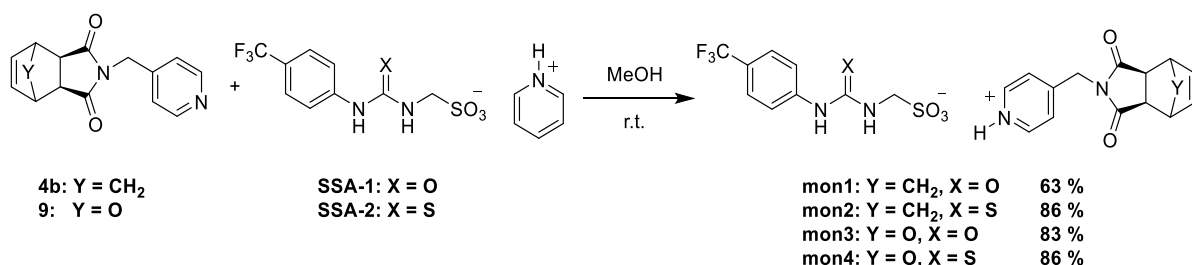
Scheme 3.5. Synthetic scheme for the preparation of NB and ONB monomers containing SSAs, **mon1** – **mon4**.

The mechanism of the reaction involved the proton transfer from the pyridinium cation in **SSA-1/SSA-2** to the pyridine group on compounds **4b** and **9** forming pyridine as a by-product. It was hypothesised that the driving force of this reaction was the formation of a weak acid and a weak base. In fact, the pyridinium on SSAs behaved as a Bronsted acid possessing a pKa of ~ 5, while it was assumed a pKa of ~ 6 for the conjugated acid of pyridine-based NB/ONB which therefore behaved as a Bronsted base. In order for this reaction to be successful, a protic polar solvent such as MeOH was needed. Due to the small difference in pKa between the reactants, the equilibrium was only partially shifted towards the product. This effect was particularly noticeable for the reaction of **4b** with **SSA-1**, where it was difficult to determine the time at which the equilibrium was reached, and therefore when product could be isolated. Due to the insolubility of both **SSA-1** and product (**mon1**) in the precipitating solvent (DCM), it was not possible to isolate **mon1** unless all the limiting reagent was consumed in the reaction. It was experimentally estimated that for the

reaction of **mon1**, equilibrium was reached after 40 minutes, while **mon2 − mon4** reached equilibrium after 2 hours. However, this could not be confirmed with certainty.

3.2.1.4.1. NMR characterisation and variable temperature (VT) studies of monomers

The formation of monomers **mon1** - **mon4** was primarily confirmed by ^{1}H NMR spectroscopy. For instance, Figure 3.7 shows the ^{1}H NMR spectrum in DMSO-d$_6$ of **mon1** (blue) compared to the spectra of reactants **4b** (red) and **SSA-1** (green).
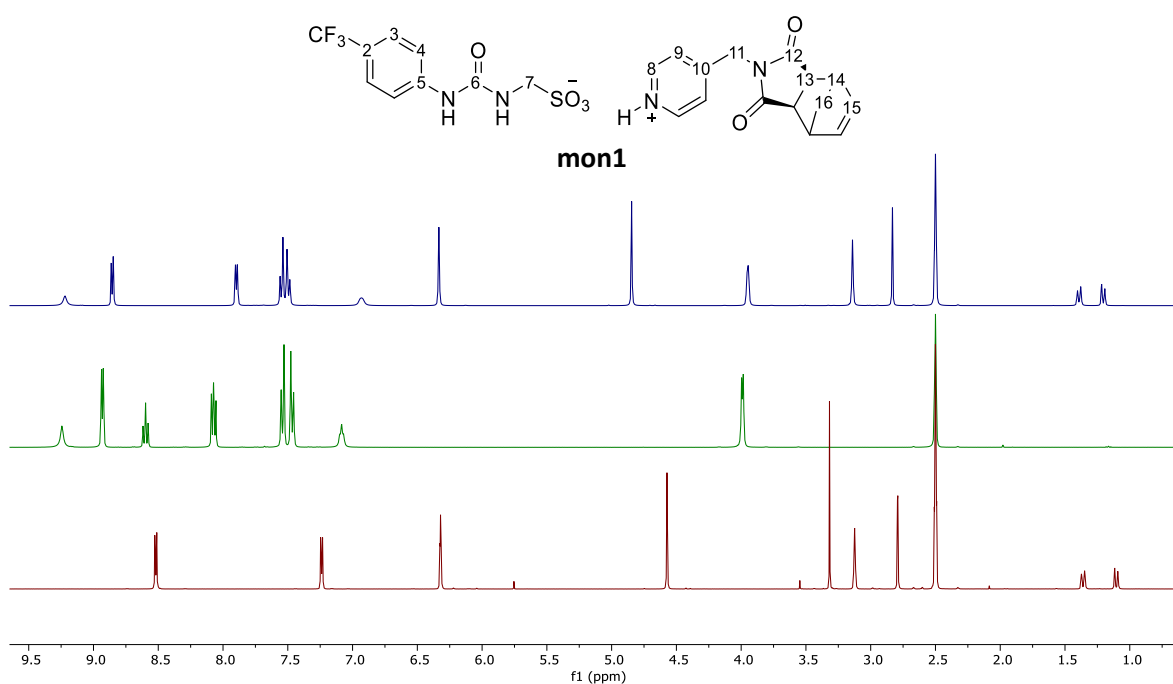
Fig. 3.7. ^{1}H NMR spectra of **mon1** (blue), **SSA-1** (green) and **4b** (red) in comparison. Structure of **mon1** with proton numbering is also shown.

It could be seen that the chemical shift of the pyridinium protons (8 and 9 in Figure 3.7) as well as proton 11 shifted downfield compared to compound **4b**, clearly indicating that the proton transfer reaction was successful. Protons 8 and 9 are two doublets at 8.86 ppm and 7.90 ppm, while proton 11 is a singlet at 4.85 ppm, each integrating for 2H (previously 8.52, 7.24 and 4.57 ppm respectively on compound **4b**). The aromatic protons on the SSA anion, 3 and 4, should couple with each other forming two doublets. However, they resonate at very close frequencies (7.51 ppm), and hence they are seen as a doublet of doublets in a pseudo second order effect. The urea NHs

123

are also visible in the spectrum as two broad singlets at 9.23 and 7.02 ppm, however their chemical shift changes according to the concentration of the sample (the more diluted, the more upfield). Protons 7, 13, 14, 15 (alkene) and 16 (bridgehead) do not considerably change their chemical shift with respect to their starting materials, and their multiplicity is retained.

Similar considerations can be made for **mon3** which is formed by anionic **SSA-1** and cationic ONB **9**. Hence, the only major difference from **mon1**, is that **mon3** possesses an O atom on the norbornene bridge, therefore the NMR spectrum does not contain the upfield bridgehead protons.

More peculiar is the case of monomers bearing the thiourea-SSA (**SSA-2**). It has been proposed by Hiscock *et al*. that the introduction of a more acidic HBD thiourea functionality in the SSA anionic component, results in the formation of a secondary structure due to a slow exchange process, where an intramolecular hydrogen bond between the sulfonate oxygen and the thiourea NH is formed[47]. This is a reversible process that has been verified through ^{1}H NMR variable temperature studies at 298 K and 333 K. This effect was found to be present on both **mon2** and **mon4**. Figure 3.8 (2) shows the NMR spectra of **mon2** at 298 K (blue) and 333 K (red): it is evident that when the monomer is at room temperature two species are present in solution (species a and b, Figure 3.8, 1), indicated by the splitting of the NH and CH_2 resonances into two peaks each that together integrate for 1H and 2H respectively (highlighted in grey, Figure 3.8, 2). These two species are the linear and the cyclic forms of the thiourea-sulfonate anion (Figure 3.8, 1). At high temperatures, however, the two NH peaks and the two CH_2 peaks coalesce together due to the breakage of the intramolecular hydrogen bond, meaning that only one species is visible in the NMR spectrum at 333 K.
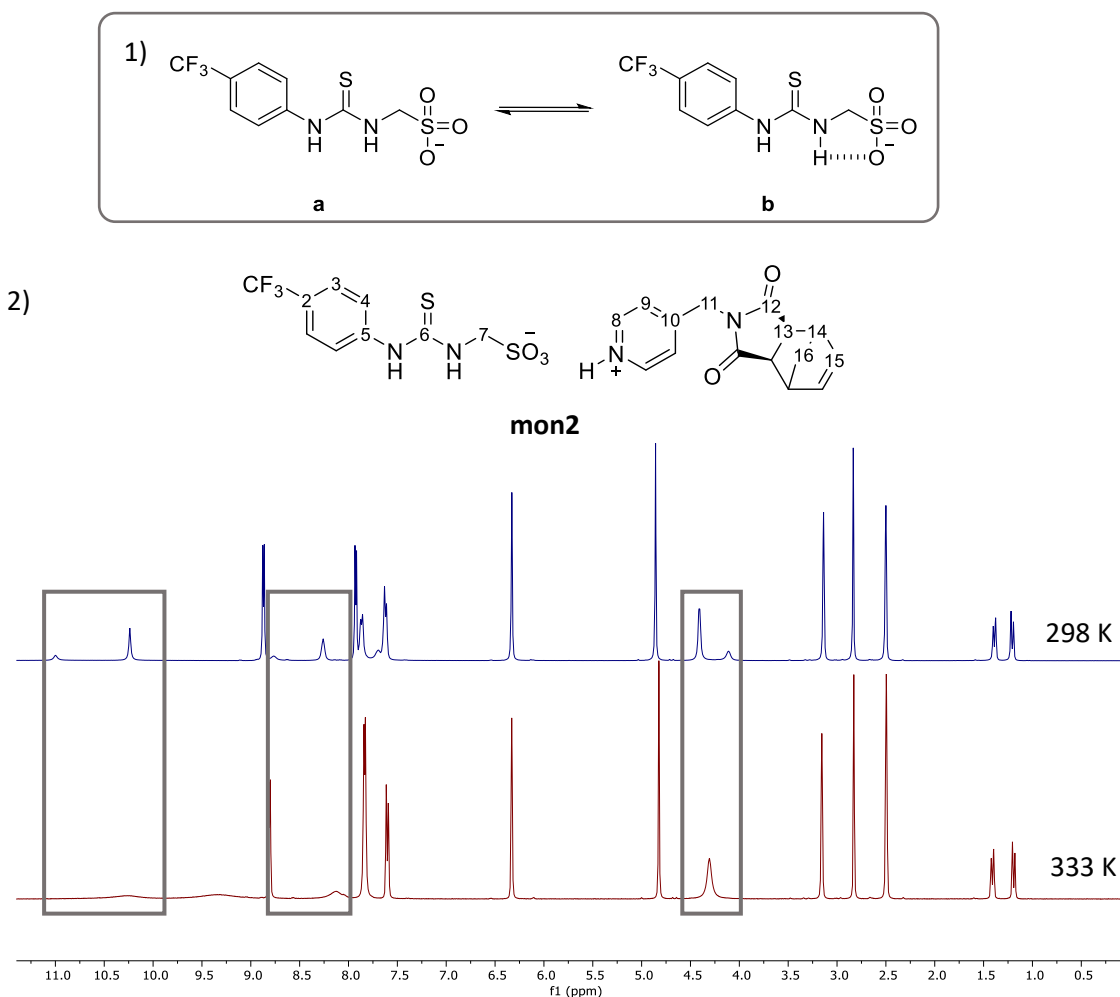
Fig. 3.8. 1) Proposed formation of a secondary structure of **SSA-2**, open form **a**, and closed form **b**. 2) ^{1}H NMR spectra of **mon2** at 298 K (red) and 300 K (blue). Highlighted in grey are the NHs protons and the CH$_2$ proton on SSA anion (proton 11).

Taking into consideration the ^{1}H NMR of **mon2** at 333 K, the aromatic region consists of protons 8 and 3 which are two doublets at 8.83 ppm and 7.71 ppm, while protons 9 and 4 resonate at the same frequencies forming a multiplet at 7.87-7.85 ppm. The aromatic protons on the SSA anion are shifted downfield compared to the same protons in **mon1**; this may be due to the presence of the more acidic sulphur atom, which due to the inductive effect, removes electron density from the protons. They therefore become deshielded and are shifted to higher chemical shifts. The CH$_2$ protons (proton 7) on the SSA anion, after heating to 333 K, are shown in the spectrum as a broad singlet at 4.33 ppm and are therefore shifted downfield in comparison to **mon1**

(3.95 ppm). The protons on the NB ring are not affected by the presence of the sulphur atom and therefore they resonate at the same frequencies found in **mon1**.

The same considerations can be made for **mon4** with the only exception that the norbornene ring possesses an O atom on the bridge instead of a CH_2 and thus no peaks are present in the range 0-2.5 ppm (Figure S25, Appendix 2).

The ^{13}C NMR spectrum of **mon1** (Figure 3.9-b) is presented here as a representative description for all of the four monomers, as their spectra are similar to one another (Figures S20, S22, S24 and S26, Appendix 2). All carbons have been assigned using a combination of HMQC (Heteronuclear Multiple Quantum Coherence) and HMBC (Heteronuclear Multiple Bond Correlation). From these studies, it was found that the carbonyl carbons 12 and 6 are the most deshielded and are found to be at 177.5 ppm and 155.0 ppm. These are followed by the quaternary aromatic carbons 5 and 10 at 154.2 ppm and 144.2 ppm. The aromatic carbons 8 and 9 are located at 142.04 ppm (more deshielded as it is close to the N atom) and 125.1 ppm, while the rest of the norbornene carbons are placed at 137.8 ppm for carbon 15, which is found to be in the typical range for the alkene carbon in norbornene, and in the range 47.7 - 40.9 ppm for carbons 13, 14, 16 and 11. Carbon 7 is a low intensity peak at 55.9 ppm; the low intensity could be due to an increase of the relaxation time caused by the proximity of carbon 7 to the SO_3 group. More peculiar is the situation for the aromatic carbons 2 and 3 in SSA, since a CF_3 group is attached to the para position in respect to the urea moiety. It is known that ^{19}F possess a quantum spin number $I = 1/2$, as it is consisting of an uneven number of protons and neutrons in its nucleus. This means that fluorine can couple with carbon in a ^{13}C NMR following the splitting rule of (n + 1). While hydrogen-carbon couplings are not seen in normal ^{13}C NMR spectra due to the C-H decoupling that prevents the splitting of the peaks, this is not possible, or it is more difficult to obtain on a carbon-fluorine coupling and thus splitting is observed[48]. The fluorine in CF_3, as shown in Figure 3.9-c, can couple with carbons 2, 3 and the CF_3 carbon itself. As a result, three quartets with different coupling constants are present in the NMR spectrum: the first coupling (the one with CF_3) generates a

quartet at 124.7 ppm with *J* = 270.7 Hz, while the coupling with carbons 2 and 3 forms two quartets at 120.9 ppm with *J* = 32.0 Hz, and 125.9 ppm with *J* = 3.7 Hz. Carbon 4 is not affected by the presence of fluorine and therefore is seen as a singlet at 117.2 ppm.
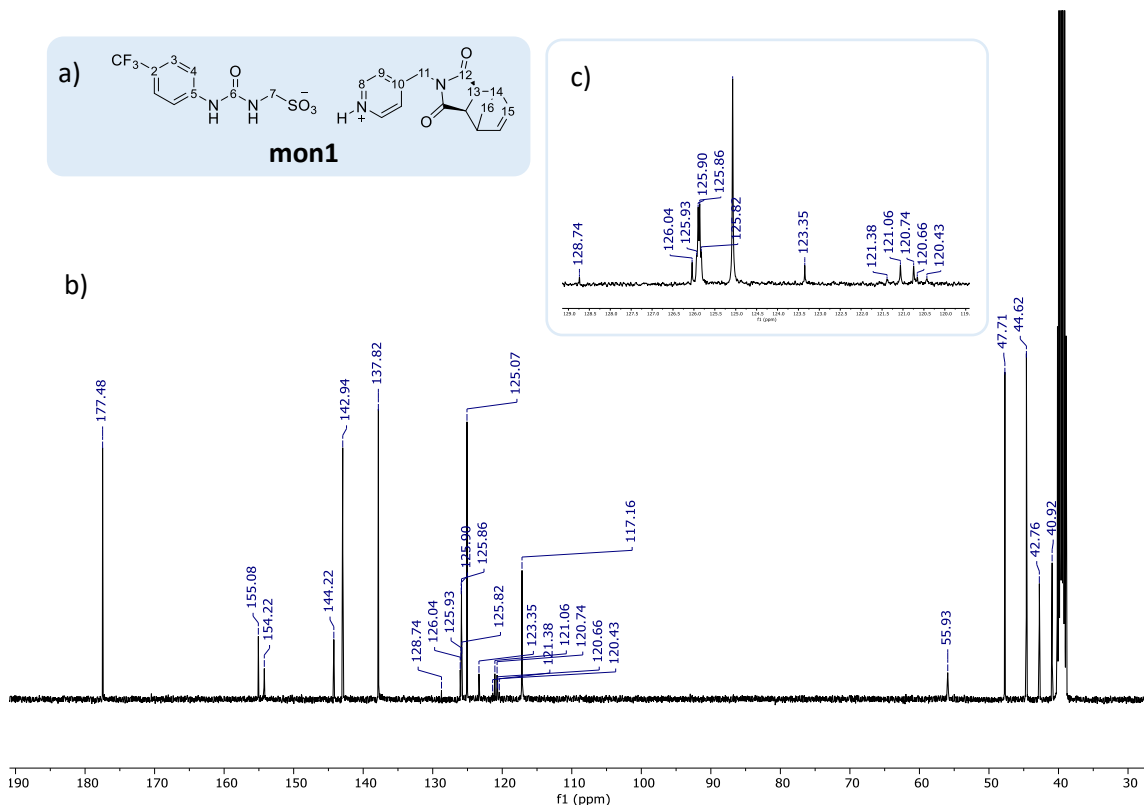
Fig. 3.9. (a) Structure of **mon1** with carbon's numbering; (b) ^{13}C NMR spectrum of **mon1** in DMSO-d_6; (c) carbon-fluorine region zoomed in.

The difference between this ^{13}C NMR spectrum compared to the other monomers relies on the presence of a more acidic sulphur atom on the urea moiety (in **mon2** and **mon4**) and the more electronegative oxygen atom on the norbornene bridge (in **mon3** and **mon4**). Consequently, the carbons closest to those atoms are deshielded and thus shifted more downfield in the spectra. For instance, carbon 6 on **mon2** and **mon4** (thiourea-based monomers) is shifted to 180.3 ppm compared to 115.1 ppm on **mon1** and **mon3** (urea-based monomers), while carbon 14 on **mon3** and **mon4** (ONB-based monomers) is shifted to 80.6 ppm compared to 44.6 ppm on **mon1** and **mon2** (NB-based monomers).

3.2.2. Polymer synthesis

As shown in Scheme 3.6, the synthesised monomers, **mon1** - **mon4**, were polymerised using the commercially available 3rd generation Grubbs catalyst (H$_2$IMes)(3-bromopyridine)$_2$-(Cl)$_2$Ru=CHPh (**G3**), in anhydrous DMF using benzaldehyde as a terminating agent. The resulting polymers (**poly1** – **poly4**) were then purified by precipitation from DCM affording **poly1** and **poly3** as brown powders (94 % and 39 % yield respectively), and **poly2** and **poly4** as dark green powders (72 % and 32 % yield respectively). In each case, the polymerisation was carried out overnight at room temperature, using a monomer to catalyst ratio [M]/[C] of 20:1 and at a monomer concentration of 0.045 M.

mon1: Y = CH$_2$, X = O
mon2: Y = CH$_2$, X = S
mon3: Y = O, X = O
mon4: Y = O, X = S

poly1: Y = CH$_2$, X = O   94 %
poly2: Y = CH$_2$, X = S   72 %
poly3: Y = O, X = O   39 %
poly4: Y = O, X = S   32 %
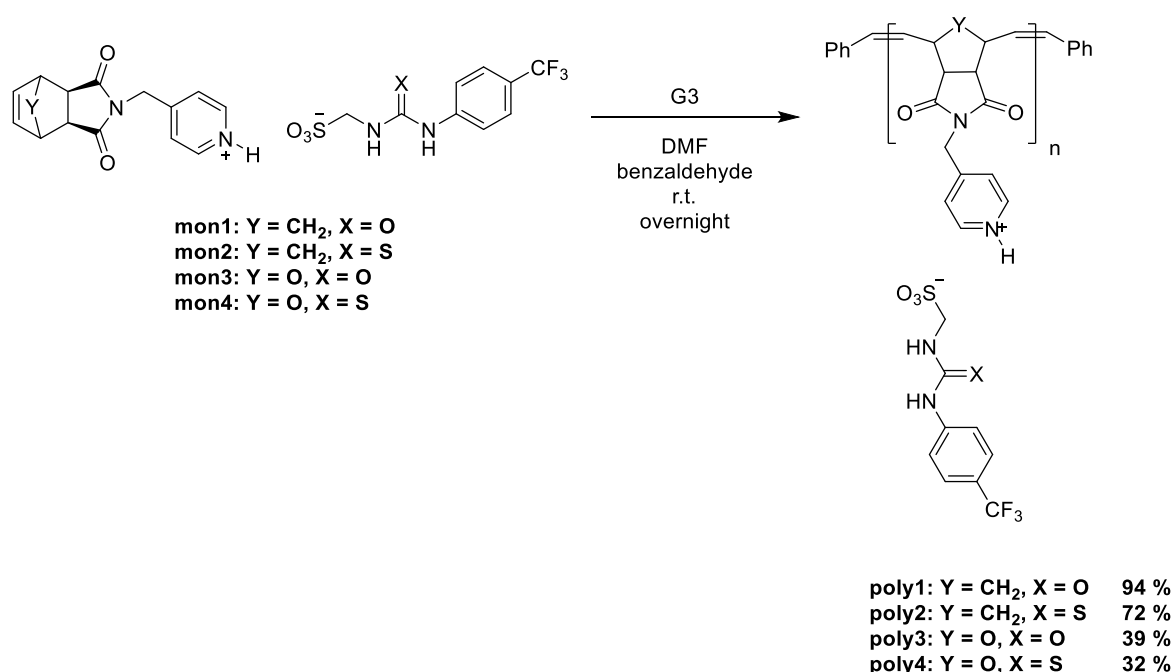
Scheme 3.6. Synthetic scheme for the preparation of homopolymers **poly1** - **poly4**, obtained by ROMP polymerisation of monomers **mon1** – **mon4** respectively, using Grubbs third generation catalyst, G3.

Obtaining the aforementioned homopolymers was not straightforward, mainly due to the insolubility of monomers in many organic solvents. The polymerisation conditions were optimised on the synthesis of **poly1**. At first, the homopolymerisation of **mon1** was carried out in polar solvents such as MeOH, MeCN and DMSO, with a monomer concentration of 0.045 M and a monomer to catalyst ratio of 20:1. However, in each case, the solvent deactivated the catalyst **G3** and hence only the unreacted monomer was present in the ^{1}H NMR spectra. Secondly, the reaction

was carried out in anhydrous DMF (as it was found in the literature to have previously been used for ROMP[49]) using the same monomer concentration and monomer to catalyst ratio. The reaction was left to stir overnight at room temperature, then terminated using ethyl vinyl ether. The ^{1}H NMR of the precipitated powder (obtained by precipitation from Et$_2$O) showed formation of a polymer as demonstrated by the typical broadening of the peaks. However, some impurities were present, which were hypothesised to be products of the hydrolysation of ethyl vinyl ether which was added in excess in the reaction mixture. The excess ethyl vinyl ether most likely, reacted with the trace H$_2$O present in DMF forming acetaldehyde (CH$_3$ doublet at 2.12 ppm and CHO quartet at 9.66) and ethanol (CH$_3$ triplet at 1.06 ppm and CH$_2$ quartet at 3.44 ppm). In addition, DMF traces were also present. Although ethanol and acetaldehyde are low boiling point and volatile liquids, it was not possible to remove them, as well as DMF traces, using a Schlenk line with heating, nor using the speed vacuum technique. This could be due to the entrapment of these small molecules within the polymer framework. In order to prevent this issue, DMF was further dried using MS 3 Å and the terminating agent was changed to benzaldehyde. In this case, the polymer was obtained by precipitation with DCM and then washed at least six time in order to remove any trace of DMF. The ^{1}H NMR, shown in Figure 3.10, was found to be free from the aforementioned impurities and only a small amount of DMF was present.

Once the conditions for the polymerisation of **mon1** were optimised, homopolymers **poly2**, **poly3** and **poly4** were synthesised. It is believed that the lower yield obtained for these three polymers was mainly due to the work up conditions, where washing the polymers multiple times with DCM led to some polymer loss. However, in the case of the ONB based polymers, **poly3** and **poly4**, the precipitation from DCM was not as successful as in the case of **poly1** and **poly2**, and only little precipitation occurred. This could be due to the higher affinity of the ONB polymers towards DMF. The introduction of the O atom on the polymer backbone might have increased the polarity of the ONB based polymers compared to the NB based ones. As a consequence, the precipitation was more difficult and some of the polymer was left behind in the

mother liquor. Even the use of more apolar solvents such as Et$_2$O and hexane did not improve the precipitation yield.

3.2.2.1. ^{1}H NMR characterisation of polymers, poly1 – poly4

As shown in Figure 3.10, formation of **poly1** was confirmed by the typical broadening of each peak. Furthermore, it was confirmed by the disappearance of the alkene peak of **mon1** at 6.33 ppm, and the appearance of a broad doublet characteristic of the *cis/trans* double bonds (proton 15) at 5.66 – 5.48 ppm. The other peaks were assigned by comparison with the NMR spectrum of **mon1** (Section 3.2.1.4.1) and by analysing its COSY NMR. In fact, the chemical shift for most of the protons was retained, however the CH$_2$ (proton 16) formed two broad singlets which were shifted downfield in comparison with **mon1** (1.89 and 1.49 ppm compared to 1.39 and 1.21 ppm). The integration of each peak was also retained and the ratio between the SSA peaks and the polymer peaks were 1:1, meaning that for each cationic repeating unit there was one anionic SSA.
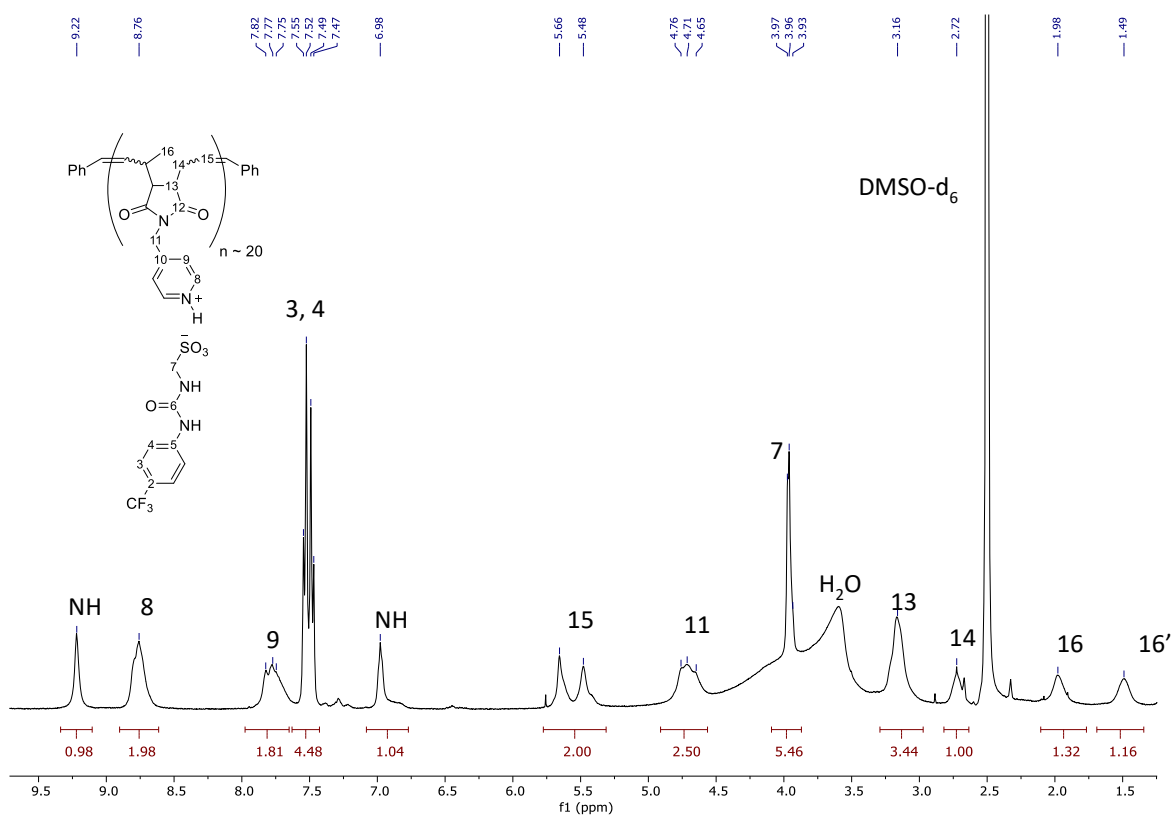
Fig. 3.10. ^{1}H NMR of **poly1** in DMSO-d$_6$ with polymer structure and peak assignment.

The polymerisation of **mon2** – **mon4** were also successful as confirmed by the ^{1}H NMR spectra of each polymer (Figures S27, S29, S31 and S33, Appendix 2). The peaks were broadened and the typical *cis/trans* alkene peak in the polymers was found to be at ~ 5 ppm in each spectrum. Homopolymers **poly2** and **poly4**, were found to behave in the same way as their respective monomers, where the thiourea-sulfonate anion formed a secondary structure at room temperature due to slow exchange (Figure 3.8). As shown in Figure 3.11, a variable temperature experiment was carried out on **poly2** demonstrating that when at high temperatures (333 K), the peaks representative of the thiourea-sulfonate anion coalesced together giving rise to one structure only. This effect is better viewed on proton 7, CH_2, on the SSA anion, which resonates at 4.29 ppm, although some of the signal is hidden by the water peak (Figure 3.11).
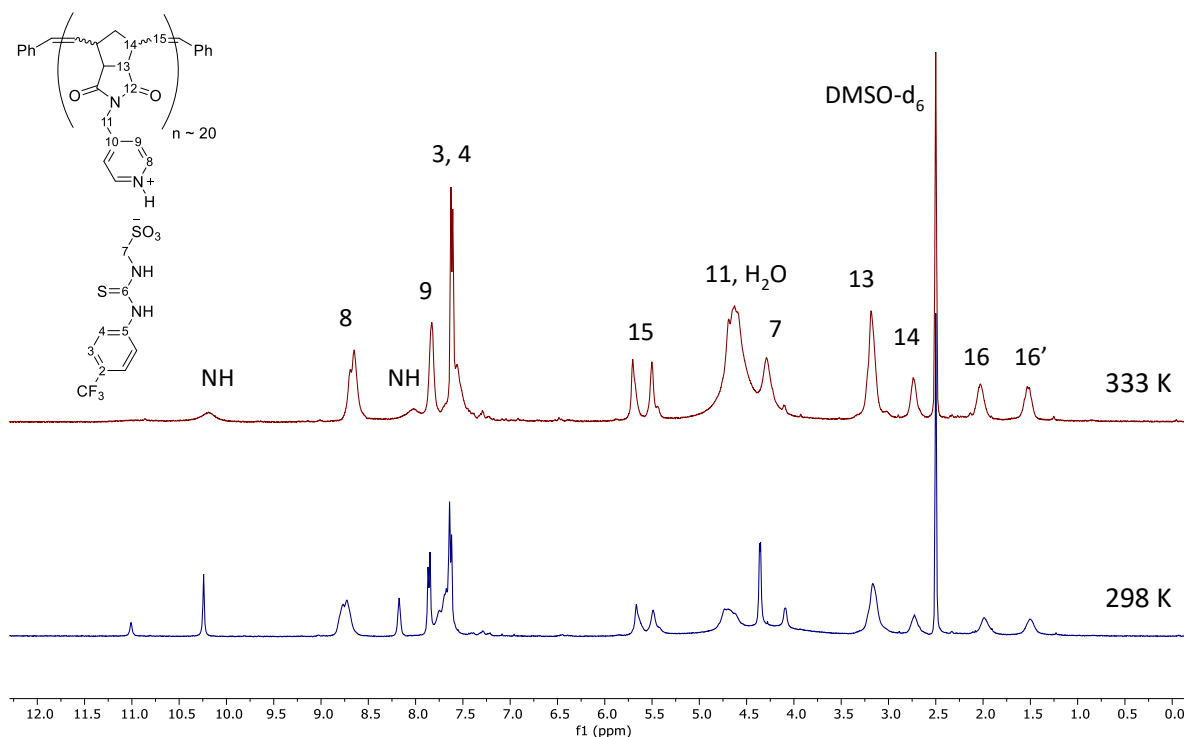
Fig. 3.11. ^{1}H NMR of **poly2** in DMSO-d_6 at 298 K and at 333 K. The homopolymer structure is shown and protons have been assigned.

^{13}C NMR spectra was obtained for all four of the polymers synthesised as shown in Figures S28, S30, S32 and S34, Appendix 2. In this case, to obtain spectra with a low signal to noise ratio,

more than 5000 scans were necessary, as well as a polymer sample of ~ 40 μg/mL. Consequently, the peaks attributed to the carbon-fluorine coupling were also visible.

3.2.2.2. Gel Permeation Chromatography (GPC) of poly1 – poly4

Molecular weights of **poly1** – **poly4** were determined using GPC chromatography (Aglient Technologies PL-GPC 50). Each polymer was dissolved in DMF with 0.1 % w/w of toluene which was added to act as the flow rate marker. The eluent used was DMF containing 0.1 % w/w lithium bromide at a flow rate of 1.0 mL/min. 100 μL of sample was injected and polymers were detected using a differential refractive index (RI) detector. The system was calibrated using 10 narrow dispersity poly(methyl methacrylate) standards (Mp = 2210000 – 1810 g/mol). The GPC analysis discussed in this section were conducted at the University of Sheffield by Samuel Harrison of the Dr. Sebastian Spain's research group .
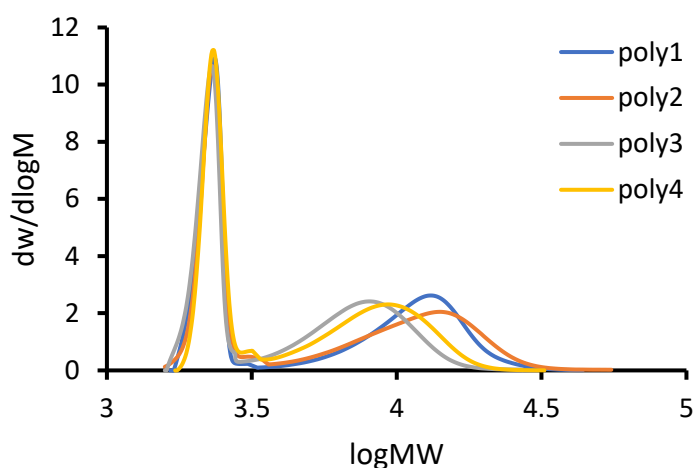
Fig. 3.12. Molecular weight profile of poly1 – poly4.

As shown in Figure 3.12, the four synthesised homopolymers presented a bimodal distribution of molecular weights, meaning that two polymer distributions with different molecular weights were formed during the reaction. This could be a result of the long reaction time used for

these four polymerisations. Since DMF was used as the reaction solvent, it was difficult to study the kinetics of the polymerisation for three main reasons: (i) deuterated DMF for NMR studies was expensive; (ii) DMF is a high boiling point, not volatile solvent, hence the NMR analysis of reaction mixture aliquots was not feasible; (iii) GPC that uses DMF as an eluent was not readily available. Therefore, the polymerisation was run overnight in order to make sure that all of the monomer was consumed by the end of the reaction. However, it was hypothesised that, due to the long reaction time, "backbiting" reactions occurred, where the active metal alkylidene at the end of the polymer chain reacted intramolecularly with another double bond along the polymer backbone giving rise to two different polymer distributions. The number average molecular weight (M_n), the weight average molecular weight (M_w) and the polydispersity index (Đ) values obtained for each polymer are shown in Table 3.1. In the case of **poly1** and **poly2**, the M_n values obtained by GPC for the two distributions, if summed together, were very similar to the theoretical one, whereas in the case of **poly3** and **poly4**, they were lower. This suggested that, although the polymerisation was left overnight, not all of the monomer reacted and thus a lower M_n was observed. However, in all four of the polymers synthesised, a very low polydispersity index was obtained, with values ranging from 1.01 to 1.24, demonstrating the great versatility of the third generation Grubbs catalyst, **G3**.

Table 3.1. Polymerisation characteristic of homopolymers **poly1** – **poly4**.

Polymer*	Yield (%)	n:G3 (th)[a]	NB:SSA[b]	M_n (th)[c]	M_n (GPC)	M_w (GPC)	Đ[d] (M_w/ M_n)
Poly1	94	20:1	1:0.90	11 100	10 600	12 400	1.17
					2 200	2 300	1.01
Poly2	72	20:1	1:1.04	11 400	10 600	13 100	1.24
					2 300	2 300	1.01
Poly3	39	20:1	1:1.11	11 100	7 100	8 200	1.15
					2 200	2 200	1.01
Poly4	32	20:1	1:1.10	11 400	8 000	9 200	1.16
					2 300	2 300	1.01

* Monomer conversion could not be determined due to the use of DMF as reaction solvent. Reaction was left overnight. [a] Theoretical feed ratio. [b] Ratio SSA anion to NB cation determined by qNMR (d = 90 s). [c] Theoretical number average molecular weight. [d] Polydispersity determined by GPC in DMF and reported relative to poly(methyl methacrylate) standards.

In order to determine whether the polymerisation disrupted the ionic bond between the SSA anion and the polyNB/polyONB cation, a relative quantitative NMR was run for each polymer using a relaxation delay of 90 seconds. By comparing integrals of interest with each other it was possible to determine the ratio between the cation and the anion within the polymer backbone. Specifically, the alkene peak (proton 15) on the polyNB/polyONB cation were integrated and compared this with the integration of the CH_2 peak (proton 7) on the urea/thiourea anion. As shown in Table 3.1 (and Figure S77, Appendix 2), the ratio of the NB cation to the SSA anion was found to be 1:1 for all four of the polymers, meaning that the ionic bond was maintained during the polymerisation. Where the integration for the SSA peaks were found to be higher than 1, it was caused by the very close proximity to another peak (proton 11) in the spectrum that might have affected the integration. Overall, it was demonstrated that for each repeating unit there was one SSA anion.

3.2.3. Physicochemical properties of NB/ONB-SSA monomers, mon1 – mon4

For the characterisation and the study of the physicochemical properties of the SSAs, the Hiscock group developed a multivalent approach which included a series of experimental techniques summarised in a flow chart shown in Figure 3.13. It is important to note that, although TEM and SEM microscopy techniques are mentioned in this flow chart, the Hiscock group demonstrated their unreliability in offering good results as the samples do not survive the method preparation[50]. For this reason, no TEM/SEM was carried out for any of the monomers synthesised, while the rest of the flow chart was used to characterise monomers **mon1** – **mon4** and compare their physicochemical properties with the SSAs (**SSA-1** and **SSA-2**).
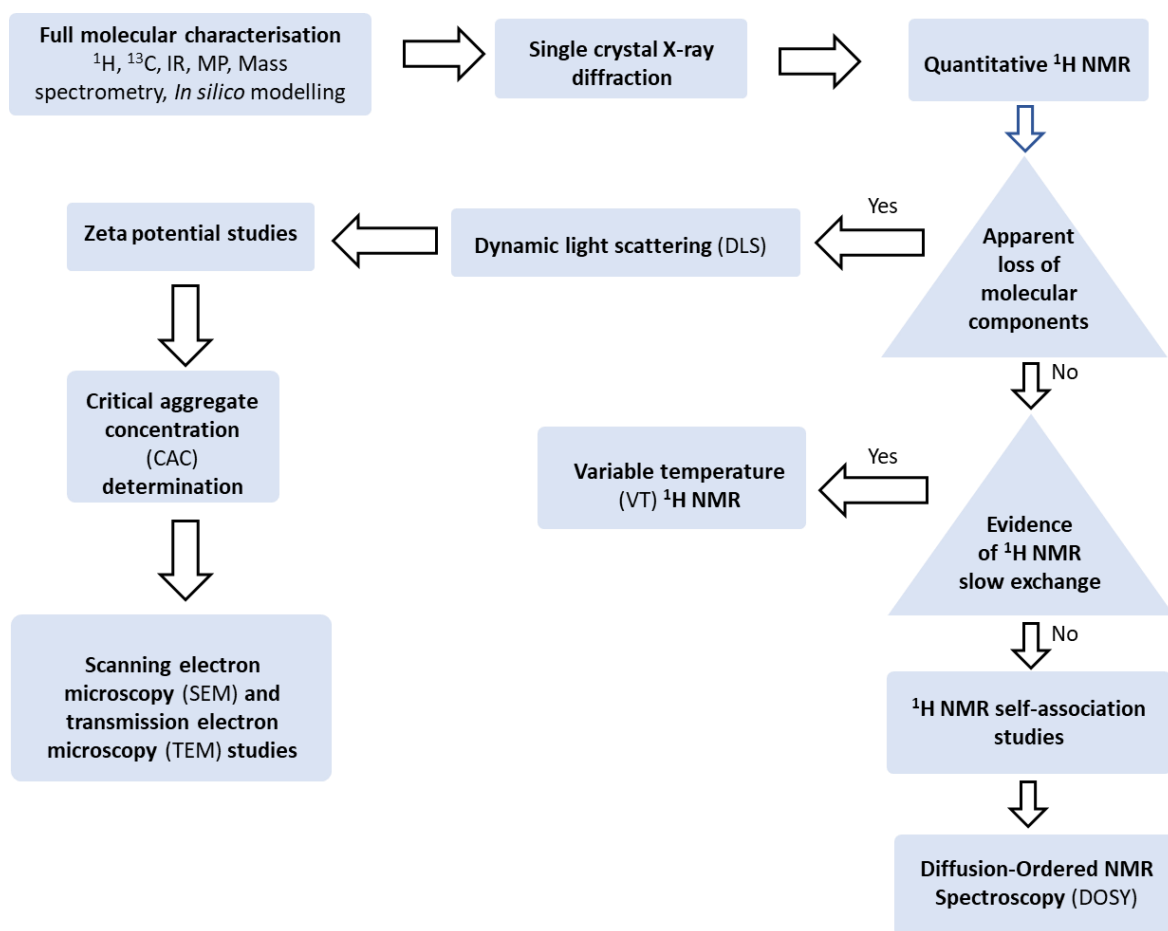
Fig. 3.13. Flow chart including all the characterisation techniques used by the Hiscock group for the analysis of the physical-chemical properties of the SSA molecules, also used for the characterisation of monomers **mon1 – mon4**[51]. Square = action; triangle = decision. Figure adapted from ref 51.

3.2.3.1. Single crystal XRD, a solid-state study

As previously mentioned in Section 3.1.2, Hiscock *et al*. studied the intermolecular binding modes adopted by the anionic component of SSAs using single crystal X-Ray diffraction (XRD)[34,35]. They found that, in the solid state, SSAs could form different packing modes thanks to the formation of intermolecular hydrogen bonds through their HBD and HBA groups and that this was strongly dependant on the counter-ion used. In particular, three situations were encountered: (i) weakly coordinating counter cations such as tetrabutylammonium (TBA) gave rise to urea/thiourea dimers; (ii) moderately coordinating counter cations such as pyridinium formed urea-anion (or thiourea-anion) tapes; (iii) strongly coordinating counter cations such as sodium or potassium formed urea-urea (or thiourea-thiourea) stacks (these are represented schematically in Figure 3.5, Section

3.1.2.). For instance, the CF$_3$ substituted benzene urea-sulphonate anion in **SSA-1** formed dimeric species when the TBA counter-ion was used. In this case, the HBD urea group hydrogen bonded to the HBA sulphonate group of another SSA anion, and because TBA was not a coordinating species, only a dimer was formed. However, when TBA was exchanged for the pyridinium cation, this acted as a competitive HBD species, and consequently a urea-sulphonate hydrogen bonded tape in the *anti*-configuration was formed. These two crystal structure images are available in the Hiscock *et al*. publication[34].

Single crystals of **mon1** and **mon2** were grown by slow evaporation from MeOH. A suitable crystal was selected, mounted at 200 K and then cooled to 100 K for collection on a SuperNova, Dual, Cu at home/neat, AtlasS2 diffractometer. Experiment on **mon1** was run by Lee Birchall, while experiment on **mon2** was run by Professor Jennifer Hiscock, both at the University of Kent. As shown in Figure 3.14, in the solid state, **mon1** (consisting of a urea-sulphonate anion and a pyridinium-based norbornene cation) formed a urea-anion tape similar to **SSA-1**. In this case the pyridinium HBD group formed a hydrogen bond with one of the oxygen atoms of the sulphonate group. However, due to the presence of a bigger, sterically hindered counter cation, **mon1** formed a staggered *syn*-stacking mode, where a hydrogen bond was formed between the urea group of one SSA anion and the sulphonate group of another SSA anion. The difference in stacking mode from *anti* to *syn* in **SSA-1** and **mon1**, could be caused by the difference in size of the counter cations. In fact, the pyridinium cation in **SSA-1** tended to be located among the urea-sulphonate anions and therefore the *anti*-configuration was energetically more favoured (crystal structure previously published[34]).

In **mon2** the same types of hydrogen bonds were formed: the HBD pyridinium hydrogen bonded to one of the oxygen atoms on the sulfonate group and at the same time, two hydrogen bonds were formed between the HBD thiourea group and the HBA sulphonate group. However, in this case, the presence of the sulphur atom on the thiourea, did not result in the formation of a tape motif as in **mon1**, but instead formed the typical thiourea-anion stacking as shown in Figure

3.15. Crystal structures of **mon3** and **mon4** could not be obtained due to time constraints and very limited availability of the instrument. However, single crystals of **mon3** and **mon4** were obtained by slow evaporation from MeOH and are ready to be analysed.
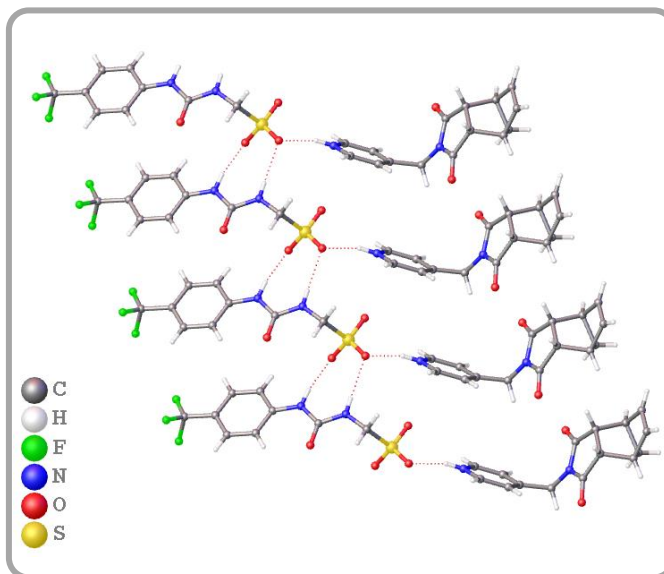
Fig. 3.14. Ball and stick representation of the single crystal X-ray structure of **mon1**, exhibiting a hydrogen bonded tape formation through the urea-anion binding mode. Crystal Data for $C_{24}H_{23}N_4O_6F_3S$ (M =552.52 g/mol): monoclinic, space group P2$_1$/c (no. 14), a = 23.527(3) Å, b = 5.5052(6) Å, c = 20.755(3) Å, β = 114.673(16)°, V = 2442.7(6) Å^3, Z = 4, T = 99.99(11) K, μ(Cu Kα) = 1.826 mm^{-1}, $Dcalc$ = 1.502 g/cm^3, 11709 reflections measured (8.272° ≤ 2Θ ≤ 142.346°), 4657 unique (R_{int} = 0.1170, R$_{sigma}$ = 0.1415) which were used in all calculations. The final R_1 was 0.0995 (I > 2σ(I)) and wR_2 was 0.2930 (all data).

In Table 3.2 the hydrogen bond distances and angles of **SSA-1**, **mon1** and **mon2** are summarised, calculated from the single-crystal X-ray structures. The **SSA-2** crystal structure was not available. These hydrogen bonds lengths were calculated as the distance from donor to acceptor (D-A) and the hydrogen bond angles were taken between D-H—A. As shown in the table, the hydrogen bond formed between the pyridinium cation and the sulphonate anion was found to be the shortest in each case with values ranging from 1.8 to 1.9 Å, while the urea (or thiourea) NHs formed hydrogen bonds with the sulphonate anion with lengths > 2.0 Å.

Table 3.2. Hydrogen bond length and angles obtained using Olex2 for **SSA-1** (previously published data), **mon1** and **mon2**. Here atoms have been numbered so that N1 is the pyridinium nitrogen which bonds O1. O1 is the oxygen bonding with two NHs. N2 and N3 are the urea nitrogen, where N2 is the one binding to O1.

	HBD	Hydrogen atom	HBA	Hydrogen bond length (D---A) (Å)	Hydrogen bond angle (D-H---A) (°)
SSA-1	N1	H1	O1	1.895 (2)	168.7 (2)
	N3	H3	O2	2.095 (2)	157.5 (2)
mon1	N1	H1	O1	1.816 (4)	151.0 (6)
	N2	H2	O1	2.161 (4)	141.8 (3)
	N3	H3	O2	2.091 (5)	167.5 (4)
mon2	N1	H1	O1	1.909 (9)	165.2 (8)
	N2	H2	O1	2.048 (9)	162.4 (8)
	N3	H3	O2	2.030 (10)	166.4 (7)
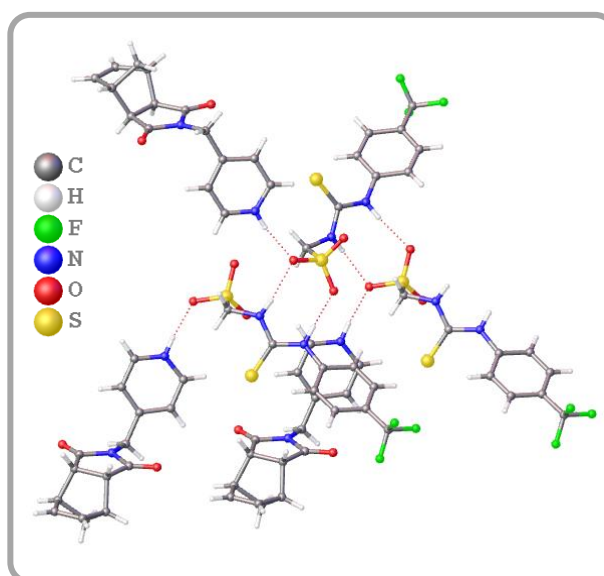
Fig. 3.15. Ball and stick representation of the single crystal X-ray structure of **mon2**, shows formation of thiourea-anion stacking. Crystal Data for $C_{24}H_{23}F_3N_4O_5S_2$ (M =568.58 g/mol): monoclinic, space group C2/c (no. 15), a = 40.110(14) Å, b = 7.8300(15) Å, c = 15.943(4) Å, β = 98.50(3)°, V = 4952(2) Å^3, Z = 8, T = 100.00(12) K, µ(Cu Kα) = 2.555 mm^{-1}, $Dcalc$ = 1.525 g/cm^3, 17086 reflections measured (8.916° ≤ 2Θ ≤ 133.192°), 4378 unique (R_{int} = 0.3577, R_{sigma} = 0.2217) which were used in all calculations. The final R_1 was 0.1771 (I > 2σ(I)) and wR_2 was 0.5056 (all data).

3.2.3.2. ESI-MS, a gas-phase study

Electrospray ionisation mass spectroscopy (ESI-MS) is a technique widely used for the analysis of both small and large molecules of different polarities[52]. ESI is a soft source of ionisation, meaning that very little energy is retained by the analyte, thus no fragmentation occurs and at the same time, non-covalent interactions (e.g., hydrogen bonds) are preserved in the gas phase. The Hiscock

group have used this technique to study the formation of intermolecular interactions on SSAs in order to determine whether the self-association of these molecules, specifically the formation of dimeric species was present in the gas phase. For instance, it was demonstrated by high resolution ESI-MS, that both SSAs used in this chapter, **SSA-1** and **SSA-2**, existed in the monomeric state [M]$^-$ and dimeric state [M+M+H]$^-$, where M is the anionic component of SSAs. This effect was specifically seen on SSAs that possessed an anionic substituent, such as the one synthesised in this study, or a carboxylic acid residue, which was also used and studied by Hiscock and co-workers[32].
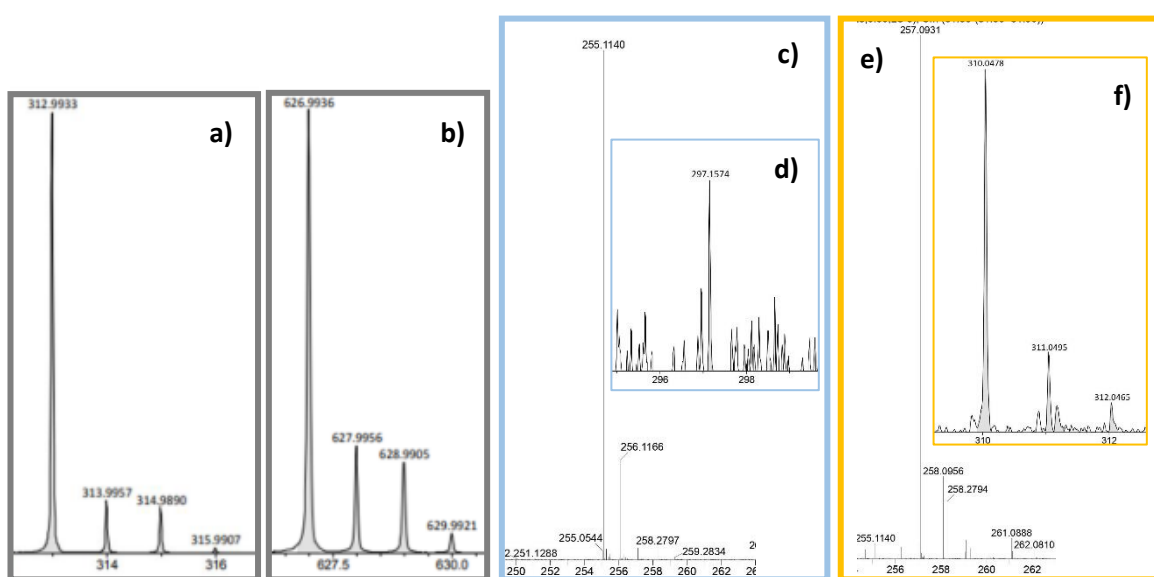
Fig. 3.16. High resolution MS spectra of: a) monomeric species and b) dimeric species of **SSA-2**; c) cationic component (NB) and d) anionic component (urea-sulphonate) of **mon1**; e) cationic component (ONB) and f) anionic component (thiourea-sulphonate) of **mon4**. Anionic components have been detected using ESI- as [M]$^-$, while cationic components have been detected using ESI+ as [M+H]$^+$. Dimeric species have been found as [M+M+H]$^-$.

For instance, as shown in the ESI-MS spectra presented in Figure 3.16, the thiourea-sulphonate anion (**SSA-2**) formed both the monomeric species [M]$^-$ with *m/z* of 312.9933 (a) and the dimeric species [M+M+H]$^-$ with *m/z* of 629.9936 (b) in the gas phase. This did not happen in the four monomers synthesised, **mon1** – **mon4**, and as shown in Figure 3.16 only the monomeric species for both cationic (NB/ONB) and anionic (urea/thiourea-sulphonate) components were present in the MS spectra. For instance, the MS spectrum (d, Figure 3.14) of **mon1** obtained in the negative ion mode (ESI-) showed an *m/z* of 297.1574, while the MS spectrum (c, Figure 3.16)

139

obtained in the positive ion mode (ESI+) showed an *m/z* of 255.1140. These were respectively the *m/z* values of the urea anion [M]$^-$ and the NB cation [M+H]$^+$ in the monomeric form and were equivalent to the calculated values (Table 3.3). In the same way, the anionic and cationic components of **mon4** were detected using ESI- and ESI+ respectively and as shown in Figure 3.16 ((e) and (f)), *m/z* of 312.0465 and 275.1034 were found for the thiourea anion and the ONB cation. However, in the case of the thiourea anion (both in **mon2** and **mon4**), *m/z* of 311.0495 and 310.0478 were detected, which could be attributed to the loss of 1H$^-$ in the first case and 2H$^-$ (more abundant) in the second case. It could be hypothesised that because the thiourea anion lost two hydrogens in the gas phase, the formation of the dimeric species was prevented.

Table 3.3. High resolution ESI-MS values calculated and found for **SSA-1**, **SSA-2** and **mon1**-**mon4**.

	m/z [M]$^-$		*m/z* [M+M+H]$^-$		*m/z* [M+H]$^+$	
	Theoretical	Actual	Theoretical	Actual	Theoretical	Actual
SSA-1	297.0162	297.0159	595.0404	595.0390	80.0500	n.a.
SSA-2	312.9928	312.9933	626.9936	629.9936	80.0500	n.a.
mon1	297.0162	297.1574	/	/	255.1128	255.1140
mon2	312.9928	312.0445	/	/	255.1128	255.1140
mon3	297.0162	297.1475	/	/	257.0921	257.0929
mon4	312.9928	312.0465	/	/	257.0921	257.0931

3.2.3.3. Quantitative ^{1}H NMR

Since 1960, quantitative NMR (qNMR) has been an important tool for quantifying the concentration and purity of small organic molecules. In particular, it has been used by the Hiscock group to initially determine, in solution state, the presence of lower- and/or higher- order structures within the sample. These structures have been hypothesised to correspond to dimers in one case and to bigger aggregates in other cases[32]. Due to their large size, higher-order structures adopt solid-like properties meaning that they cannot be observed by solution state NMR. The absolute quantification method in qNMR allows for the quantification of molecular component "lost" when integrals of interest are compared to a calibrant (a standard of known concentration). The calibrant is chosen according to specific requirements: (i) it has to be soluble in the solvent used, (ii) it has to possess low volatility, (iii) it has to be chemically inert, (iv) it has to produce a simple NMR spectrum

(singlet resonances are preferred) and most importantly (v) its peaks cannot overlap those of the analyte in order to have an effective signal integration. By knowing the concentration of the calibrant C_{cal}, the concentration of the analyte C_x of interest, their respective number of nuclei (N_{cal} and N_x) and the integral area of the internal standard I_{cal}, it is possible to determine the integral area of the analyte I_x (and therefore the percentage of higher-order structures present in the sample) using the following formula[53] :

$$\frac{I_x}{I_{cal}} = \frac{C_{cal}}{C_x} x \frac{N_x}{N_{cal}} \qquad \textbf{Eq. 3.1.}$$

In this study, monomers **mon1** − **mon4** were analysed by using two different solvent systems: (i) 1 % DCM as internal standard in DMSO-d_6 with a monomer concentration of 112 mM and (ii) 5 % EtOH as internal standard in D_2O with a monomer concentration of 5.56 mM. The qNMR results were then compared to those of **SSA-1** and **SSA-2** obtained using the same solvent systems. In both cases, the internal standard was chosen for the miscibility with the deuterated solvent and because the resonance of the ^{1}H nuclei do not overlap with those of the monomers. All experiments were carried out using a relaxation delay (d_1) of 60 seconds in order to ensure no signal loss and thus accurate integration.

It is also important to notice that at concentrations below the limit of detection of the NMR spectrometer used, it is not possible to confirm the absence of any self-associated species.

Table 3.4 summarises the results from quantitative ^{1}H NMR studies obtained for **SSA-1** and **SSA-2**, which have been carried out by the Hiscock group, and monomers **mon1** − **mon4**. As shown in Table 3.4, in a solution of DMSO-d_6 with 1 % DCM, both SSAs did not show any evident signal "loss" (0 % loss) when the integration was compared to that of the internal standard. Therefore, they tended to form lower-order structures which were hypothesised to be dimers (results confirmed by DOSY ^{1}H NMR studies). On the other hand, when aqueous conditions were used (5 % EtOH in D_2O), the results from qNMR showed an apparent "loss" of compound signal when compared to the ethanol peaks (e.g., 46 % of signal was lost in the case of **SSA-2**). It was

hypothesised that this may be due to the formation of bigger self-associated aggregates which adopted solid-like properties.

Table 3.4. Overview of the results from quantitative ^{1}H NMR studies obtained from DMSO-d_6, standardised with 1 % DCM at 112 mM and D$_2$O standardised with 5 % ethanol at 5.56 mM. The table shows the proportion, as percentage, of cation and anion of **SSA-1**, **SSA-2** and monomers **mon1** - **mon4** to become NMR silent. All quantitative ^{1}H NMR experiments were conducted with a delay time (d_1) of 60 s at 298 K.

	% Loss D$_2$O		% Loss DMSO-d_6	
	Cation	Anion	Cation	Anion
SSA-1	37	37	0	0
SSA-2	46	46	0	0
mon1	4	0.5	12	12
mon2	1.5	1.5	12.5	10.5
mon3	0	0	9	15
mon4	0	0	12.5	12.5

Interestingly, all four norbornenyl-based monomers, **mon1** – **mon4**, possessed different behaviour compared to the SSAs. As a matter of fact, the quantitative NMR results of the monomers at a concentration of 5.56 mM in D$_2$O with 5 % EtOH, showed no discernible "loss" (< 4 % loss) of signals for both the anionic and cationic components. While only about 10 % of signal was lost when monomers were dissolved in a solution of DMSO-d_6 with 1 % DCM (the highest value was 15 % for **mon3**). These results appeared to be completely in disagreement with the classical behaviour of the SSAs. We believe that this was strongly influenced by the size of the pyridinium-containing norbornenyl cation which, due to steric hindrance, prevented the formation of hydrogen bonding between the anionic component of the monomer and therefore no larger self-associated aggregates were formed in aqueous solution. On the other hand, the 10 % of signal lost in DMSO-d_6 could be caused by experimental error or could be due to favourable conditions associated with a higher solubility of monomers in this solvent system.

A representative spectrum of quantitative ^{1}H NMR of **mon1** in D$_2$O with 5 % EtOH as internal standard is shown in Figure 3.17. Quantitative ^{1}H NMR of **mon2**, **mon3** and **mon4** are shown in Appendix 2, Figures S77, S78, S79. As shown, no apparent "loss" of compound was present as the signals integrated for two protons in both anionic (orange) and cationic (blue) components.
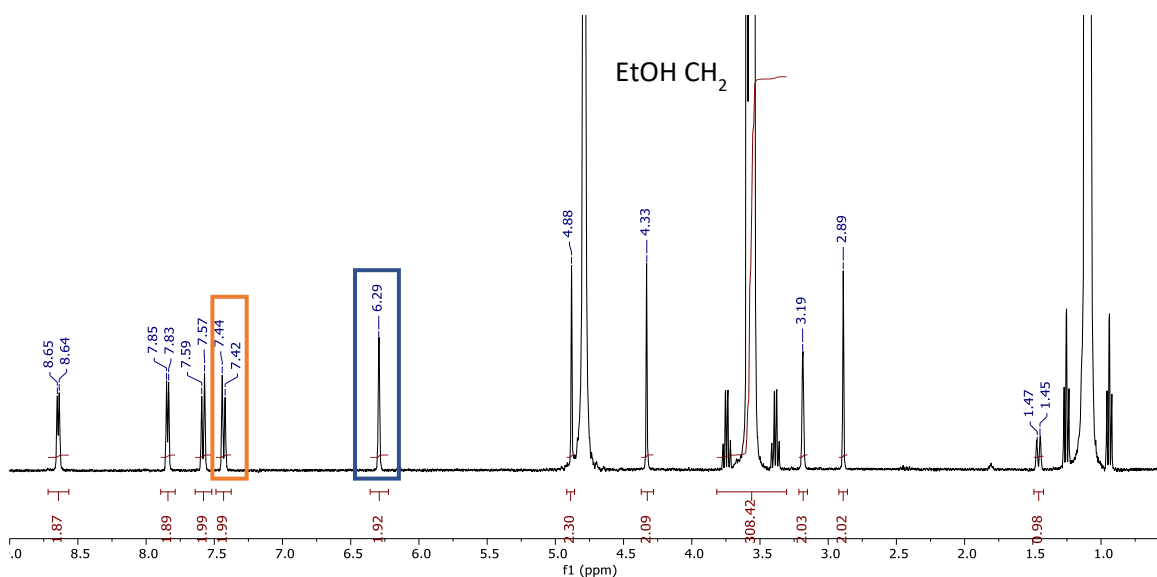
Figure 3.17. ^{1}H NMR spectrum with a delay (d_1 = 60 s) of **mon1** (5.56 mM) in D_2O/ 5 % EtOH. Comparative integration indicated 4 % of the anionic component (orange box) and 0.5 % of the cation component (blue box) has become NMR silent, concluding that no apparent loss is present in this sample.

Figure 3.18 shows an example of quantitative ^{1}H NMR of monomers (**mon1**) in DMSO-d_6 using 1 % DCM as internal standard. In this case 12 % of signal was lost for both cationic and anionic components. Quantitative ^{1}H NMR spectra of **mon2**, **mon3** and **mon4** are available in the Appendix 2 (Figures S73, S74, S75).
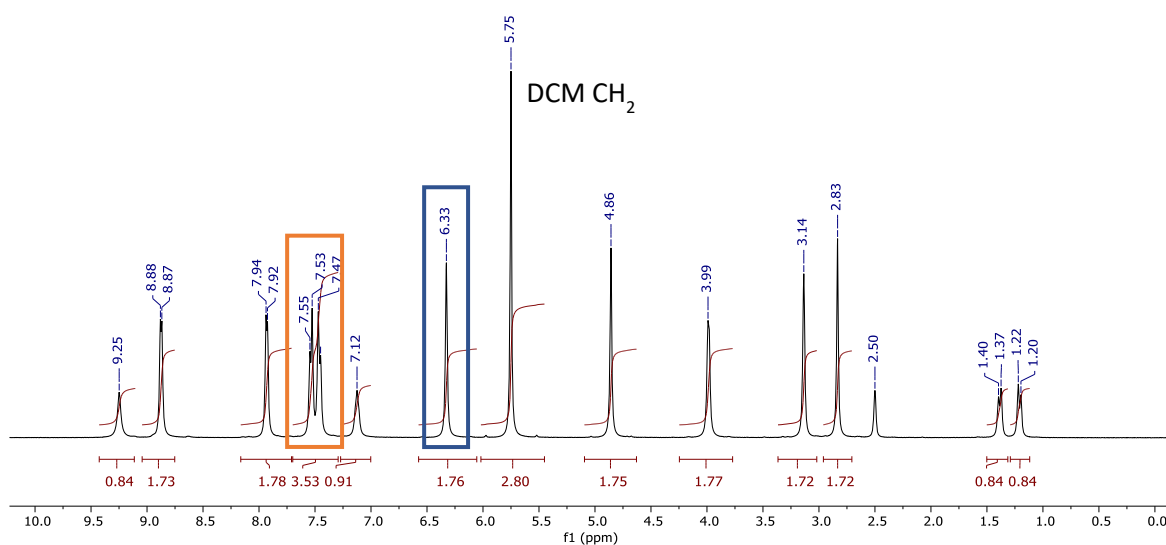
Figure 3.18. ^{1}H NMR spectrum with a delay (d_1 = 60 s) of **mon1** (112 mM) in DMSO-d_6/ 1 % DCM. Comparative integration indicated that 12 % of both cationic and anionic components of the sample have become NMR silent.

143

3.2.3.4. ¹H DOSY NMR studies

In order to further validate the results obtained by qNMR whereby all of the synthesised monomers did not form any larger self-associated structure, a series of ^{1}H NMR DOSY experiments were performed. In this case, two conditions were used: (i) 5.56 mM in D_2O with 5 % EtOH (mainly used for improving solubility of monomers in deuterated water) and (ii) 112 mM in DMSO-d_6 with 0.5 % H_2O.

Diffusion ordered spectroscopy (DOSY)[54] is a technique that allows the user to differentiate NMR signals from a mixture of molecules depending on their differences in molecular weights. More importantly, by measuring the diffusion coefficient it is possible to estimate the molecular size intended as hydrodynamic diameter (d_H) of each molecule present in the mixture. The diffusion coefficient (D) is, in fact, affected by size and shape of molecules and it is determined by the Stokes-Einstein equation:

$$D = \frac{k_B T}{3\pi\eta d_H}$$ **Eq. 3.2.**

Where k_B is the Boltzmann constant (1.38×10^{-23} kg m^2 s^{-2} K^{-1}), T is absolute temperature (K) and η is the viscosity of the solvent. Therefore, the greater the size of the molecule, the smaller the diffusion coefficient and consequently the slower the molecule will diffuse. The limitation of DOSY, however, is the approximation by which each molecule is assumed to be a spherical particle.

As shown in Table 3.5, **mon1 – mon4** did not form any large self-associated aggregates as both cation and anion exhibited a $d_H < 1.4$ nm in a solution of DMSO-d_6 with 0.5 % H_2O, and $d_H <$ 1.1 nm when dissolved in D_2O with 5 % EtOH. The results obtained in DMSO-d_6 suggested that similar to most of the SSAs synthesised by the Hiscock group[35], the anionic component of **mon1 – mon4** tended to form dimeric species (due to hydrogen bond formation). The result was that each SSA anion, within the dimer, dragged one molecule of norbornenyl cation. However, it is important to note that only about 90 % of the monomers in solution behaved in this manner. As we have mentioned before in Section 3.2.3.3, about 10 % of signal was lost in qNMR. With regards to **mon1**

– **mon4** in D_2O solution, the hydrodynamic diameter for both cation and anion were found to be lower compared to those obtained in DMSO-d_6 suggesting that only monomeric species were present in solution. This was further validated by theoretical values calculated using the "molecular weight to size calculator" supplied by Nanocoposix, for which both cationic species (NB and ONB) presented a d_H ~ 0.93 nm, while both anionic species (**SSA-1** and **SSA-2**) presented a d_H ~ 0.99 nm.

Table 3.5. Overview of diffusion coefficients and hydrodynamic diameter for **mon1 - mon4** in DMSO-d_6 and D_2O at 298 K. Errors for diffusion constants are no greater than ± 1 x 10^{-13} m^2/s.

Compound	Solvent	Cation		Anion	
		D (m^2/s)	d_H (nm)	D (m^2/s)	d_H (nm)
Mon 1	DMSO-d_6 + 0.5 % H_2O	1.67 x 10^{-10}	1.31	1.55 x 10^{-10}	1.41
Mon 2	DMSO-d_6 + 0.5 % H_2O	1.71 x 10^{-10}	1.28	1.64 x 10^{-10}	1.34
Mon 3	DMSO-d_6 + 0.5 % H_2O	1.61 x 10^{-10}	1.37	1.52 x 10^{-10}	1.44
Mon 4	DMSO-d_6 + 0.5 % H_2O	1.68 x 10^{-10}	1.31	1.63 x 10^{-10}	1.34
Mon 1	D_2O + 5 % EtOH	4.18 x 10^{-10}	1.04	3.97 x 10^{-10}	1.10
Mon 2	D_2O + 5 % EtOH	4.45 x 10^{-10}	0.98	4.17 x 10^{-10}	1.05
Mon 3	D_2O + 5 % EtOH	4.44 x 10^{-10}	0.98	4.0 x 10^{-10}	1.09
Mon 4	D_2O + 5 % EtOH	4.46 x 10^{-10}	0.98	3.94 x 10^{-10}	1.11

Figure 3.19 shows the DOSY spectrum obtained for **mon1** in DMSO-d_6 with 0.5 % H_2O. It was evident that the anion (red, peaks 1, 4 – 6 and 9) and the cation (blue, peaks 2, 3, 7, 8, 10-13) possessed very similar diffusion coefficients (D_{an} = 1.55 x 10^{-10} vs D_{cat} = 1.67 x 10^{-10} m^2/s) due to very similar molecular weights (Mw_{an} = 297.23 vs Mw_{cat} = 254.29 g/mol) and therefore sizes. In fact, from a first look, it was not possible to hypothesise whether there was a strong coordination between the two components, although the pyridinium cation was known to moderately coordinate the SSAs[34]. Similar DOSY spectra were obtained for monomers **mon2**, **mon3** and **mon4** as shown in the Appendix 2 (Figures S61, S62, S63).
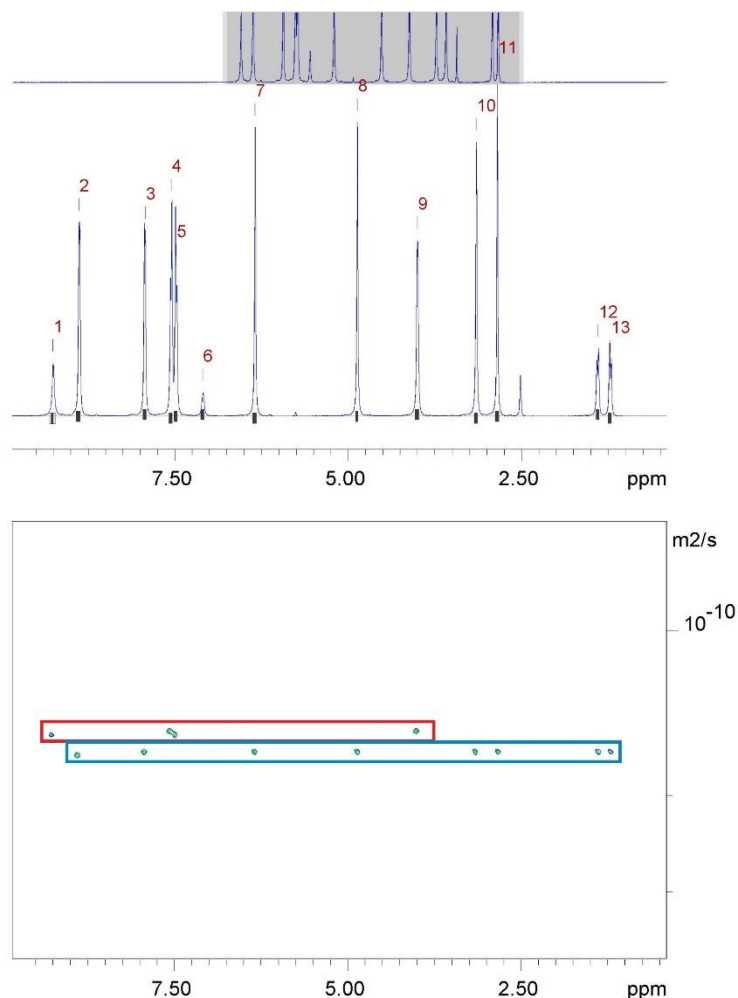
Fig. 3.19. ^{1}H DOSY NMR spectrum of **mon1** (112 mM) in DMSO-d$_6$ at 298 K. Hydrodynamic diameter of the anionic and cationic components of **mon1** were calculated to be d$_H$ = 1.41 nm and d$_H$ = 1.31 nm respectively. Peaks 1, 4-6 and 9 correspond to the anionic component of **mon1** while peaks 2, 3, 7, 8, 10-13 correspond to the cationic component of **mon1**.

It is worth noting that, typically, the thiourea-sulfonate anion (**SSA-2**) forms secondary structures where, due to a reversible slow exchange process, an intramolecular hydrogen bond exists between the sulfonate ion (HBA) and one NH (HBD) in the thiourea moiety as shown in Figure 3.20. Typically, this secondary structure **b** is not involved in the self-association process, and in the DOSY spectrum it is assumed that it diffuses at a different rate compared to the primary structure **a**. However, as shown in Figure 3.21, structure **a** and **b** (respectively peak 10 and 11) diffused at the same rate. This could be due to the fact that a dimeric structure was formed in solution where the NH on structure **b** formed a hydrogen bond with the sulfonate group in structure **a** (proposed structure **c**, Figure 3.20).

146
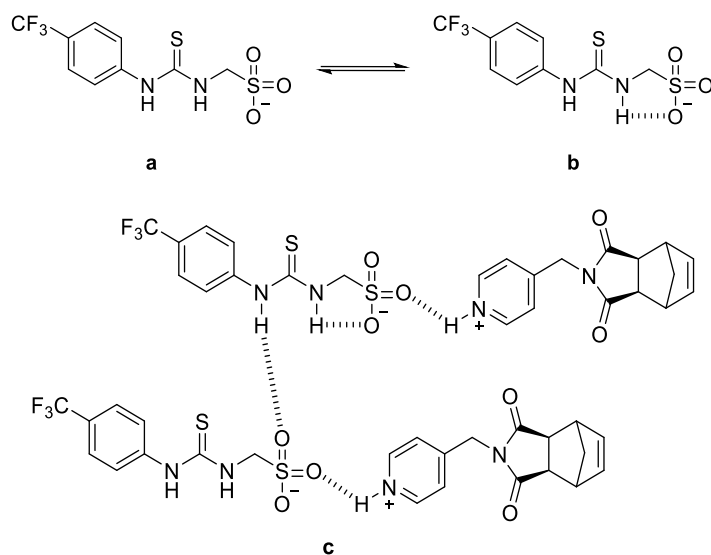
Fig. 3.20. Proposed formation of secondary structure of anionic component of **SSA-2** (structures **a** and **b**) and proposed formation of dimeric species (structure **c**) on **mon2**.
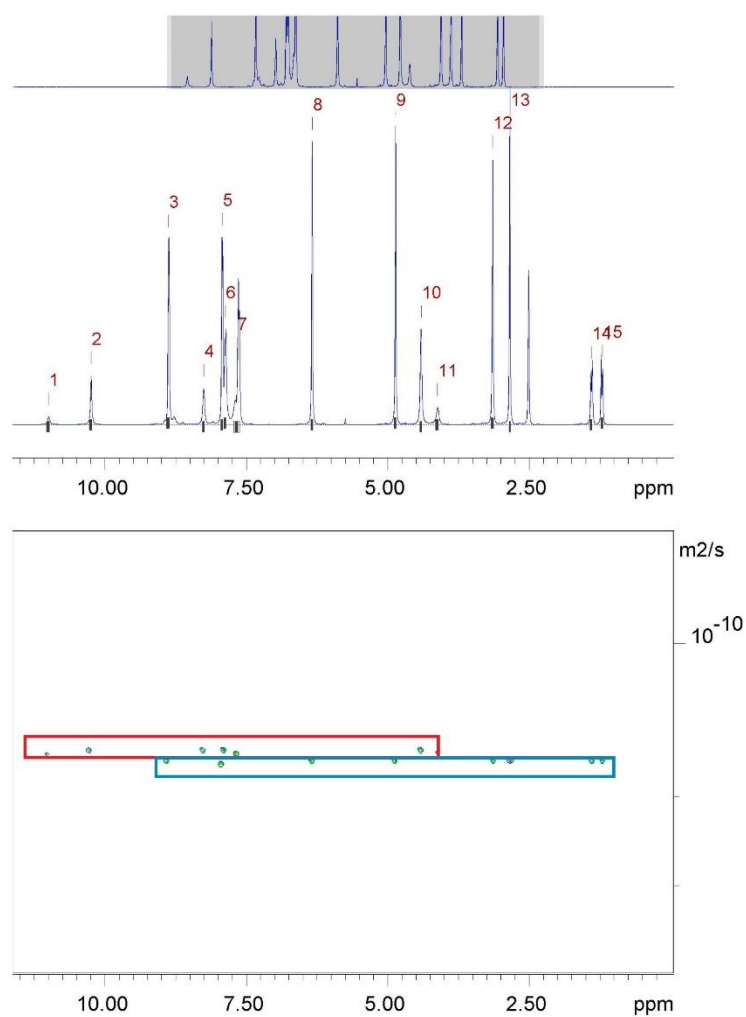
Fig. 3.21. ^{1}H DOSY NMR spectrum of **mon2** (112 mM) in DMSO-d$_6$ at 298 K. Hydrodynamic diameter of the anionic and cationic components of **mon2** were calculated to be d$_H$ = 1.34 nm and d$_H$ = 1.28 nm respectively.

Peaks 1, 2, 4, 6, 7, 10, 11 correspond to the anionic component of **mon2** while peaks 3, 5, 8, 9, 12-15 correspond to the cationic component of **mon2**.

Figure 3.22 represent the DOSY ^1H NMR spectrum of **mon1** in D_2O with 5 % EtOH. The SSA anion, highlighted in red (peaks 3, 4 and 7), had a similar molecular weight to the norbornenyl cation (highlighted in blue, peaks 1, 2, 5, 8 and 9) and thus diffused at a very similar rate (D_{an} = 3.97 x 10^{-10} vs D_{cat} = 4.18 x 10^{-10} m^2/s). Here, peaks 6 and 10 were excluded for calculation purposes as their values were affected by their proximity to the solvent peaks.
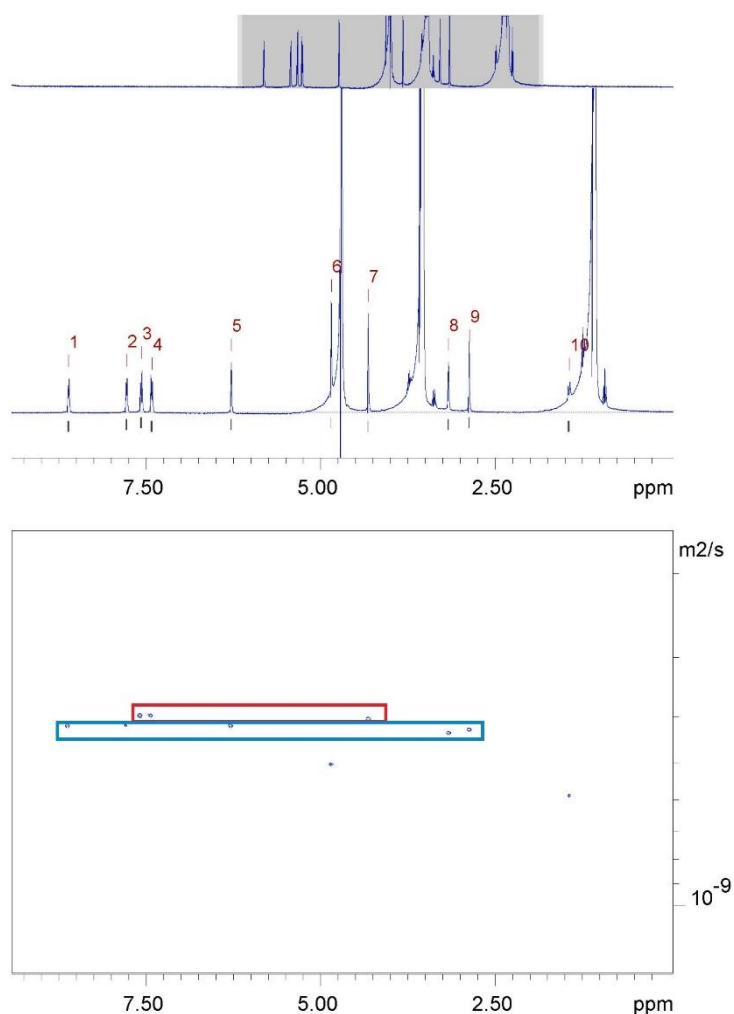
Fig. 3.22. ^1H DOSY NMR spectrum of **mon1** (5.56 mM) in D_2O with 5 % EtOH at 298 K. Hydrodynamic diameters of the anionic and cationic components of **mon1** were calculated to be d_H = 1.10 nm and d_H = 1.04 nm respectively. Peaks 3, 4 and 7 correspond to the anionic component of **mon1** while peaks 1, 2, 5, 6 and 8 – 10 correspond to the cationic component of **mon1**.

Similar DOSY spectra were obtained for **mon2**, **mon3** and **mon4** as shown in the Appendix 2 (Figures S65, S66 and S67).

3.2.3.5. ^{1}H NMR dilution studies

In order to determine the strength of the hydrogen-bonded self-association events occurring among the anionic components of each SSA, the Hiscock group developed a ^{1}H NMR dilution method which allowed for the determination of the self-association constant when compounds were dissolved in a solution of DMSO-d$_6$ (competitive solvent system to H bonds) with 0.5 % H$_2$O starting from a concentration of 112 mM. However, the drawback of this technique is that it is limited to one component, one-dimensional homogeneous aggregation. Due to the fact that **mon1** – **mon4** possessed ~ 10 % of high-order structures (as demonstrated by qNMR) in this solvent system, it could not be possible to quantify the strength of the H bonds. However, ^{1}H NMR dilution studies were performed on **mon1** – **mon4** for the qualitative determination of the presence of hydrogen-bonded events in the case of those ~ 90 % of dimeric species in solution. Samples were prepared in a series, starting from a concentration of 112 mM and then sequentially diluted to a concentration of 1.75 mM for a total of 15 samples. For each sample a ^{1}H NMR spectrum was taken and the change in chemical shift of four different protons was monitored with changes in concentration (the more diluted the sample, the more the chemical shift moves towards the upfield region). Specifically, the N-H resonances on the SSA anion and the aromatic (Ar-H) resonances on the norbornenyl cation were selected for this study.

Figure 3.23 shows the graphs of chemical shift vs concentration of **mon1** (graph a) and **mon2** (graph b) as representative models for both urea- and thiourea-based norbornenyl monomers. As shown in both graphs, there was a change in chemical shift which depended on the concentration of the monomer in solution, which provided evidence for low-order self-associated species due to hydrogen bonding formation. In particular, in **mon1** the ^{1}H nucleus that underwent the biggest change in chemical shift was the N-H represented with the orange circle, whereas in the case of **mon2**, the aromatic proton (Ar-H) represented with the grey triangle underwent the biggest change in ppm. This behaviour was also observed for **mon3** (urea-based oxanorbornenyl monomer) and **mon4** (thiourea-based oxanorbornenyl monomer), indicating that the presence of an oxygen

149

or a sulphur atom could have an effect on the hydrogen bond strength. Graphs of **mon3** and **mon4** are shown in the Appendix 2 (Figures S84, S85). Typically, thiourea-based SSAs that are slow exchange species do not participate in any of the self-association events, as the NH resonances do not show any chemical shift change[32]. However, in the case of **mon2** and **mon4** this occurred, and thus we could further validate the DOSY NMR results and the hypothesis whereby the slow exchange/secondary structure was involved in the formation of the dimeric species (Figure 3.20, c).
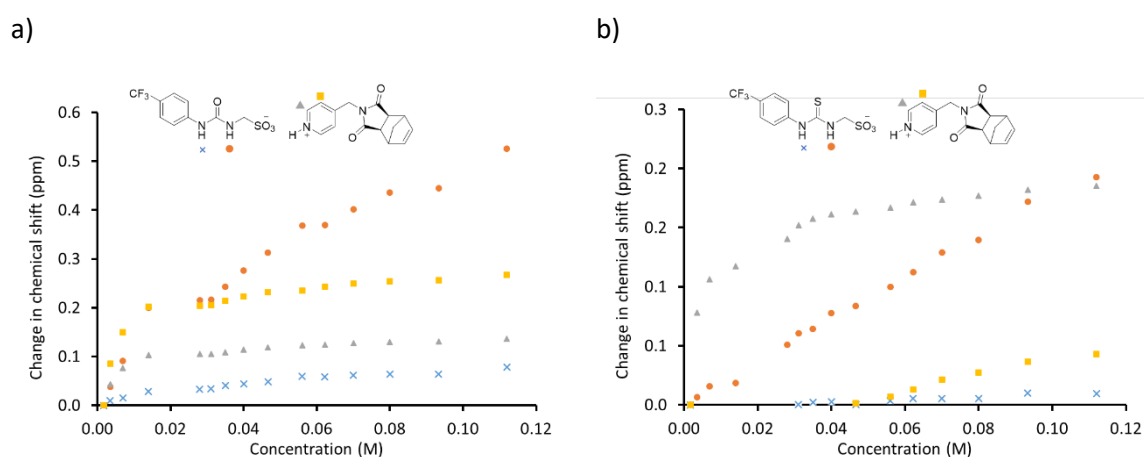
Fig. 3.23. Graph illustrating the ^{1}H NMR down-field change in chemical shift of protons with increasing concentration of **mon1** (a) and **mon2** (b) in DMSO- d_6 0.5 % H_2O (298 K).

3.2.3.6. Dynamic light scattering (DLS) and zeta potential (ZP) studies

Although it was determined by quantitative ^{1}H NMR that **mon1** – **mon4** only formed about 10 % of larger structures when dissolved in DMSO-d_6, we were interested to study their self-assembly properties using DLS and their stability by measuring the zeta potential (ZP). In particular, DLS was carried out using a concentration of **mon1** – **mon4** of 5.56 mM in H_2O with 5 % EtOH and 112 mM in DMSO, whereas ZP studies could only be carried out in water solution as DMSO damages the zeta cell.

In this study, **mon1** – **mon4** were dissolved in (i) a solution of 5 % EtOH in H_2O with a final concentration of 5.56 mM and (ii) in DMSO with a concentration of 112 mM. In both cases, the samples were heated to 40 °C to undergo an annealing process and were then cooled down to room

temperature before any measurement was taken. Since the molecules were novel and no refractive index data (RI) was available, the data were recorded without selecting any RI, thus only size distribution by intensity could be obtained (number or volume distribution could not be obtained).

Unexpectedly, as shown in Table 3.6 and Figure S86 (Appendix 2), **mon1** – **mon4** seemed to form aggregates in water solution with an intensity average diameter between 130 nm and 230 nm, with ONB-based **mon3** and **mon4** having larger particle sizes. These results were comparable to those obtained for **SSA-1**, which had a d_H of 220 nm, and **SSA-2** with a d_H of 235 nm. However, as determined by qNMR in D_2O/5 % EtOH, those monomers did not form any larger self-associated structures, therefore the DLS results obtained were not expected. It was hypothesised that these results could be due to agglomeration of smaller structures in solution that could be seen by the instrument as particles of coherent shape and size. In general, it is difficult to obtain high quality data from dispersions with agglomerated particles as too much light is scattered and hence broadened peaks can be obtained[55]. Agglomeration is enhanced with increasing concentration and this behaviour is typical of SSAs when analysed at a concentration of 112 mM in DMSO. In fact, **mon1** – **mon4** (Table 3.6 and Figure S88 of Appendix 2) as well as SSAs in general, formed large agglomerates in solution with hydrodynamic diameters above the limit of detection (d_H > 1000 nm). This was further validated by the correlation function which gave information about the signal-to-noise ratio as well as the presence of dust particles or agglomerates. The correlation function obtained for **mon1** – **mon4**, did not show a smooth single exponential decay or a linear baseline (Figure S89, Appendix 2), and these effects are always related to the presence of agglomerates or lumps. Furthermore, for each experiment, the 10 measurements taken had very different correlation functions from one another, further demonstrating the absence of homogenous particles in solution.

Upon looking at the ZP values obtained for **mon1** - **mon4** in water solution, it could be further validated the hypothesis that no larger self-associated structures and hence no aggregates were formed in solution. As a matter of fact, ZP (also termed *electrokinetic potential*) is a parameter

used to determine the stability of colloid particles or aggregates in solution. General guidelines classify particle dispersions with ZP values of ± 0 – 10 mV, ± 10 – 20 mV, ± 20 – 30 mV and ± 30 mV as highly unstable, relatively stable, moderately stable and highly stable respectively[56]. Having this in mind, it could be then concluded that the four synthesised monomers were classified as highly unstable aggregates since their ZP values ranged from -3 mV to -10 mV (Table 3.6) compared to those of **SSA-1** and **SSA-2** which possessed a ZP value of -28 mV and -21 mV respectively[32].

Table 3.6. Overview of average DLS intensity particle size distribution and ZP measurements obtained for **mon1 – mon4** at a concentration of 5.56 mM in H_2O/5 % EtOH solution and at a concentration of 112 mM in DMSO at 298 K.

	Solvent system	Concentration	d_H (nm)	Polydispersity (%)	ZP (mV)
mon 1	H_2O/5% EtOH	5.56 mM	194	15 (± 1.49)	- 3.5
mon 2	H_2O/5% EtOH	5.56 mM	131	21 (± 1.42)	- 2.9
mon 3	H_2O/5% EtOH	5.56 mM	216	17 (± 1.54)	- 4.5
mon 4	H_2O/5% EtOH	5.56 mM	226	10 (± 2.25)	- 9.5
mon 1	DMSO	112 mM	400 2800	27 (± 2.54)	n.a.
mon 2	DMSO	112 mM	403 3300	29 (± 1.19)	n.a.
mon 3	DMSO	112 mM	480 1900	35 (± 1.54)	n.a.
mon 4	DMSO	112 mM	123 2500	34 (± 3.64)	n.a.

3.2.3.7. Critical aggregate concentration (CAC) and surface tension

It was demonstrated that SSAs possessed amphiphilic properties which were responsible for the formation of large self-associated structures in solution. It has been shown, in previous work[35], by the Hiscock group that the CAC for a series of SSAs was found to be at concentrations higher than 5.56 mM; concentrations at which DLS studies were carried out showing formation of large aggregates. This was due to the fact that at low concentrations (below the CAC), monomeric units and small particles were present in solution, while at higher concentrations (above the CAC), a mixture of small and large particles could be found. This behaviour was first demonstrated by

Williams et al. in 1955 in his study of critical aggregate concentration of sodium lauryl sulphate[57].

Although self-associated structures of SSAs were present at dilute concentrations, it was only with further addition of solute molecules that it was possible to determine the CAC and therefore the presence of aggregates in solution.

Here, although we showed no formation of larger self-associated structures in water at a concentration of 5.56 mM, we were interested in studying the CAC behaviour of **mon1** - **mon4** in a 5 % EtOH/H_2O solution. The CAC was determined as a function of the change in surface tension (ST) by variation of monomer concentration. Each monomer was dissolved at its highest concentration in a solution of H_2O with 5 % EtOH (22.5 mM, 10 mM, 30 mM and 15 mM for **mon1**, **mon2**, **mon3** and **mon4** respectively) and then diluted in order to obtain at least 10 different samples with decreasing concentration. Monomer concentration and surface tension values were plotted on a graph and the CAC value, together with its ST value, was determined on the intercept of two straight lines, at the point where the surface tension no longer decreased with increasing monomer concentration (Figure 3.24).
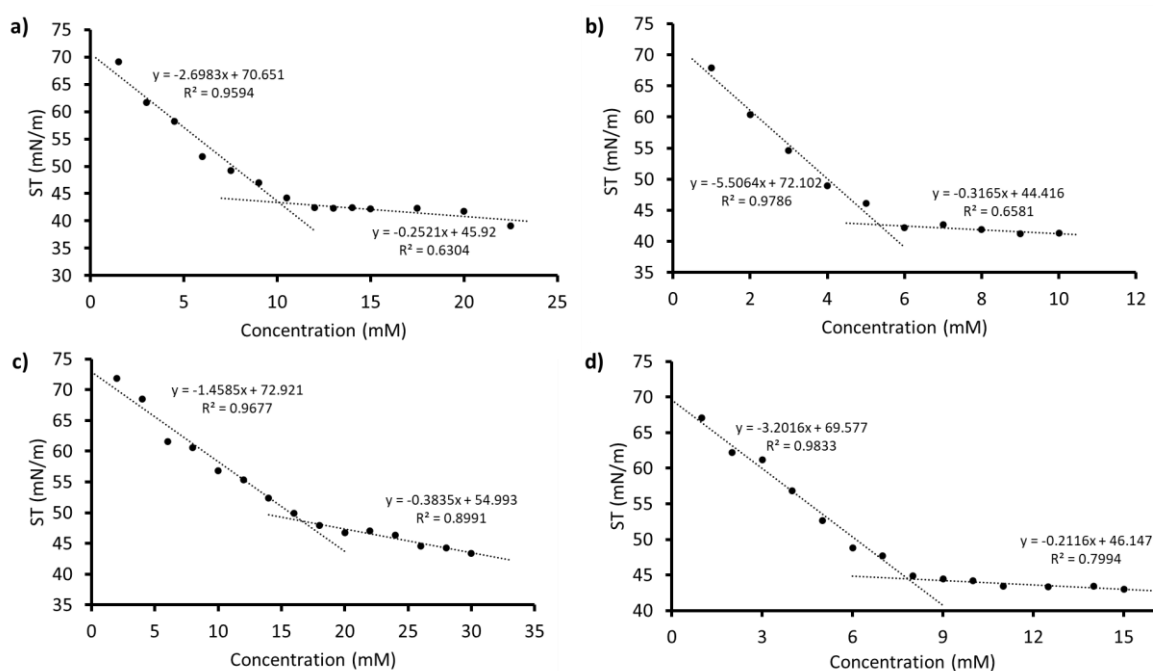
Fig. 3.24. Graphs of surface tension as a function of monomer concentration for **mon1** (a), **mon2** (b), **mon3** (c) and **mon4** (d). The CAC was calculated at the intercept of the trendline of the two series.

As shown in Figure 3.24, the surface tension for all four monomers decreased with increasing monomer concentration. The CAC was found to be higher than 5.56 mM for **mon1**, **mon2** and **mon3** (Table 3.7), meaning that the surface interface became saturated and therefore bigger aggregates only started to form at concentrations higher than 5.56 mM. The only case in which the CAC was lower than 5.56 mM was for **mon2,** which was in contradiction with the results obtained from qNMR. However, this could also be due to experimental error during line best fit. It is worth noting that **mon1** (NB-SSA-1) and **mon3** (ONB-SSA-1), which both contained the urea-based **SSA-1**, were more soluble in those conditions compared to **mon2** (NB-SSA-2) and **mon4** (ONB-SSA-2) which instead contained the thiourea-based **SSA-2**. As a consequence, the CAC was higher for urea-based monomers (10.11 and 16.68 mM) than thiourea-based monomers (5.33 and 7.84 mM). This behaviour was a general trend seen in all urea- and thiourea-based SSAs. In particular, **SSA-1** was found to have a CAC of 198 mM, while **SSA-2** had a CAC of 29 mM, which was different by more than one order of magnitude. It has been established that the presence of the thiourea group helped the formation of stronger hydrogen bonding interactions and formed more stable complexes with anions than the urea-containing molecules[35]. Furthermore, the presence of an O atom on the norbornenyl cation (ONB) slightly increased the solubility of both urea- and thiourea-based monomers in water and thus the effect was an increase in the CAC values.

Table 3.7. Critical aggregate concentration and surface tension values obtained for **mon1** – **mon4** in a solution of 5 % EtOH in water.

	C_{max} (mM)	CAC (mM)	ST (mN/m)
mon 1	22.5	10.11	43.37
mon 2	10	5.33	42.73
mon 3	30	16.68	48.60
mon 4	15	7.84	44.49

3.2.4. Physicochemical properties of polymers, poly1 – poly4

Once monomers **mon1** – **mon4**, were characterised in the solution state, the corresponding polymers, **poly1** – **poly4**, were also characterised. Specifically, the polymer size was studied using

DOSY NMR in DMSO-d_6, while the polymer self-assembly properties were studied using DLS to determine the size of the nanoparticles, ZP to determine their stability and Tensiometer to find the critical aggregate concentration. Due to the poor solubility of the four polymers in H_2O with 5 % EtOH, the solution state studies were carried out using 1 % DMSO in H_2O with a starting polymer concentration of 1 mg/mL.

3.2.4.1. Solubility studies of polymers

Solubility studies were carried out for **poly1** – **poly2** in a water solution with different percentages of DMSO and MeOH, as well as different polymer concentrations. Initially, a concentration of 3 mg/mL (5.56 mM for monomers) in 5 % EtOH/H_2O was selected in order to compare the results obtained for the polymers with the ones obtained for both SSAs and monomers, thus having a better representation of the data. However, as shown in Figure 3.25, **poly1** (named SS089-6.5) was not soluble in that solvent system and big lumps were present even after sonication at 40 °C. DMSO was selected here as it is an organic solvent with amphipathic nature that has been widely used in biological assays for its ability to dissolve poorly soluble molecules. Although, it was demonstrated to be toxic to human cells at concentrations > 10 % (v/v) through plasma membrane pore formation[58,59]. Nevertheless, it was decided that DMSO would be used in this study as no alternatives were available and as proof-of-concept studies. Thus, the solubility of **poly1** (as well as **poly2**, **poly3** and **poly4**) was tested at 1 mg/mL in 1, 5 and 10 % v/v of DMSO in water and 3 mg/mL in 5 and 10 % v/v of DMSO in water. As shown in Figure 3.25, the polymer was completely soluble, in the solvent system, only at high percentages of DMSO (1 mg/mL in 5 and 10 % DMSO; 3 mg/mL in 10 % DMSO). However, for the following characterisations, it was decided that the solution of **poly1** at 1 mg/mL with 1 % DMSO would be used, as it formed a very fine suspension in solution and at the same time a very small percentage of DMSO was used. With regards to **poly2** – **poly4**, the same behaviour was detected and the addition of an oxygen atom on the polymer backbone (**poly3** and **poly4**) did not improve the polymer solubility (Figures S99 – S102, Appendix 2).

155

Fig. 3.25. Solubility of **poly1** (compound 89-6.5) at different percentages of DMSO and MeOH in water solution.

3.2.4.2. ^{1}H DOSY NMR studies

DOSY spectroscopy is a well-established NMR method that reports the diffusion coefficients (D) for individual resonances in NMR spectra. As mentioned in Section 3.2.3.4, DOSY NMR is used determine the size of small molecules in a mixture and it has been used by Hiscock *et al*. to determine the formation of SSA dimers in DMSO-d_6. Recently, DOSY has also been used to determine the conversion[60], molecular weight[61], dispersity[62] of polymers, as well as their aggregation properties[63]. As mentioned before, the synthesised **poly1** – **poly4** formed a fine suspension in the selected solvent system (1 % DMSO in water) and therefore reliable data could not be collected by NMR spectroscopy. Thus, DOSY of polymers have been used to determine the size, intended as hydrodynamic diameter d_H, of the polymers at a concentration of 20 mg/mL in DMSO-d_6. This was used as a comparison to the DOSY data obtained for the respective monomers, rather than the analysis and determination of the polymer molecular weights.
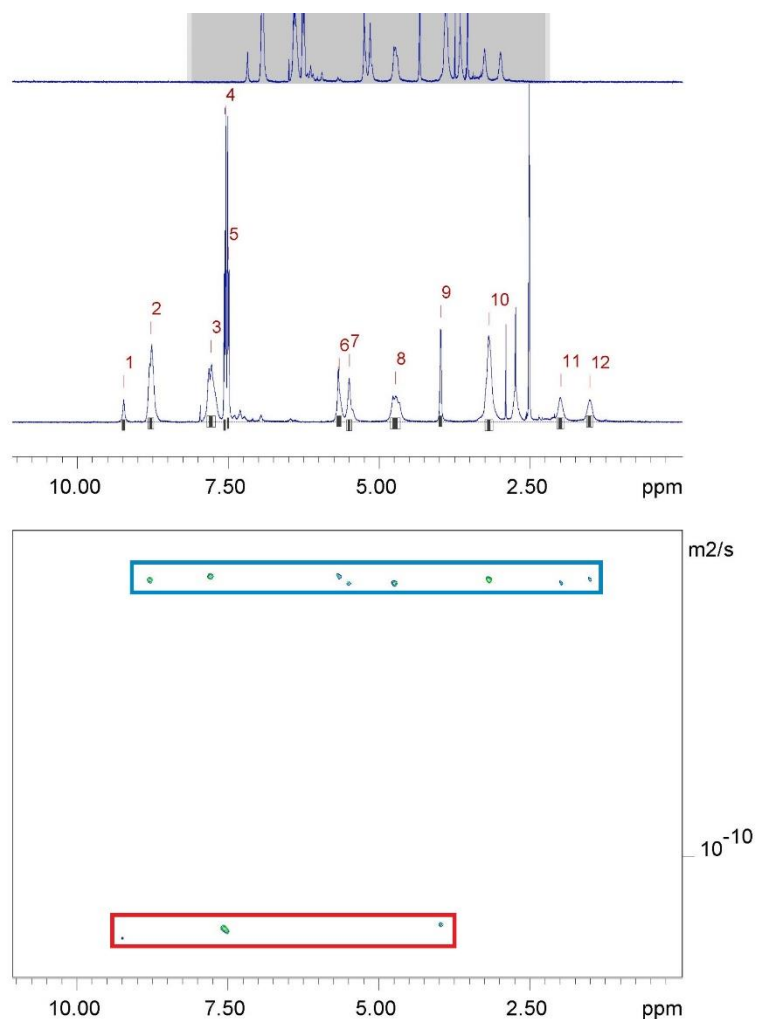
Fig. 3.26. ^{1}H DOSY NMR spectrum of **poly1** (20 mg/mL) in DMSO-d$_6$ at 298 K. Hydrodynamic diameter of the anionic and cationic components of **poly1** were calculated to be d_H = 1.59 nm and d_H = 7.31 nm respectively. Peaks 1, 4, 5 and 9 correspond to the anionic SSA, while peaks 2, 3, 6,-8, 10-12 correspond to the cationic polymer backbone.

As shown in the DOSY NMR spectrum (Figure 3.26) obtained for **poly1**, the SSA anion and the cationic polymer backbone diffused separately with different rates, revealing that the coordination between the cationic polyNB and the anionic SSA was weak, as opposed to the corresponding **mon1** (Figure 3.19), where the anionic and cationic components diffused at very similar rates. This was indeed due to the similarity in size rather than the strong coordination between the pyridinium cation and the urea-sulfonate anion. Interestingly, although the GPC analysis revealed the formation of two different molecular weight distributions (M$_n$ = 10 600 and 2 200 g/mol), the DOSY NMR spectrum did not show the diffusion of more than one polymer chain.

157

This could be due to the relatively weaker sensitivity of the NMR instrument compared to the GPC, which was able to detect and separate polymers with different lengths.

Table 3.8. Overview of diffusion coefficients and hydrodynamic diameter for polymers **poly1** – **poly4** in DMSO-d_6 at 298 K. Errors for diffusion constants are no greater than ± 1 x 10^{-12} m^2/s.

Compound	Cation		Anion	
	D (m^2/s)	d_H (nm)	D (m^2/s)	d_H (nm)
poly1	3.0 x 10^{-11}	7.31	1.38 x 10^{-10}	1.59
poly2	3.0 x 10^{-11}	7.29	1.47 x 10^{-10}	1.49
poly3	4.39 x 10^{-11}	4.99	1.58 x 10^{-10}	1.39
poly4	4.67 x 10^{-11}	4.69	1.69 x 10^{-10}	1.30

As shown in Table 3.8, the d_H of the anionic SSA on **poly1** (1.59 nm) remained relatively unchanged compared to **mon1** (1.41 nm). On the contrary, the hydrodynamic diameter for the cationic polyNB in **poly1** was 7.31 nm, which was seven times higher than the d_H of **mon1** (1.31 nm), further demonstrating the formation of a polymeric system. By comparison with the GPC results, it could be assumed that a polymer consisting of 20 repeating units (monomer conversion > 99 %) formed self-assembled structures in DMSO with an approximate d_H of 7.0 nm. In fact, **poly2** behaved similarly to **poly1** and formed cationic polyNB with d_H of 7.29 nm, while the SSA anion possessed a d_H of 1.49 nm which was similar to its monomer counterpart. The M_n values of **poly1** and **poly2** were comparable to the theoretical value (Table 3.1), indicating that all of the monomer introduced in the reaction mixture was consumed. This was different for **poly3** and **poly4**, where hydrodynamic diameters of 4.99 nm and 4.69 nm respectively (Table 3.8) were calculated by DOSY NMR for the cationic polyONB. This was consistent with the GPC results, whereby the M_n values were found to be lower than the theoretical ones (Table 3.1). This again showed that not all of the monomer was consumed during the polymerisation (monomer conversion << 90 %). Further studies are required in order to determine the reason for the poor monomer conversion of the ONB containing monomers (**mon3** and **mon4**). Longer reaction time would not be the ideal solution due to the unwanted "back-biting" side reactions. DOSY NMR spectra for **poly2**, **poly3** and **poly4** are shown in Figures S69, S70 and S71, Appendix 2.

3.2.4.3. Nanoparticles size, stability and critical aggregate concentration

As mentioned in Section 3.2.4.1, polymers **poly1 – poly4** were dissolved in a solution of 1 % DMSO in water and their self-assembly properties were studied in this solvent system. The four synthesised polymers were homopolymers consisting of the same repeating unit along the polymer chain and they possessed intrinsic amphiphilic properties. The polynorbornene backbone acted as the hydrophobic part while the SSA acted as the hydrophilic part through its sulphonate and urea groups. In order to determine the self-assembly properties of the polymers in the chosen solvent system, DLS studies were carried out.
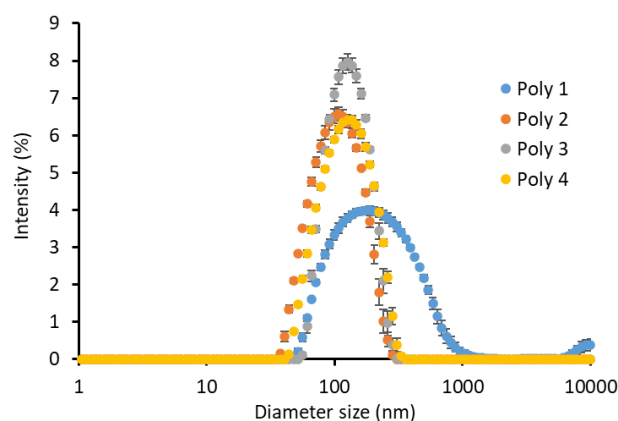
Fig. 3.27. Average intensity size distribution of polymers **poly1 – poly4** measured at a concentration of 1 mg/mL in a solution of H_2O with 1 % DMSO at 298 K.

Figure 3.27 shows the DLS size distribution of **poly1 – poly4**. In particular, **poly1** seemed to form nanoparticles with a hydrodynamic diameter that ranged between 50 nm and 1000 nm, with an average size (by intensity) of 246 nm. Whereas **poly2**, **poly3** and **poly4** formed nanoparticles in a shorter range (lower polydispersity) of 50 – 500 nm, with an average diameter of 112 nm for **poly2** and 134 nm for both **poly3** and **poly4** (Table 3.9). In order to determine the stability of the aggregates in solution, the ZP for the four polymers was measured. As shown in Table 3.9, **poly1 – poly4** possessed a ZP that ranged between + 32 mV and + 54 mV, therefore it could be assumed that highly stable aggregates were formed in solution as opposed to their corresponding monomers which formed highly unstable dispersions. Furthermore, **poly3** and **poly4** were more stable

compared to **poly1** and **poly2**, meaning that in this case the addition of the oxygen atom in the

hydrophobic backbone was a reason for further stabilisation of the aggregates.

Table 3.9. Overview of average DLS intensity particle size distribution, ZP and CAC measurements obtained for polymers **poly1 – poly4** at a concentration of 1 mg/mL in H_2O/1.0 % DMSO solution at 298 K. a = CAC of polymers could not be measured as above the solubility limit.

Polymer	Solvent system	Concentration (mg/mL)	dH (nm)	Polydispersity (%)	ZP (mV)	CAC
poly1	1% DMSO	1	246	27 (± 0.37)	+ 32	a
poly2	1% DMSO	1	112	21 (± 0.32)	+ 49	a
poly3	1% DMSO	1	134	21 (± 0.31)	+ 54	a
poly4	1% DMSO	1	134	17 (± 0.6)	+ 52	a

Once it was determined that **poly1** – **poly4** formed stable aggregates in solution, CAC

studies were carried out. Different samples were prepared by serial dilution from a stock solution

of polymer with a concentration of 1 mg/mL in 1 % DMSO/H_2O. The prepared samples were then

analysed using a Tensiometer to determine the change in surface tension (ST) with increasing

polymer concentration. As shown in Figure 3.28 the ST decreased with increasing of polymer

concentration, however, it was not possible to determine the CAC values for any of the four

polymers at that concentration range (0.1 – 1 mg/mL) and it could not be determined for

concentrations > 1 mg/mL due to the poor solubility of the polymers in the solution. This behaviour

was similar to that of the monomers (Section 3.2.3.7), where the CAC values were also found to be

higher than the concentration used for DLS studies. As demonstrated by Williams *et al.*[57], at

concentrations below the CAC small particles are present in solution and therefore these can still

be detected by the DLS.
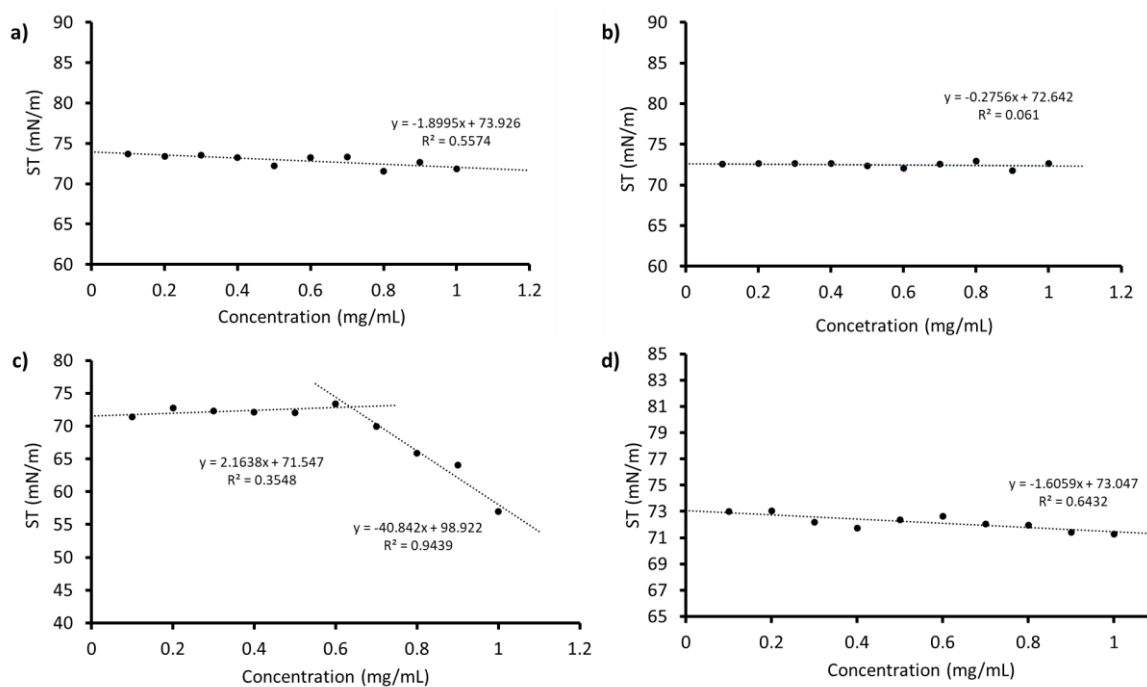
Fig. 3.28. Graphs surface tension as a function of polymer concentration for **poly1** (a), **poly2** (b), **poly3** (c) and **poly4** (d). CAC could not be calculated as it is above the solubility limit.

It is important to note that, although the DLS, ZP and CAC experiments demonstrated formation of stable aggregates in the nanometre scale, those values did not entirely match a visual analysis of the polymers at a concentration of 1 mg/mL in a solution of 1 % DMSO/H_2O. As shown in Figure 3.25 (Section 3.2.4.1), a fine suspension could be detected by the human eye. Further investigation might be required.

3.2.5. The antimicrobial activity of monomers and polymers

As previously mentioned in Section 3.1.2, SSAs have shown to act as antimicrobial agents against Gram-positive (MRSA) and/or Gram-negative (*E. coli*) bacteria of clinical interest. Hiscock *et al*. have hypothesised that the interaction between SSAs and the surface bacterial cell is mostly driven by the formation of hydrogen bonds between the HBD and HBA groups of the anionic component of SSAs and the phospholipid head groups of the bacterial cell (PE and PG) which causes cell disruption and thus, cell death[36]. On the other hand, as mentioned in Section 3.1.1, the cationic residues of

amphiphilic cationic polymers (ACPs) allow for electrostatic interactions of the polymers with the anionic groups of the lipid bilayer bacterial cell membrane. This is followed by the insertion of the hydrophobic units within the hydrophobic membrane core which then causes cell disruption[15].

The antimicrobial experiments discussed in this section were conducted at the UK Health Security Agency laboratories at Porton Down by Dr. Jessica E. Boles. Sterile LB agar plates were streaked using *Escherichia coli* DH10B or methicillin-resistant *Staphylococcus aureus* USA300 then incubated at 37 °C overnight. An initial culture was made up by inoculating Luria Broth (LB) media (5 mL) with a single colony of bacteria under sterile conditions and incubated at 37 °C with shaking overnight. The following day, overnight bacterial cultures were sub-cultured into a fresh LB medium at a starting OD_{600} (Optical Density 600 nm) of 0.01. Each compound was serially diluted across the plate with a starting concentration of 10 mM for **mon1** – **mon4** and a starting concentration of 500 µg/mL (approximately 0.9 mM) for **poly1** – **poly4**. Bacteria culture (100 µL) was aliquoted to each well giving a total well volume of 200 µL. Plates were incubated with shaking (180 rpm) at 37 °C for 18 h and the OD_{600} was determined using a Clariostar plate reader (BMG Labtech). The antibacterial activity was expressed as a minimum inhibitory concentration (MIC_{50}), the concentration required by each monomer and polymer to prevent 50 % of bacterial cell growth against Gram-positive MRSA USA300 and Gram-negative *E. coli* DH10B. Experiments could not be repeated due to time constraints. Furthermore, results for **mon3** could not be obtained as the compound was not pure at the time of the analysis (see Section 3.2.1.4).

As shown in Table 3.10 (and Figure S92, Appendix 2), **mon1** did not show any activity up to the highest measured concentration of 10 mM against both MRSA and *E. coli* bacteria. In contrast, **mon2** (Figure S93, Appendix 2) was found to be active against both Gram-positive and Gram-negative bacteria, although only at a very high concentration of 10 mM, while **mon4** (Figure S94, Appendix 2) was found to inhibit 50 % of *E. coli* growth at a concentration of 10 mM and failed against MRSA. Unfortunately, the MIC_{50} results obtained for the analysed monomers were not as promising as those obtained for a series of synthesised SSAs where the highest MIC_{50} was < 5 mM

and < 10 mM for MRSA and *E. coli* respectively[32]. For instance, **SSA-1** has been shown to have a MIC$_{50}$ of 0.35 mM against MRSA (Table 3.9), while the thiourea-sulfonate **SSA-2** did not show any antimicrobial activity.

Table 3.10. Overview of MIC$_{50}$ values determined for **SSA-1**, **SSA-2**, **mon1** - **mon4** and **poly1** - **poly4** against clinically relevant Gram-positive MRSA USA300 and Gram-negative *E. coli* DH10B after incubation at 37 °C for 18 h. Fail = compound did not inhibit bacteria growth.

	MIC$_{50}$ (mM)			MIC$_{50}$ (mM)	
Compound	MRSA	*E. coli*	Compound	MRSA	*E. coli*
SSA-1	0.35[a]	Fail[a]	**poly1**	Fail	Fail
SSA-2	Fail[a]	Fail[a]	**poly2**	Fail	Fail
mon1	Fail	Fail	**poly3**	Fail	Fail
mon2	10	10	**poly4**	Fail	Fail
mon4	Fail	10			

[a] Results are previously published by Hiscock *et al*.[32]

It can be noted that an antagonistic effect was seen when changing the cationic component from **SSA-1** (pyridinium cation) to **mon1** (pyridinium-based NB cation). The introduction of a bigger cation removed the ability of the urea-sulfonate anion to act as an antimicrobial agent against MRSA. This could be attributed to the incapability of **mon1** in forming any larger self-associated structures when added to water, compared to **SSA-1** as determined by the physicochemical properties study. On the contrary, a slight improvement was obtained when NB (**mon2**) and ONB (**mon4**) cations were added to the thiourea-sulfonate anion. In this case, while **SSA-2** was inactive towards both bacterial models, **mon2** was able to inhibit bacterial growth in both MRSA and *E. coli*, while **mon4** was selective towards Gram-negative bacteria. In this way, a synergistic effect was obtained, and it was possible to produce monomers that preferentially interact with different types of bacterial cell membrane. In fact, Gram-positive bacteria usually contain 57 % of PG and no PE, while Gram-negative bacteria are composed of 85 % PE and 15 % PG[64]. However, because of the time constraints the analysis could not be repeated more than once and therefore these results must be treated with caution. Overall, a MIC$_{50}$ concentration of 10 mM was very high compared to

results obtained for antimicrobial compounds in literature (as shown in Chapter 1, Section 1.3.2) and therefore these monomers cannot be considered antimicrobial.

In contrast to the monomers, the four synthesised polymers **poly1** – **poly4**, were found to be completely inactive towards MRSA and *E. coli* up to the highest concentration of 500 µg/mL (~ 0.9 mM) for an incubation of 18 hours (Table 3.9, Figures S95 – S98, Appendix 2). This could be due to the poor solubility of the polymers in the chosen solvent system (1 % DMSO in water), or it could be due to the polymer structure itself. It was hypothesised that in order for the SSA to act as antimicrobial, larger self-associated structures obtained through hydrogen bond formation between the SSAs anions were necessary. When the SSA anions were coordinating NB/ONB pyridinium containing cations, those bigger structures were not obtained and therefore when the monomers were polymerised, the same effect was obtained. Thus, the presence of SSA anions as monomeric units along the polymer backbone was not sufficient to obtain the necessary coordination with the phospholipid head groups and thus bacteria cell disruption was not obtained. At the same time, because the homopolymers have been designed without additional hydrophobic side chains, it was not possible to obtain the same antimicrobial activity results obtained by the polymers synthesised by Tew *et al*.[17] where the higher the number alkyl chains, the more potent the polymer was against both bacteria models. This was due to the deeper penetration of the hydrophobic units into the lipid bilayer. Finally, it was believed that because the SSA anion and the cationic polynorbornene coordinated the same area of the cell membrane, an antagonistic effect was obtained.

3.3. Conclusion

Based on the potential role of SSAs to act as antimicrobial agents against Gram-positive and/or Gram-negative bacteria, a new class of ROMP polymers containing SSAs was prepared and investigated with the intention of creating a more active SSA system.

Firstly, NB and ONB based monomers containing urea- and thiourea-sulfonate anions were synthesised and obtained cleanly via a three- or a four-step reaction. Four different monomers were synthesised: two of them (**mon1** and **mon2**) were NB based monomers and the other two (**mon3** and **mon4**) were ONB based monomers, with each of them containing either a urea-sulfonate anion (**SSA-1**) or a thiourea-sulfonate anion (**SSA-2**). The construction of four different structurally related compounds allowed for the determination of structure-activity relationship. These compounds were analysed in the solid phase, gas phase and solution state and compared with the results obtained for the isolated SSAs used in this study. While in the solid state a similar behaviour was detected for **mon1** and **mon2** compared to the SSAs, where the mildly coordinating pyridinium cation allowed for the formation of urea-anion tapes (**mon1**) and thiourea-anion stacking (**mon2**), the same cannot be said for the gas and solution state. In the gas phase only monomeric species of monomers were present as opposed to dimeric species found in **SSA-1** and **SSA-2**. The same behaviour is found in the solution state where, using quantitative NMR and DOSY, only monomeric species could be detected. This was further validated by ZP studies which determined a very high instability for monomer aggregates formed in water solution.

The previously mentioned monomers were then polymerised via ROMP using Grubbs third generation catalyst which allowed for the synthesis of four different homopolymers: **poly1** and **poly2** were polyNB based polymers, while **poly3** and **poly4** were polyONB based polymers. The polyONB based polymers were prepared with the intention of creating a more water soluble SSA-containing drug delivery system. Unfortunately, due to the polymerisation conditions, kinetic studies could not be carried out and thus homopolymers with two different types of molecular weight distributions were obtained. DLS studies of polymers in 1 % DMSO/H_2O demonstrated the formation of aggregates with average hydrodynamic diameters of 130 – 230 nm which were found to be highly stable (ZP > + 30 mV). However, visual analysis contradicted these results.

The suitability of the synthesised monomers and polymers for antimicrobial applications was evaluated by growth inhibition studies against Gram-positive MRSA and Gram-negative *E. coli*.

Unfortunately, the experiments were not successful showing that none of the polymers were active against both bacteria models up to the highest concentration of 500 μg/mL (limit of polymer solubility). Monomers **mon2** and **mon4**, showed antimicrobial activity at concentrations of 10 mM, however due to time constraints, the experiments could not be repeated and therefore the results need further validation. It can be concluded that addition of SSAs into a polyNB/polyONB backbone does not produce polymer systems with improved antimicrobial activity. However, the so formed polymers could be used as a way to deactivate the antimicrobial drugs in a novel way to prevent off-target effects. In this way the drug could be activated only when specific cells react with the polymeric aggregates to degrade the polymer backbone.

3.4. References

1   The World Health Organisation (WHO), https://www.who.int/news-room/fact-sheets/detail/antimicrobial-resistance, (accessed 31 December 2021).

2   European Centre for Disease Prevention and Control, https://www.ecdc.europa.eu/en/news-events/33000-people-die-every-year-due-infections-antibiotic-resistant-bacteria, (accessed 1 January 2022).

3   D. Ashiru-Oredope, S. Hopkins and ESPAUR Oversight Group Writing Committee ., *English surveillance programme for antimicrobial utilisation and resistance (ESPAUR): Report 2020 to 2021*, 2021.

4   H. Takahashi, G. A. Caputo and K. Kuroda, *Biomater. Sci.*, 2021, **9**, 2758–2767.

5   A. Kuroki, A. Kengmo Tchoupa, M. Hartlieb, R. Peltier, K. E. S. Locock, M. Unnikrishnan and S. Perrier, *Biomaterials*, 2019, **217**, 119249.

6   J. M. A. Blair, M. A. Webber, A. J. Baylay, D. O. Ogbolu and L. J. V. Piddock, *Nat. Rev. Microbiol.*, 2015, **13**, 42–51.

7   K. Upadhya R, L. Shenoy and R. Venkateswaran, *J. Anaesthesiol. Clin. Pharmacol.*, 2018, **34**, 46–50.

8   K. A. Brogden, *Nat. Rev. Microbiol.*, 2005, **3**, 238–250.

9   K. A. Brogden, M. Ackermann, P. B. McCray and B. F. Tack, *Int. J. Antimicrob. Agents*, 2003, **22**, 465–478.

10   M. Zasloff, *J. Occup. Environ. Med.*, 1988, **30**, 470.

11   A. A. Langham, A. S. Ahmad and Y. N. Kaznessis, *J. Am. Chem. Soc.*, 2008, **130**, 4338–4346.

12   C. Subbalakshmi and N. Sitaram, *FEMS Microbiol. Lett.*, 1998, **160**, 91–96.

13   J. R. C. García, F. Jaumann, S. Schulz, A. Krause, J. Rodríguez-Jiménez, U. Forssmann, K.

Adermann, E. Klüver, C. Vogelmeier, D. Becker, R. Hedrich, W. G. Forssmann and R. Bals, *Cell Tissue Res.*, 2001, **306**, 257–264.

14   E. M. Kohn, D. J. Shirley, L. Arotsky, A. M. Picciano, Z. Ridgway, M. W. Urban, B. R. Carone and G. A. Caputo, *Molecules*, 2018, **23**, 329.

15   K. A. Henzler Wildman, D. K. Lee and A. Ramamoorthy, *Biochemistry*, 2003, **42**, 6545–6558.

16   A. Kuroki, P. Sangwan, Y. Qu, R. Peltier, C. Sanchez-Cano, J. Moat, C. G. Dowson, E. G. L. Williams, K. E. S. Locock, M. Hartlieb and S. Perrier, *ACS Appl. Mater. Interfaces*, 2017, **9**, 40117–40126.

17   T. Eren, A. Som, J. R. Rennie, C. F. Nelson, Y. Urgina, K. Nüsslein, E. B. Coughlin and G. N. Tew, *Macromol. Chem. Phys.*, 2008, **209**, 516–524.

18   J. L. Grace, J. X. Huang, S. E. Cheah, N. P. Truong, M. A. Cooper, J. Li, T. P. Davis, J. F. Quinn, T. Velkov and M. R. Whittaker, *RSC Adv.*, 2016, **6**, 15469–15477.

19   J. L. Grace, A. G. Elliott, J. X. Huang, E. K. Schneider, N. P. Truong, M. A. Cooper, J. Li, T. P. Davis, J. F. Quinn, T. Velkov and M. R. Whittaker, *J. Mater. Chem. B*, 2017, **5**, 531–536.

20   T. D. Michl, K. E. S. Locock, N. E. Stevens, J. D. Hayball, K. Vasilev, A. Postma, Y. Qu, A. Traven, M. Haeussler, L. Meagher and H. J. Griesser, *Polym. Chem.*, 2014, **5**, 5813–5822.

21   R. Garcia Maset, A. Hapeshi, S. Hall, R. M. Dalgliesh, F. Harrison and S. Perrier, *ACS Appl. Mater. Interfaces*.

22   J. Tan, Y. Zhao, J. L. Hedrick and Y. Y. Yang, *Adv. Healthc. Mater.*, 2021, 2100482.

23   M. F. Ilker, K. Nüsslein, G. N. Tew and E. B. Coughlin, *J. Am. Chem. Soc.*, 2004, **126**, 15870–15875.

24   A. P. Kaymaz, İ. Acaroğlu-Degitz, M. A. Yapaöz, A. D. Sezer, S. Malta, B. Aksu and T. Eren, *Materialia*, 2019, **5**, 100246.

25   N. C. Süer, C. Demir, N. A. Ünübol, Ö. Yalçin, T. Kocagöz and T. Eren, *RSC Adv.*, 2016, **6**, 86151–86157.

26   N. C. Süer, T. Arasoglu, H. Cankurtaran, M. Okutan, M. Gallei and T. Eren, *Turkish J. Chem.*, 2021, **45**, 986–1003.

27   S. J. Lam, E. H. H. Wong, N. M. O'Brien-Simpson, N. Pantarat, A. Blencowe, E. C. Reynolds and G. G. Qiao, *ACS Appl. Mater. Interfaces*, 2016, **8**, 33446–33456.

28   R. Namivandi-Zangeneh, R. J. Kwan, T. K. Nguyen, J. Yeow, F. L. Byrne, S. H. Oehlers, E. H. H. Wong and C. Boyer, *Polym. Chem.*, 2018, **9**, 1735–1744.

29   L. J. White, J. E. Boles, N. Allen, L. S. Alesbrook, J. M. Sutton, C. K. Hind, K. L. F. Hilton, L. R. Blackholly, R. J. Ellaby, G. T. Williams, D. P. Mulvihill and J. R. Hiscock, *J. Mater. Chem. B*, 2020, **8**, 4694–4700.

30   L. J. White, J. E. Boles, N. Allen, L. S. Alesbrook, J. M. Sutton, C. K. Hind, K. L. F. Hilton, L. R. Blackholly, R. J. Ellaby, G. T. Williams, D. P. Mulvihill and J. R. Hiscock, *J. Mater. Chem. B*, 2020, **8**, 4694–4700.

31   J. E. Boles, R. J. Ellaby, H. J. Shepherd and J. R. Hiscock, *RSC Adv.*, 2021, **11**, 9550–9556.

32   N. Allen, L. J. White, J. E. Boles, G. T. Williams, D. F. Chu, R. J. Ellaby, H. J. Shepherd, K. K. L. Ng, L. R. Blackholly, B. Wilson, D. P. Mulvihill and J. R. Hiscock, *ChemMedChem*, 2020, **15**, 2193–2205.

33   K. K. L. Ng, M. Dimitrovski, J. E. Boles, R. J. Ellaby, L. J. White and J. R. Hiscock, *Supramol. Chem.*, 2020, **32**, 414–424.

34   L. R. Blackholly, H. J. Shepherd and J. R. Hiscock, *CrystEngComm*, 2016, **18**, 7021–7028.

35   L. J. White, N. J. Wells, L. R. Blackholly, H. J. Shepherd, B. Wilson, G. P. Bustone, T. J. Runacres and J. R. Hiscock, *Chem. Sci.*, 2017, **8**, 7620–7630.

36   G. Townshend, G. S. Thompson, L. J. White, J. R. Hiscock and J. L. Ortega-Roldan, *Chem. Commun.*, 2020, **56**, 4015–4018.

37   C. Slugovc, *Macromol. Rapid Commun.*, 2004, **25**, 1283–1297.

38   S. C. G. Biagini, S. M. Bush, V. C. Gibson, L. Mazzariol, M. North, W. G. Teasdale, C. M. Williams, G. Zagotto and D. Zamuner, *Tetrahedron*, 1995, **51**, 7247–7262.

39   M. R. Willcott, *J. Am. Chem. Soc.*, 2009, **131**, 13180–13180.

40   M. B. France, L. T. Alty and T. M. Earl, *J. Chem. Educ.*, 1999, **76**, 659–660.

41   R. B. Woodward and H. Baer, *J. Am. Chem. Soc.*, 1948, **70**, 1161–1166.

42   F. A. L. Anet, *Tetrahedron Lett.*, 1962, **3**, 1219–1222.

43   J. B. Birks, *Physics and Chemistry of the Organic Solid State Volume III*, Interscience Publishers, Inc, 1968, vol. 19.

44   S. Calvo-Losada and D. Suárez, *J. Am. Chem. Soc.*, 2000, **122**, 390–391.

45   M. W. Lee and W. C. Herndon, *J. Org. Chem.*, 1978, **43**, 518.

46   L. Rulíšek, P. Šebek, Z. Havlas, R. Hrabal, P. Čapek and A. Svatoš, *J. Org. Chem.*, 2005, **70**, 6295–6302.

47   L. J. White, S. N. Tyuleva, B. Wilson, H. J. Shepherd, K. K. L. Ng, S. J. Holder, E. R. Clark and J. R. Hiscock, *Chem. - A Eur. J.*, 2018, **24**, 7761–7773.

48   Frank J. Weigert and John D. Roberts, *J. Am. Chem. Soc.*, 1971, **93**, 2361–2369.

49   E. Ahmetali, P. Sen, N. C. Süer, B. Aksu, T. Nyokong, T. Eren and M. K. Şener, *Macromol. Chem. Phys.*, 2020, **221**, 1–14.

50   J. R. Hiscock, G. P. Bustone, B. Wilson, K. E. Belsey and L. R. Blackholly, *Soft Matter*, 2016, **12**, 4221–4228.

51   L. J. White, J. E. Boles, K. L. F. Hilton, R. J. Ellaby and J. R. Hiscock, *Molecules*, 2020, **25**, 4126.

52   M. and T. H. Ho, CS; Lam, CWS; Chan, MHM; Cheung, RCK; Law, LK; Lit, LCW; Ng, KF; Suen, *Clin Biochem Rev*, 2003, **24**, 3–12.

53   S. K. Bharti and R. Roy, *TrAC - Trends Anal. Chem.*, 2012, **35**, 5–26.

54   C. S. Johnson, *Prog. Nucl. Magn. Reson. Spectrosc.*, 1999, **34**, 203–256.

55   S. Bhattacharjee, *J. Control. Release*, 2016, **235**, 337–351.

56   J. D. Clogston and A. K. Patri, in *Methods in molecular biology (Clifton, N.J.)*, 2011, vol. 697, pp. 63–70.

57   R. J. Williams, J. N. Phillips and K. J. Mysels, *Trans. Faraday Soc.*, 1955, **51**, 728–737.

58   J. Galvao, B. Davis, M. Tilley, E. Normando, M. R. Duchen and M. F. Cordeiro, *FASEB J.*, 2014, **28**, 1317–1330.

59   M. Verheijen, M. Lienhard, Y. Schrooders, O. Clayton, R. Nudischer, S. Boerno, B. Timmermann, N. Selevsek, R. Schlapbach, H. Gmuender, S. Gotta, J. Geraedts, R. Herwig, J. Kleinjans and F. Caiment, *Sci. Rep.*, 2019, **9**, 1–12.

60   P. Lewinski, S. Sosnowski, S. Kazmierski and S. Penczek, *Polym. Chem.*, 2015, **6**, 4353–4357.

61   S. Viel, D. Capitani, L. Mannina and A. Segre, *Biomacromolecules*, 2003, **4**, 1843–1847.

62   J. Viéville, M. Tanty and M. A. Delsuc, *J. Magn. Reson.*, 2011, **212**, 169–173.

63   P. Groves, *Polym. Chem.*, 2017, **8**, 6700–6708.

64   R. F. Epand, J. E. Pollard, J. O. Wright, P. B. Savage and R. M. Epand, *Antimicrob. Agents Chemother.*, 2010, **54**, 3708–3713.

CHAPTER 4. EXPERIMENTAL SECTION

4.1. Experimental section of Chapter 2

4.1.1. Materials and instrumentations

Carbic anhydride (*endo*), 5-amino-1-pentanol, thionyl chloride and ethyl vinyl ether were obtained from Acros Organics. Glycene, poly(ethylene glycol) methyl ether (M_n 550) and third generation Grubbs catalyst were obtained from Sigma Aldrich. α-Methyl-4-(isobutyl)phenylacetic acid was obtained from Alfa Aeser. Gibco® phosphate-buffered saline (PBS) and HyClone™ foetal bovine serum (FBS) were obtained from Thermo Fisher Scientific. Porcine liver esterase was obtained from Sigma Aldrich. Gel permeation chromatography (GPC) was conducted using PL-GPC 50 Plus system by Varian Inc. equipped with 2xPLgel 5µm MIXED-C (300 x 7.5 mm) column with temperature set at 40 °C; refractive index was used for the detector and THF, stabilised with 250 ppm BHT, was the eluent; flow rate was set at 1 mL/min and sample run time was 25 minutes. DLS was performed using Zeta Sizer Nano-ZS by Malvern Instruments Limited. Transmission electron microscopy (TEM) was performed on a Jeol 1230, operating at an accelerating voltage of 80 kV and the images were recorded with a Gatan Multiscan 790 digital - 2 - camera. FTIR spectra were recorded on a Shimadzu IR-Affinity instrument. NMR spectra were obtained on a Bruker AV2 400 MHz spectrometer; the spectra were calibrated to the centre of the residual undeuterated set solvent peak and chemical shifts then reported in parts per million (ppm). Spectra were analysed using MestReNova. *In vitro* release studies were recorded using a Phenomenex Hypersil BDS column (5 µm, 100 x 4.6 mm) on a Ultimate 3000 UHPLC by Thermo Fiscer Scientific. A gradient eluent system was used starting from 28 % methanol with 0.1 % formic acid increasing to 100 % of methanol with 0.1 % formic acid. Samples were injected with a volume of 10 µL and run at 30 °C at a flow rate of 4 mL/min. Absorbance was monitored at 225 nm.

4.1.2. Synthesis of *endo/exo*-norbornenyl ibuprofen monomer (NB-ibu)

1a (*endo*)
1b (*exo*)

3a (*endo*)
3b (*exo*)

3a (*endo*)
3b (*exo*)

5a (*endo*)
5b (*exo*)
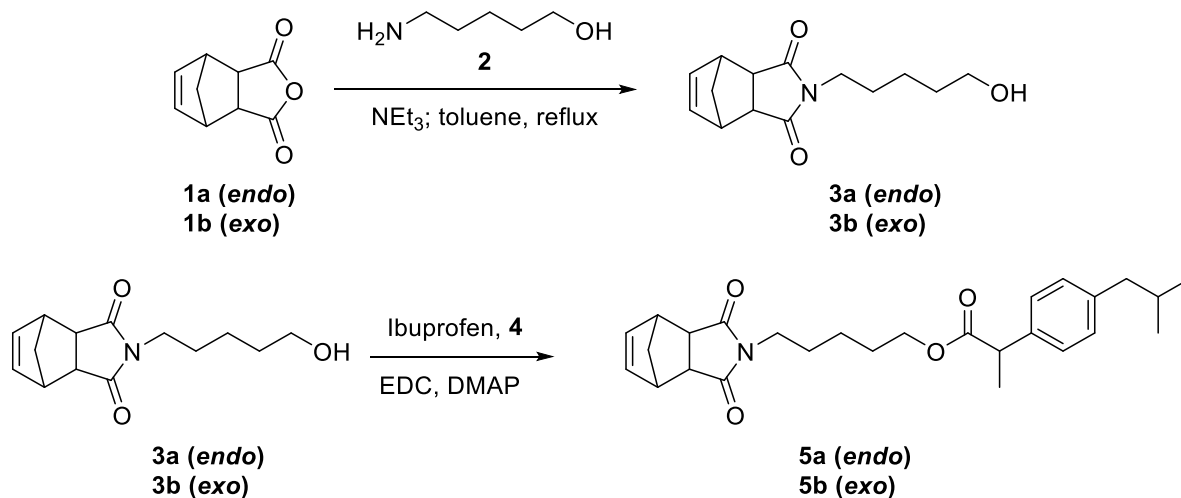
4.1.2.1. *Exo*-carbic anhydride, **1b**[1]
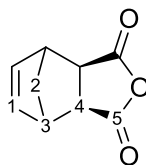
Endo-carbic anhydride **1a** (50 g, 0.3 mol) was added to a round bottom flask with condenser attached. The solid was heated at approximately 170 °C for 2h resulting in a yellow liquid. After heating, the yellow liquid was left to cool slightly and then toluene (140 mL) was added, and the solution heated at reflux in order to dissolve all the solid formed during the addition of toluene. The solution was then left to cool down to room temperature until crystallization occurred. The solvent was decanted off and the product was collected by *vacuum* filtration, washed with toluene and allowed to dry. E*xo*-carbic anhydride **1b** was purified by recrystallisation with toluene. This was repeated three times using solid/solvent ratio 1:2.5 for the first one and the second one, while for the third one the minimum amount of solvent needed to cover the solid was added. E*xo*-carbic anhydride **1b** was obtained 98 % pure (by GC analysis) as an off-white solid (7.0 g, 0.043 mol, 14 %).

m.p.: 144 – 150 °C; ^{1}H NMR (CDCl$_3$, 400 MHz) δ (ppm): 6.34 (2H, t, *J* = 1.8 Hz, 1), 3.46 (2H, t, *J* = 1.6 Hz, 3), 3.01 (2H, d, *J* = 1.45, 4), 1.67 (1H, dt, *J* = 10.3 and 1.5 Hz, 2'), 1.45 (1H, d, *J* = 10.3 Hz, 2"); ^{13}C

NMR (CDCl$_3$, 100 MHz) δ (ppm): 171.7 (*C*-5), 138.1 (*C*-1), 48.9 (*C*-4), 47.0 (*C*-3), 44.3 (*C*-2); IR ν$_{max}$ (cm^{-1}): 2999 (CH alkene), 1853 (C=O anhydride), 1772, 1217, 1082, 939, 893, 846, 767, 732, 632.

The characterization matches that reported in the literature.[1]

4.1.2.2. *N*-(hydroxypentanyl)-*cis*-5-norbornene-*endo*-2,3-dicarboximide, **3a**[2]
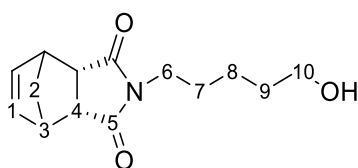
Endo-carbic anhydride **1a** (3.5 g, 21.0 mmol) and triethylamine (0.6 mL, 2.1 mmol) were added to toluene (60 mL) and stirred with gentle heating until most of the solid was dissolved. 5-Amino-1-pentanol **2** (2.2 g, 21.0 mmol) was crushed up and added to the stirring solution and a Dean-Stark trap was attached to the flask. The reaction mixture was heated at reflux for 3h, then cooled and concentrated in *vacuo* to give a yellow oil, which was dissolved in 60 mL of DCM and washed with 0.1 M HCl (1 x 30 mL) and brine (1 x 30 mL). The organic layer was dried over MgSO$_4$ and concentrated in *vacuo* to afford the title product **3a** as a yellow oil (5.1 g, 20.5 mmol, 98 %). ^{1}H NMR (CDCl$_3$, 400 MHz) δ (ppm): 6.09 (2H, t, *J* = 1.8 Hz, 1), 3.60 (2H, t, *J* = 6.5 Hz, 10), 3.39 – 3.36 (2H, m, 3), 3.33 (2H, t, *J* = 7.2 Hz, 6), 3.24 – 3.23 (2H, m, 4), 1.72 (1H, dt, *J* = 1.7 and 8.8 Hz, 2'), 1.59 – 1.52 (3H, m, 2" and 9), 1.49 – 1.42 (2H, m, 7), 1.35 – 1.37 (2H, m, 8); ^{13}C NMR (CDCl$_3$, 100 MHz) δ (ppm): 177.9 (*C*-5), 134.5 (*C*-1), 62.6 (*C*-10), 52.3 (*C*-2), 45.8 (*C*-4), 44.9 (*C*-3), 38.2 (*C*-6), 32.1 (*C*-9), 27.5 (*C*-7), 23.0 (*C*-8); IR ν$_{max}$ (cm^{-1}): 3446 (OH), 2941 (CH alkene), 1681 (C=O amide), 1398, 1336, 1155, 1051, 842, 721, 615; LC-MS (ESI): calculated [M+H]$^+$ [C$_{14}$H$_{19}$NO$_3$+H]$^+$ 250.1, found 250.2.

4.1.2.3. N-(hydroxypentanyl)-cis-5-norbornene-exo-2,3-dicarboximide 3b[2]
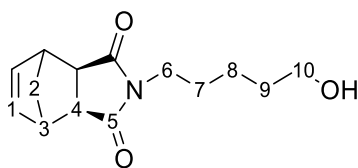
Exo-carbic anhydride **1b** (5.0 g, 30.5 mmol) and triethylamine (0.4 mL, 3.05 mmol) were added to toluene (80 mL) and stirred with gentle heating until most of the solid was dissolved. 5-Amino-1-pentanol **2** (3.2 g, 30.5 mmol) was crushed up and added to the stirring solution and a Dean-Stark trap was attached to the flask. The reaction mixture was heated at reflux for 3h, then cooled and concentrated in *vacuo* to give a yellow oil, which was dissolved in 60 mL of DCM and washed with 0.1 M HCl (1 x 30 mL) and brine (1 x 30 mL). The organic layer was dried over MgSO$_4$ and concentrated in *vacuo* to afford alcohol **3b** as a yellow oil (6.2 g, 24.7 mmol, 71 %). ^{1}H NMR (CDCl$_3$, 400 MHz) δ (ppm): 6.29 (2H, t, *J* = 1.9 Hz, 1), 3.64 (2H, t, *J* = 6.5 Hz, 10), 3.48 (2H, t, *J* = 7.4 Hz, 6), 3.27 (2H, t, *J* = 1.8 Hz, 3), 2.68 (2H, d, *J* = 1.4 Hz, 4), 1.63 – 1.56 (4H, m, 7 and 9), 1.52 (1H, dt, *J* = 1.6 and 9.9 Hz, 2'), 1.42 – 1.34 (2H, m, 8), 1.23 (1H, br d, *J* = 9.8 Hz, 2''); ^{13}C NMR (CDCl$_3$, 100 MHz) δ (ppm): 178.2 (*C*-5), 137.8 (*C*-1), 62.6 (*C*-10), 47.8 (*C*-4), 45.2 (*C*-3), 42.8 (*C*-2), 38.5 (*C*-6), 32.1 (*C*-9), 27.5 (*C*-7), 23.1 (*C*-8); IR ν$_{max}$ (cm^{-1}): 3444 (OH), 2940 (CH alkene), 2864, 1767, 1683 (C=O amide), 1396, 1344, 1327, 1287, 1153, 1055, 885, 787, 721, 642; LC-MS (ESI): calculated [M+H]$^+$ [C$_{14}$H$_{19}$NO$_3$+H]$^+$ 250.1, found 250.2.

The characterization matches that reported in the literature.[2]

4.1.2.4. Ibuprofen ester of compound 3a, 5a[3]
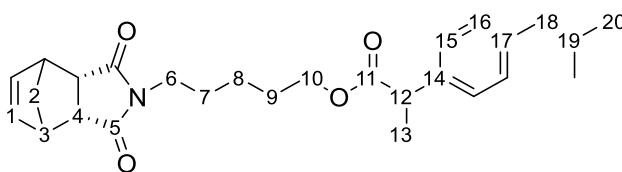
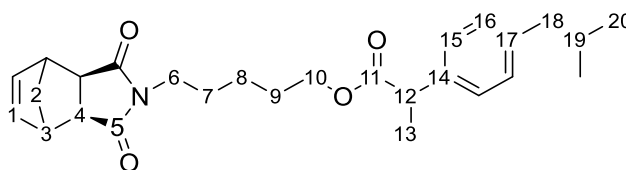To a solution of *N*-(hydroxypentanyl)-cis-5-norbornene-*endo*-2,3-dicarboximide **3b** (0.30 g, 1.2 mmol) in DCM (20 mL), were added α-methyl-4-(isobutyl)phenylacetic acid **4** (0.29 g, 1.4 mmol),

175

EDC (0.46 g, 2.4 mmol) and DMAP (0.16 g, 1.3 mmol). The reaction mixture was left to stir at room temperature for 24 hours. The solvent was concentrated in *vacuo*, EtOAc was added and the solution washed with HCl 2 M (1 x 15 mL) and water (2 x 15 mL). The organic layer was dried over MgSO$_4$, filtered and the solvent concentrated in *vacuo*. The crude product was purified by flash chromatography (EtOAc/Pet 2:3, R_f = 2.9) to afford the title compound **5a** as a colourless oil (0.20 g, 0.5 mmol, 43 %). ^{1}H NMR (CDCl$_3$, 400 MHz) δ (ppm): 7.18 (2H, d, *J* = 8.1 Hz, 15), 7.08 (2H, d, *J* = 8.1 Hz, 16), 6.07 (2H, d, *J* = 1.8 Hz, 1), 4.01 (2H, td, *J* = 6.5 and 3.3 Hz, 10), 3.67 (1H, q, *J* = 7.2 Hz, 12), 3.37 (2H, br s, 3), 3.27 (2H, t, *J* = 7.5 Hz, 6), 3.23 – 3.22 (2H, m, 4), 2.43 (2H, d, *J* = 7.2 Hz, 18), 1.83 (1H, hept, *J* = 6.8 Hz, 19), 1.72 (1H, d, *J* = 8.8 Hz, 2'), 1.59 – 1.52 (3H, m, 2" and 9), 1.47 (3H, d, *J* = 7.2 Hz, 13), 1.43 – 1.36 (2H, m, 7), 1.25 – 1.16 (2H, m, 8), 0.88 (2H, d, *J* = 6.6 Hz, 20); ^{13}C NMR (CDCl$_3$, 100 MHz) δ (ppm): 177.7 (*C*-5), 174.8 (*C*-11), 140.5 (*C*-14), 137.8 (*C*-17), 134.4 (*C*-1), 129.3 (*C*-15), 127.2 (*C*-16), 64.4 (*C*-10), 52.3 (*C*-2), 45.7 (*C*-4), 45.2 (*C*-12), 45.0 (*C*-18), 44.9 (*C*-3), 38.1 (*C*-6), 30.2 (*C*-19), 28.1 (*C*-9), 27.4 (*C*-7), 23.2 (*C*-20), 22.4 (*C*-8), 18.5 (*C*-13); IR ν$_{max}$ (cm^{-1}): 2958 (CH alkene), 1805, 1697 (C=O amide), 1400, 1308, 1165, 1400, 1308, 1165, 1096, 970, 885, 765, 716, 640, 603; LC-MS (ESI): calculated [M+H]$^+$ [C$_{27}$H$_{35}$NO$_4$+H]$^+$ 438.3, found 438.2.

4.1.2.5. Ibuprofen ester of compound **3b**, **5b** (NB-Ibu)[3]

To a solution of *N*-(hydroxypentanyl)-*cis*-5-norbornene-*exo*-2,3-dicarboximide **3b** (0.50 g, 2.0 mmol) in DCM (25 mL), were added α-methyl-4-(isobutyl)phenylacetic acid **4** (0.50 g, 2.3 mmol), EDC (0.80 g, 4.0 mmol) and DMAP (0.30 g, 2.2 mmol). The reaction mixture was left to stir at room temperature for 24 hours. The solvent was concentrated in *vacuo*, EtOAc was added and the solution washed with HCl 2 M (1 x 15 mL) and water (2 x 15 mL). The organic layer was dried over MgSO$_4$, filtered and the solvent concentrated in *vacuo* to afford monomer **5b** as a colourless oil

(0.60 g, 1.5 mmol, 74 %). ^{1}H NMR (CDCl$_3$, 400 MHz) δ (ppm): 7.19 (2H, d, J = 8.0 Hz, 15), 7.10 (2H, d, J = 8.2 Hz, 16), 6.29 (2H, t, J = 1.7 Hz, 1), 4.04 (2H, td, J = 6.5 and 2.2 Hz, 10), 3.67 (1H, q, J = 7.2 Hz, 12), 3.42 (2H, t, J = 7.6 Hz, 6), 3.28 – 3.27 (2H, m, 3), 2.67 (2H, t, J = 1.7 Hz, 4), 2.44 (1H, d, J = 1.1 Hz, 18), 1.89 - 1.79 (1H, m, 19), 1.64 - 1.50 (5H, m, 7, 9 and 2'), 1.48 (3H, d, J = 7.2 Hz, 13), 1.31 - 1.25 (2H, m, 8), 1.21 (1H, br d, J = 9.7 Hz, 2"), 0.89 (6H, d, J = 6.7 Hz, 20). ^{13}C NMR (CDCl$_3$, 100 MHz) δ (ppm): 178.1 (*C*-5), 174.8 (*C*-11), 140.5 (*C*-14), 137.8 (*C*-1 and *C*-17), 129.3 (*C*-16), 127.2 (*C*-15), 64.4 (*C*-10), 47.8 (*C*-4), 45.2 (*C*-12), 45.0 (*C*-3 and *C*-18), 42.8 (*C*-2), 38.4 (*C*-6), 30.2 (*C*-19), 28.1 (*C*-9), 27.4 (*C*-7), 23.3 (*C*-8), 22.4 (*C*-20), 18.5 (*C*-13); IR ν$_{max}$ (cm^{-1}): 2951 (CH alkene), 1769, 1730, 1695 (C=O amide), 1460, 1396, 1366, 1165, 1070, 950, 849, 787, 721, 642; LC-MS (ESI): calculated [M+H]$^+$ [C$_{27}$H$_{35}$NO$_4$+H]$^+$ 438.3, found 438.2.

4.1.3. Synthesis of *endo/exo*-norbornenyl poly(ethylene glycol) methyl ether (NB-PEG)

1a (*endo*)   7a (*endo*)   8a (*endo*)
1b (*exo*)   7b (*exo*)   8b (*exo*)

n= 12 (average)

8a (*endo*)   10a (*endo*)
8b (*exo*)   10b (*exo*)
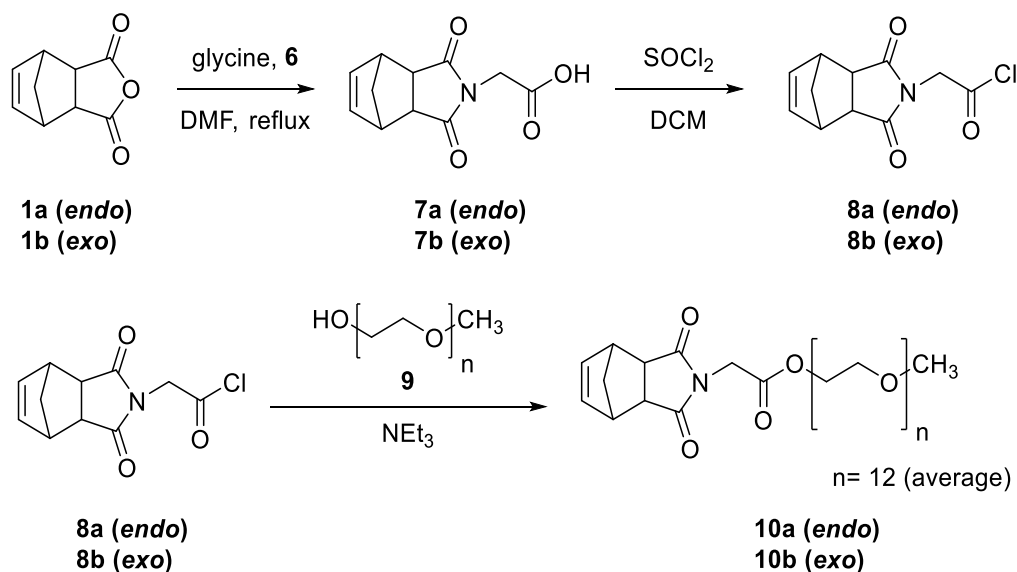
4.1.3.1. *N*-(*endo*-himoyl)-glycine, **7a**[4]
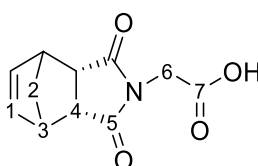
To *endo*-carbic anhydride **1a** (5.0 g, 30.5 mmol) dissolved in dry DMF (40 mL) was added glycine **6** (2.3 g, 30.5 mmol). The reaction mixture was heated at reflux for 18 hours under inert atmosphere (N$_2$), cooled to room temperature, diluted with EtOAc and washed with saturated aqueous ammonium chloride solution (5 x 40 mL). The organic phase was dried over MgSO$_4$, filtered and concentrated in *vacuo*. The residue was recrystallized twice from EtOAc (1:4 solid/solvent) giving the title product **7a** as a white crystalline solid (2.4 g, 10.7 mmol, 35 %). m.p.: 153 – 158 °C; ^{1}H NMR (CDCl$_3$, 400 MHz) δ (ppm): 6.11 (2H, t, *J* = 1.7 Hz, 1), 4.13 (2H, s, 6), 3.43 – 3.41 (2H, m, 3), 3.38 – 3.37 (2H, m, 4), 1.75 (1H, dt, *J* = 1.6 and 8.8 Hz. 2'), 1.57 (1H, br d, *J* = 8.8 Hz, 2"); ^{13}C NMR (CDCl$_3$, 100 MHz) δ (ppm): 176.9 (*C*-5), 171.7 (*C*-7), 134.6 (*C*-1), 52.3 (*C*-2), 46.2 (*C*-4), 45.0 (*C*-3), 38.8 (*C*-6); IR ν$_{max}$ (cm^{-1}): 2991 (CH alkene), 1770, 1741 (COOH), 1601 (C=O amide), 1414, 1327, 1132, 1082, 949, 885, 840, 746, 735, 717, 605, 545; LC-MS (ESI): calculated [M+Na]$^+$ [C$_{11}$H$_{11}$NO$_4$+Na]$^+$ 244.1, found 244.1.

4.1.3.2. *N*-(*exo*-himoyl)-glycine, **7b**[4]
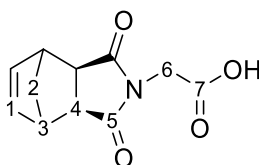
To *exo*-carbic anhydride **1b** (5.0 g, 30.5 mmol) dissolved in dry DMF (40 mL) was added glycine **6** (2.3 g, 30.5 mmol). The reaction mixture was heated at reflux for 18 hours under inert atmosphere, cooled to room temperature, diluted with ethyl acetate and washed with saturated aqueous ammonium chloride solution (5 x 40 mL). The organic phase was dried over MgSO$_4$, filtered and concentrated in *vacuo*. The residue was recrystallized twice from EtOAc (1:4 solid/solvent) giving the title product **7b** as a white crystalline solid (3.3 g, 15.0 mmol, 49 %). m.p.: 153 – 157 °C; ^{1}H NMR (CDCl$_3$, 400 MHz) δ (ppm): 6.31 (2H, t, *J* = 1.8 Hz, 1), 4.28 (2H, s, 6), 3.32 (2H, t, *J* = 1.5 Hz, 3), 2.78 (2H, d, *J* = 1.3 Hz, 4), 1.62 (1H, br d, *J* = 10.0 Hz, 2"), 1.51 (1H, dt, *J* = 1.4 and 10.0 Hz, 2'); ^{13}C NMR (CDCl$_3$, 100 MHz) δ (ppm): 177.3 (*C*-5), 172.0 (*C*-7), 138.0 (*C*-1), 48.1 (*C*-4), 45.4 (*C*-3), 42.9 (*C*-2),

39.1 (*C*-6); IR ν_{max} (cm^{-1}): 2991 (CH alkene), 1734 (COOH), 1660 (C=O amide), 1420, 1321, 1204, 1173, 939, 885, 816, 783, 696, 634, 611; LC-MS (ESI): calculated [M+Na]$^+$ [C$_{11}$H$_{11}$NO$_4$+Na]$^+$ 244.1, found 244.1.

The characterization matches that reported in the literature.[4]

4.1.3.3. *N*-(*endo*-himoyl)-glycinoyl chloride, **8a**[4]
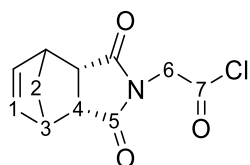
Thionyl chloride (5 mL) was added to *N*-(*endo*-himoyl)-glycine **7a** (1 g, 4.5 mmol). The reaction mixture was heated to reflux overnight at 75 °C and then thionyl chloride in excess was removed initially by rotary evaporator and then under Schlenk line affording the title product **8a** as a white powder (1.0 g, 4.1 mmol, 91 %). m.p.: 151 – 161 °C; ^{1}H NMR (CDCl$_3$, 400 MHz) δ (ppm): 6.15 (2H, br s, 1), 4.48 (2H, s, 6), 3.44 (2H, br s, 3), 3.38 (2H, br s, 4), 1.77 (1H, br d, *J* = 8.9 Hz, 2'), 1.58 (1H, br d, *J* = 8.9 Hz, 2''); ^{13}C NMR (CDCl$_3$, 100 MHz) δ (ppm): 176.1 (*C*-5), 168.0 (*C*-7), 134.7 (*C*-1), 52.3 (*C*-2), 47.9 (*C*-4), 46.2 (*C*-3), 45.1 (*C*-6); IR ν_{max} (cm^{-1}): 2991 (CH alkene), 1701 (COCl), 1653 (C=O amide), 1412, 1319, 1173, 978, 885, 719, 604.

4.1.3.4. *N*-(*exo*-himoyl)-glycinoyl chloride, **8b**[4]
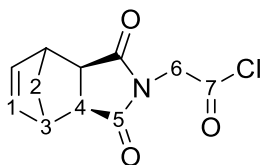
Thionyl chloride (5 mL) was added to *N*-(*exo*-himoyl)-glycine **7a** (1 g, 4.5 mmol). The reaction mixture was heated to reflux overnight at 75 °C and then thionyl chloride in excess was removed initially by rotary evaporator and then under Schlenk line affording the title product **8b** as a white

powder (1.2 g, 4.2 mmol, 94 %). m.p.: 152 – 162 °C; ^{1}H NMR (CDCl$_3$, 400 MHz) δ (ppm): 6.32 (2H, t, J = 1.9 Hz, 1), 4.62 (2H, s, 6), 3.34 (2H, t, J = 1.7 Hz, 3), 2.79 (2H, s, 4), 1.56 (2H, br s, 2' and 2''); ^{13}C NMR (CDCl$_3$, 100 MHz) δ (ppm): 177.3 (*C*-5), 171.7 (*C*-7), 138.0 (*C*-1), 48.1 (*C*-2), 45.5 (*C*-4), 42.9 (*C*-3), 39.1 (*C*-6); IR ν$_{max}$ (cm^{-1}): 2980 (CH alkene), 1805 (COCl), 1701 (C=O amide), 1404, 1308, 1165, 1097, 970, 928, 885, 817, 766, 716, 640, 604.

The characterization matches that reported in the literature.[4]

4.1.3.5. *N*-(*endo*-himoyl)-glycine poly(ethylene glycol) ester, **10a**[4]
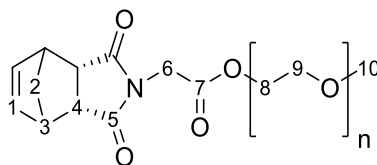
To a solution of *N*-(*endo*-himoyl)-glycinoyl chloride **8a** (0.9 g, 3.8 mmol) in anhydrous DCM (25 mL), were added poly(ethylene glycol) methyl ether (*M*$_n$ 550) **9** (1.9 mL, 3.8 mmol) and triethylamine (1 mL, 7.5 mmol). The reaction was left to stir overnight at room temperature under N$_2$. The organic phase was washed with 2 M HCl (2 x 30 mL) and brine (1 x 30 mL). The organic layer was dried over MgSO$_4$, filtered and concentrated in *vacuo* to afford the title product **10a** as a yellow oil (2.5 g, 3.3 mmol, 87 %). ^{1}H NMR (CDCl$_3$, 400 MHz) δ (ppm): 6.14 (2H, br s, 1), 4.26 (2H, t, J = 4.6 Hz, 8), 4.11 (2H, s, 6), 3.64 (48H, br s, PEG), 3.56 – 3.53 (2H, m, 9), 3.41 (2H, br s, 3), 3.38 (3H, s, 10), 3.35 (2H, br s, 4), 1.75 (1H, br d, J = 8.8 Hz, 2'), 1.56 (1H, br d, J = 8.8 Hz, 2''); ^{13}C NMR (CDCl$_3$, 100 MHz) δ (ppm): 176.8 (*C*-7), 166.6 (*C*-5), 134.6 (*C*-1), 71.9 (*C*-8), 70.5 (*C*-PEG), 68.8 (*C*-9), 64.7 (*C*-6), 59.1 (*C*-10), 52.3 (*C*-2), 46.2 (*C*-4), 44.9 (*C*-3), 39.1 (*C*-8); IR ν$_{max}$ (cm^{-1}): 2866 (CH alkene), 1749 (C=O ester), 1705 (C=O amide), 1414, 1199, 1174, 1096, 947, 843, 719, 615; LC-MS (ESI): calculated [C$_{12}$H$_{13}$NO$_4$ + (OC$_2$H$_4$)] 742.6, found 742.5.

4.1.3.6. *N*-(*exo*-himoyl)-glycine poly(ethylene glycol) ester **10b** (NB-PEG)[4]
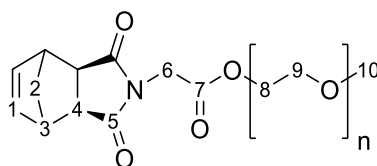
To a solution of *N*-(*exo*-himoyl)-glycinoyl chloride **8b** (1.0 g, 4.2 mmol) in anhydrous DCM (30 mL), were added poly(ethylene glycol) methyl ether (M_n 550) **9** (2.1 mL, 4.2 mmol) and triethylamine (1.2 mL, 8.3 mmol). The reaction was left to stir overnight at room temperature under N_2. The organic phase was washed with 2 M HCl (2 x 30 mL) and brine (1 x 30 mL). The organic layer was dried over MgSO$_4$, filtered, and concentrated in *vacuo* to afford a yellow oil monomer **10b** (2.7 g, 3.6 mmol, 86 %). ^{1}H NMR (CDCl$_3$, 400 MHz) δ (ppm): 6.30 (2H, t, *J* = 1.7 Hz, 1), 4.29 (2H, t, *J* = 4.9 Hz, 8), 4.26 (2H, s, 6), 3.65 (48H, s, PEG), 3.56 – 3.54 (2H, m, 9), 3.38 (3H, s, 10), 3.32 (2H, t, *J* = 1.6, 3), 2.76 (2H, d, *J* = 1.3 Hz, 4), 1.73 (1H, br d, *J* = 10.0 Hz, 2"), 1.53 (1H, dt, *J* = 1.5 and 10 Hz, 2'); ^{13}C NMR (CDCl$_3$, 100 MHz) δ (ppm): 177.2 (*C*-5), 167.0 (*C*-7), 138.0 (*C*-1), 71.9 (*C*-9), 70.6 (*C*-PEG), 68.8 (*C*-9), 64.9 (*C*-8), 59.1 (*C*-10), 48.0 (*C*-4), 45.5 (*C*-3), 42.9 (*C*-2), 39.4 (*C*-6); IR v$_{max}$ (cm^{-1}): 2887 (CH alkene), 1805 (C=O ester), 1780, 1703 (C=O amide), 1404, 1308, 1213, 1165, 1146, 1096, 970, 912, 885, 779, 766, 716, 766, 640, 509; LC-MS (ESI): calculated [$C_{12}H_{13}NO_4$ + (OC_2H_4)] 742.6, found 742.5.

The characterization matches that reported in the literature for a similar compound.[4]

4.1.4. Homopolymerisation

4.1.4.1. *Exo*-norbornenyl ibuprofen homopolymer **poly5b**[4]
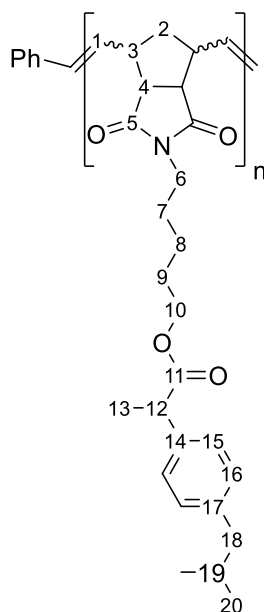
Under an inert atmosphere, the 3rd generation Grubbs catalyst (3.0 mg, 0.0034 mmol) was dissolved in anhydrous DCM (1.5 mL) and added to monomer **5b** (30.0 mg, 0.069 mmol). During the reaction the colour changed from a green solution to a pale brown solution. The reaction was stirred for 10 minutes after which it was terminated by addition of three drops of ethyl vinyl ether and stirred for further 20 minutes. The solvent was removed in *vacuo* until a minimum amount of solvent was left. The polymer was purified by precipitation from diethyl ether affording a brown solid **poly5b** (29.4 mg, 98 %). ^{1}H NMR (CDCl$_3$, 400 MHz) δ (ppm): 7.21 – 7.18 (2H, m, 15), 7.10 – 7.08 (2H, m, 16), 5.61 (2H, br d, *cis/trans*, 1), 4.06 – 3.98 (2H, m, 10), 3.71 – 3.65 (1H, m, 12), 3.44 – 3.39 (2H, m, 6), 3.28 – 3.27 (1H, m, 3), 3.10 – 2.93 (2H, br m, 2), 2.67 (1H, br s, 4), 2.45 – 2.43 (2H, m, 18), 1.87 – 1.81 (1H, m, 19), 1.62 – 1.46 (8H, m, 7, 9 and 13), 1.29 – 1.20 (2H, br m, 8), 0.91 – 0.88 (6H, m, 20); ^{13}C NMR (CDCl$_3$, 100 MHz) δ (ppm): 178.2 (*C*-5), 174.7 (*C*-11), 140.5 (*C*-14), 137.8 (*C*-17),132.1 (*C*-1), 129.3 (*C*-15), 127.2 (*C*-16), 64.4 (*C*-10), 50.8 (*C*-2), 45.1 (*C*-12), 45.0 (*C*-18), 38.4 (*C*-6), 30.2 (*C*-19), 28.1 (*C*-7), 27.3 (*C*-9), 23.2 (*C*-8), 22.4 (*C*-20), 18.6 (*C*-13); IR ν$_{max}$ (cm^{-1}): 2951, 1728, 1693, 1452, 1394, 1341, 1163, 1070, 968, 849, 777; GPC: M$_n$ = 11 116, M$_w$ = 14 111, Đ = 1.27.

4.1.4.2. *Exo*-norbornenyl poly(ethylene glycol) methyl ether homopolymer **poly10b**[4]
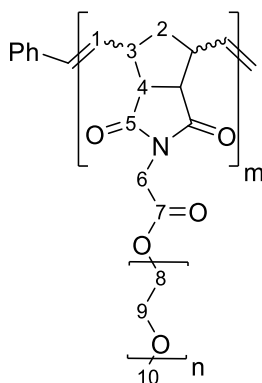
Under an inert atmosphere, the 3rd generation Grubbs catalyst (3.0 mg, 0.0034 mmol) was dissolved in anhydrous DCM (1.5 mL) and added to monomer **10b** (51.0 mg, 0.069 mmol). During the reaction the colour changed from a green solution to a pale brown solution. The reaction was stirred for 10 minutes after which was terminated with three drops of ethyl vinyl ether and stirred for further 20 minutes. The solvent was removed in *vacuo* until a minimum amount of solvent was left. The polymer was purified by precipitation from diethyl ether affording a brown sticky solid **poly10b** (45.8 mg, 92 %). ^{1}H NMR (CDCl$_3$, 400 MHz) δ (ppm): 5.66 (2H, br d, *cis/trans*, 1), 4.27 (4H, br m, 6 and 8), 3.66 (44H, br s, PEG), 3.56 – 3.54 (2H, m, 9), 3.38 (3H, s, 10), 3.27 – 2.80 (4H, br m, 3 and 4), 2.16 (1H, br s, 2), 1.58 (1H, br s, 2'); ^{13}C NMR (CDCl$_3$, 100 MHz) δ (ppm): 177.4 (*C*-5), 166.9 (*C*-7), 131.8 (*C*-1), 71.9 (*C*-8), 70.6 (*C*-PEG), 68.8 (*C*-9), 64.9 (*C*-6), 59.0 (*C*-10); IR ν$_{max}$ (cm^{-1}): 2870, 1746, 1705, 1414, 1206, 1094, 1034, 949, 851; GPC: M$_n$ = 10 984, M$_w$ = 14 907, Đ = 1.36.

4.1.5. Copolymerisation

4.1.5.1. Block copolymer **poly5b-b-poly10b**[4]

Under an inert atmosphere, the 3rd generation Grubbs catalyst (3.0 mg, 0.0034 mmol) was dissolved in anhydrous DCM (1.5 mL) and added to monomer **5b** (30.0 mg, 0.069 mmol). During the reaction the colour changed from a green solution to a pale brown solution. After 10 minutes, a solution of monomer **10b** (51.0 mg, 0.069 mmol) in anhydrous DCM (0.3 mL) was added to the former reaction mixture and left to stir for 10 minutes. The reaction was then terminated by three drops of ethyl vinyl ether and stirred for further 20 minutes. The solvent was removed in *vacuo* until a minimum amount of solvent was left. The polymer was purified by precipitation from diethyl ether affording a brown sticky solid **poly5b-b-poly10b [64:36]** (64.6 mg, 80 %); **poly5b-b-poly10b [50:50]** (1.8 g, 65 %). ^{1}H NMR (CDCl$_3$, 400 MHz) δ (ppm): 7.18 − 7.16 (2H, m, 20), 7.09 − 7.06 (2H, m, 21), 5.63 (2H, br d, *cis/trans*, 1), 4.28 − 4.15 (4H, br m, 6 and 8), 4.04 − 3.99 (2H, br m, 15), 3.64 (40H, s, PEG), 3.56 − 3.53 (2H, m, 9), 3.37 (3H, s, 10), 3.26 − 2.65 (6H, br m, 3, 4 and 11), 2.43 (2H, d, *J* = 7.0 Hz, 23), 2.26 − 2.10 (2H, br m, 2), 1.86 − 1.80 (1H, m, 24), 1.59 − 1.45 (8H, m, 12, 14 and 18), 1.24 (2H, br s, 13), 0.88 (6H, d, *J* = 6.5 Hz, 25); ^{13}C NMR (CDCl$_3$, 100 MHz) δ (ppm): 178.2 (*C*-5), 174.7 (*C*-16), 140.5 (*C*-19), 137.8 (*C*-22), 131.8 (*C*-1), 129.3 (*C*-20), 127.2 (*C*-21), 71.9 (*C*-9), 70.6 (*C*-PEG), 70.5 (*C*-8), 68.8 (*C*-15), 64.4 (*C*-10), 59.0 (*C*-6), 45.2 (*C*-23), 45.0 (*C*-2), 30.2 (*C*-24), 28.1 (*C*-12), 27.3 (*C*-14), 23.2 (*C*-

13), 22.4 (*C*-25), 18.6 (*C*-18); IR ν_{max} (cm^{-1}): 2947, 2866, 1697, 1396, 1348, 1325, 1167, 1096, 953, 849, 766. **Poly5b-b-poly10b [64:36]**: Quantitative ^{1}H NMR (d = 90 s): 64 % poly-**5b** (NB-Ibu), 36 % poly-**10b** (NB-PEG); GPC: M_n = 19 318, M_w = 24 905, Đ = 1.29. **poly5b-b-poly10b [50:50]**: Quantitative ^{1}H NMR (d = 90 s): 50 % poly-**5b** (NB-Ibu), 50 % poly-**10b** (NB-PEG); GPC: M_n = 19 627, M_w = 28 294, Đ = 1.44.

4.1.5.2. Statistical copolymer **poly5b-co-poly10b**[4]
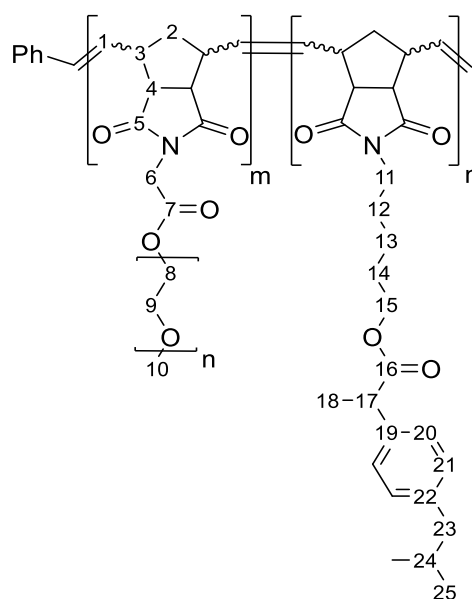
Under an inert atmosphere, the 3rd generation Grubbs catalyst (1.0 mg, 0.011 mmol) was dissolved in anhydrous DCM (0.5 mL) and added to a solution of monomer **5b** (10.0 mg, 0.023 mmol) and monomer **10b** (17.0 mg, 0.023 mmol) in anhydrous DCM (0.1 mL). During the reaction the colour changed from a green solution to a pale brown solution. The reaction mixture was left to stir for 1 hour after which the reaction was terminated with three drops of ethyl vinyl ether and stirred for further 30 minutes. The solvent was removed in *vacuo* until a minimum amount of solvent was left. The polymer was purified by precipitation from diethyl ether affording a brown sticky solid **poly5b-co-poly10b [63:37]** (20.4 mg, 76 %); **poly5b-co-poly10b [60:40]** (0.95 g, 76 %). ^{1}H NMR (CDCl$_3$, 400 MHz) δ (ppm): 7.18 − 7.16 (2H, m), 7.09 − 7.06 (2H, m), 5.63 (2H, br d, *cis/trans*), 4.28 − 4.15 (4H, br m), 4.04 − 3.99 (2H, br m), 3.64 (40H, s), 3.56 − 3.53 (2H, m), 3.37 (3H, s), 3.26 − 2.65 (6H, br m),

2.43 (2H, d, J = 7.0 Hz), 2.26 – 2.10 (2H, br m), 1.86 – 1.80 (1H, m), 1.59 – 1.45 (8H, m), 1.24 (2H, br s), 0.88 (6H, d, J = 6.5 Hz); IR ν_{max} (cm^{-1}): 2947, 2866, 1697, 1396, 1348, 1325, 1167, 1096, 953, 849, 766. **Poly5b-co-poly10b [63:37]**: quantitative ^{1}H NMR (d = 90 s): 63 % poly-**5b** (NB-Ibu), 37 % poly-**10b** (NB-PEG); GPC: M_n = 19 263, M_w = 26 191, Đ = 1.36. **Poly5b-co-poly10b [60:40]**: quantitative ^{1}H NMR (d = 90 s): 60 % poly-**5b** (NB-Ibu), 40 % poly-**10b** (NB-PEG); GPC: M_n = 23 914, M_w = 30 730, Đ = 1.56.

4.1.6. Synthesis of norbornene monomers bearing an imine bond

11   **13a**
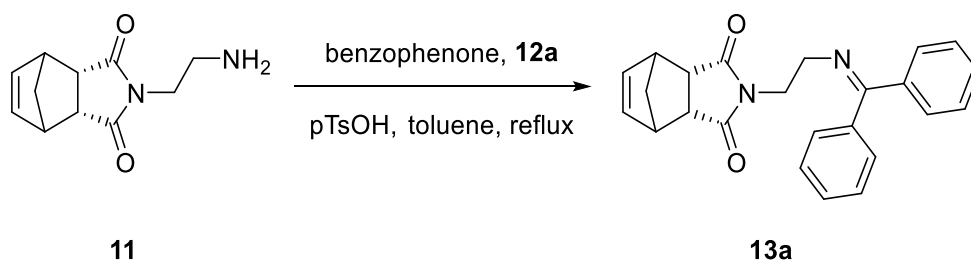
4.1.6.1. *Endo-N*-(2-aminoethyl)-5-norbornene-2,3-dicarboximide, **11**[5]
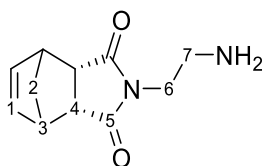
To a solution of *endo*-carbic anhydride **1a** (2.0 g, 12.0 mmol) in toluene (100 mL) was added ethylene diamine (6.4 mL, 96.0 mmol) dropwise. The reaction mixture was heated at reflux overnight using a Dean Stark apparatus. Toluene and ethylene diamine in excess were removed *in vacuo*. A further amount of toluene (100 mL) was added to the crude until everything was dissolved. The organic layer was extracted with water (3 x 50 mL) followed by extraction of the aqueous layer with DCM (3 x 50 mL). The combined organic layer was dried over MgSO$_4$, filtered and concentrated *in vacuo* affording the pure product **11** as a yellow oil which turned solid after few minutes (0.9 g, 4.4 mmol, 36 %). m.p.: 113 – 117 °C; ^{1}H NMR (CDCl$_3$, 400 MHz) δ (ppm): 6.12 (2H, s, 1), 3.48 -3.41 (4H, m, 3 and 7), 3.29 (2H, br s, 4), 2.78 (2H, t, J = 6.3 Hz, 6), 1.76 (1H, d, J = 8.8 Hz, 2'), 1.57 – 1.56 (3H, m, 2" and NH$_2$); ^{13}C NMR (CDCl$_3$, 100 MHz) δ (ppm): 178.0 (*C*-5), 134.6 (*C*-1), 52.3 (*C*-2), 45.9

(*C*-4), 44.9 (*C*-3), 41.5 (*C*-7), 40.1 (*C*-6); IR ν_{max} (cm^{-1}): 3381 (NH$_2$), 2997 (CH alkene), 2941, 2860, 1692 (C=O amide), 1622, 1490, 1491, 1335, 843, 777, 725, 415; LC-MS (ESI): calculated [M+H]$^+$ [C$_{11}$H$_{14}$N$_2$O$_2$+H]$^+$ 207.1, found 207.2.

The characterization matches that reported in the literature[5].

4.1.6.2. Ketoprofen methyl ester, **12c**[6]
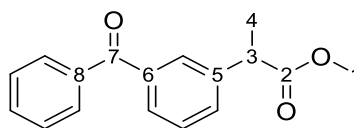
To a solution of ketoprofen (0.25 g, 1.0 mmol) in MeOH (4 mL), H$_2$SO$_4$ (30 μL, 0.56 mmol) was added and the reaction mixture was heated to reflux and stirred for 2 hours. The reaction mixture was cooled down and the solvent evaporated in vacuo. A colourless oil was formed, this was dissolved in DCM (25 mL) and washed with saturated NaHCO$_3$ solution (2 x 20 mL) and water (1 x 20 mL). MgSO$_4$ was added, filtered and the solvent evaporated in vacuo affording **12c** as a colourless oil (0.22 mg, 0.82 mmol, 82 %). ^{1}H NMR (CDCl$_3$, 400 MHz) δ (ppm): 7.82 – 7.42 (9H, m, Ar), 3.82 (1H, q, *J* = 7.2 Hz, 3), 3.69 (3H, s, 1), 1.55 (3H, d, *J* = 7.2, 4); ^{13}C NMR (CDCl$_3$, 100 MHz) δ (ppm): 196.6 (*C*-7), 174.6 (*C*-2), 141.0 (*C*-5), 138.1 and 137.6 (*C*-6 and *C*-8), 132.6 – 128.4 (*C*-Ar), 52.3 (*C*-1), 45.4 (*C*-3), 18.6 (*C*-4); IR ν_{max} (cm^{-1}): 1734 (COOH), 1656 (C=O), 1597, 1446, 1282, 1207, 1165, 704, 642; LC-MS (ESI): calculated [M+H]$^+$ [C$_{17}$H$_{16}$O$_3$+CH$_3$OH+H]$^+$ 301.1, found 301.1.

4.1.6.3. *Endo*-(2-diphenyl imine)-ethyl-5-norbornene-2,3-dicarboximide, **13a**[7]
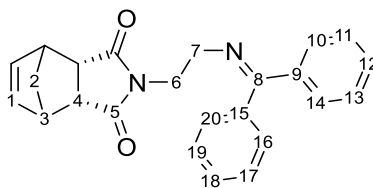
Endo-N-(2-aminoethyl-5-norbornene-2,3-dicarboximide **11** (0.9 g, 4.4 mmol) and benzophenone **12a** (0.5 g, 2.9 mmol) were dissolved in toluene (30 mL) fallowed by the addition of *p*-toluenesulfonic acid (7.6 mg, 0.01 mmol). The reaction mixture was heated to reflux using a Dean-Stark trap. After 24 hours of reflux, the reaction mixture was cooled down to room temperature and then washed with water (2 x 20 mL) and brine (1 x 20 mL). The organic layer was dried over $MgSO_4$, filtered and the solvent removed *in vacuo*. The crude product was purified by flash chromatography (EtOAc/PET 3:2) affording **13a** as a colourless oil which turned solid after one month (0.4 g, 1.1 mmol, 37 %). m.p.: 92 – 96 °C; ^1H NMR ($CDCl_3$, 400 MHz) δ (ppm): 7.57 (2H, d, *J* = 7.50 Hz, 19 and 20), 7.47 – 7.42 (3H, m, 12,13 and 14), 7.40 – 7.31 (3H, m, 16, 17 and 18), 7.14 (2H, d, *J* = 7.2 Hz, 10 and 11), 5.99 (2H, s, 1), 3.69 (2H, t, *J* = 6.4 Hz, 6), 3.44 (2H, t, *J* = 6.4 Hz, 7), 3.37 (2H, s, 3), 3.25 (2H, s, 4), 1.70 (1H, d, *J* = 8.9 Hz, 2'), 1.52 (1H, d, *J* = 8.8 Hz, 2"); ^{13}C NMR ($CDCl_3$, 100 MHz) δ (ppm): 177.7 (*C*-5), 130.1 (*C*-9 and 15), 134.4 (*C*-1), 128.7 (*C*-19 and *C*-20), 128.6 (*C*-12, *C*-13 and *C*-14), 128.3 (*C*-8), 128.1 (*C*-16, *C*-17 and *C*-18), 127.7 (*C*-10 and *C*-11), 52.1 (*C*-2), 51.1 (*C*-7), 45.8 (*C*-4), 44.9 (*C*-3), 39.4 (*C*-6); IR v_{max} (cm^{-1}): 2985 (CH alkene), 1688 (N=C), 1429, 1329, 1169, 989, 763, 696, 642; LC-MS (ESI): unavailable due to fragmentation.

4.2. Experimental section of Chapter 3

4.2.1. Materials and instrumentation

All solvents and starting materials were purchased from known chemical suppliers or available stores and used without any further purification unless specifically stipulated. The NMR spectra were obtained using a Bruker AV2 400 MHz or AVNEO 400 MHz spectrometer. The spectra were calibrated to the centre of the residual undeuterated set solvent peak and chemical shifts then reported in parts per million (ppm). Spectra were analysed using MestReNovaNMR. FTIR spectra were recorded on a Shimadzu IR-Affinity instrument. Tensiometry measurements were undertaken using the Biolin Scientific Theta Attension optical tensiometer. The data was processed using Biolin OneAttension software. A Hamilton (309) syringe was used for the measurements. The melting

point for each compound was measured using Stuart SMP10 melting point apparatus. GPC was performed on an Aglient Technologies PL-GPC 50 Integrated GPC System fitted with a differential refractive index (RI) detector. Separation was performed using a pair of Agilent PLgel 5 μm Mixed-D columns (7.8 × 300 mm) fitted with a matching guard column (7.8 × 50 mm) at 50 °C. The eluent was DMF containing 0.1 % w/w lithium bromide at a flow rate of 1.0 mL/min. Toluene was added to sample preparation solvent at 0.1 % w/w to act as the flow rate marker. The system was calibrated using 10 narrow dispersity poly(methyl methacrylate) standards (Mp = 2210000 − 1810 g/mol). Data was analysed using Agilent GPC/SEC software version A.02.01. DLS and Zeta Potential studies were carried out using Anton Paar LitesizerTM 500 and processed using KalliopeTM Professional. Cellular growth curve measurements obtained using Thermo Scientific Multiscan Go 1510-0318C plate reader and recorded using the SkanIt Software 4.0 and a Clariostar plater reader using MARS data analysis software. High-resolution mass spectrometry was performed using a Bruker microTOF-Q mass spectrometer and spectra recorded and processed using Bruker's Compass Data Analysis software.

4.2.2. Synthesis of Norbornene intermediates
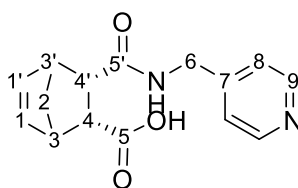

Y = CH$_2$ 1a (*endo*)
          1b (*exo*)
Y = O   7

Y = CH$_2$ 3a (*endo*)
          3b (*exo*)
Y = O   8

Y = CH$_2$ 4a (*endo*)
          4b (*exo*)
Y = O   9

4.2.2.1 Compound **3a**

Endo-carbic anhydride (0.16 g, 0.98 mmol) and 4-(aminomethyl)pyridine (0.1 mL, 0.98 mmol) were dissolved in DCM (20 mL) and reacted together at room temperature for 1 hour. Precipitation occurred after 2 minutes. After 1 hour the flask was placed in an ice bath and the white precipitate filtered and washed with cold DCM (0.24 g, 0.87 mmol, 90 %). m.p.: 198 – 202 °C; ^{1}H NMR (dmso-d_6, 400 MHz) δ (ppm): 11.63 (1H, s, OH), 8.46 (2H, d, J = 5.9 Hz, 9), 8.34 (1H, t, J = 5.9 Hz, NH), 7.24 (2H, d, J = 5.9 Hz, 8), 6.19 (1H, dd, J = 5.4 and 2.9 Hz, 1), 5.94 (1H, dd, J = 5.4 and 2.9 Hz, 1'), 4.22 (2H, qd, J = 16.3 and 5.9 Hz, 6), 3.20 (2H, ddd, J = 51.1, 10.3 and 3.3 Hz, 4 and 4'), 2.99 (2H, br d, J = 24.2 Hz, 3 and 3'), 1.28 (2H, br dd, J = 33.3, 17.5 Hz, 2); ^{13}C NMR (dmso-d_6, 100 MHz) δ (ppm): 173.5 (*C*-5), 171.5 (*C*-5'), 149.3 (*C*-9), 148.9 (*C*-7), 135.1 (*C*-1), 133.5 (*C*-1'), 122.1 (*C*-8), 48.4 (*C*-4), 48.2 (*C*-4'), 46.8 (*C*-2), 45.2 (*C*-3 and *C*-3'), 41.1 (*C*-6); IR v_{max} (cm^{-1}): 3283 (CH alkene), 2967 (CH), 1697 (COOH), 1652 (C=O amide), 1546, 1336, 1261, 1203, 1066, 1018, 910, 794, 680, 526; LC-MS (ESI): calculated [M+H]$^+$ [$C_{15}H_{16}N_2O_3$+H]$^+$ 273.1 , found 273.1.

4.2.2.2. Compound **4a**[8]
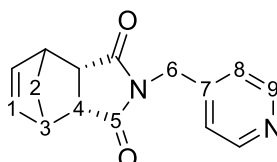
Freshly prepared 5 M methanolic HCl (20 mL) was added to compound **3a** (0.3 g, 1.1 mmol). The reaction mixture was heated at 50 °C for 1 hour until the compound was completely dissolved. The solvent was then removed *in vacuo* affording a white powder which was dissolved in DCM (20 mL) and washed with saturated NaHCO$_3$ solution (3 x 20 mL) and brine (2 x 20 mL). The organic layer was dried over MgSO$_4$, filtered and evaporated *in vacuo* affording a white powder (0.23 g, 0.89 mmol, 81 %). m.p.: 119 - 124 °C; ^{1}H NMR (CDCl$_3$, 400 MHz) δ (ppm): 8.56 (2H, d, J = 4.2 Hz, 9), 7.21 (2H, d, J = 5.8 Hz, 8), 5.07 (2H, t, J = 3.6 and 1.9 Hz 1), 4.5 (2H, s, 6), 3.47 – 3.38 (4H, m, 3), 3.33 (2H, dd, J = 2.8 and 1.5 Hz, 4) 1.75 (1H, dt, J = 8.8 and 1.5 Hz, 2), 1.56 (1H, d, J = 8.8 Hz, 2'); ^{13}C NMR (CDCl$_3$, 400 MHz) δ (ppm): 177.2 (*C*-5), 150.0 (*C*-7), 144.5 (*C*-9), 134.5 (*C*-1), 123.5 (*C*-8), 52.3 (*C*-2),

45.9 (*C*-3), 45.1 (*C*-4), 41.0 (*C*-6); IR v_{max} (cm^{-1}): 3248 (CH alkene), 2985 (CH), 1697 (C=O amide), 1695, 1602, 1395, 1330, 1313, 1170, 1124, 908, 840, 744, 723, 630, 617, 582; LC-MS (ESI): calculated [M+H]$^+$ [C$_{15}$H$_{14}$N$_2$O$_2$+H]$^+$ 255.1 , found 255.1.

4.2.2.3. Compound **3b**
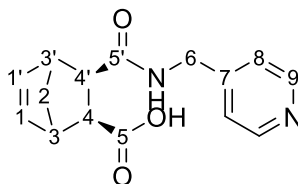
Exo-carbic anhydride (0.16 g, 0.98 mmol) and 4-(aminomethyl)pyridine (0.1 mL, 0.98 mmol) were dissolved in DCM (20 mL) and reacted together at room temperature for 1 hour. Precipitation occurred after 2 minutes. After 1 hour the flask was placed in an ice bath and the white precipitate filtered and washed with cold DCM (0.18 g, 0.70 mmol, 71 %). m.p.: 187 - 189 °C; ^{1}H NMR (dmso-d$_6$, 400 MHz) δ (ppm): 11.92 (1H, br s, OH), 8.52 (1H, t, *J* = 5.9 Hz, NH), 8.47 (2H, dd, *J* = 6.2 and 2.8 Hz, 9), 7.27 (2H, d, *J* = 6.0 Hz, 8), 6.24 – 6.21 (2H, m, 1 and 1'), 4.27 (2H, ddd, *J* = 53.8, 16.3, 5.9 Hz, 6), 2.95 (1H, s, 3), 2.79 (1H, s, 3'), 2.55 (1H, d, *J* = 10.5 Hz, 4), 2.34 (1H, dd, *J* = 9.6 and 1.7 Hz, 4'), 2.25 (1H, d, *J* = 8.2 Hz, 2), 1.25 (1H, dt, *J* = 8.3 and 1.8 Hz, 2'); ^{13}C NMR (dmso-d$_6$, 100 MHz) δ (ppm): 174.4 (*C*-5), 172.8 (*C*-5'), 149.4 (*C*-9), 148.6 (*C*-7), 138.2 (*C*-1), 138.0 (*C*-1'), 122.1 (*C*-8), 46.9 (*C*-4), 46.7 (*C*-4'), 46.6 (*C*-3'), 45.0 (*C*-2), 43.6 (*C*-3), 41.1 (*C*-6); IR v_{max} (cm^{-1}): 3302 (CH alkene), 1705 (COOH), 1647 (C=O amide), 1543, 1327, 1257, 1205, 1024, 794, 729, 615, 528; LC-MS (ESI): calculated [M+H]$^+$ [C$_{15}$H$_{16}$N$_2$O$_3$+H]$^+$ 273.1 , found 273.1.

4.2.2.4. Compound **4b**[8]
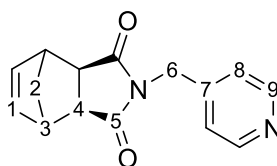
Freshly prepared 5 M methanolic HCl (40 mL) was added to compound **3b** (1.5 g, 5.5 mmol). The reaction mixture was heated at 50 °C for 1 hour until the compound was completely dissolved. The solvent was then removed *in vacuo* affording a colourless oil which was dissolved in DCM (40 mL) and washed with saturated $NaHCO_3$ solution (3 x 40 mL) and brine (2 x 20 mL). The organic layer was dried over $MgSO_4$, filtered and evaporated *in vacuo* affording a white powder (2.4 g, 9.2 mmol, 83 %). m.p.: 152 - 154 °C; ^{1}H NMR (dmso-d_6, 400 MHz) δ (ppm): 8.53 – 8.50 (2H, m, 9), 7.33 -7.19 (2H, m, 8), 6.32 (2H, t, *J* = 1.9 Hz, 1), 4.57 (2H, s, 6), 3.12 (2H, t, *J* = 1.8 Hz, 3), 2.79 (2H, d, *J* = 1.4 Hz, 4), 1.36 (1H, dt, *J* = 9.8 and 1.6 Hz, 2), 1.10 (1H, d, *J* = 9.7 Hz, 2); ^{13}C NMR (dmso-d_6, 100 MHz) δ (ppm): 177.4 (*C*-5), 150.0 (*C*-9), 144.8 (*C*-7), 137.7 (*C*-1), 122.5 (*C*-8), 47.4 (*C*-4), 44.6 (*C*-3), 42.5 (*C*-2), 40.6 (*C*-6); IR v_{max} (cm^{-1}): 1683 (C=O amide), 1598, 1431, 1390, 1328, 1172, 1074, 941, 894, 821, 779, 731, 621, 588; LC-MS (ESI): calculated [M+H]$^+$ [$C_{15}H_{14}N_2O_2$+H]$^+$ 255.1 , found 255.1.

4.2.2.5. Compound **7**[9]
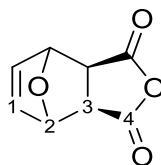
Maleic anhydride (5.0 g, 50.0 mmol) was dissolved in THF (20 mL) and furan (3.3 mL, 45.0 mmol) was added dropwise into the solution. The reaction mixture was left to stir for an hour until precipitation occurred. The white crystals were collected by suction filtration and washed with cold THF (3.5 g, 21.2 mmol, 47 %). m.p.: 106-109 °C; ^{1}H NMR (CDCl$_3$, 400 MHz) δ (ppm): 6.59 (2H, t, *J* = 0.9 Hz, 1), 5.47 (2H, t, *J* = 0.9 Hz, 2), 3.19 (2H, s, 3); ^{13}C NMR (CDCl$_3$, 100 MHz) δ (ppm): 169.9 (*C*-4), 137.0 (*C*-1), 82.2 (*C*-2), 48.7 (*C*-3); IR v_{max} (cm^{-1}): 1857 (C=O anhydride), 1778, 1211, 1145, 1083, 1018, 947, 921, 877, 732, 634.

### 4.2.2.6. Compound **8**
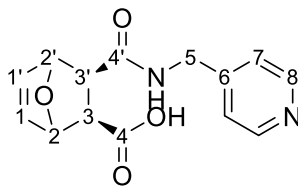
Exo-7-oxanorborn-5-ene-2,3-dicarboxylic anhydride **7** (0.2 g, 1.2 mmol) and 4-(aminomethyl)pyridine (0.14 mL, 1.4 mmol) were dissolved in DCM (20 mL) and reacted together at room temperature for 1 hour. Precipitation occurred after 2 minutes. After 1 hour the flask was placed in an ice bath and the white precipitate filtered and washed with cold DCM (0.29 g, 1.03 mmol, 85 %). m.p.: 137 – 140 °C; ^{1}H NMR (dmso-d_6, 400 MHz) δ (ppm): 8.47 (2H, d, J = 6.1 Hz, 8), 8.26 (1H, t, J = 5.9 Hz, NH), 7.28 (2H, d, J = 6.1 Hz, 7), 6.46 (2H, ddd, J = 4.2, 1.7 and 1.5 Hz, 1 and 1'), 5.11 (1H, s, 2), 4.96 (1H, s, 2'), 4.27 (2H, ddd, J = 27.7, 16.3 and 5.8 Hz, 5), 2.65 (2H, q, J = 20.8 and 9.2 Hz, 3 amd 3'); ^{13}C NMR (dmso-d_6, 100 MHz) δ (ppm): 172.8 (*C*-4), 171.1 (*C*-4'), 149.4 (*C*-8), 148.6 (*C*-6), 136.9 (*C*-1), 136.5 (*C*-1'), 122.2 (*C*-7), 80.6 (*C*-2), 79.0 (*C*-2'), 46.7 (*C*-3), 46.4 (*C*-3'), 41.3 (*C*-5); IR v_{max} (cm^{-1}): 3327 (CH alkene), 1701 (COOH), 1655 (C=O amide), 1521, 1213, 1186, 1043, 1010, 904, 822, 713, 615, 515; LC-MS (ESI): calculated [M+H]$^+$ [C$_{14}$H$_{14}$N$_2$O$_4$+H]$^+$ 275.1 , found 275.1.

4.2.2.7. Compound **9**[8]
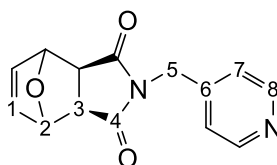
Freshly prepared 5 M methanolic HCl (70 mL) was added to compound **8** (2.6 g, 9.5 mmol). The reaction mixture was heated at 50 °C for 1 hour until the compound was completely dissolved. The solvent was then removed *in vacuo* using a rotary evaporator. Saturated NaHCO$_3$ solution (100 mL) was added into the flask and the product extracted with DCM (5 x 50 mL). The organic layer was then washed with brine (2 x 20 mL), dried over MgSO$_4$, filtered and the solvent removed *in vacuo* affording a white powder (1.9 g, 7.3 mmol, 77 %). m.p.: 158 -160 °C; ^{1}H NMR (CDCl$_3$, 400 MHz) δ

(ppm): 8.55 (2H, d, J = 5.8 Hz, 8), 7.18 (2H, d, J = 6.0 Hz, 7), 6.55 (2H, t, J = 0.9 Hz, 1), 5.32 (2H, t, J = 0.9 Hz, 2), 4.65 (2H, s, 5), 2.93 (2H, s, 3); ^{13}C NMR (CDCl$_3$, 100 MHz) δ (ppm): 175.8 (C-4), 150.3 (C-8), 144.1 (C-6), 136.7 (C-1), 122.5 (C-7), 81.2 (C-2), 47.7 (C-3), 41.4 (C-5); IR v_{max} (cm^{-1}): 3039 (CH alkene) 1694 (C=O amide), 1603, 1420, 1396, 1342, 1188, 1013, 918, 876, 791, 700, 650, 602; LC-MS (ESI): calculated [M+H]$^+$ [C$_{14}$H$_{12}$N$_2$O$_3$+H]$^+$ 257.1 , found 257.1.

4.2.3. Synthesis of SSA intermediates

10: X = O
11: X = S

12

SSA-1: X = O
SSA-2: X = S

4.2.3.1. Compound SSA-1[10]

1-Isocyanato-4-(trifluoromethyl)benzene (1.2 mL, 5.8 mmol) was added to a stirring solution of aminomethanesulfonic acid (0.65 g, 5.8 mmol) in anhydrous pyridine (30 mL) under an inert atmosphere. The mixture was heated to 60 °C overnight. The suspension formed was filtered and washed with EtOAc (20 mL) affording a white powder (1.6 g, 4.3 mmol, 74 %). m.p.: 170 – 174 °C; ^{1}H NMR (dmso-d$_6$, 400 MHz) δ (ppm): 9.24 (1H, s, NH-6), 8.96 – 8.90 (2H, m, 8), 8.60 (1H, tt, J = 7.8 and 1.6 Hz, 10), 8.11 – 8.03 (2H, m, 9), 7.54 (2H, d, J = 8.6 Hz, 4), 7.47 (2H, d, J = 8.6 Hz, 3), 7.08 (1H, t, J = 6.1 Hz, NH-7), 3.99 (2H, d, J = 5.6 Hz, 7); ^{13}C NMR (dmso-d$_6$, 100 MHz) δ (ppm): 154.2 (C-6), 146.1 (C-10), 144.2 (C-5), 142.4 (C-9), 127.2 (C-8), 126.2 (q, J = 3.7 Hz, C-3), 124.5 (q, J = 270.5 Hz, CF$_3$), 121.3 (q, J = 32.1 Hz, C-2), 117.2 (C-4), 56.0 (C-7); IR v_{max} (cm^{-1}): 3334 (NH), 3070 (NH salt), 1697 (C=O urea), 1604, 1531 (C-F), 1325 (S=O sulfonate), 1178, 1097, 1033, 842, 756, 680, 594, 516; HRLC-MS (ESI): sulfonate-urea ion, calculated [M]$^-$ [C$_9$H$_8$F$_3$N$_2$O$_4$S]$^-$ 297.0162, found 297.1475.

4.2.3.2. Compound SSA-2[10]

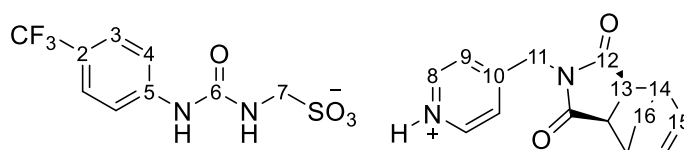1-Isothiocyanato-4-trifluoromethylbenzene (0.5 g, 2.4 mmol) was added to a suspension of aminomethanesulfonic acid (0.24 g, 2.2 mmol) in anhydrous pyridine (6 mL) under an inert atmosphere. The reaction mixture was heated at 60 °C overnight and taken to dryness giving a yellow sticky oil. EtOAc (20 mL) was added into the flask forming a white solid which was filtered and washed with EtOAc (0.72 g, 1.9 mmol, 85 %). m.p.: 133 - 135 °C; ^{1}H NMR (dmso-d$_6$, 333 K, 400 MHz) δ (ppm): 10.20 (1H, br s, NH-5), 8.90 (2H, d, J = 5.5 Hz, 8), 8.56 (1H, t, J = 7.8 Hz, 10), 8.14 (1H, br s, NH-7) 8.03 (2H, t, J = 6.7 Hz, 9), 7.83 (2H, br s, 4), 7.61 (2H, d, J = 8.3 Hz, 3), 4.34 (2H, br s, 7); ^{13}C NMR (dmso-d$_6$, 100 MHz) δ (ppm): 180.3 (*C*-6), 146.4 (*C*-10), 143.6 (*C*-5), 142.3 (*C*-8), 127.3 (*C*-9), 125.5 (q, J = 3.6 Hz, CF$_3$), 124.5 (q, J = 271.4 Hz, *C*-3), 123.4 (q, J = 31.8 Hz, *C*-2), 121.7 (*C*-4), 60.0 (*C*-7); IR ν$_{max}$ (cm^{-1}): 3310 (NH), 3072 (NH salt), 1614, 1548 (C-F), 1325 (S=O sulfonate), 1219 (C=S thiourea), 1165, 1107, 1039, 848, 761, 686, 594; HRLC-MS (ESI): sulfonate-urea ion, calculated [M]$^-$ [C$_9$H$_8$F$_3$N$_2$O$_3$S$_2$]$^-$ 312.9928, found 312.0445.

4.2.4. Synthesis of norbornene/oxanorbornene (NB/ONB) monomers containing SSAs

4b: Y = CH$_2$
9: Y = O

SSA-1: X = O
SSA-2: X = S

mon1: Y = CH$_2$, X = O
mon2: Y = CH$_2$, X = S
mon3: Y = O, X = O
mon4: Y = O, X = S
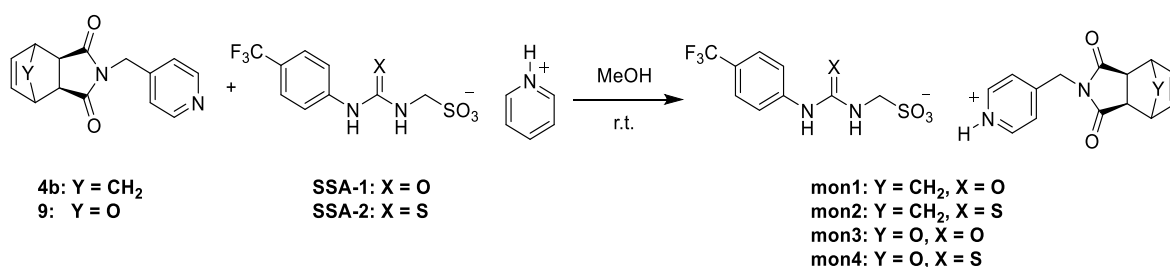
4.2.4.1. Monomer 1, mon1

Compound **4b** (0.10 g, 0.4 mmol) was added to a solution of compound **10** (0.10 g, 0.27 mmol) in MeOH (40 mL) and the reaction mixture left to stir at room temperature for 40 minutes. MeOH was then evaporated *in vacuo* affording a colourless film. DCM (15 mL) was added into the flask and left until the product started forming a white suspension in solution. This was then filtered and washed with DCM in order to remove any excess of **compound 4** and the white powder dried under Schlenk line (0.09 g, 0.17 mmol, 63 %). m.p.: 189 - 190 °C; ^{1}H NMR (dmso-d$_6$, 400 MHz) δ (ppm): 9.22 (1H, br s, NH-5), 8.86 (2H, d, J = 6.0 Hz, 8), 7.90 (2H, d, J = 5.9 Hz, 9), 7.52 (4H, dd, J = 12.9 and 8.1 Hz, 3 and 4), 6.93 (1H, br s, NH-7), 6.34 – 6.33 (2H, m, 15), 4.85 (2H, s, 11), 3.95 (2H, s, 7), 3.14 (2h, s, 14), 2.83 (2H, s, 13), 1.39 (1H. d. J = 9.8 Hz, 16), 1.20 (1H, d J = 9.8 Hz, 16'); ^{13}C NMR (dmso-d$_6$, 100 MHz) δ (ppm): 177.4 (*C*-12), 155.1 (*C*-6), 154.2 (*C*-10), 144.2 (*C*-5), 142.8 (*C*-8), 137.8 (*C*-15), 125.9 (q, J = 3.7 Hz, *C*-3), 125.1 (*C*-9), 124.7 (q, J = 270.7 Hz, CF$_3$), 120.9 (q, J = 32.0 Hz, *C*-2), 117.2 (*C*-4), 55.9 (*C*-7), 47.7 (*C*-13), 44.6 (*C*-14), 42.7 (*C*-16), 40.9 (*C*-11); IR ν$_{max}$ (cm^{-1}): 1699 (C=O amide), 1604 (C=O urea),1546 (C-F), 1390 (S=O sulfonate), 1321, 1215, 1165, 1110, 1026, 846, 719, 599; HRMS (ESI): sulfonate-urea ion, calculated [M]$^-$ [C$_9$H$_8$ F$_3$N$_2$O$_4$S]$^-$ 297.0162, found 297.1475; norbornene-pyridinium ion, calculated [M+H]$^+$ [C$_{15}$H$_{14}$N$_2$O$_2$+H]$^+$ 255.1128, found 255.1140.

4.2.4.2. Monomer 2, **mon2**
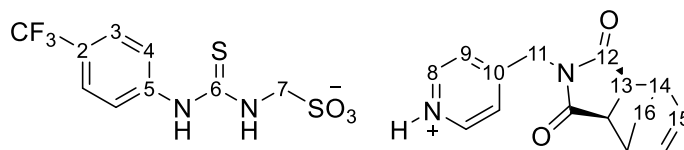
Compound **4b** (0.40 g, 1.58 mmol) was added to a solution of compound **11** (0.50 g, 1.31 mmol) in MeOH (100 mL) and the reaction mixture left to stir at room temperature for 2 hours. MeOH was then evaporated *in vacuo* affording a colourless film. DCM (25 mL) was added into the flask and left until the product started forming a white suspension in solution. The white powder was then filtered and washed with DCM in order to remove any excess of compound **4b** (0.64 g, 1.13 mmol, 86 %). m.p.: 176 - 178 °C; ^{1}H NMR (dmso-d$_6$, 333 K, 400 MHz) δ (ppm): 10.21 (1H, br s, NH-5), 8.83

(2H, d, J = 6.2 Hz, 8), 8.12 (1H, br s, NH-7), 7.87 – 7.85 (4H, m, 9 and 4), 7.61 (2H, d, J = 8.4 Hz, 3), 6.33 (2H, s, 15), 4.84 (2H, s, 11), 4.33 (2H, s, 7), 3.15 (2H, s, 14), 2.83 (2H, s, 13), 1.41 (1H, d, J = 9.8 Hz, 16), 1.20 (1H, d, J = 9.7 Hz, 16'); ^{13}C NMR (dmso-d_6, 100 MHz) δ (ppm): 180.3 (C-6), 177.5 (C-12), 155.6 (C-10), 143.7 (C-5), 142.6 (C-8), 137.9 (C-15), 125.6 (q, J = 4.0 Hz, C-3), 125.2 (C-9), 124.5 (q, J = 271.4 Hz, CF$_3$), 123.4 (q, J = 31.6 Hz, C-2), 121.7 (C-4), 60.1 (C-7), 47.8 (C-13), 44.7 (C-14), 42.8 (C-16), 41.0 (C-11); IR v_{max} (cm^{-1}): 3269 (NH), 3074 (NH salt, CH alkene), 1700 (C=O amide), 1552 (C-F), 1396 (S=O sulfonate), 1319, 1259 (C=S thiourea), 1153, 1124, 1068, 1026, 891, 844, 777, 731, 611; HRMS (ESI): sulfonate-urea ion, calculated [M]$^-$ [C$_9$H$_8$F$_3$N$_2$O$_3$S$_2$]$^-$ 312.9928, found 312.0445; norbornene-pyridinium ion, calculated [M+H]$^+$ [C$_{15}$H$_{14}$N$_2$O$_2$+H]$^+$ 255.1128, found 255.1140.
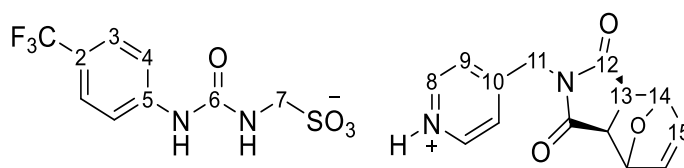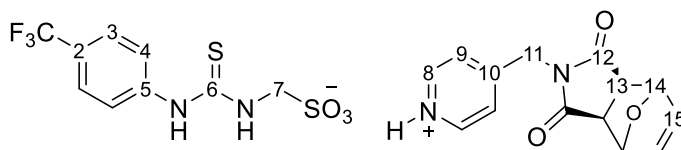
4.2.4.3. Monomer 3, **mon3**

Compound **9** (0.12 g, 0.48 mmol) was added to a solution of compound **10** (0.15 g, 0.40 mmol) in MeOH (100 mL) and the reaction mixture left to stir at room temperature for 2 hours. MeOH was then evaporated *in vacuo* affording a colourless oil. DCM (25 mL) was added into the flask and left until the product started forming a white suspension in solution. The white suspension was then filtered and washed with DCM in order to remove any excess of compound **9**. The filtered solid was then dissolved in deionised H$_2$O in a sonicator bath heated to 40 °C for 30 minutes. This was necessary in order to remove any trace of MeOH. H$_2$O was then removed in *vacuo* affording a pale pink powder, (0.18 g, 0.33 mmol, 83 %). m.p.: 158 - 161 °C; ^{1}H NMR (dmso-d_6, 400 MHz) δ (ppm): 9.23 (1H, br s, NH-5), 8.87 (2H, d, J = 6.5 Hz, 8), 7.81 (2H, d, J = 6.5 Hz, 9), 7.51 (4H, dd, J = 17.2 and 8.6 Hz, 3 and 4), 7.02 (1H, br s, NH-7), 6.60 (2H, s, 15), 5.22 (2H, s, 14), 4.89 (2H, s, 11), 3.97 (2H, d, J = 4.7 Hz, 7), 3.09 (2H, s, 13); ^{13}C NMR (dmso-d_6, 100 MHz) δ (ppm): 176.3 (C-12), 155.4 (C-10), 154.2 (C-6), 144.2 (C-5), 142.6 (C-8), 136.5 (C-15), 125.7 (q, J = 3.8 Hz, C-3), 124.7 (q, J = 270.9 Hz, CF$_3$), 124.3 (C-9), 120.9 (q, J = 31.9 Hz, C-2), 117.1 (C-4), 80.6 (C-14), 55.9 (C-7), 47.6 (C-13), 40.6 (C-
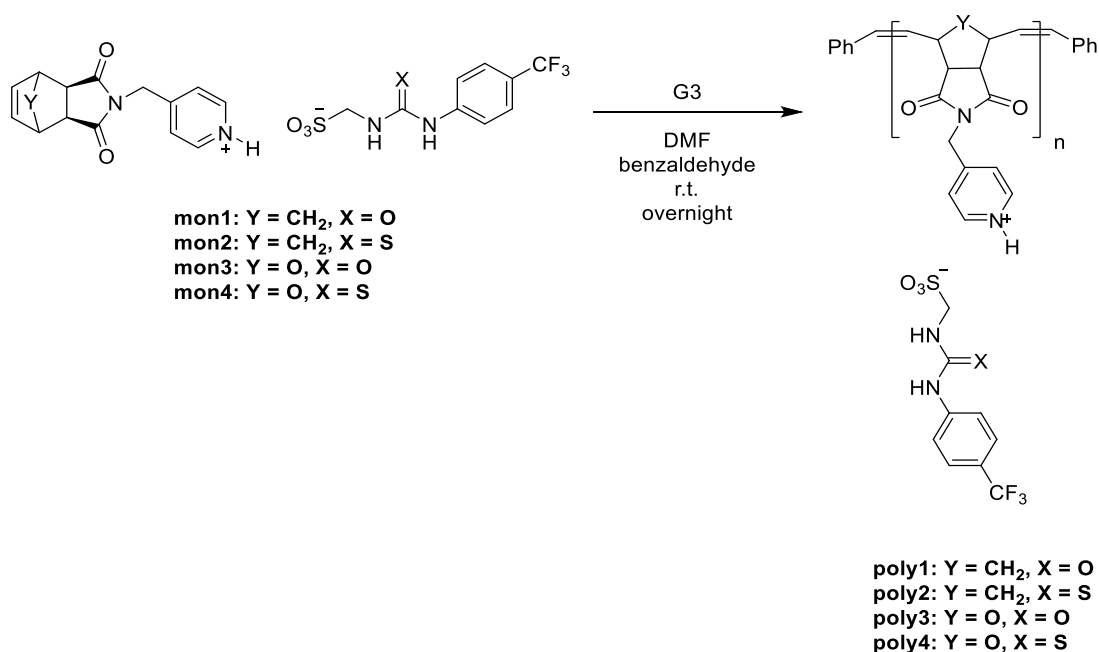
11); IR v_{max} (cm^{-1}): 3282 (NH), 2985 (CH alkene), 1697 (C=O amide), 1602 (C=O urea), 1541 (C-F), 1394 (S=O sulfonate), 1330, 1228, 1172, 1066, 997, 906, 840, 723, 619; HRMS (ESI): sulfonate-urea ion, calculated [M]$^-$ [C$_9$H$_8$ F$_3$N$_2$O$_4$S]$^-$ 297.0162, found 297.1475; norbornene-pyridinium ion, calculated [M+H]$^+$ [C$_{14}$H$_{12}$N$_2$O$_3$+H]$^+$ 257.0921, found 257.0931.

4.2.4.4. Monomer 4, **mon4**

Compound **9** (0.50 g, 1.20 mmol) was added to a solution of compound **11** (0.62 g, 1.63 mmol) in MeOH (100 mL) and the reaction mixture left to stir at room temperature for 2 hours. MeOH was then evaporated *in vacuo* affording a colourless film. DCM (25 mL) was added into the flask and left until the product started forming a white suspension in solution. This was then filtered and washed with DCM in order to remove any excess of compound **9** and the white powder dried under Schlenk line (0.80 g, 1.40 mmol, 86 %). m.p.: 169 - 173 °C; ^{1}H NMR (dmso-d$_6$, 333 K, 400 MHz) δ (ppm): 8.82 – 8.75 (2H, m, 8), 7.83 (2H, br s, 4), 7.71 (2H, d, *J* = 6.7 Hz, 9), 7.62 (2H, d, *J* = 8.6 Hz, 3), 6.60 (2H, t, *J* = 0.9 Hz, 15), 5.21 (2H, t, *J* = 1.0 Hz, 14), 4.84 (2H, s, 13), 4.28 (2H, br s, 7), 3.08 (2H, s, 11); ^{13}C NMR (dmso-d$_6$, 100 MHz) δ (ppm): 180.2 (*C*-6), 176.4 (*C*-12), 155.3 (*C*-10), 143.6 (*C*-5), 142.9 (*C*-8), 136.6 (*C*-15), 125.6 (q, *J* = 3.2 Hz, *C*-3), 124.5 (q, *J* = 271.3 Hz, CF$_3$), 124.3 (*C*-9), 123.4 (q, *J* = 32.4 Hz, *C*-2), 121.6 (*C*-4), 80.7 (*C*-13), 60.1 (*C*-7), 47.6 (*C*-11), 40.7 (*C*-14); IR v_{max} (cm^{-1}): 3250 (NH), 3066 (NH salt/CH alkene), 1701 (C=O amide), 1637, 1546 (C-F), 1396 (S=O sulfonate), 1317, 1238 (C=S thiourea), 1151, 1107, 1004, 914, 842, 705, 613, 590; HRMS (ESI): sulfonate-urea ion, calculated [M]$^-$ [C$_9$H$_8$N$_2$O$_3$S$_2$]$^-$ 312.9928, found 312.0445; norbornene-pyridinium ion, calculated [M+H]$^+$ [C$_{14}$H$_{12}$N$_2$O$_3$+H]$^+$ 257.0921, found 257.0931.

4.2.5. Synthesis of polyNB-SSA/polyONB-SSA homopolymers

mon1: Y = CH$_2$, X = O
mon2: Y = CH$_2$, X = S
mon3: Y = O, X = O
mon4: Y = O, X = S

G3
DMF
benzaldehyde
r.t.
overnight

poly1: Y = CH$_2$, X = O
poly2: Y = CH$_2$, X = S
poly3: Y = O, X = O
poly4: Y = O, X = S

4.2.5.1. General synthetic procedure for the preparation of homopolymers, **poly1 – poly4**[11]

poly1   X = O, Y = CH$_2$
poly2   X = S, Y = CH$_2$
poly3   X = O, Y = O
poly4   X = S, Y = O
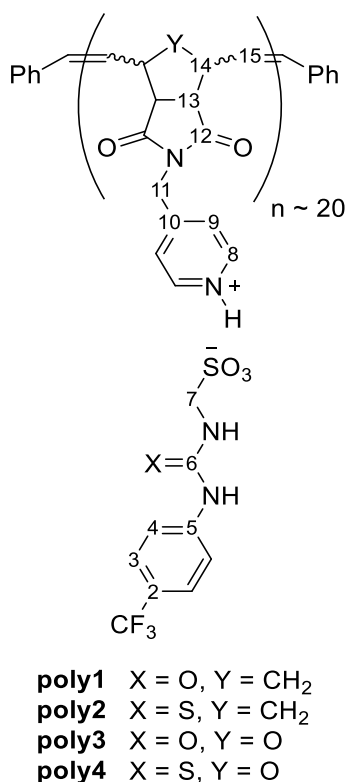
A solution of Grubbs third generation in dry DMF was added to a solution of monomer (**mon1 – mon4**) in dry DMF under inert atmosphere using a catalyst/monomer ratio of 1:20 and 2 mg/mL of catalyst in DMF. The reaction was left to stir overnight, followed by the addition of 50 µL of

benzaldehyde as terminating agent and left to stir for 30 minutes. The product was obtained by precipitation from DCM (1:2 v/v DMF:DCM for **poly1** and **poly2**; 1:2.5 v/v DMF:DCM for **poly3** and **poly4**) which was washed 6 times with DCM and filtered in order to remove any traces of DMF.

Poly1 was obtained as a light brown powder (0.2 g, 94 %). ^{1}H NMR (dmso-d_6, 400 MHz) δ (ppm): 9.22 (1H, s, NH-5), 8.76 (2H, br s, 8), 7.98 – 7.65 (2H, m, 9), 7.63 – 7.43 (4H, m, 3 and 4), 5.57 (2H, d, J = 70.5 Hz, 15 cis & trans), 4.91 – 4.56 (2H, m, 11), 3.97 (2H, d, J = 5.3 Hz, 7), 3.16 (2H, br s, 13), 2.72 (2H, s, 14), 1.98 (1H, s, 16), 1.49 (1H, s, 16'); ^{13}C NMR (dmso-d_6, 100 MHz) δ (ppm): 177.9 (C-12), 162.3 (C-6), 154.2 (C-5), 144.2 (C-10), 143.0 (C-8), 131.5 (C-15), 125.7 (q, J = 3.4 Hz, C-3), 124.6 (q, J = 271.0 Hz, CF$_3$), 124.5 (C-9), 120.9 (q, J = 31.7 Hz, C-2), 117.2 (C-4), 56.0 (C-7), 52.1 (C-13), 50.9 (C-14), 44.7 (C-16) 40.6 (C-11); GPC: M_n = 10 600 and 2 200 g/mol, M_w = 12 400 and 2 300 g/mol, Đ = 1.17 and 1.0.

Poly2 was obtained as a dark green powder (0.14 g, 72 %). ^{1}H NMR (dmso-d_6, 333 K, 400 MHz) δ (ppm): 10.19 (1H, br s, NH-5), 8.69 – 8.65 (2H, m, 8), 8.02 (1H, br s, NH-7), 7.83 (2H, br s, 9), 7.63 – 7.56 (4H, m, 3 and 4), 5.60 (2H, d, J = 81.3 Hz, 15, cis & trans), 4.63 (2H, s, 11), 4.29 (2H, s, 7), 3.19 (2H, s, 13), 2.73 (2H, s, 14), 2.03 (1H, s, 16), 1.52 (1H, s, 16'); ^{13}C NMR (dmso-d_6, 100 MHz) δ (ppm): 180.2 (C-6), 177.8 (C-12), 143.6 (C-8), 131.6 (C-15), 125.8 (C-3), 124.4 (q, J = 271.0 Hz, CF$_3$), 124.4 (C-9), 122.2 (C-2), 120.4 (C-4), 60.1 (C-7), 52.1 (C-13), 50.8 (C-14), 44.7 (C-16), 41.0 (C-11); GPC: M_n = 10 600 and 2 300 g/mol, M_w = 13 000 and 2 300 g/mol, Đ = 1.24 and 1.0.

Poly3 was obtained as a light brown powder (0.12 g, 39 %). ^{1}H NMR (dmso-d_6, 400 MHz) δ (ppm): 9.20 (1H, s, NH-5), 8.76 (2H, br s, 8), 7.77 (2H, br s, 9), 7.53 (4H, q, J = 8.77 Hz, 3 and 4), 6.87 (1H, s, NH-7), 5.85 (2H, d, J = 90.2 Hz, 15 cis & trans), 4.95 – 4.49 (4H, m, 11 and 14), 3.95 (2H, d, J = 4.4 Hz, 7), 3.55 (2H, br s, 13); ^{13}C NMR (dmso-d_6, 100 MHz) δ (ppm): 175.6 (C-12), 154.2 (C-6), 144.2 (C-5), 143.2 (C-8), 131.6 (C-15), 125.8 (q, J = 3.6 Hz, C-3), 124.7 (q, J = 271.0 Hz, CF$_3$), 124.5 (C-9), 120.9 (q, J = 32.0 Hz, C-2), 117.2 (C-4), 79.9 (C-14), 56.0 (C-7), 53.5 (C-13), 41.0 (C-11); GPC: M_n = 7 100 and 2 200 g/mol, M_w = 8 200 and 2 200 g/mol, Đ = 1.15 and 1.0.

Poly4 was obtained as a dark green powder (0.10 g, 32 %). ^{1}H NMR (dmso-d_6, 333 K, 400 MHz) δ (ppm): 10.19 (1H, br s, NH-5), 8.69 – 8.60 (2H, m, 8), 8.01 (1H, br s, NH-7), 7.82 (2H, br s, 4), 7.62 (2H, d, J = 8.3 Hz, 9), 7.55 – 7.47 (2H, br m, 3), 5.87 (2H, d, J = 96.4 Hz, 15 cis & trans), 4.95 – 4.49 (4H, m, 11 and 14), 4.22 (2H, s, 7), 3.55 (2H, s, 13); ^{13}C NMR (dmso-d_6, 100 MHz) δ (ppm): 180.2 (C-6), 175.6 (C-12), 143.6 (C-5 and C-8), 131.5 (C-15), 125.5 (C-3), 124.4 (q, J = 271.4 Hz, CF$_3$), 124.3 (C-9), 122.2 (C-2), 121.4 (C-4), 60.1 (C-7), 53.5 (C-13), 52.5 (C-14), 40.1 (C-11); GPC: M_n = 8 000 and 2 300 g/mol, M_w = 9 200 and 2 300 g/mol, Đ = 1.16 and 1.0.

4.2.6. Sample preparation for antimicrobial screening[12]

Preparation of Luria Broth media (LB): Yeast extract (5 g), tryptone (10 g) and sodium chloride (10 g) were dissolved in dH$_2$O (1 L) then divided into bottles and autoclaved.

Preparation of Luria Broth (LB) agar plates: Agar (6 g) was added to LB (400 mL) and autoclaved. Once cool, the LB agar was poured into sterile petri dishes under sterile conditions and allowed to set. LB plates were stored at 4 °C until use.

Preparation of bacterial plates: Sterile LB agar plates were streaked using *Escherichia coli* DH10B or methicillin-resistant *Staphylococcus aureus* USA300 then incubated at 37 °C overnight.

Preparation of Inoculum: An initial culture was made up by inoculating LB media (5 mL) with a single colony of bacteria under sterile conditions and incubated at 37 °C with shaking overnight. The following day, overnight bacterial cultures were subcultured into fresh LB medium to a starting OD$_{600}$ of 0.01.

Preparation of MIC well microplate: Each compound was serially diluted across the plate with a starting concentration of 10 mM for **mon1 – mon4** and 500 µg/mL for **poly1 – poly4**. Bacteria culture (100 µL) of was aliquoted to each well giving a total well volume of 200 µL. Plates were incubated with shaking (180 rpm) at 37 °C for 18 h and the OD$_{600}$ was determined using a Clariostar plate reader (BMG Labtech).

4.3. References

1   L. T. Birchall, S. Shehata, C. J. Serpell, E. R. Clark and S. C. G. Biagini, *J. Chem. Educ.*, 2021, **98**, 4013–4016.

2   Y. C. Teo and Y. Xia, *Macromolecules*, 2015, **48**, 5656–5662.

3   B. Neises and W. Steglich, *Angew. Chemie Int. Ed. English*, 1978, **17**, 522–524.

4   S. C. G. Biagini and A. L. Parry, *J. Polym. Sci. Part A Polym. Chem.*, 2007, **45**, 3178–3190.

5   L. T. Birchall, S. Shehata, S. McCarthy, H. J. Shepherd, E. R. Clark, C. J. Serpell and S. C. G. Biagini, *Polym. Chem.*, 2020, **11**, 5279–5285.

6   R. Moumne, S. Lavielle and P. Karoyan, *J. Org. Chem.*, 2006, **71**, 3332–3334.

7   R. Wang, M. Ma, X. Gong, G. B. Panetti, X. Fan and P. J. Walsh, *Org. Lett.*, 2018, **20**, 2433–2436.

8   S. C. G. Biagini, S. M. Bush, V. C. Gibson, L. Mazzariol, M. North, W. G. Teasdale, C. M. Williams, G. Zagotto and D. Zamuner, *Tetrahedron*, 1995, **51**, 7247–7262.

9   M. B. France, L. T. Alty and T. M. Earl, *J. Chem. Educ.*, 1999, **76**, 659–660.

10   L. R. Blackholly, H. J. Shepherd and J. R. Hiscock, *CrystEngComm*, 2016, **18**, 7021–7028.

11   E. Ahmetali, P. Sen, N. C. Süer, B. Aksu, T. Nyokong, T. Eren and M. K. Şener, *Macromol. Chem. Phys.*, 2020, **221**, 1–14.

12   J. E. Boles, R. J. Ellaby, H. J. Shepherd and J. R. Hiscock, *RSC Adv.*, 2021, **11**, 9550–9556.

CHAPTER 5. SUMMARY AND FUTURE WORK

5.1. Summary of Chapter 1

The ring opening metathesis polymerisation (ROMP) became, in the late 1990's, one of the most versatile living polymerisation methods for the preparation of different materials used in a variety of applications. Living polymerisations are a type of chain transfer polymerisation where the termination step does not occur and therefore the polymer is kept "alive" during the propagation step (Chapter 1, Section 1.1.1). The greatest contribution towards the development of such polymerisation is attributed to Y. Chauvin, R. H. Grubbs and R. R. Schrock who in 2005 received together the Nobel Prize in chemistry for the development of the metathesis method in organic synthesis (reaction of olefins via carbon-carbon exchange)[1]. ROMP involves the polymerisation of strained cyclic olefines (norbornene (NB) and 7-oxanorbornene (ONB) being the most used ones) mediated by a metal alkylidene catalyst based on group VI and VIII metals, such as Mo and Ru. Due to its living behaviour, ROMP does not possess a termination step and hence control over molecular weight (M_n is proportional to the monomer conversion), as well as homo and block architecture is possible. Furthermore, ROMP allows for the preparation of polymers with a very narrow distribution of the molecular weights (Đ < 1.5).

Since the 1960's many catalysts have been developed for ROMP and Chapter 1 gives a brief overview of those most important. Those that are now commercially available are the molybdenum catalysts synthesised by Schrock and the ruthenium-alkylidene initiators developed by Grubbs. Among the Schrock and Grubbs catalysts, Grubbs third generation (**G3**) is the most widely used one as it possesses several advantages including stability towards air and moisture, high functional group tolerance, high propagation rate and control over molecular weight distribution.

Thanks to the versatility of the ROMP initiators, many research groups have employed ROMP polymerisation for the realisation of biologically related polymers. This includes targeted delivery systems of drugs[2] or nucleic acids[3], antimicrobial polymers[4], carbohydrates[5] and peptide[6]

containing polymers as well as synthetic mimics of DNA and RNA[7,8] in the form of delivery vehicles. Chapter 1 highlights some of the recent literature on the use of ROMP for biological purposes and focus the attention on ROMP for drug delivery systems to be used in cancer therapy and ROMP as antimicrobial agents. These two are the main topics that this PhD project has focused on. Chapter 2 discusses the preparation of ROMP nanoparticles for the delivery of ibuprofen, while Chapter 3 discusses the development of antimicrobial ROMP polymers consisting of a novel class of antibiotics called SSAs (self-associating amphiphilic salts).

5.2. Summary and future work of Chapter 2

In this chapter a novel class of polymer-drug conjugates (drugs covalently bonded to a polymer backbone) containing ibuprofen, an NSAID drug, was successfully prepared using the ROMP polymerisation. Firstly, ibuprofen and PEG based norbornene (NB) monomers (**5b** and **10b**) were synthesised in a three and four step reaction respectively. Thanks to the presence of -COOH and -OH functionalities in the ibuprofen and PEG moieties, it was possible to link them to the NB ring via an ester bond, which could eventually undergo hydrolysis. The formation of both monomers, **5b** and **10b**, was mainly confirmed by ^{1}H NMR and LC-MS, the latter identifying a distribution of m/z in the case of monomer **10b** caused by the presence of PEG which is a polymer chain itself.

Monomers **5b** and **10b** were then polymerised using the **G3** initiator which allowed for the preparation of homopolymers **poly5b** and **poly10b** possessing a narrow distribution of the molecular weights. GPC chromatography showed formation of homopolymers consisting of a very low dispersity index Đ of 1.27 and 1.36 for **poly5b** and **poly10b** respectively, whereas ^{1}H NMR exhibited peak broadening upon formation of the polymers with very little changes in the chemical shift when compared to their monomer counterparts. ^{1}H NMR spectroscopy was also used to determine the rate of homopolymerisation, showing that both monomers **5b** and **10b** completely converted to their respective polymers **poly5b** and **poly10b** in less than 5 minutes. Although **G3** catalyst is a very active initiator for ROMP, it needs to be handled carefully as it can oxidise over

time and therefore it can lose its activity. It was demonstrated, in this study, that the use of oxidised **G3** formed **poly5b** and **poly10b** with dispersity index greater than 2.0 and M_n values almost one order of magnitude greater than the theoretical one. Kinetic studies also showed longer monomer conversion times of 4 hours for **5b** and 40 minutes for **10b**.

The copolymerisation of both ibuprofen and PEG containing NB monomers allowed for the preparation of statistical (**poly5b-co-poly10b**) and block (**poly5b-b-poly10b**) copolymers. In both cases, quantitative ^{1}H NMR was used to determine the NB-Ibu/NB-PEG ratio within the polymer backbone resulting in the formation of four copolymers with different hydrophobic/hydrophilic ratios. Thanks to the hydrophobic and hydrophilic properties of NB-Ibu and NB-PEG, it was possible to form self-assembly morphologies in aqueous environment. These were studied by DLS and TEM which showed formation of both small (d ~ 20 nm) and big (d ~ 100 nm) spherical aggregates in the case of **poly5b-b-poly10b**, while **poly5b-co-poly10b** gave rise to single chain nanoparticles which then aggregated and precipitated in water to from big random agglomerates. Due to the broad distribution of particle size obtained in the case of block copolymers, it could not be assumed that micellar structures were formed. This is because the micellization is an equilibrium phenomenon that leads to the formation of micelles with uniform size (narrow distribution). It was demonstrated that changing the organic solvent (acetone, THF, acetonitrile) for nanoprecipitation as well as the NB-Ibu/NB-PEG ratio within the polymer chain (50:50 vs 36:64) did not drastically alter the size of nanoparticles, showing the versatility of the synthesised block copolymers.

Finally, the release of ibuprofen was investigated for **poly5b-b-poly10b [50:50]** self-assembled in acetone, THF and acetonitrile, and for **poly5b-co-poly10b [60:40]** self-assembled from acetonitrile. Due to time constrain, the realising studies could not be carried out for the statistical copolymers in the acetone/water and THF/water systems. It was demonstrated that the drug release, carried out at 40 °C, from both block and statistical copolymers was successful when strong alkaline environment (pH = 14.3) was used, and no major differences were detected for the three block copolymers self-assemblies investigated. A slower release was obtained in the case of

block copolymers due to ibuprofen being less readily available for hydrolysis in bigger polymeric nanoparticles (> 90 % in 10 %) compared to single chain nanoparticle systems adopted by statistical copolymers (~ 90 % in 2 hours). This demonstrated the importance of using a specific sequence within the polymer backbone in order to obtain nanoparticles with specific size and morphology and consequently slow realising processes. When systems that best mimic the physiological conditions, such as PBS, FBS and PLE were used, no polymer degradation was observed for a period of up to four days. However, this can demonstrate the stability of the prepared nanoparticles meaning that no drug might be released before being delivered to the site of action. Despite the good results have been obtained only under basic conditions, the release of ibuprofen from polymeric nanoparticles could be studied under mild acidic conditions, due to the low pH existing in the tumour extracellular environment (pH ~ 5.0 − 7.0)[9]. Furthermore, the so obtained nanoparticles could not only be used for cancer therapy, but they could also be used in chemoprevention as well as treatment of rheumatoid arthritis and general inflammation management, with the purpose of reducing the gastrointestinal and renal side effects associated with the oral administration of NSAIDs.

In order to obtain systems that could release the drug under mild acidic pH, another approach was taken. Attempts to form an imine bond between the NB ring and the drug was carried out. For this purpose, ketoprofen, a derivative of ibuprofen that contains a ketone group was employed. The reaction conditions used between the primary amine NB-NH$_2$ **11** and ketoprofen **12b** or ketoprofen methyl ester **12c**, included (i) catalytic pTsOH in toluene using a Dean-Stark trap, (ii) catalytic pyrrolidine in DCM and molecular sieves 4 Å and (iii) stoichiometric Ti(OEt)$_4$ in THF under anhydrous conditions. Despite the efforts put into the development of these new drug system, no successful linkage could be obtained.

Further work could explore different linkages between the polymer backbone and the drug with the aim of inducing controlled release in the presence of specific physiological environments, and its effects in cells. In particular the system could be tuned to allow for the slow enzymatic

release of ibuprofen by esterase enzymes as it has been shown in other polymer nanoparticle systems[10]. For example, studies at different concentration of PLE could be carried out, as well as the employment of different esterase enzymes could be investigated. Furthermore, more labile linkages, such as hydrazone bonds, could be also employed between the polymer backbone and ibuprofen as they could hydrolyse at mild acidic pH, such those present in the tumour microenvironment (see Section 1.3.1.1, Chapter 1). A possible reaction pathway obtained by a modification from literature[11] is shown in Scheme 5.1.
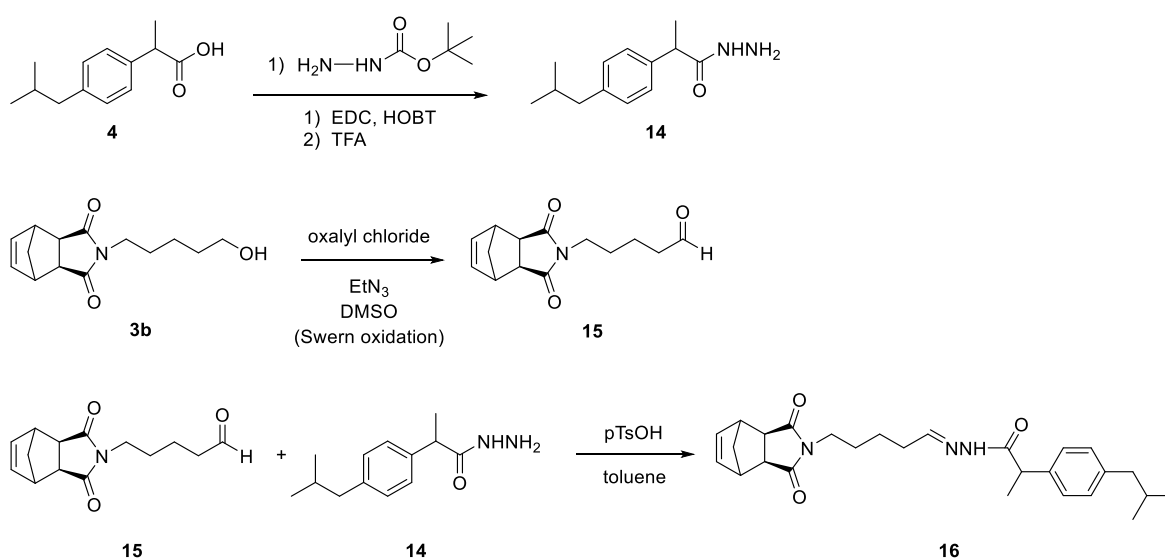
Scheme 5.7. Possible reaction pathway for the synthesis of a new ibuprofen containing NB monomer consisting of a hydrazone link.

Another future work could investigate the reaction of non-terminated **poly5b** with poly(ethylene glycol) methyl ether acrylate (M_n = 480 and/or M_n = 2000) (**mPEG-acrylate**) which would act both as the terminating agent of the polymerisation and as the hydrophilic portion of the block copolymer (the cross-metathesis synthesis of methyl acrylate has been previously studied for the transformation of terpenoids[12]). In this way, a novel amphiphilic copolymer (**poly5b-b-acryl-PEG**) could be synthesised for the preparation of polymeric NPs that would possess micellar structure (core-shell structure) with narrower size distribution compared to those obtained in the case of the **poly5b-b-poly10b** investigated in this study. Its self-assembly properties could be

studied using both DLS and TEM, and the releasing processes of ibuprofen could also be investigated under both physiological conditions and mild acidic pHs.
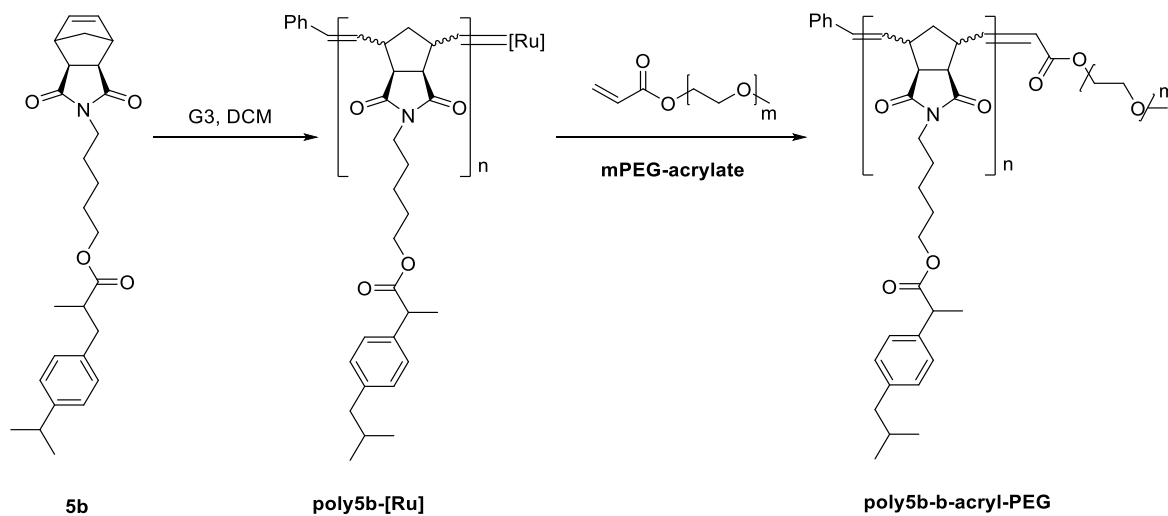
Scheme 5.8. Possible schematic route for the preparation of a novel amphiphilic block copolymer, **poly5b-b-acryl-PEG**, obtained by the cross-metathesis of active ibuprofen homopolymer, **poly5b-[Ru]** and **mPEG-acrylate**.

5.3. Summary and future work of Chapter 3

In this chapter novel antimicrobial polymers possessing quaternary pyridinium cations and SSA (supramolecular self-associating amphiphiles) anions were prepared and tested for their antimicrobial activity against both Gram-positive and Gram-negative bacteria. SSAs are urea/thiourea sulfonate-based salts prepared by the Hicock group at the University of Kent. The anionic component of SSAs possesses both HBA (hydrogen bond accepting) and HBD (hydrogen bond donating) groups which allow for the preparation of aggregates through self-association processes (Chapter 3, Section 3.1.2). SSAs have previously shown to act as antimicrobial agents against MRSA and/or *E. coli* bacteria, although in some cases high concentrations of SSAs were required in order to inhibit 50 % of bacterial cell growth[13]. In this study, ROMP polymers were used both as drug carriers and antimicrobial polymers, with the intention of gaining synergistic effect between the polymer carrier and the SSA drug, and hence determine whether and improvement in the SSA antimicrobial activity could be obtained.

In order to achieve that, norbornene (NB) and oxanorbornene (ONB) monomers containing a pyridine moiety (**4b** and **9**) were first synthesised and then each reacted with two selected SSAs, urea-sulfonate anion (**SSA-1**) and thiourea-sulfonate anion (**SSA-2**), to obtain four different structurally related monomers, **mon1 – mon4**. **Mon1** and **mon2** were NB based monomers, while **mon3** and **mon4** were ONB based monomers. **Mon1** and **mon3** contained **SSA-1** as the counterion, while **mon2** and **mon4** contained **SSA-2** as the counterion. The so formed monomers were then polymerised using Grubbs third generation catalyst (**G3**) in DMF at room temperature, using benzaldehyde as terminating agent and purified by precipitation from DCM. Homopolymers **poly1** and **poly2** were obtained with high yields, 94 % and 72 % respectively, while the polyONB homopolymers, **poly3** and **poly4** were obtained with low yields of 39 % and 32 % respectively. This was hypothesised to be due to poor work up conditions, for which polymers could only partially be precipitated from the reaction mixture, but also for incomplete conversion of the monomers (M_n (GPC) < M_n (Th)). DMF was the solvent chosen for the polymerisation, due to poor solubility of the monomers in many organic solvents. However, the selected solvent did not allow for the kinetic studies to be carried out, and therefore the polymerisations were left overnight in order to obtain complete conversion of the monomers. The analysis of the distribution of the polymer chain for **poly1 – poly4** were carried out using GPC chromatography. GPC analysis showed formation of two different distributions of the molecular weights for each of the four polymers. This was probably due to the long reaction time which caused "backbiting" side reactions to happen (see Chapter 1, Section 1.2.2.4 for the explanation of "backbiting" reactions). Unfortunately, to due GPC instrument unavailability, these results were the only ones obtained from all the experiments that were carried out. However, formation of polymers was previously confirmed by ^{1}H NMR, which showed typical peak broadening.

Monomers **mon1 – mon4** were studied in the solid phase (XRD), gas phase (MS) and solution state (qNMR, DOSY NMR, DLS, Tensiometry) and then compared to the results obtained for **SSA-1** and **SSA-2** alone. Single crystal XRD analysis were carried out for **mon1** and **mon2**, while

due to time constrain and instrument unavailability, **mon3** and **mon4** could not be analysed. It was determined that, in the solid state, **mon1** and **mon2** behaved similarly to **SSA-1** and **SSA-2**. In fact, they both formed self-associating structures due to formation of hydrogen bonds between the monomeric units. **Mon1** formed a staggered *syn*-stacking mode, while **mon2** formed the thiourea-anion stacking mode typical of the sulphur containing SSAs, rather than a tape motif adopted by **mon1**. On contrary, the behaviour of the four synthesised monomers is different compared to **SSA-1** and **SSA-2** in both gas phase and solution state. In these cases, all of the monomers showed formation of monomeric species rather than the typical dimeric or higher order species obtained for the SSAs. Using ESI-MS in negative and positive modes, only the m/z values of the urea anion $[M]^-$ and the NB/ONB cation $[M+H]^+$ in the monomeric form could be detected.

In the solution state different techniques were used to determine the formation of self-associating species. All the tests were carried out in two different solvent systems: (i) 5 % EtOH in water and (ii) DMSO. While it was determined that both **SSA-1** and **SSA-2** tended to form higher order structures in water solution and dimeric species in DMSO, this could not be determined for **mon1 − mon4**. Both qNMR and DOSY NMR analysis on **mon1 − mon4** showed formation of monomeric species in water and dimeric species in DMSO. For instance, with DOSY NMR, hydrodynamic diameters of d_H 1.0 - 1.1 nm in water and d_H 1.3 - 1.4 nm in DMSO for cation and anion in each monomer could be determined. Despite the results obtained by qNMR and DOSY, where no larger self-associating structures were detected, nanoparticle size distribution (DLS) and stability (zeta potential, ZP) were analysed for **mon1 − mon4** (5 % MeOH/H_2O solution at a concentration of 5.56 mM). Unexpectedly, DLS showed formation of aggregates in water with average diameter between 130 nm and 230 nm, however ZP determined a high instability for these aggregates (~ -5 mV). It was, therefore, hypothesised that these results could be due to agglomeration of smaller structures in solution that could be seen by the DLS as particles of coherent shape and size. However, ZP confirmed the absence of large structures in solution. Nevertheless, studies on CAC were carried out and it was found that the concentration for which

aggregates started to form in 5 % MeOH/H$_2$O was, for **mon1 – mon4**, above 5.56 mM (DLS studies concentration). This could mean that the surface interface became saturated and therefore bigger aggregates only started to form at concentrations higher than 5.56 mM.

Homopolymers, **poly1 – poly4**, were also characterised in the solution state but not in the solid and gas states. DOSY NMR was carried out to determine the size of polymer aggregates in DMSO. The cationic polymer backbone was shown to possess d$_H$ ~ 7.3 nm (**poly1** and **poly2**) and d$_H$ ~ 5.0 nm (**poly3** and **poly4**), while the SSA anions remained unchanged (d$_H$ ~ 1.5 nm). These results demonstrated that a week coordination is formed between the cationic polymer backbone and the anionic SSA, as they diffuse at different rates in the DOSY experiment. The nanoparticle size and stability of **poly1 – poly4** was studied in 1 % DMSO/H$_2$O with a concentration of 1 mg/mL (a polymer suspension was obtained). This was the solvent system selected for the studies of antimicrobial activity. DLS analysis showed that all of the four polymers could form aggregates in solution with an average diameter between 130 nm and 250 nm. Differently from their monomer counterparts, the so formed aggregates were shown to be relatively stable as the ZP was > +30 mV. Tensiometry analysis on **poly1 – poly4** was carried out, however it was not possible to determine the CAC at concentrations up to 1 mg/mL.

Finally, antimicrobial studies on both monomers and polymers were carried out against Gram-positive and Gram-negative bacteria. The antibacterial activity was expressed as a minimum inhibitory concentration (MIC$_{50}$), the concentration required by each monomer and polymer to prevent 50 % of bacterial cell growth against Gram-positive MRSA USA300 and Gram-negative *E. coli* DH10B models. While experiments failed in the case of **poly1 – poly4** at concentrations up to 500 µg/mL and for **mon1** at concentrations up to 10 mM, **mon2** could inhibit 50 % of MRSA USA300 and *E. coli* DH10B growth at a concentration of 10 mM. Whereas **mon4** failed against MRSA but possessed a MIC$_{50}$ of 10 mM against *E. coli*. Experiments could not be carried out for **mon3** due to the presence of MeOH traces in the crude product at the time the antimicrobial tests were carried out. However, the results were not promising in comparison to those obtained for the SSAs alone,

meaning that the addition of a cationic polymer to SSAs had an antagonistic effect towards the SSAs antimicrobial activity.
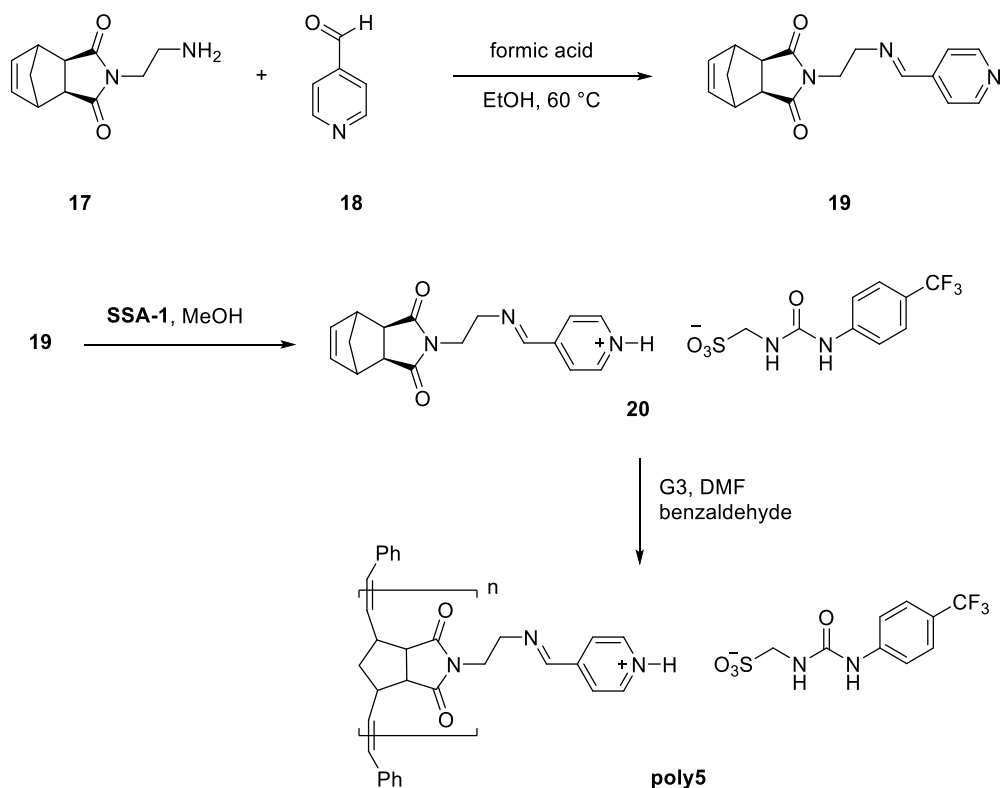
Scheme 5.9. Possible reaction scheme for the preparation of homopolymer **poly5**. In the first step NB-NH$_2$ **17** could react with pyridine-4-carboxaldehyde **18** to form compound **19** consisting of an imine bond between the two reactants[18,19]. This could be followed by the proton transfer reaction between compound **19** and **SSA-1** to afford the possible monomer **20**. The latter could then be polymerised using **G3** as the initiator and DMF as the solvent.

Despite the unsuccessful results, the synthesised polymeric systems could be seen as ideal delivery vectors for SSAs as they would remain inactive during their circulation to the desired site of action and therefore, SSAs would be safely delivered. For this reason, it would be interesting to prepare polymeric drug delivery systems where the SSAs could be released in proximity to the bacteria outer surface due to metabolic processes such as hydrolysis under mild acidic pHs. It is known from literature that pH influences the occurrence and distribution of microorganisms[14,15]. According to what pH they thrive, microbes are classified into acidophiles (pH 0.1 – 5.4), neutrophiles (pH 5.4 – 7.0) and alkalophiles (pH 7.0 – 11.5)[16]. For instance, *E. coli* has the ability to

grow at moderate acidic pH of 4.0 − 5.0 and therefore is classified as an acidophile[17]. A new polymer-SSA deliver system could be constructed so that an imine bond between NB and SSA is formed. This way SSA could be delivered towards the bacteria cell membrane where the acidic environment would hydrolyse the imine bond and consequently release the SSA. Scheme 5.3 shows a possible synthetic pathway for the preparation of a novel ROMP homopolymer (**poly5**) consisting of molecules of SSAs covalently bonded to the polymer backbone via imine bond.

5.4. References

1   MLA style: The Nobel Prize in Chemistry 2005. NobelPrize.org. Nobel Media AB 2021. Wed. 9 Jun 2021., https://www.nobelprize.org/prizes/chemistry/2005/summary/, (accessed 10 June 2021).

2   P. Bertrand, C. Blanquart and V. Héroguez, *Biomolecules*, 2019, **9**, 60.

3   R. Gareth Davies, V. C. Gibson, M. B. Hursthouse, M. E. Light, E. L. Marshall, M. North, D. A. Robson, I. Thompson, A. J. P. White, D. J. Williams and P. J. Williams, *J. Chem. Soc. Perkin 1*, 2001, 3365–3381.

4   M. N. Islam, B. Aksu, M. Güncü, M. Gallei, M. Tulu and T. Eren, *J. Polym. Sci.*, 2020, **58**, 872–884.

5   T. Debsharma, B. Schmidt, A. Laschewsky and H. Schlaad, *Macromolecules*, 2021, **54**, 2720–2728.

6   P. Kelly, P. Anand, A. Uvaydov, S. Chakravartula, C. Sherpa, E. Pires, A. O'Neil, T. Douglas and M. Holford, *Int. J. Environ. Res. Public Health*, 2015, **12**, 12543–12555.

7   M. Lis, F. Dorner, G. N. Tew and K. Lienkamp, *Langmuir*, 2016, **32**, 5946–5954.

8   A. Ö. Tezgel, P. Jacobs, C. M. Backlund, J. C. Telfer and G. N. Tew, *Biomacromolecules*, 2017, **18**, 819–825.

9   F. Danhier, O. Feron and V. Préat, *J. Control. Release*, 2010, **148**, 135–146.

10 C. O'Sullivan and C. Birkinshaw, *Polym. Degrad. Stab.*, 2002, **78**, 7–15.

11 V. Vijayakameswara Rao, S. R. Mane, A. Kishore, J. Das Sarma and R. Shunmugam, *Biomacromolecules*, 2011, **13**, 221–230.

12 H. Bilel, N. Hamdi, F. Zagrouba, C. Fischmeister and C. Bruneau, *Green Chem.*, 2011, **13**, 1448–1452.

13 N. Allen, L. J. White, J. E. Boles, G. T. Williams, D. F. Chu, R. J. Ellaby, H. J. Shepherd, K. K. L. Ng, L. R. Blackholly, B. Wilson, D. P. Mulvihill and J. R. Hiscock, *ChemMedChem*, 2020, **15**, 2193–2205.

14 Q. Jin and M. F. Kirk, *Front. Environ. Sci.*, 2018, **6**, 1–15.

15 T. A. Krulwich, G. Sachs and E. Padan, *Nat. Rev. Microbiol.*, 2011, **9**, 330–343.

16 S. Sivaramakrishnan and R. T. V. Vimala, in *Bacterial Bioflocculant for Multifunctional Features*, Academic Press, 2022, pp. 7–68.

17 Y. Xu, Z. Zhao, W. Tong, Y. Ding, B. Liu, Y. Shi, J. Wang, S. Sun, M. Liu, Y. Wang, Q. Qi, M. Xian and G. Zhao, *Nat. Commun.*, 2020, **11**, 1–13.

18 S. Zai, H. Gao, Z. Huang, H. Hu, H. Wu and Q. Wu, *ACS Catal.*, 2012, **2**, 433–440.

19 S. Shamim, S. Murtaza and M. F. Nazar, *J. Chem. Soc. Pakistan*, 2016, **38**, 494–503.